UNIVERSITY OF CALIFORNIA SAN DIEGO

Vibrational Damping of Composite Materials

A dissertation submitted in partial satisfaction of the requirements for the degree

Doctor of Philosophy

in

Materials Science and Engineering

by

Janet M. Biggerstaff

Committee in charge:

Professor John Kosmatka, Chair
Professor Vistasp Karbhari
Professor Vitali Nesterenko
Professor M. Lea Rudee
Professor Michael Sailor

2006

The dissertation of Janet Biggerstaff is approved, and it is acceptable in quality and for publication on microfilm:

_____

_____

_____

_____

_____

Chair

University of California San Diego

2006

DEDICATION

There are many people who made this possible. I would like to thank my advisor, Professor John Kosmatka, who gave me invaluable counsel and guidance over the past ten years. I'd also like to thank NASA-Glenn for their funding of this research, and Oral Mehmed for his assistance with this project.

The members of my dissertation committee, Professor Vistasp Karbhari, Professor Vitali Nesterenko, Professor M. Lea Rudee, and Professor Michael Sailor have generously given their time and expertise. I thank them for their contributions.

I am grateful to have received assistance from many great students through the years, including Howard Nestman, Tony Stotts, Brandon Farmer, Phu Nguyen, Devon Johnson, Jon Carter, Stanley Mak, Ma Zhixin, and Marc Robinson. Fellow grad students Kevin Napolitano and Geoff Appuhn were both tremendously helpful and made life in the lab more fun, although their best advice might have been picks for the football pool.

I'd like to thank my parents for always being there, and for encouraging me to go after whatever I want in life.

A special thank you goes to my husband, Bob, who supported me through this very long process. I know it wasn't easy to hear "just another six months" for so many years.

This is dedicated to the two reasons this dissertation took five years longer than it should have: my precious daughters Natalie and Sophie. Now Mommy can finally "stop working on the 'puter."

TABLE OF CONTENTS

LIST OF FIGURES

LIST OF TABLES

ACKNOWLEDGEMENTS

Chapter 4 is a reprint, in part, of the material published in 1999 in the *Journal of Composite Materials* titled "Damping Performance of Cocured Graphite/Epoxy Composite Laminates with Embedded Damping Materials" Volume 33, pages 1457-1469. The dissertation author was the primary investigator and co-authored the article with advisor J. B. Kosmatka.

Chapter 5 will be submitted, in part, for publication to the *Journal of Composite Materials* with the title "Shear Measurements of Cocured Viscoelastic Damping Materials". The dissertation author was the primary investigator and co-authored the article with advisor J. B. Kosmatka.

Chapter 6 will be submitted, in part, for publication to *Composites, Part A* with the title. "Directional Damping Properties of Slotted Acrylic". The dissertation author was the primary investigator and co-authored the article with advisor J. B. Kosmatka.

Chapter 7 will be submitted, in part, for publication to the *Journal of Composite Materials* with the title "Addition of Particulate Tougheners to Increase Damping of Composite Laminates". The dissertation author was the primary investigator and co-authored the article with advisor J. B. Kosmatka.

Chapter 8 will be submitted, in part, for publication to *Mechanics of Advanced Materials and Structures* with the title "The Development of Electroviscoelastic Materials As Active Vibrational Dampers". The dissertation author was the primary investigator and co-authored the article with advisor J. B. Kosmatka.

VITA

1995	B.S., University of Kentucky
1999	M.S., University of California San Diego
1995-2001	Research Assistant, University of California San Diego
2006	Ph.D., University of California San Diego

PUBLICATIONS

Biggerstaff, J. M., and J. B. Kosmatka, 1998. "Damping Performance of Cocured Composite Laminates with Embedded Viscoelastic Layers", *SPIE Proceedings on Smart Structures and Materials*, **3327**:107-114.

Biggerstaff, J. M., and J.B. Kosmatka, 1999. "Damping Performance of Cocured Graphite/Epoxy Composite Laminates with Embedded Damping Materials", *Journal of Composite Materials*, **33**:1457-1469.

Biggerstaff, J. M., and J. B. Kosmatka, 1999. "Shear Measurements of Viscoelastic Damping Materials Embedded in Composite Plates", *SPIE Proceedings on Smart Structures and Materials*, **3672**:82-92.

Biggerstaff, J. M., and J. B. Kosmatka, 1999. "Directional Damping Material for Integrally Damped Composite Plates", *SPIE Proceedings on Smart Structures and Materials*, **3672**:368-374.

Biggerstaff, J. M., and J. B. Kosmatka, 2000. "Effect of Particulate Toughеners on the Damping of Composite Laminates", *SPIE Proceedings on Smart Structures and Materials*, **3989**:531-538.

Biggerstaff, J. M., and J. B. Kosmatka, 2002. "Electroviscoelastic Materials As Active Dampers", *SPIE Proceedings on Smart Structures and Materials*, **4695**:345-350.

Biggerstaff, J. M., and J. B. Kosmatka, 2006. "Shear Measurements of Cocured Viscoelastic Damping Materials", submitted for publication to *Journal of Composite Materials*

Biggerstaff, J. M., and J. B. Kosmatka, 2006. "Directional Damping Properties of Slotted Acrylic", submitted for publication to *Composites, Part A*

Biggerstaff, J. M., and J. B. Kosmatka, 2006. "Addition of Particulate Toughеners to Increase Damping of Composite Laminates", submitted for publication to *Journal of Composite Materials*

Biggerstaff, J. M., and J. B. Kosmatka, 2006. “The Development of Electroviscoelastic Materials As Active Vibrational Dampers”, submitted for publication to *Mechanics of Advanced Materials and Structures*

ABSTRACT OF THE DISSERTATION

Vibrational Damping of Composite Materials

by

Janet M. Biggerstaff

Doctor of Philosophy in Materials Science and Engineering

University of California, San Diego, 2006

Professor John Kosmatka, Chair

The purpose of this research was to develop new methods of vibrational damping in polymeric composite materials along with expanding the knowledge of currently used vibrational damping methods. A new barrier layer technique that dramatically increased damping in viscoelastic damping materials that interacted with the composite resin was created. A method for testing the shear strength of damping materials cocured in composites was developed. Directional damping materials, where the loss factor and modulus could be tailored by changing the angle, were produced and investigated. The addition of particles between composite prepreg layers to increase damping was studied. Electroviscoelastic materials that drastically changed properties such as loss factor and modulus with an applied voltage were manufactured and tested.

Chapter 1 Introduction

The use of polymeric composites composed of fibers (graphite, Kevlar, glass) embedded in a polymer matrix has increased tremendously in the past 30 years. Figure 1-1 shows a diagram of a polymer composite composed of unidirectional layers. Composites have many advantages over metals such as increased stiffness and strength-to-weight ratio, tailorability, corrosion resistance, radar absorption, and tailorable thermal expansion coefficient. Composites are now used in a wide range of applications such as aerospace structures, automobiles, boats, biomedical products, sporting goods, and civil structures. Vibrations are undesirable in many of these systems, causing problems that range from noise to fatigue failure. Vibrations are especially problematic in aerospace structures: in aircraft, the engine vibrations can cause problems in the fan blades and throughout the airframe structure while space satellites do not have air, a natural damper, to reduce vibrations initiated by instruments or thermal expansion and contraction.

Metallic structures are typically made up of many more parts than composite structures and thus have more sources for energy dissipation. A large portion of the damping for most structures is obtained from the friction of the joints, bolts, rivets, etc. Composite structures often don't have as many parts and typically have bonded joints so they have fewer sources of energy dissipation.[1] Therefore although composite materials have more inherent damping than metals, composite structures

may have no more or even less damping than an equivalent metal structure. A comparison of the loss factors of various materials is shown in Figure 1-2.

The advantages of composites – in particular their high strength-to-weight ratio and tailorability – make them ideal for aircraft. Over the past thirty years composites have become standard design materials for both military and commercial aircraft. Initially boron/epoxy composites were used on the tail skins of the F-14 and F-15 fighter aircraft.[2] Currently composites make up approximately 24% by weight of the F-22 and cover the exterior of the B2 stealth bomber. Commercially, by the mid-1980's composites were used in more than 350 airline components.[3] The Airbus A380, which is set to go into service in March 2006, has an airframe that is 25% composite, the most of any commercial aircraft.[4] Figure 1-3 shows some examples of the percent composite material by weight of commercial and military aircraft.

One critical aircraft component is the turbine engine fan blade. A jet engine has two sets of turbine blades: the initial set compresses the air flowing through the engine and a second set in the exhaust stream. The second set experiences very high temperatures and therefore are not candidates for composites but there are several reasons composites would be well suited for the 1st stage compressor blades. Graphite/epoxy composite blades are significantly lighter (increasing the engine efficiency), tougher (more able to withstand object strikes), more durable, and quieter than titanium blades.[5,6] Most fan blades are still made with titanium although General Electric has graphite/epoxy fan blades in its GE90-115B engine, which powers the Boeing 777.[7] Clearly, damping turbine blades to reduce the vibrational stresses would

considerably increase the reliability and lifespan of the blade. In the mid 1990's J. Kosmatka, A. Lapid, and O. Mehmed conducted studies on the insertion of viscoelastic materials into the composite as a method of damping the blades; this testing was performed on flat and pretwisted plates.[8] G. Appuhn then continued the research by making fan blades, shown in Figure 1-4 at the NASA-Glenn Dynamic Spin Rig, with embedded viscoelastic damping material.

Figure 1-5 shows the various techniques used to increase the vibrational damping. There are two types of damping, inherent and additive. Inherent damping is derived from the properties of the composite, such as the resin or fibers. Additive damping, also known as integral damping, involves embedding damping materials into the composite. Additive damping can be added either by inserting damping layers between composite plies or by adding damping particles into the resin.

The purpose of this research was to explore various methods of vibrational damping of composite materials; several different approaches were used with the overall intention of improving the damping of composite fan blades. First, currently utilized embedded viscoelastic damping layers were improved. This had an immediate impact as they were embedded in the UCSD damped composite fan blades that were spin tested at NASA-Glenn.[5] The inability to predict or measure the shear modulus of the embedded damping materials led to the development of shear tests that could directly measure the shear modulus. This is essential for finite element modeling of fan blades and other applications. Concerns about embedding layers of low-modulus material in parts such as fan blades that experience high

loads prompted the exploration of adding particles to the samples with the intent of increasing damping without drastically lowering the bending and shear modulus.

Two other areas of research involve looking at tailorable damping materials. Sometimes only a certain mode needs damping - the chordwise mode is particularly problematic in the fan blades – and there are times when damping is not desirable, such as when the frequency is far from resonance. One tailorable damping method, directional damping material, damps each mode differently and thus the damping angle would be chosen for the specific structure. The other tailorable damping method explored uses electroviscoelastic materials (materials that change modulus and loss factor with an applied voltage) and are active dampers, meaning they could be turned on and off as needed. A potential application would be for fan blades during spin-up, when they experience stronger vibrations at different frequencies than they do once they reach operating speed.

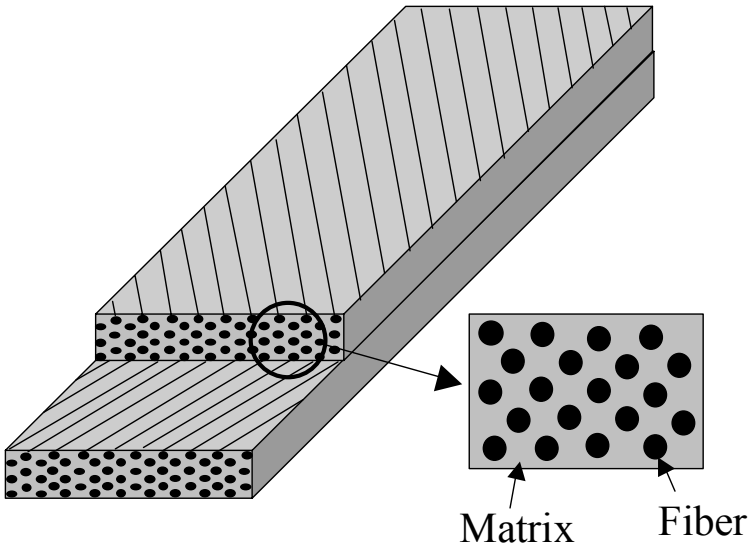

Figure 1-1. Composite plies with unidirectional fibers in a resin matrix.

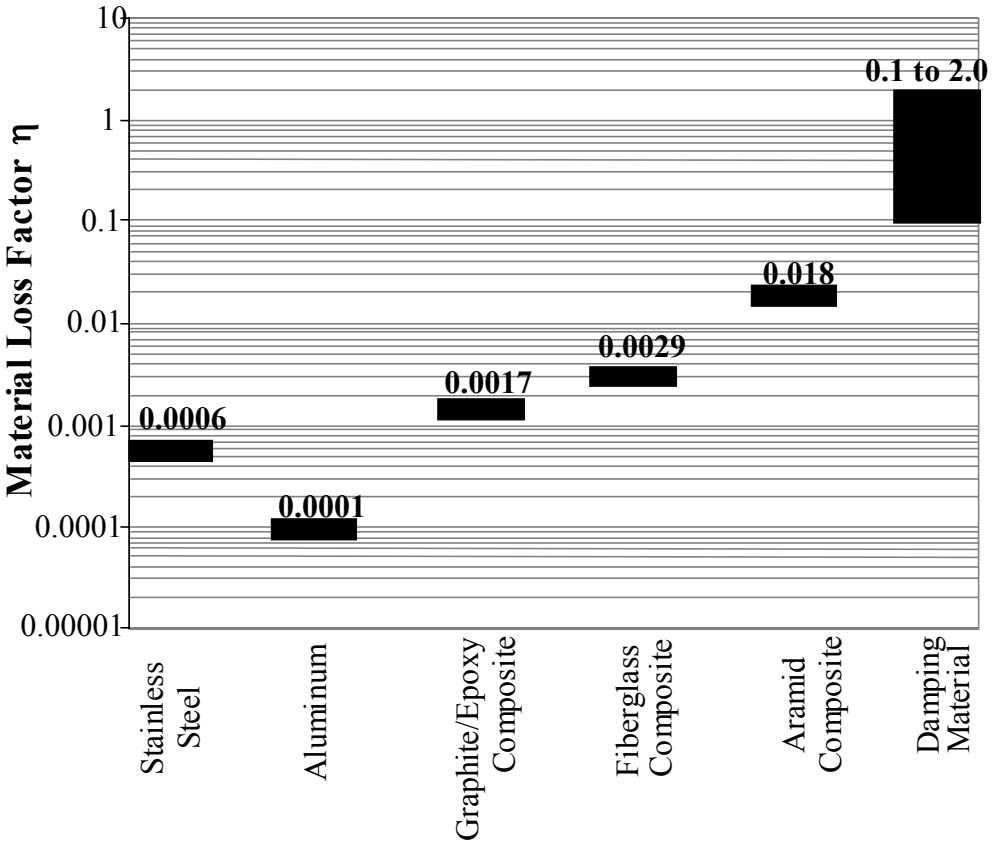

Figure 1-2. Loss factors of various materials in bending.

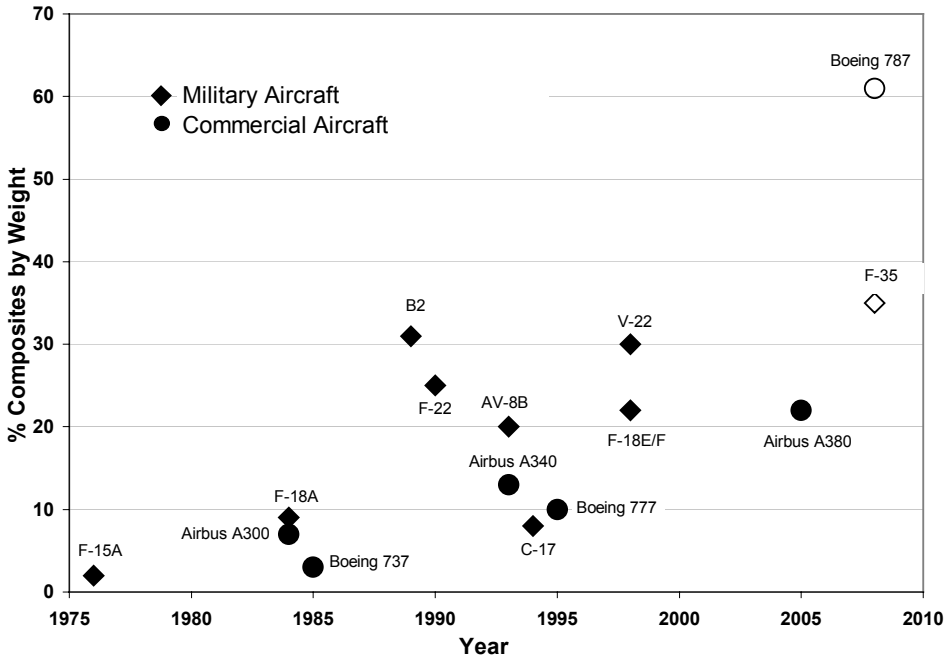

Figure 1-3. Composite weight percent of various aircraft.[2,4,9,10]

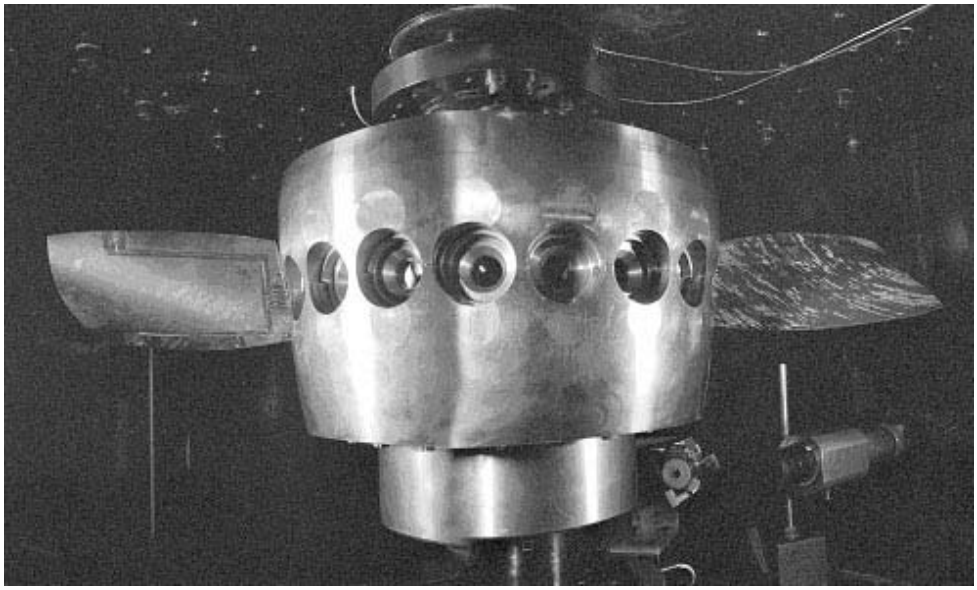

Figure 1-4. Dynamic Spin Rig at NASA Glenn ready to test two fan blades.[5]

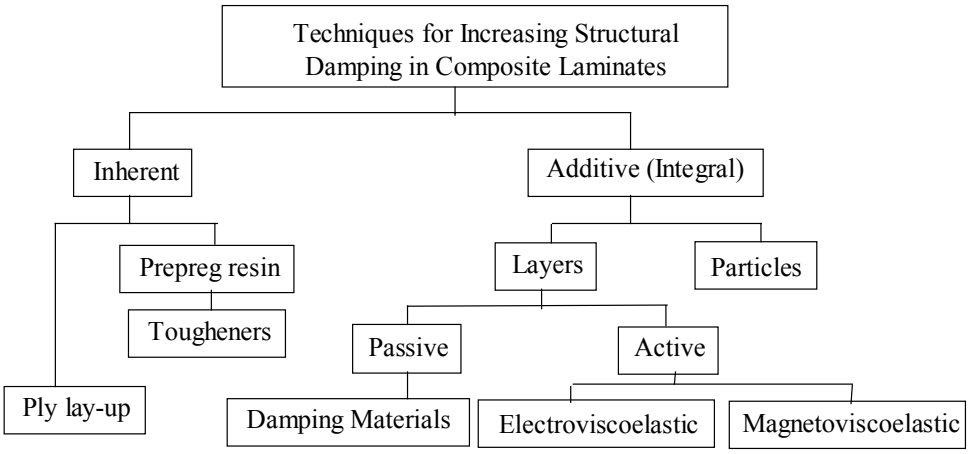

Figure 1-5. Flow chart of techniques used to increase structural damping in composite laminates.

1.1 Inherent Composite Damping

There are many factors that affect damping in composite materials, such as the matrix material, volume fractions, fiber orientation, fiber surface, fiber interaction, and fiber length and diameter.[11] The first choice a designer typically makes is what type of material to use. Figure 1-6 shows the damping of composites with three types of fiber and several resins.[12] The aramid composite has much more damping than either the fiberglass or graphite does because of inherent material properties. The aramid samples varied only slightly with resin type, fiber angle, and fabric vs. unidirectional fibers because the damping comes from the fiber, not the resin or friction from the fibers. The loss factors of the fabric fiber graphite and fiberglass samples, however, were much higher than the unidirectional fiber samples. This is because the damping is mainly a result of the resin and friction from fiber motion. Figure 1-7 demonstrates how varying the fiber volume fraction changes the loss factor. There is only a

substantial increase in loss factor below 30% fiber volume, which is too low for most applications.

Changing the fiber angle can significantly alter the damping of a composite laminate. Adams et. al. proposed a 2-D strain energy models that describes the damping mechanisms in unidirectional orthotropic composite materials as consisting of three different loss factors: longitudinal damping η_x, transverse damping η_y, and longitudinal shear damping η_{xy}.[13,14,15] The total damping is the sum of the three components. Each component behaves very differently over the orientation angles. In 1991 Hwang and Gibson used a 3-D strain energy model which determines that the damping mechanism consists of six stress components, only three of which are contributed significantly to the energy dissipation: longitudinal, transverse shear, and longitudinal shear.[16] Although the components are different from the Adams model the total damping is quite similar. Figure 1-8 and Figure 1-9 show what the 2-D and 3-D curves, respectively, look like for a carbon fiber/epoxy matrix composite.

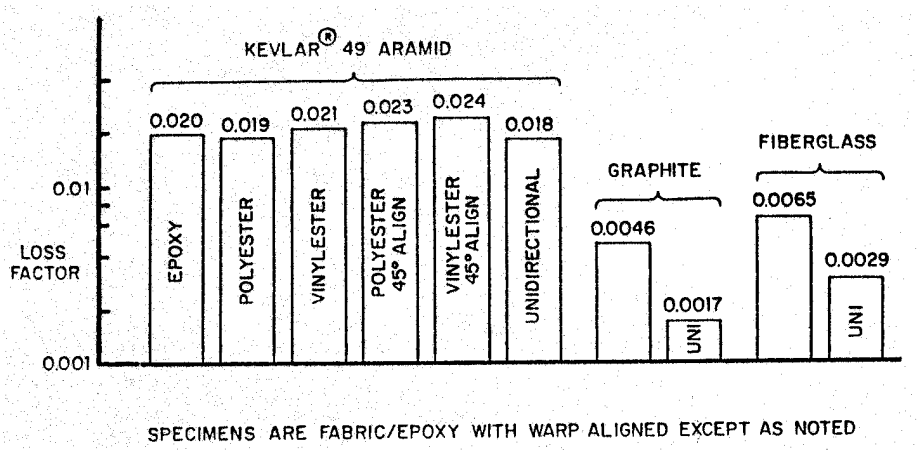

Figure 1-6. Damping of composites with various combinations of fiber and resin.[12]

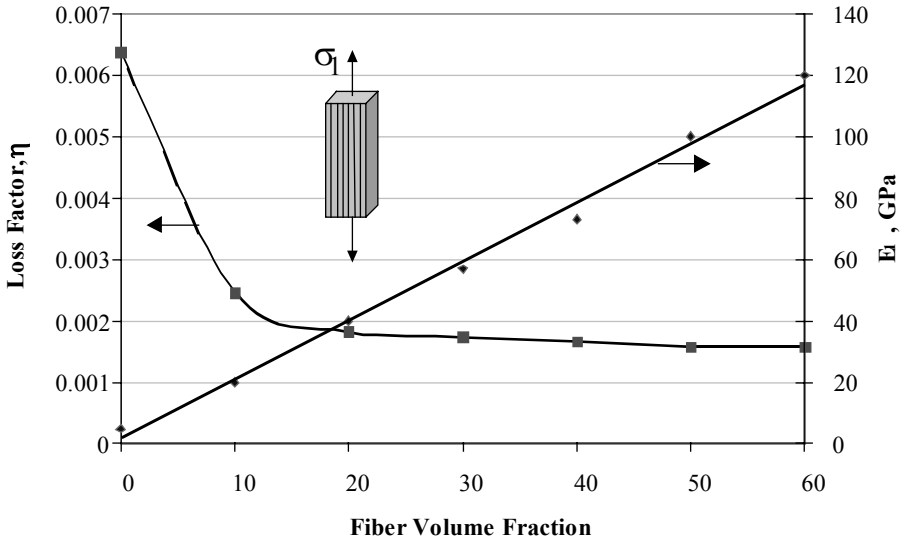

Figure 1-7 Loss Factor (η) and Modulus (E_1) of a composite sample with varied fiber volume fraction loaded along the fiber direction.[47]

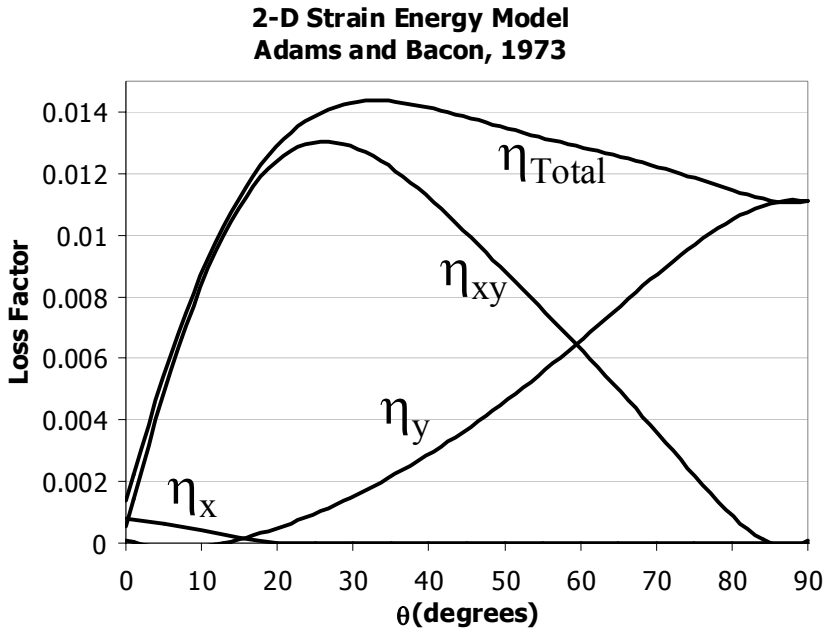

Figure 1-8. Components of damping for 2-D Strain Energy Model.[13]

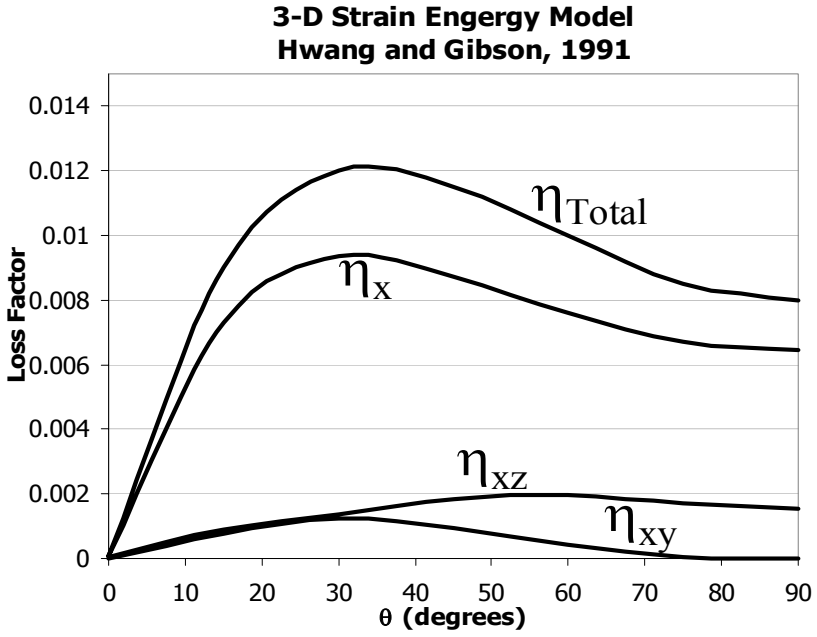

Figure 1-9. Components of damping for 3-D Strain Energy Model.[16]

1.2 Embedded Viscoelastic Damping Material Layers

One method of increasing damping in composite materials is to add damping material. Viscoelastic materials (VEMs) provide vibrational damping by dissipating strain energy in the form of thermal energy when sheared. Common damping materials include rubber blends, acrylics, nitrile phenolics, and polyurethanes; a list of some commercially available damping materials is shown in Table 1-1. Ideally, the optimal damping treatment is designed before the manufacturing process, but for an existing structure, add-on damping treatments such as constrained-layer damping must be used. Add-on treatments aren't usually as effective as embedded treatments. They also add more mass to the system than embedded treatments because the contraining layer only serves to increase the shear in the damping material and typically does not add to the structural integrity of the system. Considering that composites are often chosen because of their low strength-to-mass ratio, mass can be very critical. When the damping is optimized, the damping layer can be placed in the highest strain region for the vibrational mode or modes that need damping. Therefore less material is needed and greater damping can be achieved.

The choice of a damping material can also be a complicated process. The modulus and loss factor of VEMs vary tremendously with both temperature and frequency. Figure 2-4 and Figure 2-5 show the shear modulus and loss factor, respectively, of a very common damping material, 3M ISD112. The shear modulus varies from less than 2 psi to over 3000 psi and the loss factor varies from 0.000008 to

0.997. Each VEM has unique properties, so the designer must choose a damping material with the optimal properties for each structure.

In the late 1980's "cocuring" viscoelastic damping material in composite materials was proposed.[17] Cocuring refers to the process of inserting materials within composite laminates before the composite is cured, therefore the embedded materials undergo the temperature and pressure cycle that is necessary to cure the composite. There were numerous concerns about cocuring the viscoelastic damping materials in composites, such as would the damping material be degraded during the cure, would there be delaminations in the composites, would the damping material creep or squeeze out of the composite, etc. Specific tests were not performed to answer these questions, but in the 1990s numerous researchers have embedded VEM material in composites and have shown to be successful in greatly increasing the damping of composite structures.[19-31] Although no degradation was directly observed, a few of these papers also presented analytical predictions, and the damping is often not as high as predicted.[22,23,31] In 1996 Maly and Johnson demonstrated that cocuring viscoelastic damping materials changes the viscoelastic material properties and decreases the damping capabilities of most materials.[18] The reason for the change, however, was not explored.

Table 1-1. Common commercially available damping materials.

Manufacturer	Product	Type of material	Standard Thickness
3M	ISD 112	Acrylic adhesive	0.005”
	ISD 113	Acrylic adhesive	0.005”
	ISD 130	Acrylic adhesive	0.005”
	AF32	Nitrile phenolic adhesive	0.010”
Avery Dennison	FasTape 1125	Acrylic adhesive	0.005”
	FasTape 1182	Acrylic adhesive	0.002”
	FasTape 1191	Rubber/acrylic blend adhesive	0.011”
	FasTape 1158	Acrylic adhesive with embedded fibers	0.004”
EAR	CN-06	Thermoplastic alloy	Variable, must be hot-pressed to desired thickness
Soundcoat	Dyad 606	polyurethane	0.020”

1.3 Embedded Particles in Composite Resin

There are many concerns with embedding layers of viscoelastic damping material. The modulus of the damping material is typically several orders of magnitude less than that of the composite, so adding the damping material layer leaves a soft or low stiffness layer. If the damping material could instead be placed throughout the resin matrix, the overall modulus might be slightly decreased (assuming the amount of resin remains the same) but there wouldn’t be such an extreme discontinuity in modulus. Currently, rubber is commonly added to the matrix

to toughen the composite. When a crack is progressing through the composite, the elastic energy stored in the rubber during stretching is dissipated when the particles fail.[32] These particles wouldn't seem to work for damping, however, because 1) damping requires a non-elastic material and 2) no particle failure is expected. If the particles are not completely elastic, however, then some damping will occur. Also, if the particles are discreet, then there could be damping from the particle/matrix interface interaction.

Other researchers have added different particles to composites, such as thermoplastic powders and whiskers[33], carbon fiber filaments[34], and tin-zinc alloy particles[35]. The thermoplastic powders and whiskers were added for toughness and the damping properties were not investigated. The damping characteristics of the composites with both the carbon fiber filaments and the tin-zinc alloy particles were studied. The carbon fiber filaments increased the damping in the transverse modes but only slightly in the longitudinal modes. The tin-zinc particles increased the damping but of course added weight and so would be undesirable in most applications. Commercially, composite manufacturers and prepreggers such as Newport Composites and Fiberite offer composites with toughened epoxies. The damping of these composites has not been reported.

1.4 Electroviscoelasticity and Magnetoviscoelasticity

The ability to tailor damping response is very desirable. Structures such as space satellites see tremendous temperature shifts and there is no single damping material that has desirable damping characteristics throughout the entire range.

Currently several layers of damping material with differing properties must be applied to produce damping throughout the entire range. These structures are often very weight-critical, however, and adding extra layers of damping material is undesirable. Ideally one layer of damping material could be applied and its properties varied with the temperature and/or frequency of the structure.

The change in viscosity of fluids with particle suspensions when an electric field is applied is called an electrorheological (ER) response. The viscosity of ER fluids can increase several orders of magnitude when electric fields on the order of 1kV/mm are applied across them. The response takes less than 1 ms. The increase in viscosity is attributed to the energy required to disassociate the electric field induced structures.[36] This phenomena was first patented by Winslow in 1947.[37]

Magnetorheological (MR) fluids contain magnetizable particles, and, analogous to ER fluids, their viscosity changes with applied magnetic field. Several types of MR dampers are currently marketed.[38] One advantage MR fluids have over ER fluids is that MR fluids have a larger change in modulus for comparable power required. [39] A disadvantage is that MR dampers typically use iron particles, which have a high density and adds mass to the system.

Because the viscosity can be so readily changed, ER and MR fluids in dashpot-type dampers are useful in a variety of applications. Often, however, a self-supporting material is necessary. In 1990 Shiga et. al. suspended poly(methacrylic acid) cobalt(II) salt (PMACo) particles containing small amounts of adsorbed water in silicone polymer gels, making a electroviscoelastic material.[40] First, the particle

volume content necessary to see the electroviscoelastic effect was examined; Figure 1-10 shows that at least 30% particle volume fraction is needed to see a change in shear storage modulus with an applied field. Then it was demonstrated that by applying an electric field the modulus increased and loss factor curve changed. Figure 1-11 and Figure 1-12 show how the modulus and the loss tangent (or loss factor), respectively, change with an applied field and vary with the frequency of the applied shear strain.[41] The loss factor is especially interesting because at very low frequencies the sample with the applied electric field has a higher loss factor while at high frequencies the sample with no applied field has a higher loss factor. The frequencies range for many applications is higher than the 100 Hz. maximum frequency tested in this study. Other particles such as doped poly(p-phenylenes) were studied in subsequent papers with similar results.[42,43,44]

Magnetoviscoelastic gels have also been developed, mainly by the same researchers who developed electroviscoelastic gels, by embedding iron particles in silicone.[45] Figure 1-13 shows how the storage modulus changes with applied magnetic field and strain frequency. The process is demonstrated to be repeatable, as shown in Figure 1-14.

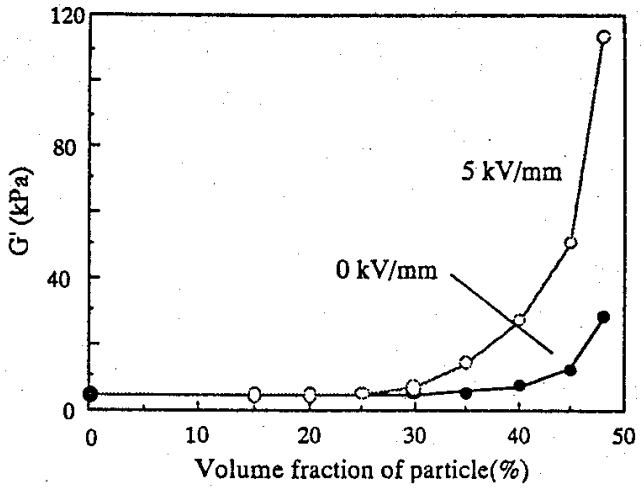

Figure 1-10. Effect of volume fraction of dispersed PMACo particles in a silicone gel on the shear storage modulus of the gel under an electric field.[44]

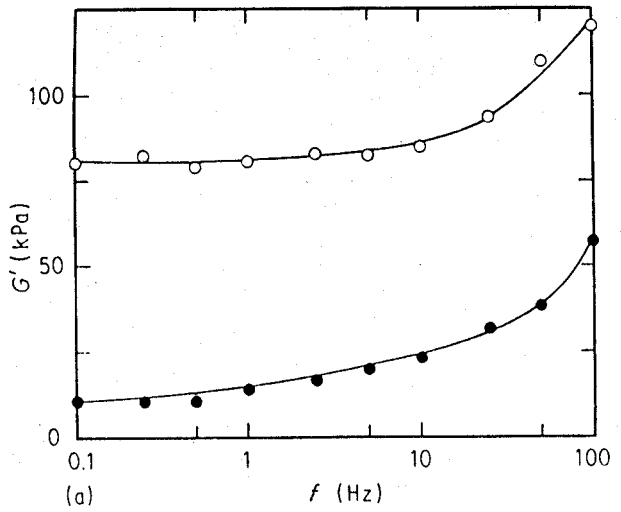

Figure 1-11. Shear storage modulus of a silicone gel with ER particles excited at a sinusoidally varying shear strain $\gamma = \gamma_o \sin 2\pi ft$ without an electric field (O) and with a 4kV/mm (•) applied field.[41]

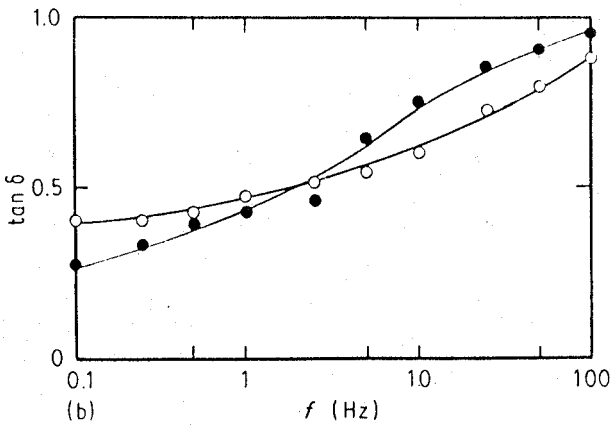

Figure 1-12. Loss tangent or loss factor of a silicone gel with ER particles excited at a sinusoidally varying shear strain $\gamma = \gamma_0 \sin 2\pi ft$ without an electric field (O) and with a 4kV/mm (•) applied field. [41]

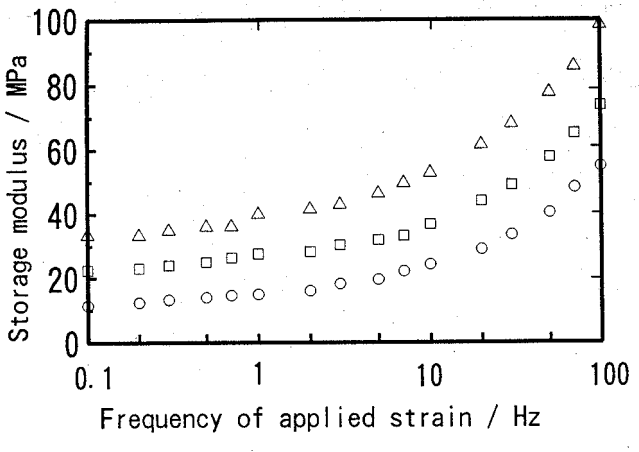

Figure 1-13. Storage shear modulus of silicone gel with iron particles with varied frequency of applied strain and various magnetic fields: (O) 0kA/m, (□) 43.2 kA/m, and (Δ) 59.2 kA/m.[45]

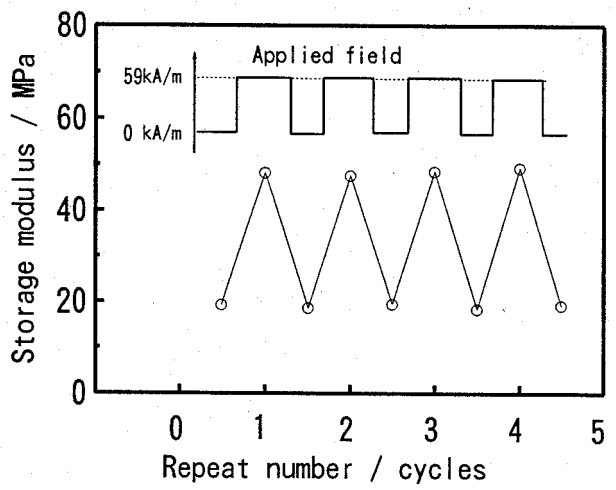

Figure 1-14. Repeatability of the magnetoviscoelastic effect for silicone gel with iron particles.[45]

1.5 Dissertation Outline

Chapter 2 provides the fundamental equations used for modeling and damping viscoelastic materials, which is used in the majority of this research. Sample manufacturing and testing methods are presented in Chapter 3.

Chapter 4 describes the testing on a variety of viscoelastic materials (VEMs) used for damping the composites. A cure temperature study was performed to determine whether variations in cure temperature affected the damping capabilities of common VEMs. Next tests were performed on VEMs that were cocured in the composite, meaning they were embedded in the composite before it was cured and then went through the cure cycle with the composite. It was shown that the epoxy infiltrated most of the VEMs and as a result lowered their damping capacity. A barrier layer was then developed to prevent the epoxy from infiltrating the VEM.

Traditional shear tests could not adequately test a cocured VEM so a method was developed after looking at variables such as sample manufacturing, test area, and strain rate. Chapter 5 describes the test and the results obtained, which included comparisons of VEMs, cocured vs. secondarily bonded VEMs, barrier layers, and VEMs with embedded mesh.

The desire to create a tailorable damping material where certain vibrational modes would be more damped than others led to the development of a directional damping material where the stiffness and damping properties vary with material orientation. Basic VEMs behave isotropically, meaning their stiffness and damping properties are the same in all directions. This research, described in Chapter 6, begins by creating a directional damping layer by cutting slots out of acrylic sheets at various angles and then sandwiching that layer between polycarbonate sheets. Isotropic materials were used so that the directionality of a composite would not interfere with the directionality of the damping layer. The stiffness and damping were measured for the bending, torsion, and chordwise modes of vibration.

Chapter 7 discusses the research of adding three types of toughening particles between the layers of graphite/epoxy prepreg. The damping and tensile and bending modulus of the samples with particles were compared to samples with layers of VEM or other additives such as a layer of epoxy.

Many applications need damping over a wide frequency and temperature range. No single damping materials have desirable damping characteristics throughout the entire range, and there are numerous applications where the damping is

not necessary or beneficial, such as when the vibrating frequency is far from a resonance frequency. The ability to tailor the damping response is highly desirable. Electroviscoelastic materials (EVEMs), discussed in Chapter 8, are materials that change properties such as stiffness and damping when a voltage is applied across the thickness. The goal of this research was to develop an EVEM that could be used to actively control vibrations by using a single EVEM layer.

Chapter 2 Damping Fundamentals

This chapter explains the methods for calculating and modeling damping and reviews the models for viscoelastic material.[46]

2.1 Complex Modulus and Damping Definitions for Viscoelastic Materials

The shear modulus (G) of an elastic material is defined as the shear stress (τ) as a function of time (t) divided by the shear strain (γ) as a function of time:

$$G = \frac{\tau(t)}{\gamma(t)} \tag{2-1}$$

The viscosity of a viscous material (μ) is defined as the shear stress divided by the strain rate ($\dot{\gamma}$):

$$\mu = \frac{\tau(t)}{\dot{\gamma}(t)} \tag{2-2}$$

If a sinusoidal shear stress

$$\tau(t) = \tau_o \sin \omega t \tag{2-3}$$

is applied to an elastic material at a frequency ω, the strain is in-phase with the stress:

$$\gamma(t) = \frac{\tau_o}{G} \sin \omega t \tag{2-4}$$

If the same sinusoidal stress is applied to a viscous material, the strain rate is defined as

$$\dot{\gamma}(t) = \frac{\tau(t)}{\mu} \tag{2-5}$$

From equation 2-5 it can be seen that the maximum strain rate occurs when the stress is a maximum and minimum when the stress is a minimum, or the strain rate is in-phase with the stress. The strain, however, is the integral of the strain rate and is therefore 90^o out of phase with the stress:

$$\gamma(t) = -\frac{\tau_o}{\mu\omega}\cos\omega t \tag{2-6}$$

Figure 2-1 shows the relationship of a sinusoidal load and the resulting strain on an elastic and viscoelastic body. Figure 2-2 shows the relationship if stress and strain vectors are used to describe the behavior. For a viscoelastic material, the stress and strain are out-of-phase by an angle δ^o. The angle δ^o is greater than 0^o (the angle for an elastic material) and less than 90^o (the angle for a viscous material).

To show how the modulus is composed of an in-phase and an out-of-phase component, a complex moduli nomenclature is typically used. The out-of-phase portion of the vector, whether it's stress, strain, or modulus, is multiplied by the imaginary number *i* so it is represented in the imaginary plane. Therefore for an applied stress, τ, the measured strain γ^* is the combination of the in-phase and out-of-phase portions:

$$\gamma^* = \gamma' + i\gamma'' \tag{2-7}$$

Figure 2-3 shows how the strain vector is decomposed in the complex plane.

The complex modulus G* is then defined as

$$G^* = G' + iG'' \tag{2-8}$$

where G' is the in-phase portion of the modulus, also called the storage modulus, and G" is the out-of-phase portion, also called the loss modulus. The in-phase and out-of-phase components of the shear modulus, G' and G", respectively, are defined as

$$G' = \frac{\tau'}{\gamma} \quad \text{and} \quad G'' = \frac{\tau''}{\gamma} = G'\eta \tag{2-9}$$

where γ is the applied strain and η is the loss modulus, which is defined as

$$\eta = \tan\delta = \frac{\tau''}{\tau'} = \frac{\gamma''}{\gamma'} = \frac{G''}{G'} \tag{2-10}$$

If the angle is 0^o (the response is in-phase with the applied force, as for an elastic material) then the loss factor is zero. If the angle is 90^o (the response is out-of-phase with the applied force, as for a viscous material) then the loss factor is equal to infinity.

Similarly, Young's modulus (E) and Poisson's ration (υ) are also represented in the imaginary plane. Young's modulus is defined as the longitudinal stress (σ) divided by the longitudinal strain (δ):

$$E = \frac{\sigma(t)}{\delta(t)} \tag{2-11}$$

Poisson's ratio (υ) is defined as the strain in the transverse direction, $\varepsilon_{transverse}$, divided by the strain in the longitudinal direction, $\varepsilon_{longitudinal}$, when there is an displacement in the longitudinal direction:

$$\upsilon = -\frac{\varepsilon_{transverse}}{\varepsilon_{longitudinal}} \tag{2-12}$$

The minus sign is so that most materials have a positive Poisson's ratio. Both Young's modulus and Poisson's ratio can be defined using the same complex nomenclature as the shear modulus:

$$E^* = E' + iE'' \tag{2-13}$$

$$\upsilon^* = \upsilon' + i\upsilon'' \tag{2-14}$$

In practice, however, Poison's ratio is rarely expressed in the complex form.

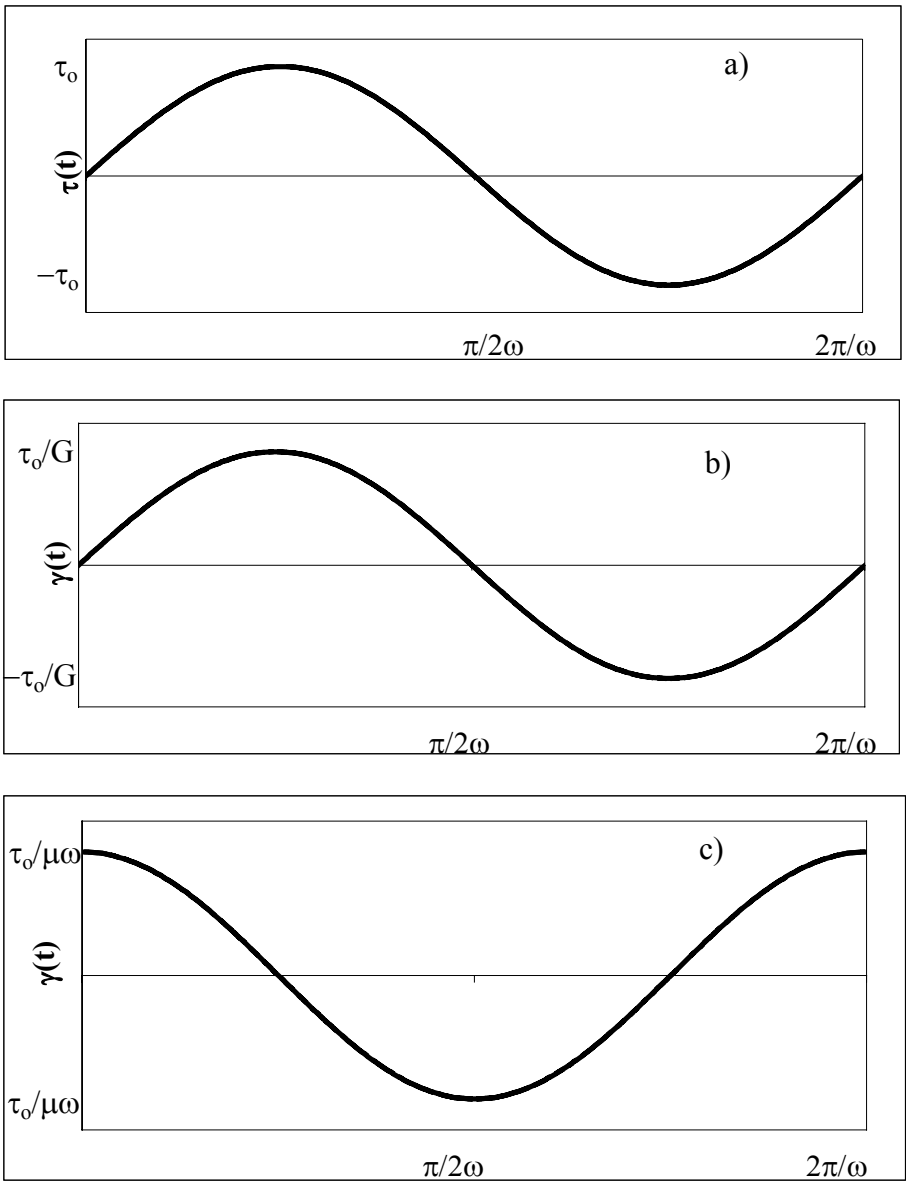

Figure 2-1. Demonstration of a) sinusoidal load applied to a material, b) the resulting strain on an elastic body, and c) the resulting strain on a viscous body.

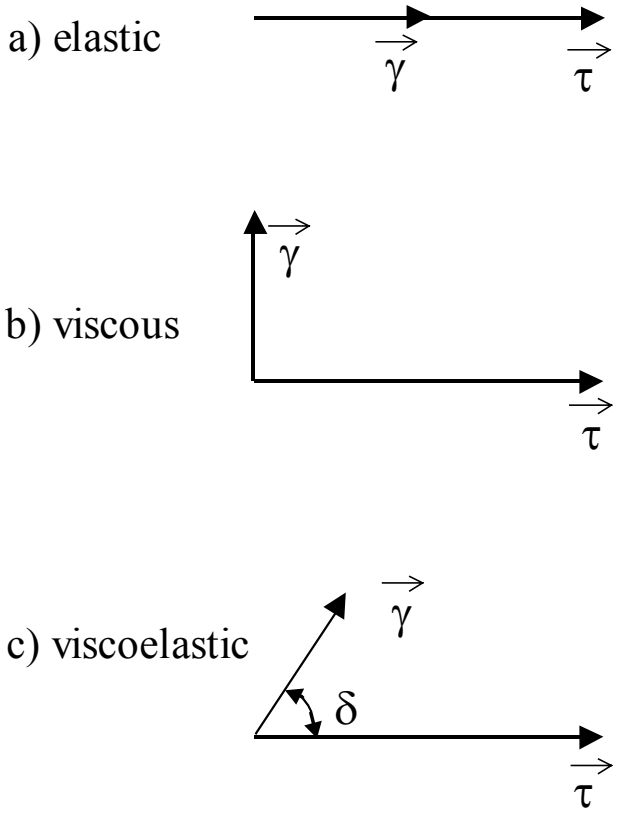

Figure 2-2. Stress and strain vectors for a) an elastic material (stress and strain are in-phase), b) a viscous material (stress and strain are 90^o out-of-phase), and c) a viscoelastic material (stress and strain are δ^o out-of-phase).

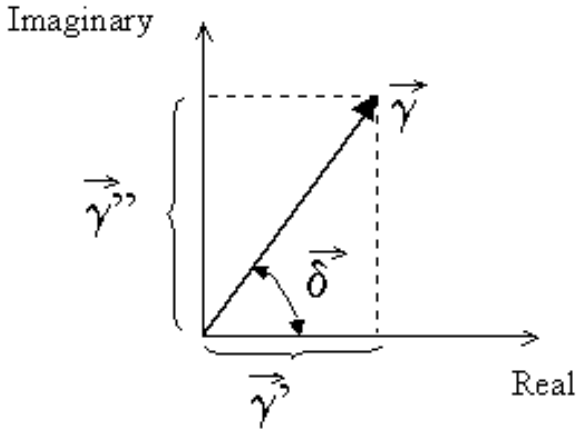

Figure 2-3. The strain vector γ decomposed into real (γ') and imaginary (γ") portions.

2.2 Viscoelastic Material Modeling

It is very difficult to model or even curvefit the behavior of viscoelastic material properties because they are highly dependent on temperature and frequency.[3-8] A simple way of describing the viscoelastic materials is to think of them as polymer chains. At high temperatures the materials have a low modulus because the chains are "soft" and can easily move past one another. At low temperatures the materials have a higher modulus because the chains are more rigid. Similarly, at low frequencies the chains have time to move past each other and therefore the material has a low modulus; at high frequencies the chains don't have time to move and thus the material has a higher modulus. The maximum loss factor tends to occur at the frequency and temperature ranges that are at the shear modulus "transition region", which is the region where the modulus is rapidly changing. Figure 2-4 and Figure 2-5 show how the shear modulus and loss factor of a typical damping material, 3M ISD 112, vary with temperature and frequency. The behavior changes tremendously over a large temperature and frequency range so the behavior is plotted on a $\log_{10}$ scale. The gray area emphasizes the frequency range that is most typically used in engineering applications. This material is chosen because its loss factor is a maximum within this frequency range.

The simplest mechanical models that can simulate viscoelastic material behavior are composed of springs and dashpots. The shear stress in an elastic spring is linearly proportional to the shear strain

$$\tau(t) = G\gamma(t) \tag{2-15}$$

where τ is the shear stress, γ is the shear strain, and G is the shear modulus. Here G could also be expressed as G' because the stress and strain are completely in-phase. The shear stress in a viscous dashpot is linearly proportional to the shear strain rate:

$$\tau(t) = \mu\dot{\gamma}(t) \tag{2-16}$$

where μ is the shear viscosity, and $\dot{\gamma}$ is the shear strain rate. Viscoelastic materials are neither proportional to strain or strain rate; they are somewhere in-between. A combination of the two equations is called the generalized standard viscoelastic model:

$$\tau(t) = G\gamma(t) + \mu\dot{\gamma}(t) \tag{2-17}$$

This can be represented by a spring and dashpot in parallel, which is called a Kelvin-Voigt model, shown in Figure 2-6 a). If the two elements were in series, as shown in Figure 2-6 b), then the shear stress would be the same in each element:

$$\tau(t) = G\gamma_1(t) = \mu\dot{\gamma}_2(t) \tag{2-18}$$

where γ_1 is the strain in the spring and $\dot{\gamma}_2$ is the strain rate in the dashpot. The total strain is equal to the sum of the strains and the constitutive relation can be calculated as:

$$\tau(t) + (\mu / G)\dot{\tau}(t) = \mu\dot{\gamma}(t) \tag{2-19}$$

This is called a Maxwell model. Neither the Kelvin-Voigt nor the Maxwell unit sufficiently model viscoelastic materials. When combined, however, the models do a better job of modeling some viscoelastic materials but only in particular frequency

ranges. Typical three-parameter models are shown in Figure 2-7. The constitutive relation for both three parameter models has the same form:

$$\tau(t) + A(\dot{\tau}(t)) = B(\gamma(t)) + C(\dot{\gamma}(t)) \tag{2-20}$$

where A, B, and C are terms made up of shear modulus (G) and viscosity (μ) terms but are typically just curvefit from experimental data. For the three parameter Kelvin-Voight model A, B, and C are equal to

$$A = \frac{\mu}{G_1 + G_2}, \quad B = \frac{G_1 G_2}{G_1 + G_2}, \text{ and } \quad C = \frac{\mu G_2}{G_1 + G_2} \tag{2-21}$$

and for the Maxwell model A, B, and C are equal to

$$A = \frac{\mu}{G_2}, \quad B = G_1, \text{ and } \quad C = \mu + \frac{\mu G_1}{G_2} \tag{2-22}$$

where G_1, G_2, and μ are defined in Figure 2-7. When additional springs and dashpots are added the terms A, B, and C become more complex. When generalized to include more parameters, the constitutive relation becomes:

$$\tau(t) + \sum_{i=1}^{q} A_i \left(\frac{\partial^i \tau(t)}{\partial t^i}\right) = B(\gamma(t)) + \sum_{j=1}^{q} C_j \left(\frac{\partial^j \gamma(t)}{\partial t^j}\right) \tag{2-23}$$

This equation does a better job of fitting the data but quickly becomes very large.

The shear modulus of the material is written as $\overline{G}$; the shear modulus of the three parameter model (Equation 2-20) can easily calculated in the Laplace domain. Once converted to the frequency domain the shear modulus is

$$\overline{G}(i\omega) = \frac{\overline{\tau}(i\omega)}{\overline{\gamma}(i\omega)} = \frac{B + (i\omega)C}{1 + (i\omega)A} \tag{2-24}$$

By simply multiplying the numerator and denomenator of $\overline{G}$ by the complex conjugate of the denomenator, $\overline{G}$ can divided into its real and imaginary parts:

$$\overline{G}(i\omega) = \frac{B + (i\omega)C}{1 + (i\omega)A} * \frac{1 - (i\omega)A}{1 - (i\omega)A} = \frac{B + AC\omega^2}{1 + A^2\omega^2} + i\frac{\omega(C - AB)}{1 + A^2\omega^2} \tag{2-25}$$

where the storage modulus is equal to the first term

$$G'(i\omega) = \frac{B + AC\omega^2}{1 + A^2\omega^2} \tag{2-26}$$

the second term is the loss modulus

$$G''(i\omega) = \frac{\omega(C - AB)}{1 + A^2\omega^2}. \tag{2-27}$$

and the loss factor is the loss modulus divided by the shear modulus

$$\eta = \frac{G''}{G'} = \frac{\omega(C - AB)}{B + AC\omega^2} \tag{2-28}$$

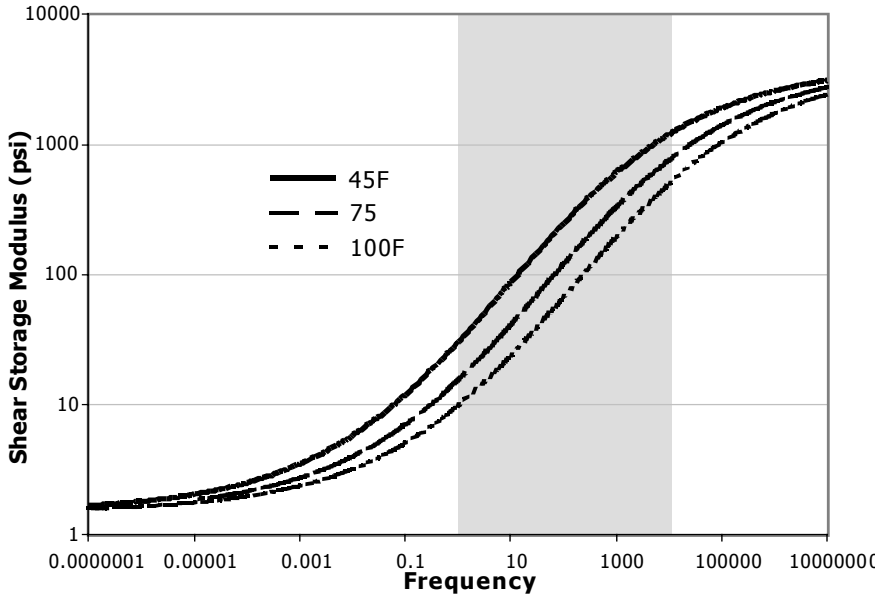

Figure 2-4. Shear Modulus of 3M ISD 112 viscoelastic damping material at varying temperatures. The shaded area represents the typical useful frequency range.

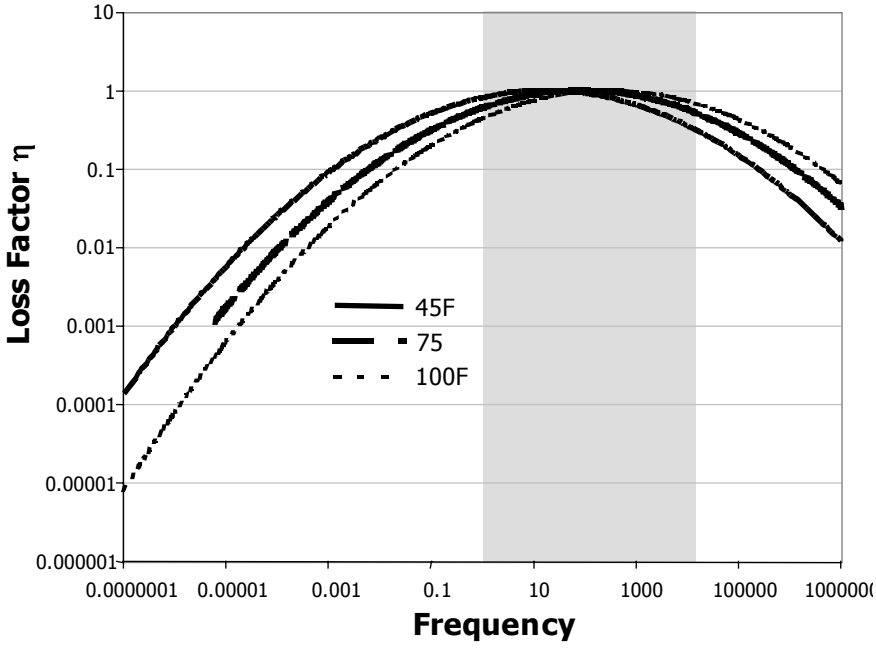

Figure 2-5. Loss Factor of 3M ISD 112 viscoelastic damping material at varying temperatures. The shaded area represents the typical useful frequency range.

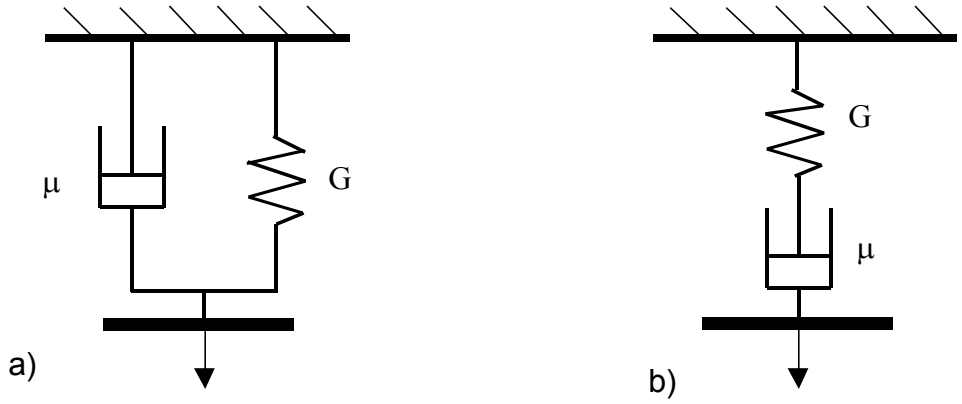

Figure 2-6. Two parameter material models: a) Kelvin-Voigt Model, b) Maxwell Model.

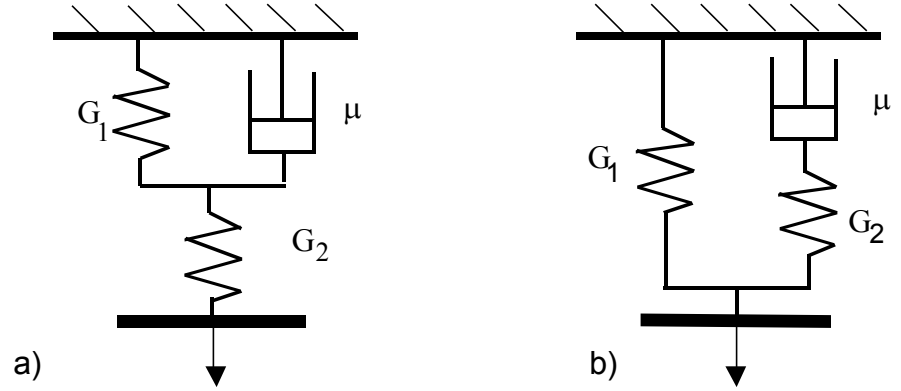

Figure 2-7. Three parameter material models: a) three parameter Kelvin-Voigt Model, and b)three parameter Maxwell Model.

2.2.1 Fractional Derivatives and Four Parameter Model

Another way to define viscoelastic material properties would be to say that they are proportional to a factor that is between the strain and the strain rate. [9-14] This model assumes the stress is proportional to a fractional derivative of the strain,

$$\tau(t) = G' \frac{d^{\alpha} \gamma_{(t)}}{dt^{\alpha}} \tag{2-29}$$

also expressed as

$$\tau(t) = G' D^{\alpha} \gamma_{(t)} \tag{2-30}$$

If $\alpha = 0$, then G' = G and the equation becomes the linear elastic spring equation. If $\alpha = 1$, the G' = μ and the equation becomes the linear viscous dashpot equation. Therefore for the viscoelastic case α should be between 0 and 1. The fractional derivative equation alone cannot represent viscoelastic material behavior, but when used in a three parameter model it greatly increases the modeling capability. The generalized fractional derivative model is simply the generalized standard model with fractional derivatives rather than integer derivatives:

$$\tau(t) + \sum_{i=1}^{q} A_i (D^{\alpha_i} \tau(t)) = B(\gamma(t)) + \sum_{j=1}^{p} C_j (D^{\beta_j} \gamma(t)) \tag{2-31}$$

where α and β are between 0 and 1. The generalized fractional derivative equation does a much better job of curvefitting the data than the generalized standard model. By curvefitting experimental data it is seen that typically $\alpha \cong \beta$. The model with the least number of variables that provides the best curvefit is the three parameter Maxwell Model in which the dashpot is replaced with a fractional derivative element. This model is called the Four-parameter model. Here, $\alpha \cong \beta$ and p and q are equal to one in the generalized fractional derivative equation. The constitutive relation describing this model is:

$$\tau(t) + A(D^{\alpha}\tau(t)) = B(\gamma(t)) + C(D^{\alpha}\gamma(t)) \tag{2-32}$$

The shear modulus of the material is written as $\overline{G}$ and is defined as the stress divided by the shear strain. In the frequency domain (after conversion from the Laplace domain), the stress is:

$$\overline{G}(i\omega) = \frac{\overline{\tau}(i\omega)}{\overline{\gamma}(i\omega)} = \frac{B + (i\omega)^{\alpha} C}{1 + (i\omega)^{\alpha} A} \tag{2-33}$$

There are several steps required to get the real and imaginary parts of the storage modulus. First, both the numerator and denominator are multiplied by the conjugate of the denominator. Because *i* is raised to a fractional power, the conjugate is not the typical 1-$(i\omega)^{\alpha}$A, which it would be if α were an integer. To find the conjugate, the fractional power must be cleared by using the mathematical identity:

$$i^{\alpha} = \cos(\tfrac{\alpha\pi}{2}) + i\sin(\tfrac{\alpha\pi}{2}) \tag{2-34}$$

to get:

$$\overline{G}(i\omega) = \frac{B + C\omega^{\alpha}[\cos(\tfrac{\alpha\pi}{2}) + i\sin(\tfrac{\alpha\pi}{2})]}{1 + A\omega^{\alpha}[\cos(\tfrac{\alpha\pi}{2}) + i\sin(\tfrac{\alpha\pi}{2})]} \tag{2-35}$$

which can be rearranged to separate the real and imaginary sections of the numerator and denominator and then multiplied by the complex conjugate:

$$\overline{G}(i\omega) = \frac{[B + C\omega^{\alpha}\cos(\tfrac{\alpha\pi}{2})] + iC\omega^{\alpha}\sin(\tfrac{\alpha\pi}{2})}{[1 + A\omega^{\alpha}\cos(\tfrac{\alpha\pi}{2})] + iA\omega^{\alpha}\sin(\tfrac{\alpha\pi}{2})} \bullet \frac{[1 + A\omega^{\alpha}\cos(\tfrac{\alpha\pi}{2})] - iA\omega^{\alpha}\sin(\tfrac{\alpha\pi}{2})}{[1 + A\omega^{\alpha}\cos(\tfrac{\alpha\pi}{2})] - iA\omega^{\alpha}\sin(\tfrac{\alpha\pi}{2})} \tag{2-36}$$

Once multiplied through, equation (2-36) becomes:

$$\overline{G}(i\omega) = \frac{B + (BA + C)\omega^{\alpha} \cos(\frac{\alpha\pi}{2}) + C\omega^{\alpha} A + i(C - BA)\omega^{\alpha} \sin(\frac{\alpha\pi}{2})}{1 + 2A\omega^{\alpha} \cos(\frac{\alpha\pi}{2}) + A^2\omega^{2\alpha}} \quad (2\text{-}37)$$

The storage modulus is the real part of equation (2-37):

$$G' = \mathrm{Re}[\overline{G}(i\omega)] = \frac{B + (BA + C)\omega^{\alpha} \cos(\frac{\alpha\pi}{2}) + C\omega^{2\alpha} A}{1 + 2A\omega^{\alpha} \cos(\frac{\alpha\pi}{2}) + A^2\omega^{2\alpha}} \quad (2\text{-}38)$$

and the loss modulus is the imaginary part of equation (2-37):

$$G'' = \mathrm{Im}[\overline{G}(i\omega)] = \frac{(C - BA)\omega^{\alpha} \sin(\frac{\alpha\pi}{2})}{1 + 2A\omega^{\alpha} \cos(\frac{\alpha\pi}{2}) + A^2\omega^{2\alpha}} \quad (2\text{-}39)$$

The loss factor is the imaginary divided by the real, or the loss modulus divided by the storage modulus:

$$\eta = \frac{\mathrm{Im}[\overline{G}(i\omega)]}{\mathrm{Re}[\overline{G}(i\omega)]} = \frac{(C - BA)\omega^{\alpha} \sin(\frac{\alpha\pi}{2})}{B + (BA + C)\omega^{\alpha} \cos(\frac{\alpha\pi}{2}) + C\omega^{2\alpha} A} \quad (2\text{-}40)$$

From looking at curvefit data the physical meaning of the unknowns is determined:

$$B = G_e \quad (2\text{-}41)$$

where G_e is the equilibrium modulus (or the storage modulus when $\omega \cong 0$). When the glassy modulus is much greater than one, the α term can be approximated by

$$\alpha = \frac{2}{\pi} \tan^{-1}(\eta_{\max}) \qquad \text{for four-parameter model} \quad (2\text{-}42)$$

$$\alpha = 1 \qquad \text{for three-parameter model} \quad (2\text{-}43)$$

where η_{max} is the maximum loss factor. The next term, A, can be obtained by taking the derivative of the loss factor with respect to frequency and setting it equal to zero for maximum loss factor

$$A = \sqrt{\frac{G_e}{G_g}} \frac{1}{(2\pi f_{\eta\max})^{\alpha}} \tag{2-44}$$

where G_g is the glassy modulus (or the storage modulus when $\omega \to \infty$) and $f_{\eta max}$ is the frequency at which the maximum loss factor occurs. Finally, C is calculated by equating G_g to G' at infinite frequency

$$C = AG_g \tag{2-45}$$

The values are demonstrated in Figure 2-8, which shows how the shear modulus and loss factor vary with frequency. Figure 2-9 and Figure 2-10 show how the three and four parameter model calculated storage moduli and loss factors compare with experimental data.

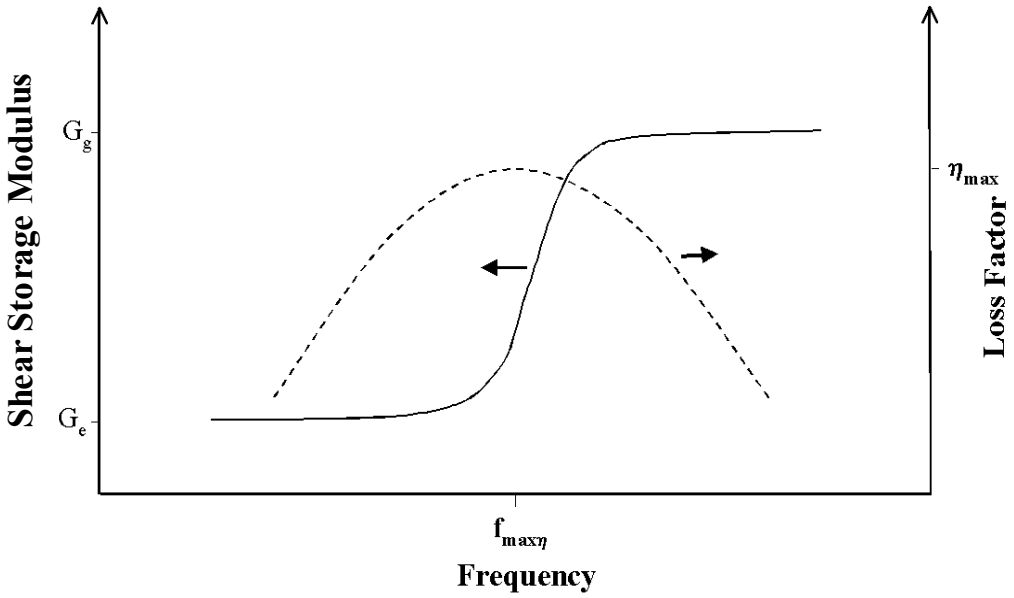

Figure 2-8. Shear modulus and loss factor variation with frequency for a typical viscoelastic material.

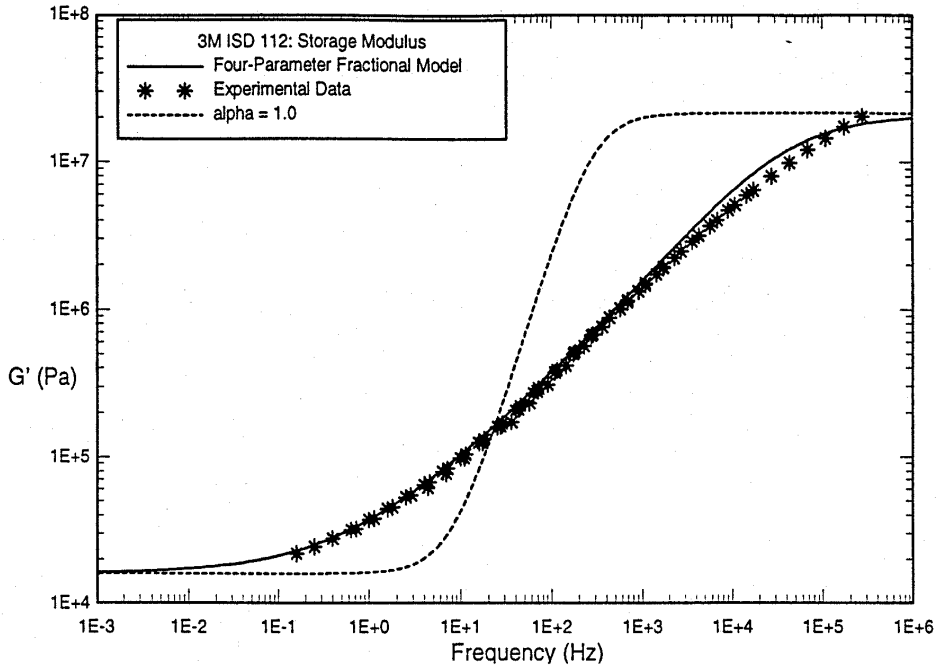

Figure 2-9. Storage modulus for 3M ISD 112 viscoelastic damping material. The experimental data provided by 3M is plotted along with the storage modulus of the three parameter model (labeled as alpha = 1) and four parameter model which uses fractional derivatives.[51]

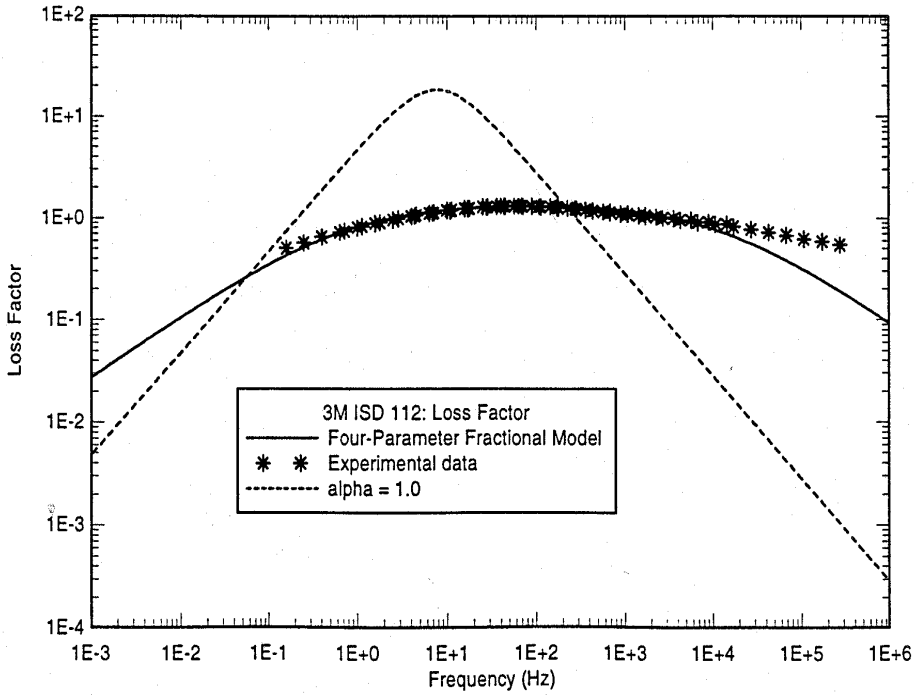

Figure 2-10. Loss factor for 3M ISD 112 viscoelastic damping material. The experimental data provided by 3M is plotted along with the storage modulus of the three parameter model (labeled as alpha = 1) and four parameter model which uses fractional derivatives.[51]

2.2.2 GHM Model and Anelastic Displacement Fields

There are two other models that describe viscoelastic behavior: the Golla-Hughes-McTavish (GHM) model and the Anelastic Displacement Fields (ADF) model.[58,59] The GHM model uses a series of mini-oscillators, shown in Figure 2-11, which are repeated 2 to 5 times. The material complex modulus is given, in the Laplace domain, as:

$$G^*(s) = G_r(1+h(s)) = G_r\left[1+\sum_{j=1}^{n}\hat{\alpha}_j\frac{s^2+2\hat{\zeta}\hat{\omega}_j s}{s^2+2\hat{\zeta}\hat{\omega}_j s+\hat{\omega}_j{}^2}\right] \tag{2-46}$$

where $\hat{\alpha}_j, \hat{\omega}_j$, and $\hat{\varsigma}_j$ are constants obtained by curve-fitting; each repeating unit therefore has three unknowns. Figure 2-12 shows how the GHM loss modulus fit compares to the four parameter fractional derivative model and experimental values of 3M ISD 112.

The ADF model assumes the total displacement field consists of two parts, the elastic and the anelastic:

$$u(x,t) = u^E(x,t) + u^A(x,t) \tag{2-47}$$

where u^E is the elastic displacement and u^A is the anelastic displacement. Figure 2-13 shows a diagram of the ADF model. The material complex modulus in the frequency domain, G*, is given as:

$$G^* = G_r\left(1 + \sum_{n=1}^{N} \Delta_n \frac{(\omega/\Omega_n)^2}{1+(\omega/\Omega_n)^2}\right) + iG_r\left(\sum_{n=1}^{N} \Delta_n \frac{(\omega/\Omega_n)^2}{1+(\omega/\Omega_n)^2}\right) \tag{2-48}$$

where G_r is the static or equilibrium modulus, Ω_n is the inverse of the relaxation time constant, and Δ_n is the relaxation magnitude, and N is the number of anelastic displacement fields. Figure 2-14 and Figure 2-15 show how the ADF fits experimental modulus and loss factor data for one and three displacement fields, respectively. Three displacement fields give a nice curve-fit but requires the determination of seven unknowns: G_r, Ω_1, Ω_2, Ω_3, Δ_1, Δ_2, and Δ_3.

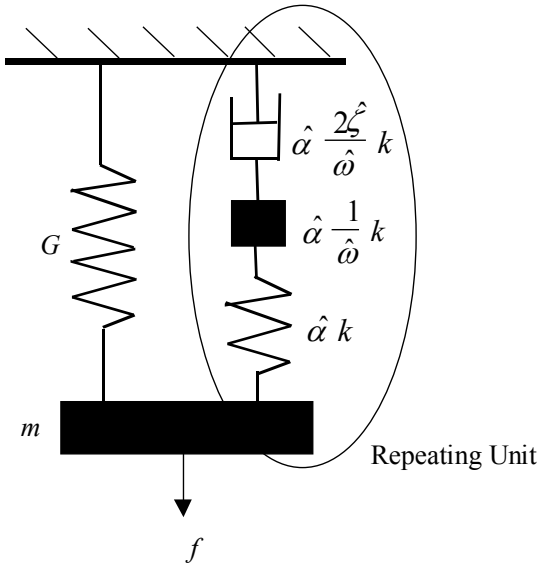

Figure 2-11. GHM material model.[58]

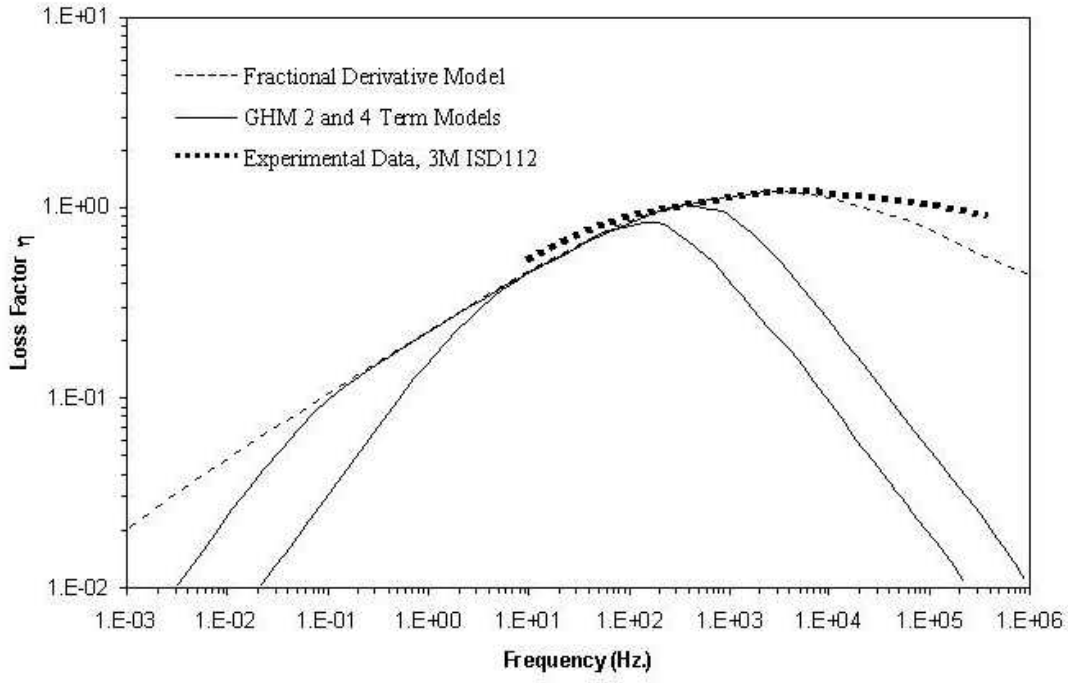

Figure 2-12. Two and four GHM mini-oscillator term fits of loss factor as compared to the four parameter fractional derivative model and 3M ISD 112 experimental data.[58]

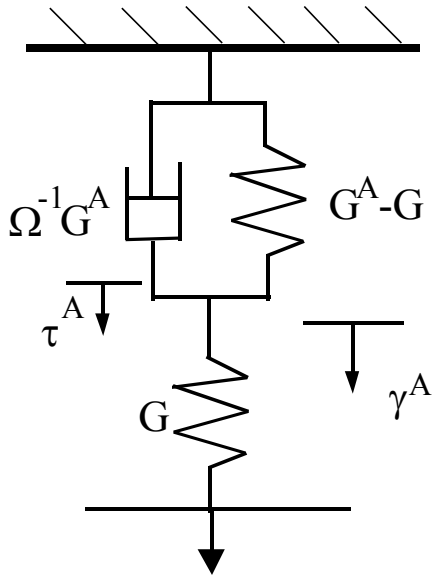

Figure 2-13. Anelastic Displacement Field (ADF) diagram. [59]

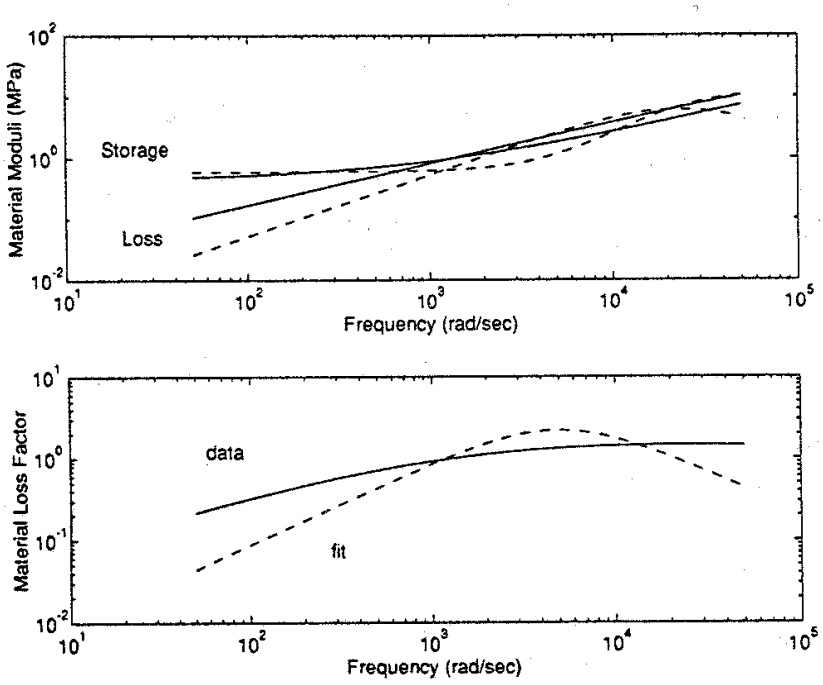

Figure 2-14. One ADF storage and loss modulus and loss factor fit of 3M ISD 112 viscoelastic damping material data. The solid lines are the experimental data and the dashed lines are the curvefits. [59]

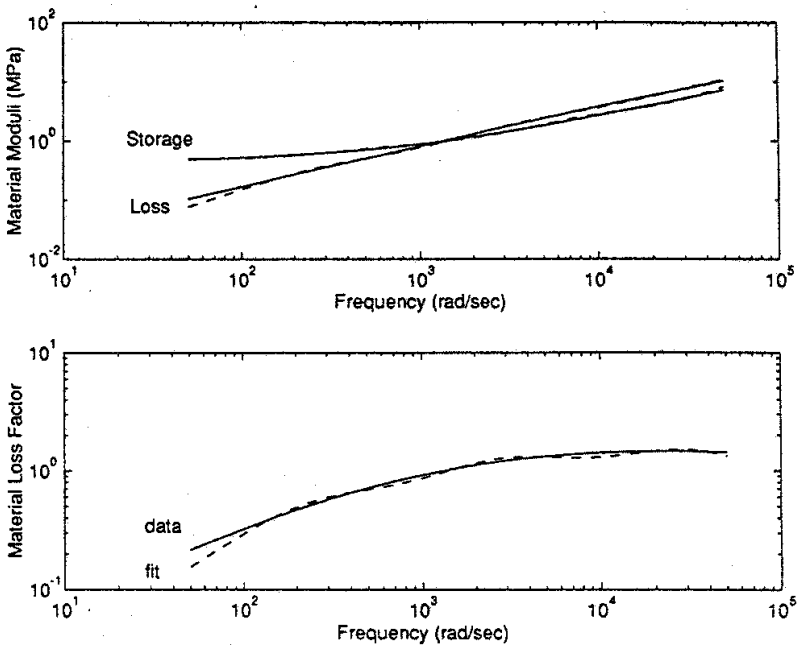

Figure 2-15. Three ADF storage and loss modulus and loss factor fit of 3M ISD 112 viscoelastic damping material data. [59]

2.2.3 Temperature Effects

The properties of a material, such as modulus (both shear and Young's) and loss factor, vary not only with frequency but also with temperature; often the variation can be several orders of magnitude with a relatively small temperature change. This large effect on properties necessitates the inclusion of temperature in viscoelastic models. Figures Figure 2-4 and Figure 2-5 show how these properties shift as the temperature changes for 3M ISD-112.

Often, experimental data cannot be collected over a sufficiently large frequency range. Data that has been collected over a certain frequency range at varying temperatures can be shifted to determine the properties over a wider frequency range. Figure 2-16 a) shows an example of how the modulus and loss

factor could change with temperature. Figure 2-16 b) shows how the curves can be shifted so that data is plotted over a wider frequency range. The temperature at which this curve is accurate is the reference temperature T_o; in this example T2 is equal to T_o. The property curves at any other temperature will simply be shifted left or right, depending on whether the temperature goes up or down; this phenomenon is called the temperature-frequency superposition principle.

A common way of describing the material behavior is by plotting the modulus and loss factor versus a reduced frequency ω_r, which can be defined as

$$\omega_r = \omega * \alpha_T(T) \tag{2-49}$$

where ω is the frequency and α_T is the temperature shift function, which is a relation to the reference temperature. If the temperature is T_o, then α_T will be equal to one and ω_r will equal ω. Figure 2-17 shows an experimental values plot of the shift factor vs. temperature for a common viscoelastic damping material, 3M ISD 112. To be able to include the shift factor into an equation for modulus or loss factor the data must be curve fitted. The basis of the most of the equations used to describe the α_T vs. temperature curve is the Williams-Landell-Ferry (WLF) equation, which was originally developed for the viscosity of polymers

$$\log \alpha_T = \frac{-C_1(T - T_o)}{C_2 + T - T_o} \tag{2-50}$$

where C_1 and C_2 are constants determined by curvefitting, T_o is the chosen reference temperature, and T is the temperature at which α_T is determined.[60,61] James Eichenlaub and Lynn Rogers expanded on the WLF equation to improve the α_T curvefit[62]:

$$\log \alpha_T = \frac{-\frac{1000 C_1 C_2}{T_o^{\,2}}(T - T_o)}{C_2 + T - T_o} \tag{2-51}$$

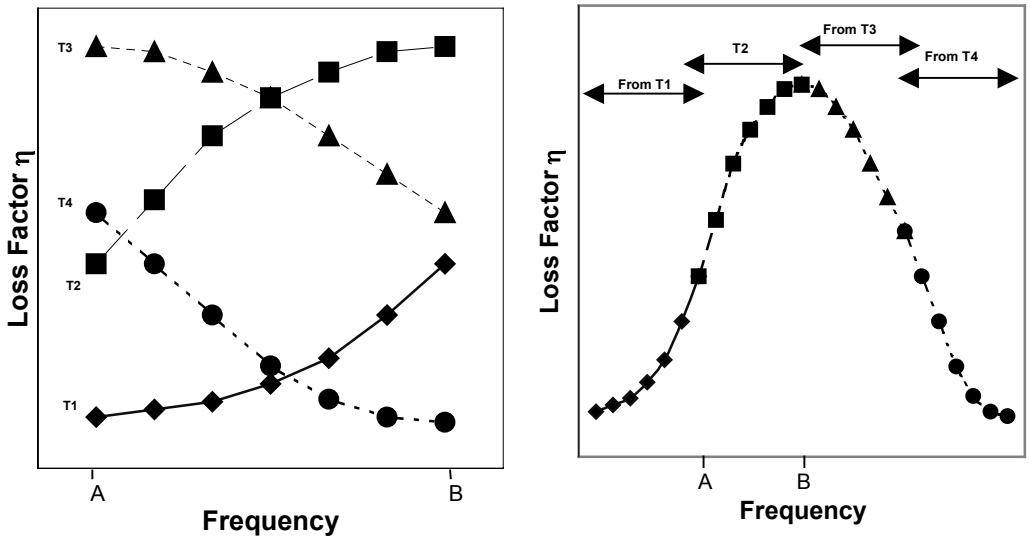

Figure 2-16. a) Loss factor vs. frequency at various temperatures. b) Data from plot a) shifted so that data is shown over a greater frequency range; this is called the temperature frequency superposition principal. In this example T2 is the reference temperature.

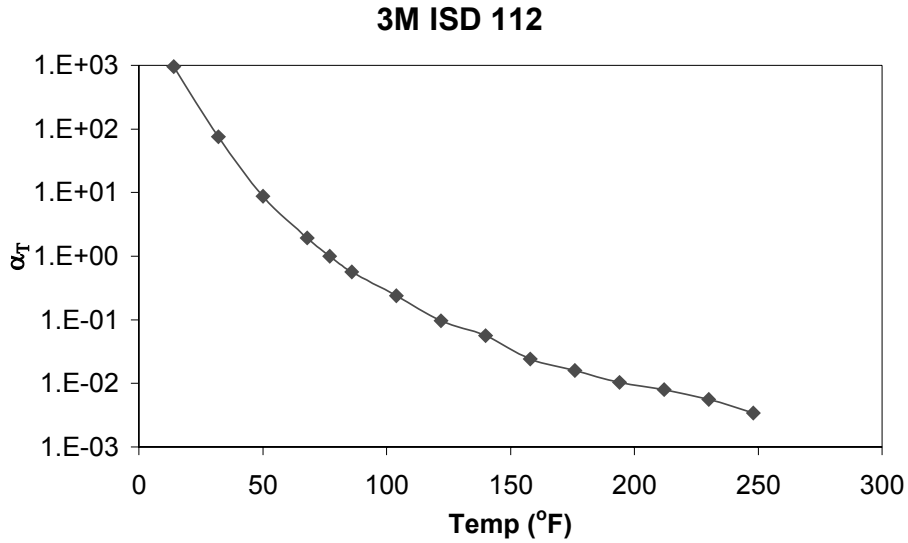

Figure 2-17. Temperature shift α_T factor vs. temperature for 3M ISD 112 viscoelastic damping material. The reference temperature is 75^{o}F (α_T = 1 at 75^{o}F).

2.2.4 Combining Temperature and Frequency Effects

To correctly predict the behavior of viscoelastic materials frequency and temperature effects both must be taken into account. Good curvefits can be produced, at least over relatively small temperature ranges, by taking the four-parameter fractional derivative model and combining it with the a shift factor equation such as the modified WLF equation, making it a six-parameter model. The shift factor equation adds two unknowns, so the modulus and loss factor equations have six total unknowns:

$$G' = \frac{B + (BA + C)\left\{\omega * \exp\left(\frac{-\frac{1000 C_1 C_2}{T_o^{\,2}}(T - T_o)}{C_2 + T - T_o}\right)\right\}^{\alpha} \cos(\frac{\alpha\pi}{2}) + C\left\{\omega\left(\frac{-\frac{1000 C_1 C_2}{T_o^{\,2}}(T - T_o)}{C_2 + T - T_o}\right)\right\}^{2\alpha} A}{1 + 2A\left\{\omega\left(\frac{-\frac{1000 C_1 C_2}{T_o^{\,2}}(T - T_o)}{C_2 + T - T_o}\right)\right\}^{\alpha} \cos(\frac{\alpha\pi}{2}) + A^2\left\{\omega\left(\frac{-\frac{1000 C_1 C_2}{T_o^{\,2}}(T - T_o)}{C_2 + T - T_o}\right)\right\}^{2\alpha}}$$

(2-52)

and

$$\eta = \frac{(C - BA)\omega\left\{\exp\left(\frac{-\frac{1000 C_1 C_2}{T_o^{\,2}}(T - T_o)}{C_2 + T - T_o}\right)\right\}^{\alpha} \sin(\frac{\alpha\pi}{2})}{B + (BA + C)\left\{\omega * \exp\left(\frac{-\frac{1000 C_1 C_2}{T_o^{\,2}}(T - T_o)}{C_2 + T - T_o}\right)\right\}^{\alpha} \cos(\frac{\alpha\pi}{2}) + C\left\{\omega * \exp\left(\frac{-\frac{1000 C_1 C_2}{T_o^{\,2}}(T - T_o)}{C_2 + T - T_o}\right)\right\}^{2\alpha} A}$$

(2-53)

Equations 2-52 and 2-53 are simply Equations 2-38 and 2-40, respectively, with the frequency ω replaced with the reduced frequency ω_r from Equation 2-49 and the temperature shift function α_T from Equation 2-51. For T equal to T_o, these equations are the same as Equations 2-38 and 2-40.

Chapter 3 Manufacturing and Experimental Methods

This chapter describes the manufacturing and experimental methods used in this research. In general, graphite/epoxy unidirectional prepreg composite was used, although this research could apply to any reinforced polymeric composite. This chapter gives an overview of standard methods of determining damping then describes the specific methods used in this research.

3.1 Manufacturing

A variety of standard polymeric prepreg composites were used in this work. All materials were donated by either the manufacturer or local companies that use polymeric composites. After each prepreg ply was added the laminate is placed under vacuum, which ranged from 0.4 to 0.6 atmospheres, for at least 5 minutes. Once the lay-up was complete the laminate is left under vacuum overnight. The laminate was then placed on the tooling plate, typically stainless steel or aluminum, and prepared for an autoclave cure. The autoclave bagging sequence is shown in Figure 3-1. A release film was first laid down on the plate to prevent the resin from sticking to the plate. This not only made clean up easier but also allowed the laminate to expand and contract independent of the tooling. Because of the difference in coefficients of thermal expansion, if the composite bonded to the plate they would buckle during cool-down after the cure. On top of the release film was a peel ply layer. The peel ply gave the composite its surface finish. The laminate was then placed on the peel ply and another layer of peel ply was laid on the top of the laminate. Breather/bleeder

cloth was the next layer. Breather/bleeder cloth provided a path for the vacuum and soaked up excess resin. The final layer was the outer bagging material, which was attached around the edges of the tooling with a sealant tape. Once the bagging process was complete, the entire part was placed in an autoclave. The autoclave used can reach 650^{o}F and 10.2 atmospheres (150 psi) pressure. A typical cure cycle is shown in Figure 3-2.

Resin contents of the composites were measured by acid digestion. Small samples were cut from the laminate. Each sample was massed and the specific gravity was measured by weighing it in water. The samples were then placed in sealed crucibles with concentrated nitric acid. They were then heated in an industrial microwave and the hot pressurized nitric acid dissolves the epoxy. After being rinsed and dried overnight, the fibers were massed. From these measurements resin and fiber mass and volume content could be easily calculated along with the void content.

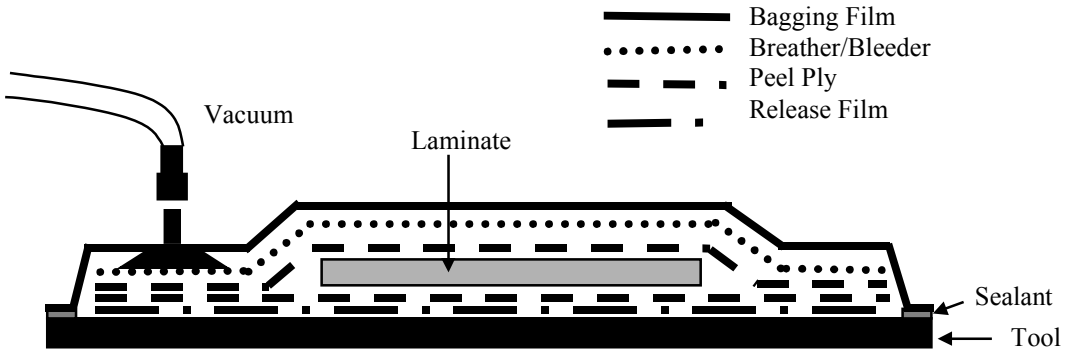

Figure 3-1. Autoclave bagging sequence.

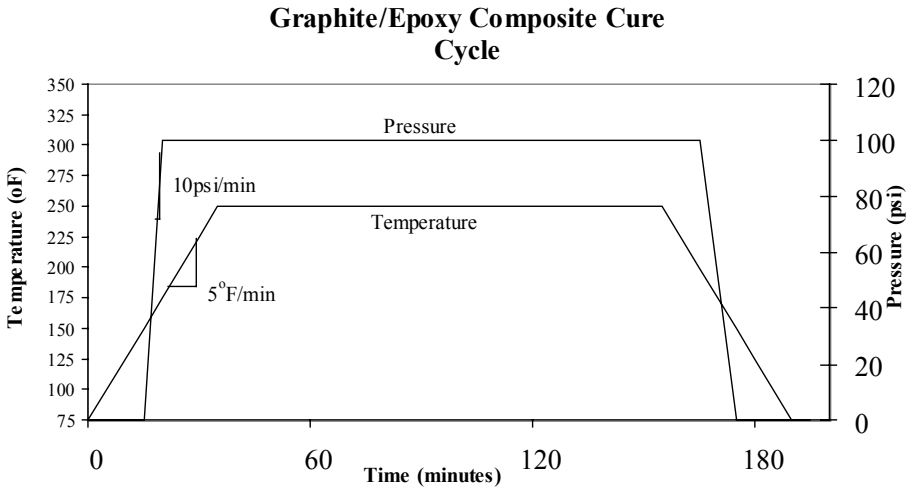

Figure 3-2. Typical polymeric composite cure cycle.

3.2 Experimental

There are numerous ways of calculating the dynamic mechanical properties such as the modulus and damping values of a material. The chosen method depends on numerous factors such as modulus of the material, desired frequency and temperature

range, and equipment availability. Methods used include beam tests[63], impulse tests[64,65], torque tests[66], relaxation tests and creep tests[67], and tests using a Dynamic Mechanical Thermal Analyzer (DMTA). In all of these tests factors such as clamping conditions, temperature stability (for non temperature variability tests), and air friction (especially for large displacements) must be accounted for.

There is no standard accepted technique only for composites, although the most commonly used is a variation on the beam technique. With the beam technique, a cantilevered sample is excited by a shaker, vibration transducer, or speaker and the response is measured by an accelerometer, vibration transducer, or laser vibrometer. The various types of beams are shown in Figure 3-3. The-self supporting beam is called the uniform beam. The other two types, Oberst and Sandwich, are for soft materials; the materials are applied to a base beam with known properties. The properties of the system are then measured and those properties, along with the base beam properties, are used to back out the properties of the applied material. The Oberst beam is designed to test the damping material in extension and the sandwich beam tests it in shear.

The DMTA uses a variety of set-ups, shown in Figure 3-4 and described in ASTM Standard D 4065-94, including three-point bending, dual cantilever bending, linear shearing, tension and compression. The main problem with the DMTA is that most cannot go above 200 Hz. frequency. Most have time temperature superposition functions, but they are not always accurate at frequencies much greater than 200 Hz.

Another interesting measurement technique, which was designed specifically for composites, are impulse tests.[65] Figure 3-5 and Figure 3-6 show the apparatus for the flexural and extensional tests. The beams are excited with an impulse from an electromagnetic hammer with an attached force transducer. The vibrational response is measured by an eddy current probe for the samples in flexure and an accelerometer for the extensional tests.

The beam method and the impulse method use the half-power bandwidth method to measure the damping of the beams. A frequency response curve showing points used in the half power bandwidth method is shown in Figure 3-7. The loss factor η is then calculated as

$$\eta = \frac{\omega_2 - \omega_1}{\omega_n} \tag{3-1}$$

where ω_2 and ω_1 are the half power point frequencies and ω_n is the natural frequency of the mode of vibration. This method is only good for loss factors less than approximately 0.1.[68] At greater loss factors, the frequency response data must be curvefit. A simple model of the structure is first made consisting of a spring, dashpot, and mass and the equation of motion is used. The equation of motion is then solved for the output is divided by the input; for example if the output is acceleration and the input is force, as in the case for a force hammer and an accelerometer, solve the equation of motion for acceleration divided by force. Laplace transforms are used to make the math much simpler. Once the output over input equation is determined it is divided up into real and imaginary terms, then the loss factor is simply the imaginary

portion divide by the real. Fortunately software such as LMS's Cada-X perform these calculations, although the data must sometimes be hand-fit in cases where the curves had a lot of scatter and the Cada-X fits weren't satisfactory.

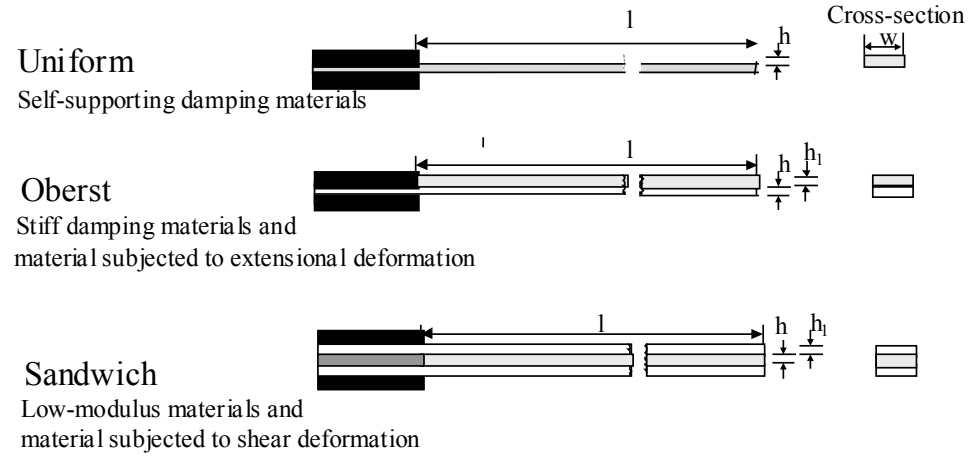

Figure 3-3. Beams used in damping calculations.

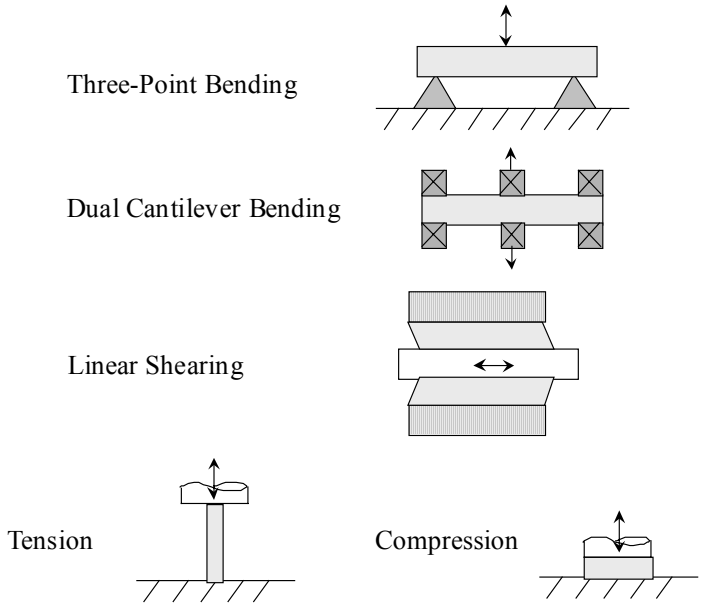

Figure 3-4. DMTA test configurations.

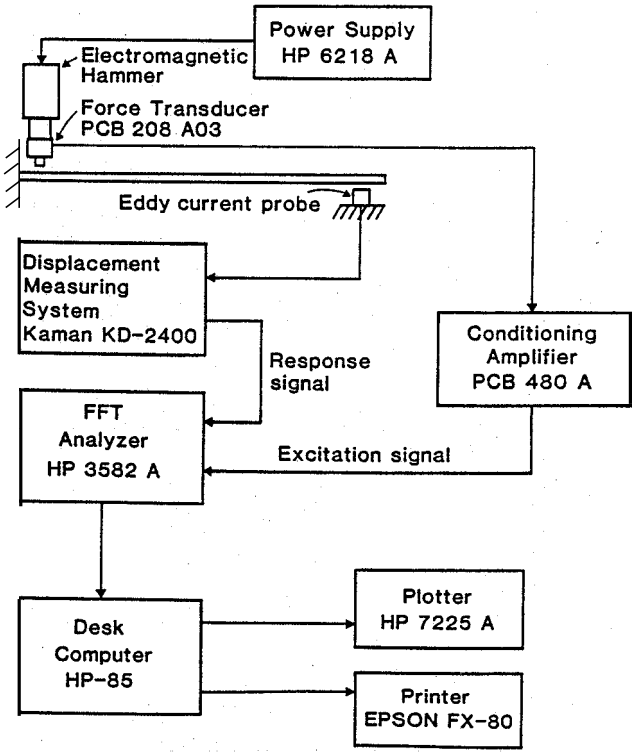

Figure 3-5. Flexural vibration apparatus for impulse tests.[65]

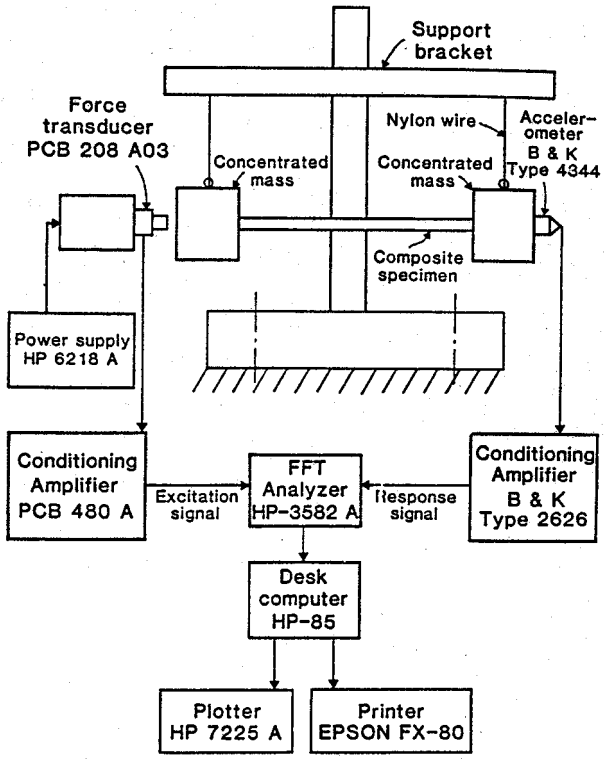

Figure 3-6. Extensional vibration apparatus for impulse tests. [65]

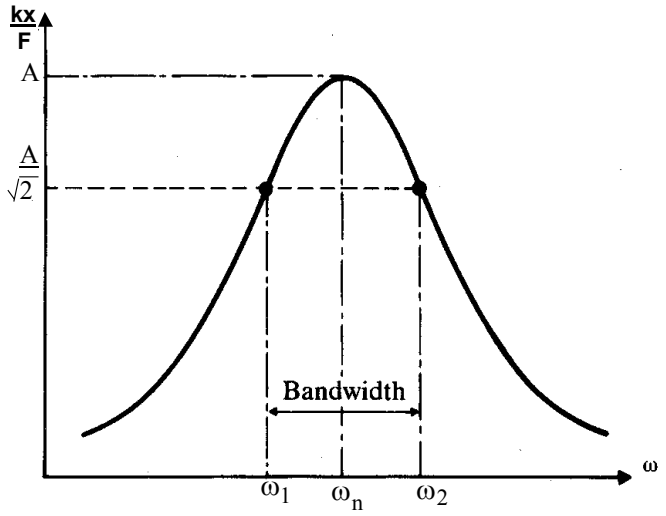

Figure 3-7. Frequency response curve showing half power points.

3.2.1 Vibrations tests – bending modes

Vibration tests were performed on samples in order to obtain natural frequency and damping results; these tests are similar to the sandwich beam tests described in Section 3.2, with the advantage that these tests used non-contacting excitation and measurement. The beams were clamped on one end and the length was varied to obtain results at various frequencies. A speaker was used to provide a broad band excitation. A Polytec PI laser vibrometer was used to measure beam velocity response. Figure 3-8 shows the test set-up.

Frequency response function (FRF) curves were generated by the vibrometer computer program. The damping was measured with LMS's Cada X software, which curvefit the data as described in the Section 3.2. The data was also checked by manually fitting the magnitude of the generated FRFs in the frequency domain. Typically one specimen was tested per sample and each specimen point was analyzed twice and the two values were averaged; damping values were typically within 1% of each other. All bending tests were performed at room temperature, although testing at elevated temperatures along with lower temperatures is often desirable. Most of the tests in this research were for comparison purposes so room temperature was the simplest way to test.

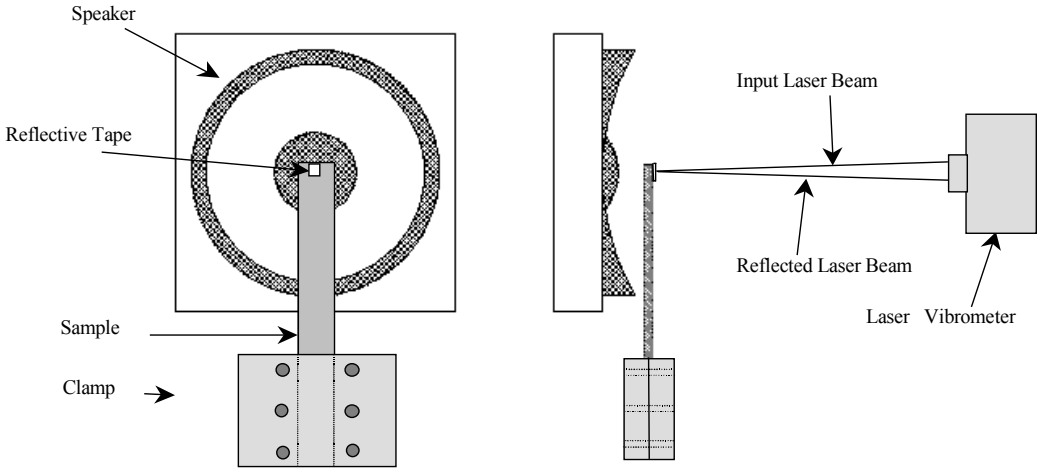

Figure 3-8. Test set-up for bending tests.

3.2.2 Vibrations tests – axial mode

Vibrations tests performed on the axial mode of vibration were similar to the tests performed on the bending modes. The main difference is that the axial mode cannot be excited by a speaker and therefore must be excited by a shaker. Figure 3-9 shows the axial mode set-up. The calculations were performed the same as in the bending mode tests.

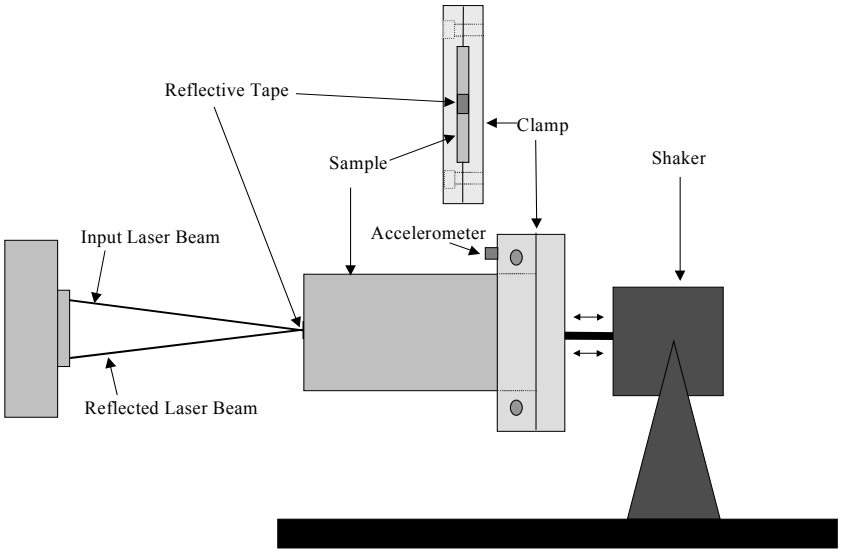

Figure 3-9. Test set-up for axial tests.

Chapter 4 Temperature Tests and Barrier Film

When damping materials are embedded within a composite, the viscoelastic material experiences the temperature cycle of the cure. Most of the commercially available damping materials have maximum recommended temperatures below that of the composite cure cycles. How the performance of damping materials is affected by curing at various temperatures is unknown. Moreover, it is unknown if there is an interaction between the lamina matrix (epoxy) and the damping material.

There are three objectives to this chapter: 1) to document the reduction in damping performance of embedded damping layers cocured into a composite laminate, 2) to experimentally investigate the effect of cure temperature on damping performance, and 3) to prove experimentally that interaction between the damping material and resin (epoxy) is occurring and is reducing damping performance. The first goal was achieved by making cocured composites and comparing their damping performance with samples that had been secondarily bonded (where the sides were cured separately and then bonded with the damping material). The second goal of studying cure temperature effects on damping materials simply involved cocuring a variety of damping materials over a range of cure temperatures. The third goal was accomplished by initially ruling out the effects of the high temperatures and pressures undergone in the cure cycle and then demonstrating that it was epoxy penetration into the damping material that was reducing the damping performance. The cure cycle was ruled out as the cause of the decrease in damping when secondarily bonded samples

that had been run through temperature and pressure cure cycles did not reduce the damping to the cocured level. The epoxy interaction was shown to be the cause of the decrease in damping after samples that had decreased resin penetration, either because of cocuring with lower resin content prepreg or because of an impenetrable layer placed between the resin and damping material, were shown to have an increase in damping.

4.1 **Cure Temperature Study**

The damping materials selected are listed in Table 4-1, where E is Young's Modulus and η is the effective loss factor. All data was obtained from manufacturers' data sheets except for AF32, which was taken from "Cocured Viscoelastic Composites" by Maly and Johnson.[18] Layers of the damping materials were embedded and cocured in the polymeric composite laminate. The prepreg, made by Cape Composites, had intermediate modulus graphite fibers and an epoxy with a cure temperature variable from 250^{o}F to 350^{o}F.

Table 4-1. Damping materials used in cure temperature tests.

Manufacturer	Product	Properties
3M	ISD 112	E = 17.4 to 406 psi, η = 0.6 to 1.0
	ISD 130	E = 13.86 to 218 psi, η = 0.38 to 0.89
	AF 32	E = 1 x 10^4 to 2.2 x 10^4 psi, η = 0.11 to 0.2
Avery Dennison	FasTape 1125 HL	E = 36.3 to 4785 psi, η = 0.7 to 1.9
	FasTape 1191 UHA	E = 27.6 to 130.5 psi, η = 0.12 to 2.5
Soundcoat	Dyad 606	E = 2446.2 to 4.5 x 10^4, η = 0.58 to 1.2

The layup for the cure temperature test plates was $[0/\pm 15/\text{damping material}]_s$. Control samples were also made where the damping layer was replaced with a 90^o ply. Samples were made at 250^oF, 300^oF, and 350^oF) The manufacturer's autoclave cure cycle recommendations were followed: the 250^oF samples were cured for 2 hours, the 300^oF samples for 1 ½ hours, and the 350^oF samples for 1 hour, all at 100 psi. The plate were made 3 ½" by 8" and were later cut into 1" by 7 ½" beams for testing.

Vibration tests were performed on the beams in order to obtain natural frequency and damping results for the first (and, when possible, second) bending mode. The beams were clamped on one end, with the length varying from 3" to 6" in 1" increments to obtain results over a frequency range, typically from 50 Hz. to 250 Hz. for the first bending mode. Some samples were also tested at different beam lengths to better characterize a frequency range. A speaker was used to provide a broad band excitation from 0 - 1000 Hz. A Polytec PI laser vibrometer was used to measure beam velocity response. The damping was measured with LMS's Cada PC software, which uses a time domain multi-degree-of-freedom curvefitter. The data was also checked by manually fitting the magnitude of the generated FRFs in the frequency domain. One specimen was tested per sample and each specimen point was analyzed twice and the two values were averaged; damping values were typically within 1% of each other. The coherence was excellent near resonance. All tests were performed at room temperature.

The effective loss factor of the control samples varied from 0.0014 to 0.0018; Figure 4-1 shows the damping vs. frequency for the control samples cured at 250^oF,

300°F, and 350°F. The frequencies were the 1st and 2nd bending mode frequencies for 6", 5", 4", and 3" beam lengths. Compared with the amount of damping in the beams with damping material, the variation in the control samples is insignificant.

Figures 4-2 to 4-7 show the cure temperature data for beams with embedded ISD 112, FasTape 1125, Dyad 606, AF32, FasTape 1191, and ISD 130, respectively. Beams made with ISD 112 show a slight decrease in damping with cure temperature above 250°F, although there seems to be no consistent pattern between the samples cured at 300°F and 350°F. 3M recommends that ISD 112 can withstand temperature maximums of 300°F. The FasTape 1125 sample appears to have slightly more damping after cured at 350°F. Avery recommends a maximum continuous operating temperature of 250°F, although it does allow intermittent operating temperature of 350°F. Dyad 606 decreases in damping from the 250°F cure sample to the 300°F cure sample, then drastically increases in damping for the 350°F cure sample. Soundcoat recommends Dyad 606 should not experience 350°F for more than 15 minutes. The 350°F cure samples had obviously changed during cure. The sample thickness had increased, indicating possible volatile gas formation. The Dyad 606 was also "squeezed out" of the laminate when clamped to be tested. The 6" data point was not included because of this problem. AF32 250°F cure samples showed significantly less damping than the 300°F and 350°F cure samples. Because AF32 is an adhesive that itself must be cured, the 250°F sample may not have completely cured. 3M recommends AF32 cure temperatures between 250°F and 450°F. Damping in FasTape 1191 samples does not appear to be consistently affected by cure temperature. At

approximately 113 Hz. the sample cured at 350°F had an effective loss factor 0.04 less than that of the samples cured at 250°F and 300°F; otherwise the data was similar. Avery recommends a maximum continuous operating temperature of 230° F, although it does allow intermittent operating temperature of 300° F. Damping for ISD 130 appears to slightly decrease with cure temperature. The maximum decrease in effective loss factor, however, is quite minor: 0.005 at 80 Hz. 3M recommends that ISD 130 can withstand temperature maximums of 300°F.

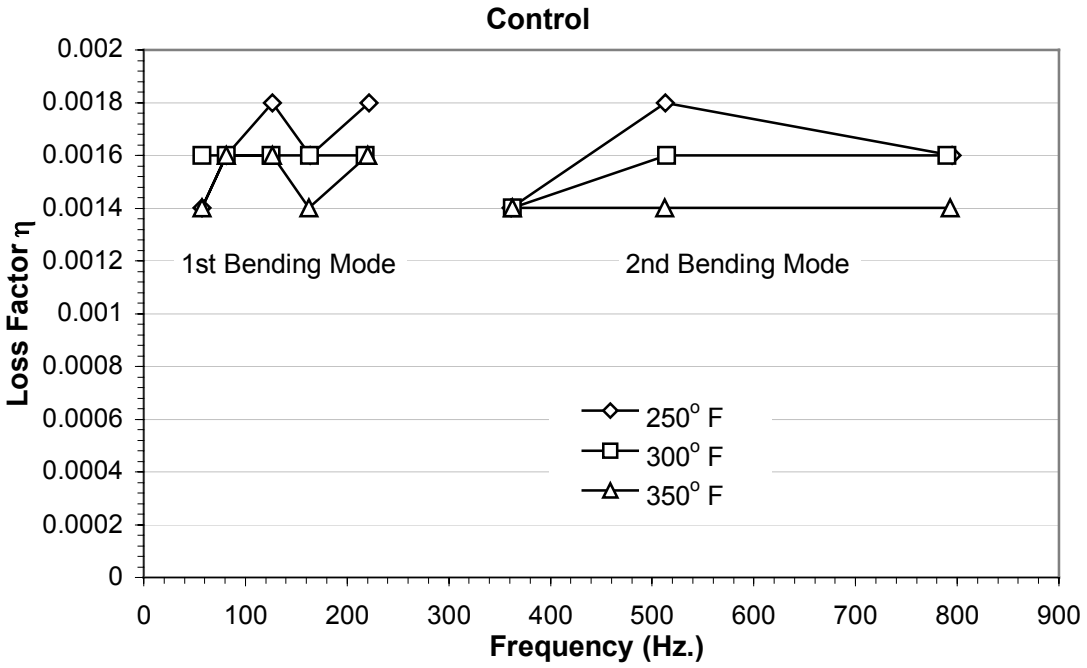

Figure 4-1. Loss factor of graphite/epoxy control samples (no damping) cured at 250° F, 300° F, and 350° F and tested over a range of beam lengths to vary the frequency.

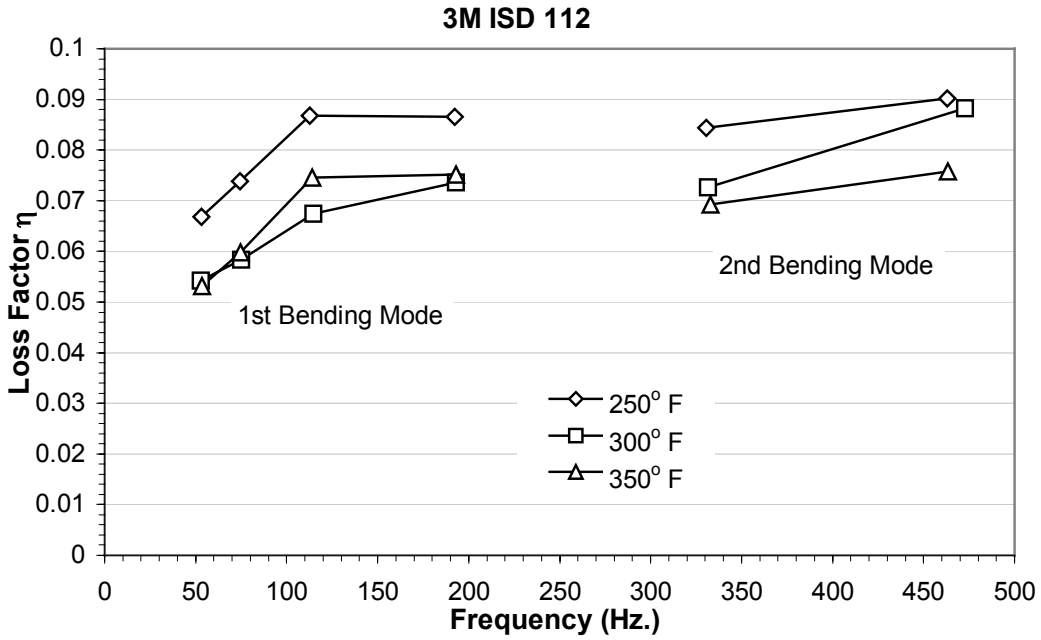

Figure 4-2. Loss factor of graphite/epoxy samples with an embedded 3M ISD 112 damping layer cured at 250° F, 300° F, and 350° F and tested over a range of beam lengths to vary the frequency. First and second bending modes are shown.

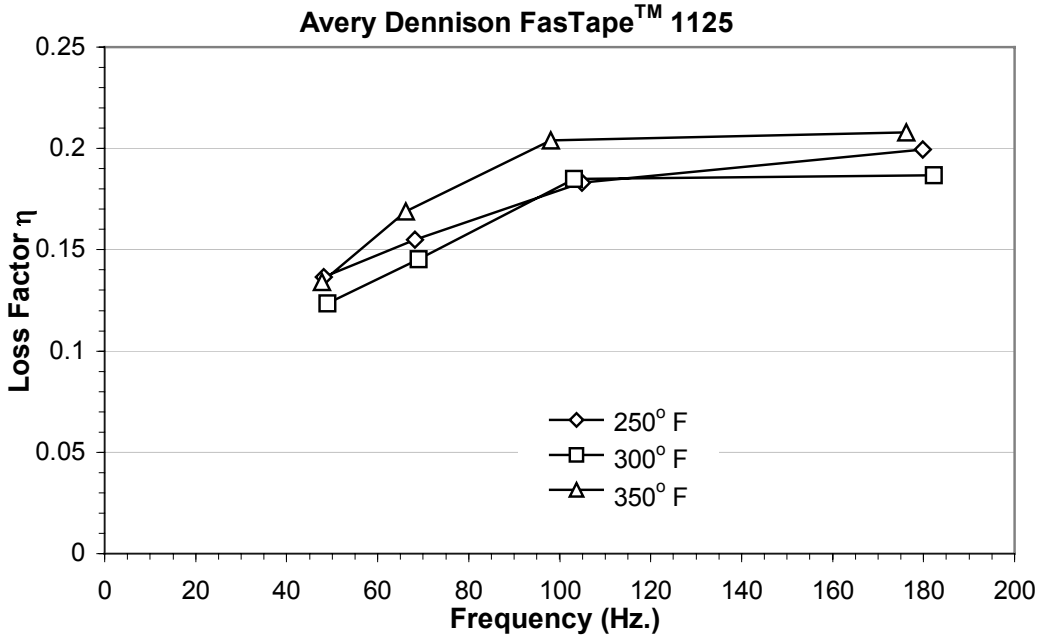

Figure 4-3. Loss factor of graphite/epoxy samples with an Avery Dennison FasTape 1125 damping layer cured at 250° F, 300° F, and 350° F, tested over a range of beam lengths to vary the frequency.

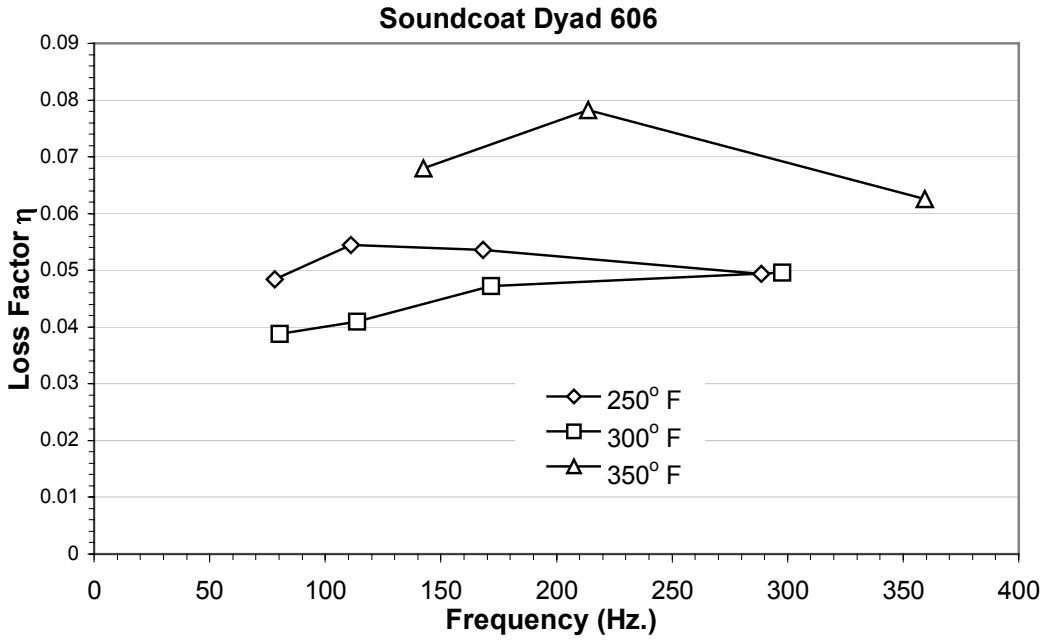

Figure 4-4. Loss factor of graphite/epoxy samples with an embedded Soundcoat Dyad damping layer cured at 250° F, 300° F, and 350° F, tested over a range of beam lengths to vary the frequency.

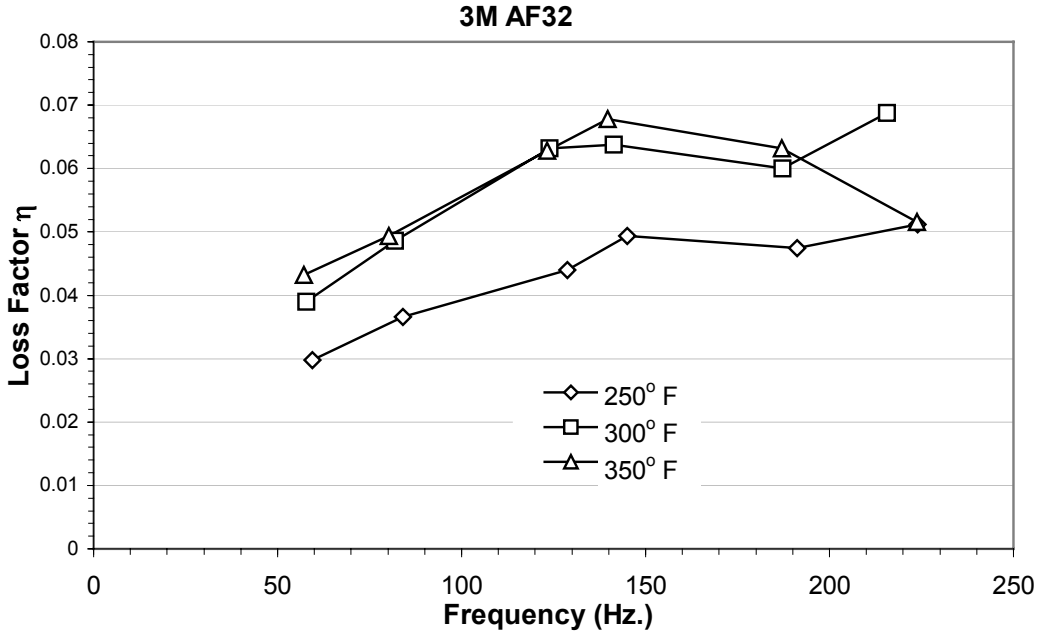

Figure 4-5. Loss factor of graphite/epoxy samples with an embedded Soundcoat Dyad damping layer cured at 250° F, 300° F, and 350° F, tested over a range of beam lengths to vary the frequency.

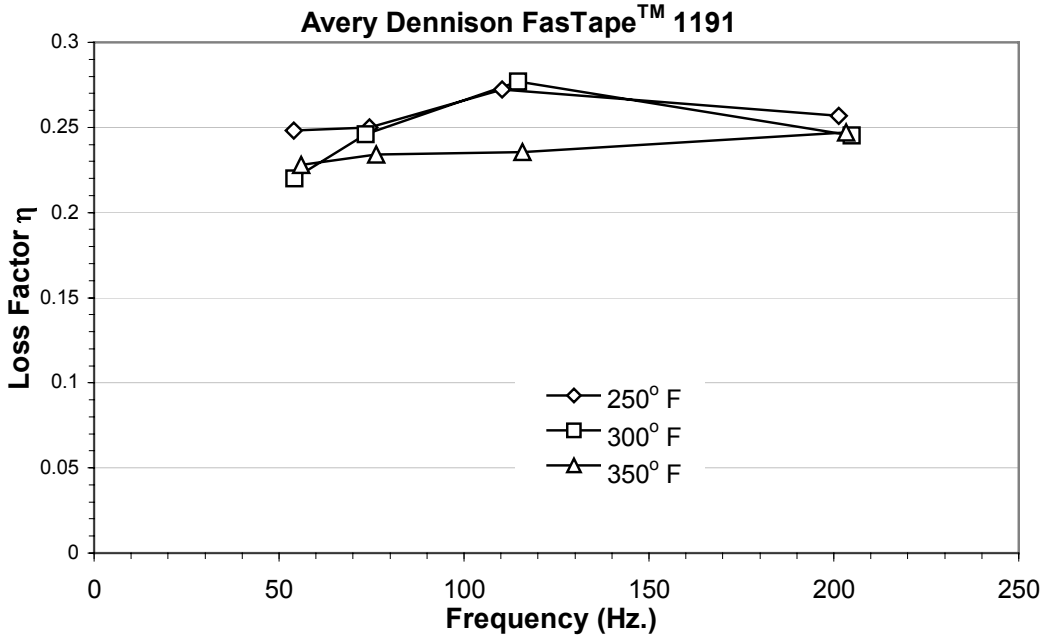

Figure 4-6. Loss factor of graphite/epoxy samples with an embedded Avery Dennison FastTape™ 1191 damping layer cured at 250° F, 300° F, and 350° F, tested over a range of beam lengths to vary the frequency.

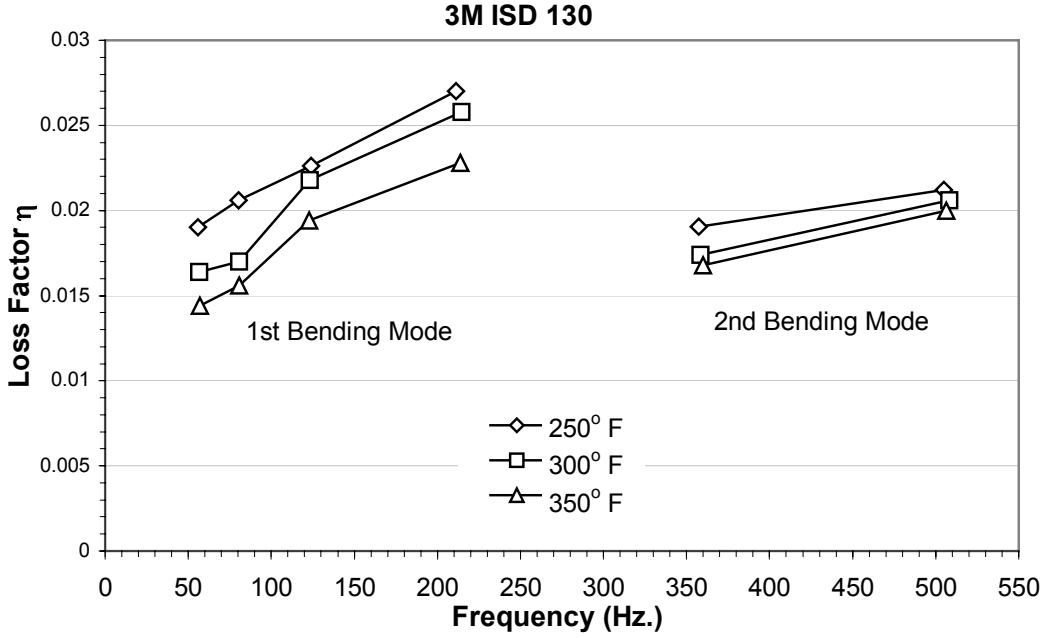

Figure 4-7. Loss factor of graphite/epoxy samples with an embedded 3M ISD 130 damping layer cured at 250° F, 300° F, and 350° F, tested over a range of beam lengths to vary the frequency.

4.2 Cocured Composite Damping Reduction Study

The cocured and secondarily bonded samples were made from Newport Composite NCT 301-G150, an intermediate modulus polymeric low temperature cure prepreg. Two commonly used damping materials, Avery FasTape 1125 and 3M ISD 112, were chosen as the damping materials for these tests.

Both cocured and secondarily bonded samples were cured at 250^{o}F and 100 psi for 3 hours. The layup for these plates was $[0/+15/-15/+15/0/\text{damping material}]_s$. Because each side of the secondarily bonded plates was cured separately, the laminate had to be symmetric not only through the entire thickness but also on each side. There were three sets of secondarily bonded samples: 1) secondarily bonded, 2) secondarily bonded then the entire sample run through a temperature cycle identical to that of the composite cure, 3) secondarily bonded then the entire sample run through a pressure cycle identical to that of the composite cure. These plates were made 3 ½" by 8" and cut into 1" by 7 ½" beams for testing. Testing was identical to that used in the cure temperature test study.

The first step was to make cocured samples and compare them with the secondarily bonded samples. Next, secondarily bonded samples were run them through temperature and pressure cycles identical to the cure cycle. Figure 4-8 and Figure 4-9 show the difference between cocured and secondarily bonded samples for FasTape 1125 and ISD 112, respectively. FasTape 1125 cocured samples had an 8.1% to 33.7% lower effective loss factor than the secondarily bonded samples. FasTape 1125 secondarily bonded samples run through temperature and pressure cycles show a

decrease in damping at low frequencies but still aren't as low as the cocured sample. ISD 112 cocured samples had approximately a 60.8% lower effective loss factor than the secondarily bonded samples. ISD 112 samples run through temperature and pressure cycles show no consistent change in damping and still have tremendously more damping than the cocured sample. These tests indicate that the application of temperature and pressure cycles were not the reason for the decrease in damping seen in cocured laminates.

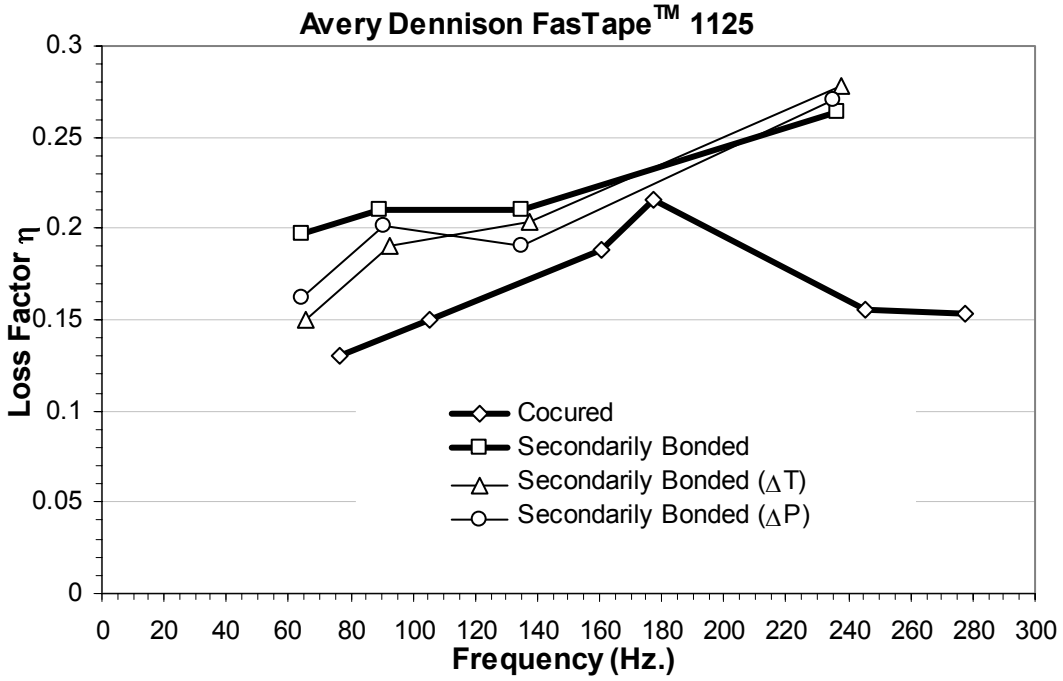

Figure 4-8. Loss factors of graphite/epoxy samples with a layer of Avery Dennison FasTape 1125 that were cocured, secondarily bonded, and secondarily bonded then run through temperature (ΔT) and pressure (ΔP) cycles. Tests were performed over a range of beam lengths to vary the frequency of the first bending mode.

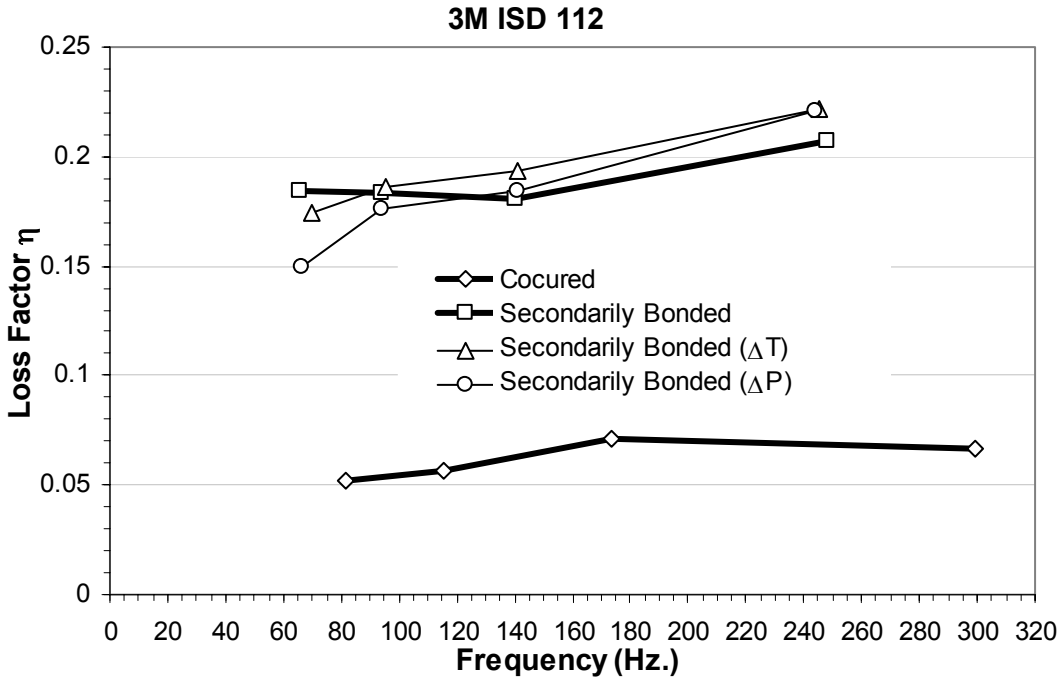

Figure 4-9. Loss factors of graphite/epoxy samples with a layer of 3M ISD 112 that were cocured, secondarily bonded, and secondarily bonded then run through temperature (ΔT) and pressure (ΔP) cycles. Tests were performed over a range of beam lengths to vary the frequency of the first bending mode.

4.3 Epoxy-Damping Material Interaction Study

The material, layup, and damping materials used are identical to those used in the cocure damping reduction study. The testing procedure is the same as described in the cured temperature test section.

This study was to determine whether the resin was penetrating the damping material. Microscope observations indicated physical changes in the damping material. The secondarily bonded damping material tended to "pull out" of the

laminate when cut and bulged out when clamped. The damping material in the cocured sample was not as pliable and did not pull or bulge out when cut and clamped.

If the epoxy was penetrating the damping material, then reducing the resin should reduce the resin available for penetration and thus potentially increase the damping. Prebleeding was used to reduce the resin content. Prebled plates were made by taking the top and bottom sections of the uncured plates and laying them up with an adsorbent glass cloth that would "bleed away" some of the resin. The plates were heated up to 150^{o}F at 100 psi for 5 to 10 minutes. This temperature allowed the resin to flow but wasn't high enough to start to cure the part over such a short time. The plates were then removed, bonded together with the damping material, and run through a normal cure cycle. Resin content tests verified that the resin content was significantly decreased by prebleeding. The samples prebled for ten minutes had a final resin content of approximately 22.5 wt. %, as compared to approximately 31wt. % for the original cocured sample. Attempting to further reduce resin content by prebleeding for more than 10 minutes was found to produce resin starved regions (i.e. dry fibers).

As shown in Figure 4-10 and Figure 4-11, prebleeding did slightly increase the damping in both FasTape 1125 and ISD 112, respectively. This indicated the resin was probably causing a decrease in damping, but the resin could not be reduced further and there was still a large discrepancy between the cocured and secondarily bonded samples.

The final step was to place a barrier layer on both sides of the damping material to prevent resin penetration. Polyimide film, 0.002" thick, was selected as the barrier layer between the damping material and epoxy resin. The surface of the polyimide film was roughened with a scouring pad and cleaned with isopropyl alcohol to improve bonding with the epoxy and damping material. To ensure the film wouldn't contract during cure it was heated to 250^{o}F for 30 minutes and cooled to room temperature before being assembled into the laminate. Figure 4-12 and Table 2 show the loss factors of the samples cocured with the polyimide film between the FasTape 1125 damping material and the epoxy compared to the secondarily bonded sample and the cocured sample without the film; samples cocured with the polyimide film between 3M 112 damping material and the epoxy are shown in Figure 4-13 and Table 4-3. Also shown are the damping values of a control sample, which was made with a 0^{o} composite ply in place of the damping material, and a sample with embedded polyimide film (no damping material). The polyimide film increased the effective loss factor in FasTape 1125 samples by 15.7% to 92.3% over the cocured samples without the film. In ISD 112 samples the increase over cocured without the film was at least 168%. The damping is above the secondarily bonded levels across the tested frequency range for the FasTape 1125 samples. The reason for this is suspected to be poor bonding between the damping material and the polyimide film. The polyimide film showed insignificant damping; the composite sample with only polyimide film showed no more damping than the control sample. The damping values in both the control sample and sample with embedded polyimide film were only 1 to 2% of the

damping values of the samples with embedded damping material. Damping for the ISD 112 samples is only slightly below the secondarily bonded levels at frequencies below 100 Hz. and is approximately the same above 100 Hz. This verifies the role of epoxy interaction in reducing the damping in cocured samples.

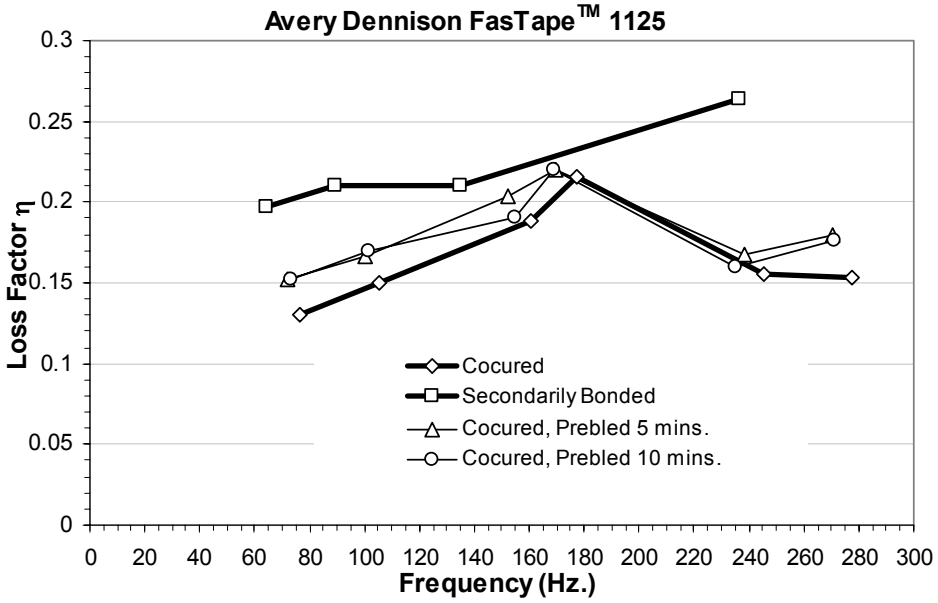

Figure 4-10. Loss factors of graphite/epoxy samples with a layer of Avery Dennison FasTape 1125 that were cocured, secondarily bonded, and cocured after prebleeding 5 or 10 minutes. Tests were performed over a range of beam lengths to vary the frequency of the first bending mode.

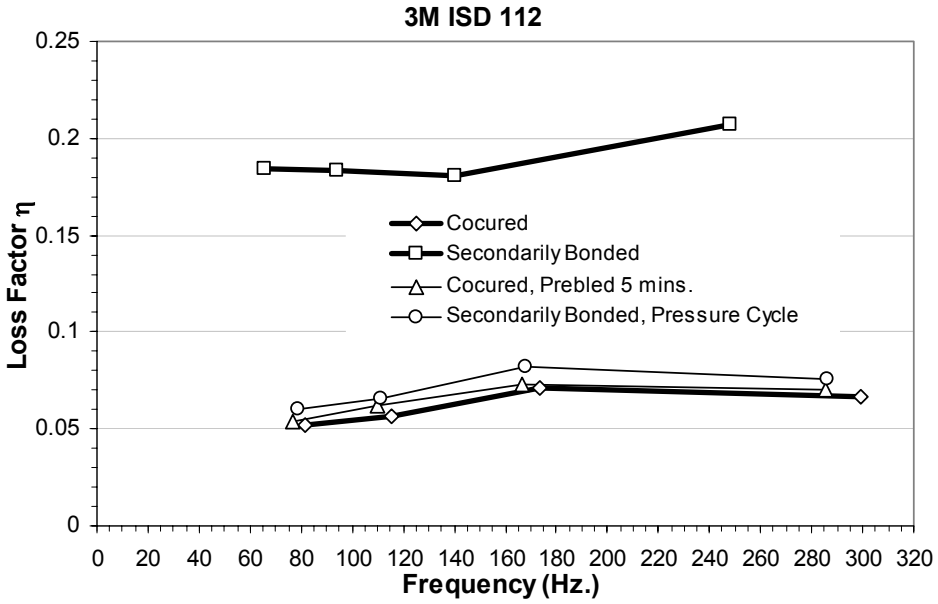

Figure 4-11. Loss factors of graphite/epoxy samples with a layer of 3M ISD 112 that were cocured, secondarily bonded, and cocured after prebleeding 5 or 10 minutes. Tests were performed over a range of beam lengths to vary the frequency of the first bending mode.

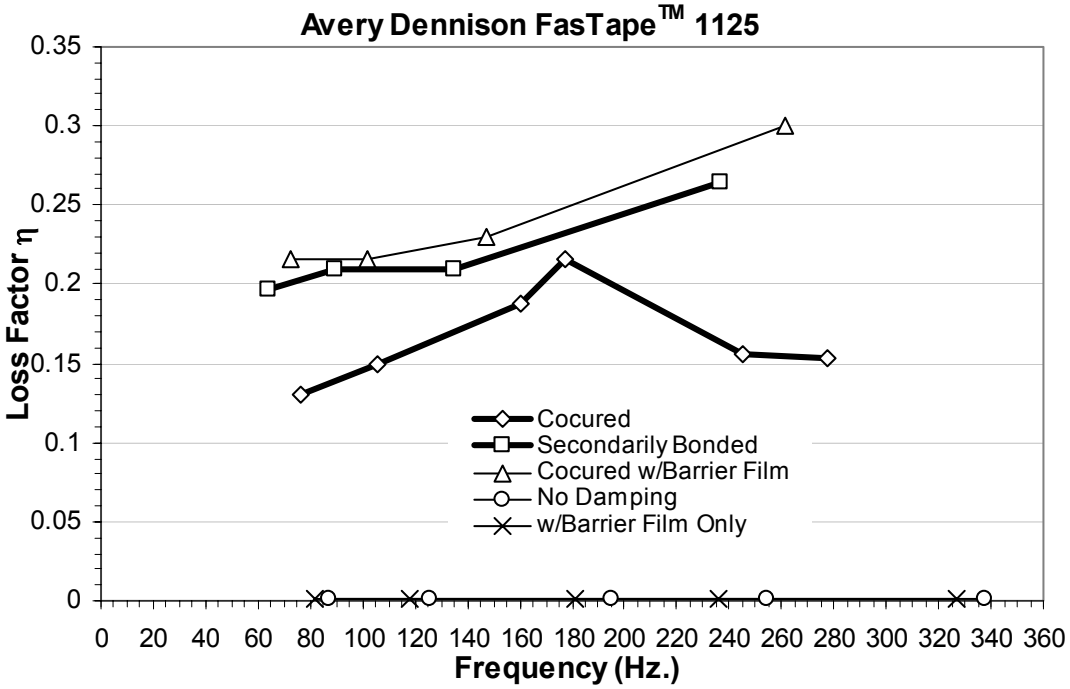

Figure 4-12. Loss factors of graphite/epoxy samples with a layer of FasTape 1125 that were cocured, secondarily bonded, and cocured with polyimide film separating the damping material and epoxy. Also included are the control sample and a sample with embedded polyimide film only.

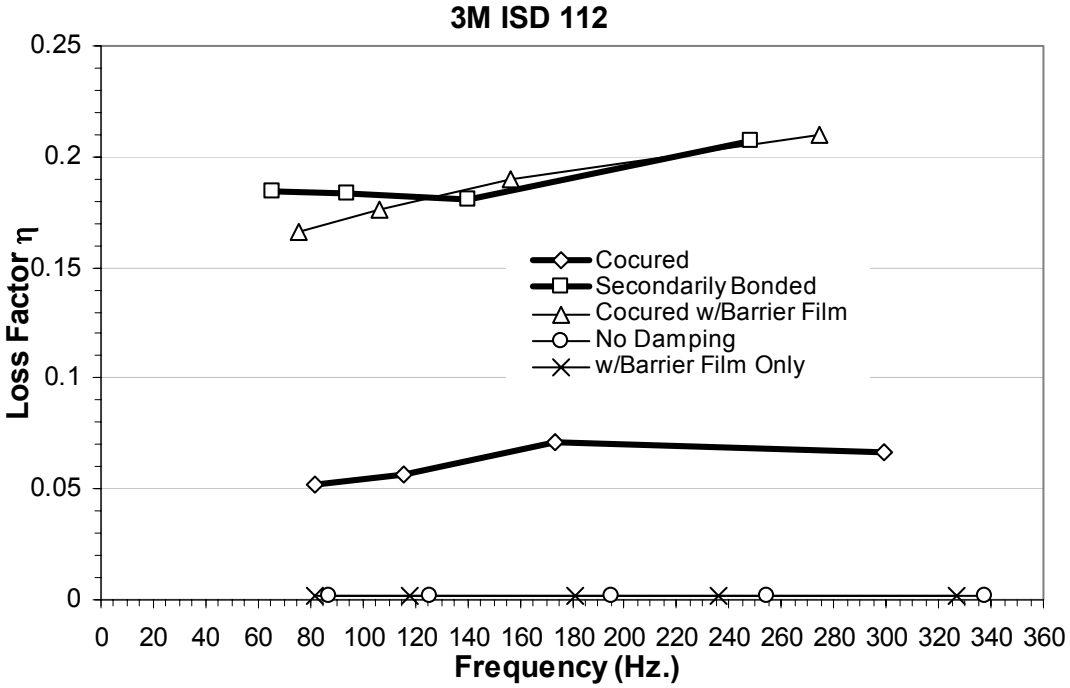

Figure 4-13. Loss factors of graphite/epoxy samples with a layer of ISD 112 that were cocured, secondarily bonded, and cocured with polyimide film separating the damping material and epoxy. Also included are the control sample and a sample with embedded polyimide film only.

Table 4-2. Frequency and effective loss factor of data shown in Figure 4-12.

Baseline (No damping)				with 3M ISD 112					
composite lamimate		with polyimide barrier layer		Cocured		Cocured w/PI barrier layer		Secondarily bonded	
ω(Hz.)	η_{eff}	ω(Hz.)	η_{eff}	ω(Hz.)	η_{eff}	ω(Hz.)	η_{eff}	ω(Hz.)	η_{eff}
87.39	0.0018	81.59	0.0017	81.83	0.052	75.90	0.17	65.60	0.18
125.88	0.0017	117.64	0.0018	115.64	0.057	106.10	0.18	93.90	0.18
195.31	0.0017	181.43	0.0016	173.72	0.071	156.40	0.19	140.63	0.18
254.62	0.0017	235.54	0.0017	299.17	0.067	274.50	0.21	248.13	0.21
337.96	0.0018	326.51	0.0019						

Table 4-3. Frequency and effective loss factor of data shown in Figure 4-13.

Baseline (No damping)				with Avery Dennison FasTape™ 1125					
composite lamimate		with polyimide barrier layer		Cocured		Cocured w/PI barrier layer		Secondarily bonded	
ω(Hz.)	η_{eff}	ω(Hz.)	η_{eff}	ω(Hz.)	η_{eff}	ω(Hz.)	η_{eff}	ω(Hz.)	η_{eff}
87.39	0.0018	81.59	0.0017	76.70	0.131	72.70	0.216	64.05	0.197
125.88	0.0017	117.64	0.0018	105.67	0.150	102.00	0.216	89.40	0.210
195.31	0.0017	181.43	0.0016	160.50	0.188	147.50	0.230	134.81	0.210
254.62	0.0017	235.54	0.0017	177.00	0.216	261.00	0.300	236.32	0.264
337.96	0.0018	326.51	0.0019	245.20	0.156				
				277.50	0.154				

4.4 Conclusions

Cocuring damping materials in polymeric composite materials greatly increases the damping of the structure. The damping capabilities of the tested damping materials, however, decrease significantly when cocured. The cause of the decrease was demonstrated to be the interaction of the epoxy with the damping material. Samples that had been prebled and thus had a lower resin content were shown to increase the damping levels, but not tremendously. Substantial increases in damping occurred when a polyimide film barrier layer was placed between the damping layer and the epoxy before curing to prohibit damping material/epoxy interaction. The polyimide film increased the effective loss factor in FasTape 1125 samples by 15.7% to 92.3% over the cocured samples without the film. In ISD 112 samples the increase over cocured without the film was at least 168%. The resulting damping levels were very close to those achieved by secondarily bonding.

The damping materials tested were not greatly affected by cure temperature, with the exception of Soundcoat Dyad 606. Soundcoat Dyad 606 had greater damping

with a 350^{o}F cure temperature but appeared to have undergone considerable material changes. There were small differences in the other samples, but typically not great enough that cure temperature should be dictated by damping material performance.

This chapter is a reprint, in part, of the material published in 1999 in the *Journal of Composite Materials* titled "Damping Performance of Cocured Graphite/Epoxy Composite Laminates with Embedded Damping Materials" Volume 33, pages 1457-1469. The dissertation author was the primary investigator and co-authored the article with advisor J. B. Kosmatka.

Chapter 5 Shear Tests

The objective of this investigation was to measure the shear moduli of a variety of cocured damping materials. This gave an indication as to what extent cocuring changed viscoelastic material properties. Also, the shear moduli of viscoelastic materials cured with barrier layers to prevent the epoxy interaction were measured. Another goal was to determine the benefits of placing a "scrim cloth", or loosely woven mesh, in between two layers of damping material.

This experimental research program concentrated on the following five areas: (1) determine the minimum specimen shear area needed to get consistent measurements, (2) perform tests at a series of strain rates to measure the variation of modulus with strain rate, (3) illustrate the differences in the initial and secondary shear moduli for the various cocured damping materials, (4) compare different barrier films for protecting the damping material during cure, (5) investigate what effect an embedded loose weave scrim cloth has on the behavior of the damped specimens.

5.1 Manufacturing and Testing

Testing the shear strength of the viscoelastic layer cocured in composite samples posed several problems. The standard tests used to determine shear response in a composite sample, ASTM D 3518M-94 ($\pm$45 laminate test) and ASTM D 5379M-93 (V-notched test) do not work in this situation; they are designed for the shear of the entire composite laminate rather than a single layer. Typical single lap or double lap shear tests for adhesive materials simply call for bonding the material between metal

plates and then place the plates in tension, such as ASTM D 1002-94. The shear test method ASTM D 1002-94 was used as a general guideline for these tests, with the exception that a double-lap test is used to make the plates symmetric. In this study the material had to be cocured, however, and since prepreg is flexible, spacers were necessary to keep the layers parallel during the cure. Figure 5-1 shows the configuration before and after assembly. Composite release film was placed around the end of each spacer to prevent resin transfer during curing and load transfer during testing. The composite sections have a layup of $[0^o/+15^o/-15^o/+15^o/0^o]$. The spacers have the same layup except 0^o layers were added to keep the thickness uniform. The number of 0^o layers depended on the thickness of the material to be tested. An intermediate modulus 250^oF cure graphite/epoxy unidirectional prepreg was used to make the samples. Six specimens were made per sample. An Instron machine was used to perform the shear tests at a strain rate of 0.05"/minute, except for the varying strain rate tests where the strain rate varies from 0.002"/minute to 2"/minute. The loads were measured directly from the Instron machine. An extensiometer was used to measure the displacement during the testing. The shear angle γ can easily be calculated from the displacement:

$$\gamma = \tan^{-1}\frac{x}{t} \tag{5-1}$$

where t is the thickness of the shear sample and x is the measured displacement. The shear stress, τ, is defined as the shear load divided by the shear area and the shear

modulus, G, is defined the shear stress divided by the shear angle. Plots were typically made of the shear stress τ vs. the shear angle γ.

Vibration tests were performed on the beams in order to obtain natural frequency and damping results for the first bending mode, first torsion mode, and first chordwise mode. The plates were 3.5" wide and were cantilevered with a length of 6". A speaker was used to provide a broad band excitation from 0 - 2000 Hz. The input into the speaker was used as the reference and a Polytec PI laser vibrometer was used to measure beam velocity response. The damping was measured with LMS's Cada X software, which uses a time domain multi-degree-of-freedom curvefitter. One specimen was tested per sample and each specimen point was analyzed twice and the two values were averaged; damping values were typically within 1% of each other. The coherence was excellent near resonance. All tests were performed at room temperature.

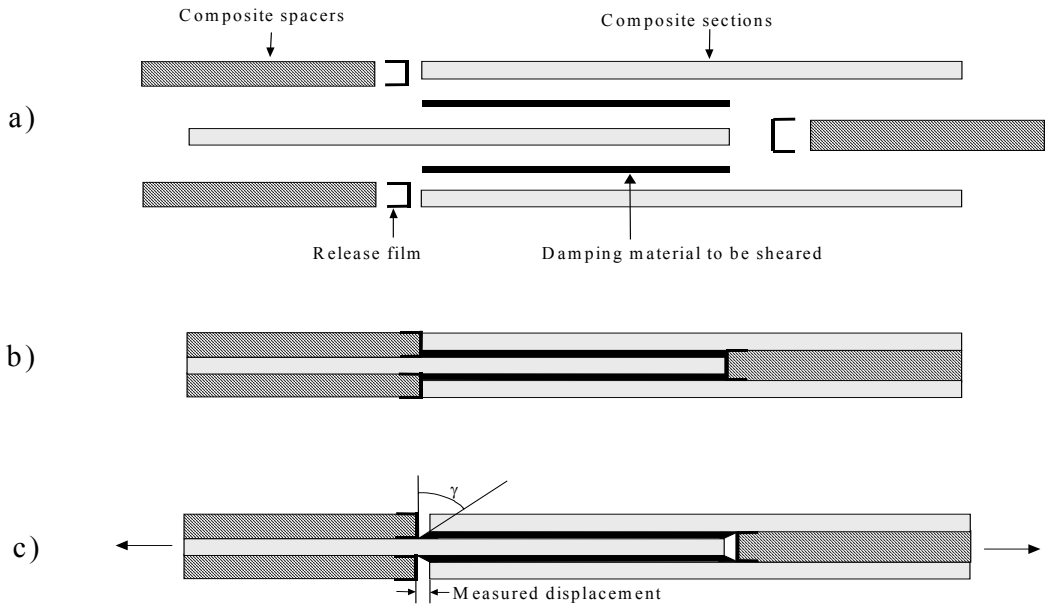

Figure 5-1 a) –c). Shear test samples. a) shows the samples before assembly. The composite sections have a layup of [0^o/+15 ^{o} /-15 ^{o} /+15 ^{o} /0 ^{o}]. The spacers have the same layup except 0 ^{o} layers were added to keep the thickness the same as in the middle, where the damping material adds thickness. b) shows the assembled sample, and c) shows the sample under load.

5.2 Determination of Minimum Test Specimen Shear Area

The first objective was to determine the shear area for the tests. The area needed be large enough so that edge effects are negated, but if too large the samples would become difficult to test and require large amounts of material. Avery FasTape 1125 (FT1125) was the damping material used for this study. The sample width was 1" and four shear lengths, 1", 2", 3" and 4" were tested. Six specimens were tested per sample and the strain rate was 0.005"/minute. Figure 5-2 shows the stress vs. strain curve for these tests. One representative stress vs. strain curve is shown for

each sample, here and throughout this chapter. It is seen that there are two moduli for each sample, an initial linear modulus and a secondary strain-dependent modulus; the moduli are shown in Table 5-1. The initial linear modulus is relatively small in comparison to the secondary strain-dependent modulus. The initial modulus is highest for the 1" sample (106.1 psi), and decreases in the 2", 3", and 4" samples (66.3 psi, 60.4 psi, and 57.6 psi, respectively). The 1" and 2" samples have similar secondary moduli (1004.8 psi and 1061.9 psi, respectively), as do the 3" and 4" samples (894.7 psi and 875.0 psi). When looking at the stress-strain plots in Figure 5-2 it is seen that the 4" sample curve is almost identical to the 3" sample curve and since the modulus is only slightly lower (and within the standard deviation) it was assumed that the edge effects were almost negligible at the 4" length. Therefore the remaining samples were made with a shear length of 4".

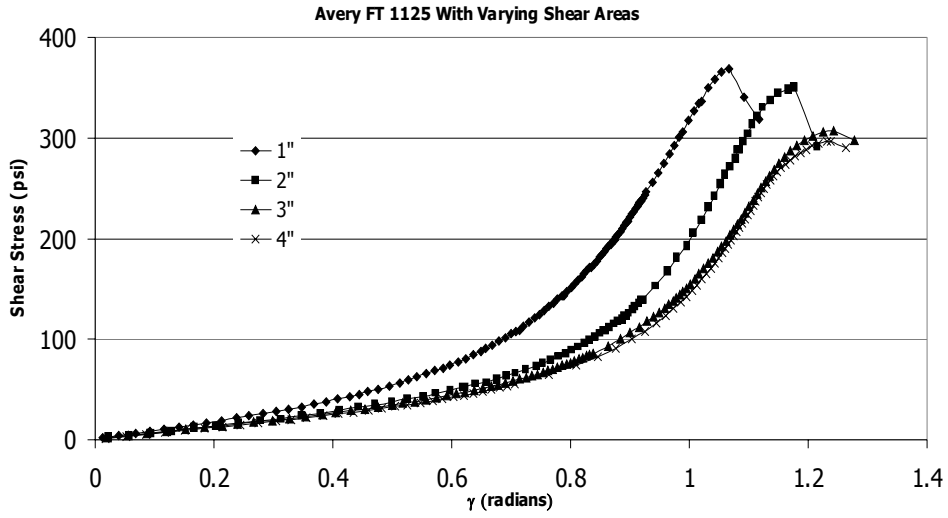

Figure 5-2. Shear Stress vs. Shear Angle γ for cocured Avery FT 1125 samples made in 1", 2", 3" and 4" lengths. The strain rate was 0.01"/minute. The shear modulus values are shown in Table 3.

Table 5-1. Moduli of samples shown in Figure 5-2.

Sample	Initial Shear Modulus (psi)	Secondary Shear Modulus (psi)
Avery FT 1125, 1" x 1" shear area	106.1 ± 4.7	1004.8 ± 26.9
Avery FT 1125, 1" x 2" shear area	66.3 ± 1.3	1061.9 ± 50.6
Avery FT 1125, 1" x 3" shear area	60.4 ± 4.1	894.7 ± 53.2
Avery FT 1125, 1" x 4" shear area	57.6 ± 1.6	875.0 ± 99.3

5.3 Variable strain rate tests

The viscoelastic damping materials used in these tests have properties that vary tremendously with frequency and temperature; therefore it is reasonable to assume that the properties will also vary with shear strain rate. Shear tests were performed on graphite/epoxy samples with cocured FT 1125. Previously, it was shown that during the cure cycle, epoxy often interacts with the damping material, usually reducing the effective damping. [69] To prevent this problem, a barrier layer was placed between the damping material and composite, so tests were also performed on samples with the barrier film Tedlar. Tests were performed at strains of 0.002"/min, 0.05"/min, 0.3"/min, and 2"/min. Figure 5-3 shows the variation in initial shear moduli with strain rate. The modulus of the sample without Tedlar has a small variation from the 0.002"/min strain rate to the 0.05"/min strain rate (2.6 psi, which is within the standard deviation) then increases dramatically (30.3 psi from 0.5"/min to 0.3"/min and 25.7 psi from 0.3"/min to 2"/min). The sample with Tedlar shows an 11 psi increase in modulus from 0.002"/min to 0.05"/min and a much greater increase (25.4 psi from 0.5"/min to 0.3"/min and 23.3 psi from 0.3"/min to 2"/min) at higher strain

rates. Because many of these samples went to very high strains before failing, 0.05”/min was chosen as the strain rate.

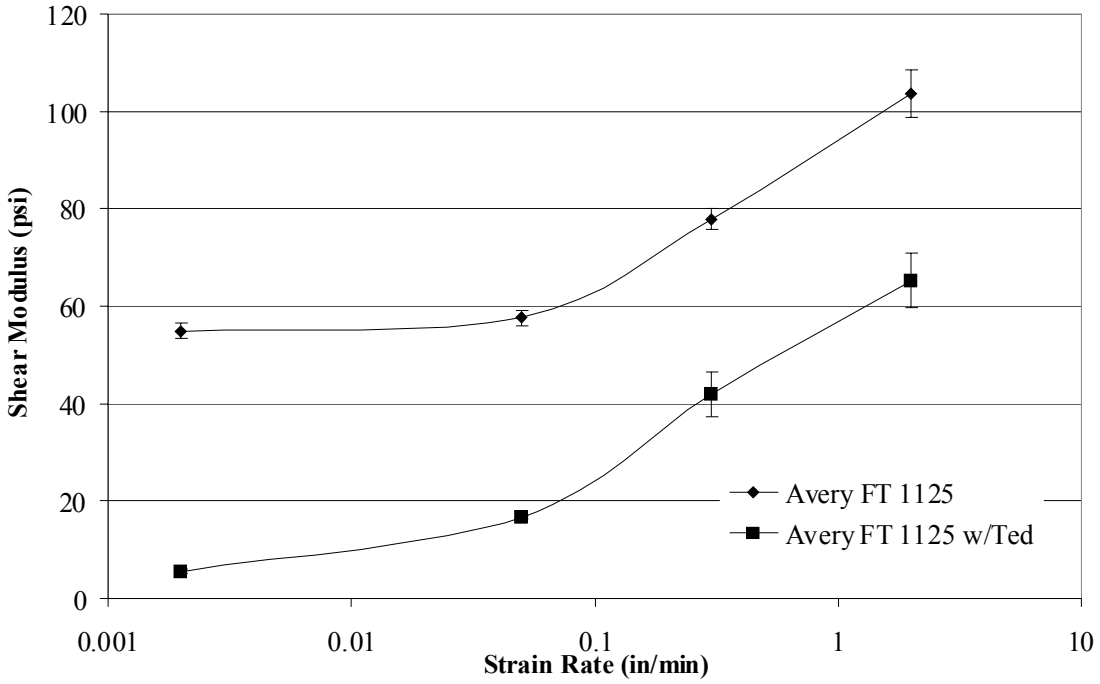

Figure 5-3. Shear modulus vs. strain rate for cocured Avery FT 1125 and Avery 1125 with a Tedlar barrier layer.

5.4 **Shear moduli of cocured damping materials**

The next objective was to illustrate the differences in the stress-strain curves, and the initial and secondary shear moduli for the various cocured damping material. No barrier films were used in these tests (the next section investigates damping materials with barrier layers). The strain rate used is very small (0.05”/min) so the initial modulus is equivalent to the static (or near-zero frequency) modulus on a material nomogram. While the static shear modulus don’t show how the modulus

would change over the various frequencies, it gives a comparison as to how different the modulus of the cocured damping layer is to damping material that had not been cocured. Shear strain tests were performed on graphite epoxy samples cocured with eight materials: five acrylics (Avery FT 1125, Avery FT 1182, 3M ISD 112, 3M ISD 113, and 3M ISD 130), an acrylic/rubber blend (Avery 1191), an acrylic with embedded glass fibers (Avery 1158) and a thermoplastic alloy (EAR CN-06). Figure 5-4 shows the shear stress vs. shear strain curve for five acrylic-based damping materials and Figure 5-5 show the shear stress vs. shear strain curve for the other three materials. The acrylic samples and Avery 1191 all showed an initial linear modulus and a secondary strain-dependent modulus, while the EAR CN-06 and Avery 1158 stayed mostly linear. Table 5-2 lists initial moduli taken from the stress vs. strain curves in Figure 5-4 and Figure 5-5 along with the manufacturer listed modulus for 0.1 Hz. (the lowest frequency the 3M material plots show, extrapolated for EAR and Avery Dennison materials) at room temperature. In general the cocured samples had a higher modulus than the manufacturer's listed modulus, with the exceptions of EAR CN-06 and Avery FT 1191. The moduli of all of the acrylic cocured samples ranged from 1.5 (ISD-130) to 10.4 (ISD-112) times higher than the manufacturer's listed moduli. This moduli increase was due to the infiltration of the epoxy resin into the damping material during the cure cycle. The Avery FT 1191 sample had almost the same shear modulus as the manufacturer's listed modulus and since this material is a rubberized adhesive it appears that epoxy did not infiltrate it during the cure cycle. The reason for the decrease in modulus for EAR CN-06 is unknown, but this material

was supplied in a 0.060" thickness that was hot-pressed to 0.006" for the current tests and thus this operation may have reduced the shear modulus.

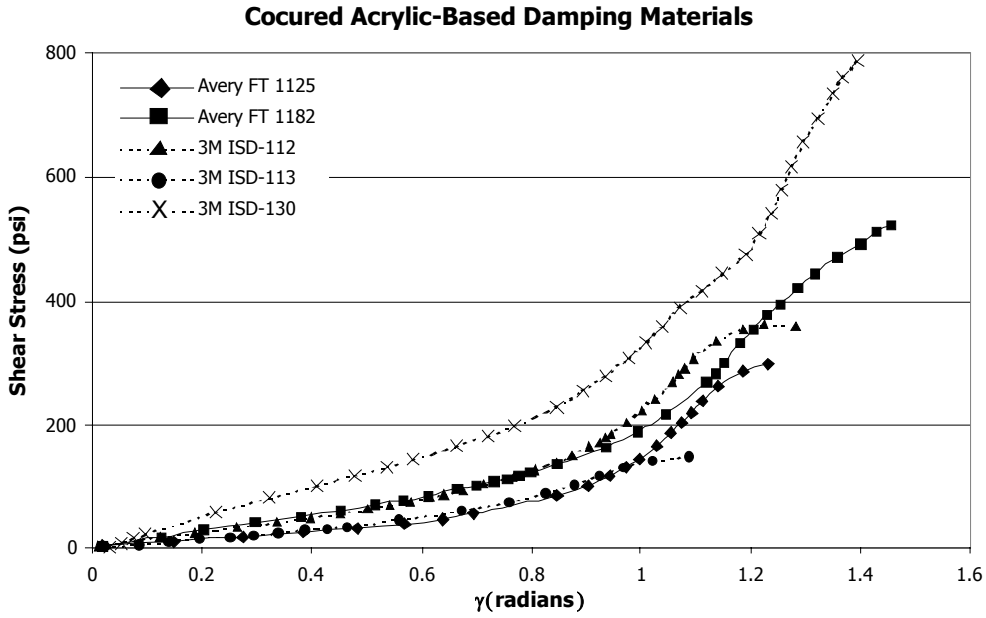

Figure 5-4. Shear stress vs. shear angle γ for acrylic-based cocured damping materials manufactured by Avery Dennison (---) and 3M (—).

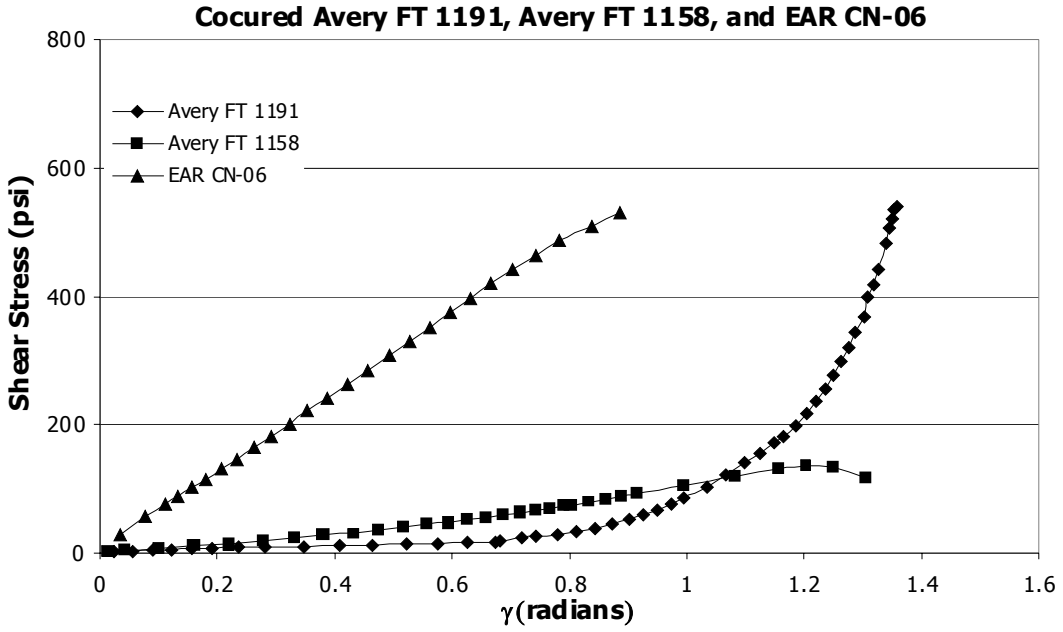

Figure 5-5. Shear stress vs. shear angle γ for Avery FT 1191 (♦), Avery FT 1158 (■), and EAR CN-06 (▲) cocured damping materials.

Table 5-2. Experimental moduli of cocured damping materials, manufacturer's listed moduli at 0.1 Hz. and ambient temperature, and % difference from the manufacturer's moduli.

Damping Material	Initial Shear Modulus of Cocured Sample (psi)	Manufacturers' Listed Shear Modulus at 0.1Hz. and Ambient Temperature (psi)	Difference
Avery FT 1125	57.6 ± 1.6	17.4	231%
Avery FT 1182	129.7 ± 1.0	18.9	586%
Avery FT 1191	22.6 ± 2.2	24.7	-8.5%
Avery FT 1158	72.9 ± 9.0	no data given	---
3M ISD-112	113.6 ± 2.6	10.9	942%
3M ISD-113	67.6 ± 1.4	7.5	801%
3M ISD-130	213.8 ± 23.2	145.0	47.4%
EAR CN-06	573.7 ± 40.0	4,833	-88.1%

5.5 Comparison of different barrier film materials

Previously, it's been shown that during the cure cycle, epoxy often interacts with the damping material, often reducing the effective damping.[69] To prevent this problem, a barrier layer was placed between the damping material and composite. The barrier layer successfully increased the damping to the predicted levels. Kapton polyimide film was the barrier layer used in the original test, primarily because of its availability. Other films were investigated, and two that were found to meet the requirements of being very thin and able to withstand the 250^{o}F to 350^{o}F standard cure temperature were Tedlar and polyester. Samples were made with the three films as barrier layers, described in Table 5-3; Avery FT 1125 was the damping material used. The first concern is the damping level, and therefore vibrations tests were performed on graphite/epoxy composite samples made with a [0/+15/-15/+15/0/barrier layer/FT 1125/barrier layer/0/+15/-15/+15/0] layup. The films had slightly different thicknesses, but not enough to affect the natural frequencies, shown in Figure 5-6a. The loss factor of three modes of interest (first bending, first torsion, and first chordwise) are shown in Figure 5-6b. Tedlar had a slightly higher loss factor in the first bending mode (0.25 compared to 0.22 and 0.23 for Kapton and polyester, respectively), but the three samples were very similar in the torsion and chordwise modes.

Graphite/epoxy composite samples were made with the three barrier layers on either sided of FT 1125 damping material. Calculations were made of the entire "damping sandwich", meaning the thickness used to determine the angle γ was that of

the damping material plus the barrier layers. The shear stress vs. shear angle curve for composite samples made with barrier layers on either side of FT 1125 damping material are shown in Figure 5-7. The initial modulus was slightly higher for the sample with FT 1125 and Tedlar (16.6 psi) than for the samples with FT 1125 and Kapton (13.3 psi) and Avery FT 1125 and polyester (11.5 psi). The sample with FT 1125 and a Tedlar barrier layer, however, had a much higher secondary modulus (1927 psi compared to 711 psi for FT 1125 with Kapton and 671 psi for FT 1125 with polyester). At low strains the damping material shear was dominant, but at high strains the damping material was observed to be debonding from the barrier layer, indicating the high strain (secondary) shear modulus is a measure of bond strength. Although damping materials embedded within composites should never experiences strains that high, this indication of superior bonding could make Tedlar better in fatigue and creep.

Graphite/epoxy composite samples were made with each of the three barrier films and no damping material; shear test results are plotted in Figure 5-8. Polyester and Kapton films had similar shear moduli (118.0 psi and 116.2 psi, respectively which were less than half the shear modulus of Tedlar (260.9 psi). Using the moduli of the barrier layers and the moduli of the "damping sandwich", the moduli of the damping material cured with the barrier layers could be calculated to see how it compares to the manufacturer's given modulus. Figure 5-9 shows the shear angles and thicknesses of the damping layer, barrier layer, and damping sandwich. The

modulus of the damping layer (G_{DL}), barrier layer (G_{BL}), and sandwich (G_{SW}) are defined, in order, as follows:

$$G_{DL} = \frac{\tau}{\gamma_{DL}} \tag{5-2}$$

$$G_{BL} = \frac{\tau}{\gamma_{BL}} \tag{5-3}$$

$$G_{SW} = \frac{\tau}{\gamma_{SW}} \tag{5-4}$$

where τ is a given shear stress, and γ_{DL}, γ_{BL}, and γ_{SW} are the shear angles of the damping layer, barrier layer, and sandwich, respectively. The shear angles are defined as follows:

$$\gamma_{DL} = \tan^{-1} \frac{x_{DL}}{t_{DL}} \tag{5-5}$$

$$\gamma_{BL} = \tan^{-1} \frac{x_{BL}}{t_{BL}} \tag{5-6}$$

$$\gamma_{SW} = \tan^{-1} \frac{x_{SW}}{t_{SW}} \tag{5-7}$$

where x_{DL}, x_{BL} and x_{SW} are the displacements of the damping layer, barrier layer and sandwich, respectively, and t_{DL}, t_{BL}, and t_{SW} are the thicknesses of the damping layer, barrier layer and sandwich, respectively. To solve for G_{DL} we need to find γ_{DL}. The thickness of the damping layer is known so the only unknown is the displacement of the damping layer, which is the displacement of the sandwich minus the total displacement of the barrier layers:

$$x_{DL} = x_{SW} - x_{BL} \tag{5-8}$$

The displacement of the sandwich can be determined by substituting Equation 5-7 into Equation 5-4 and then solving for the displacement:

$$x_{DL} = t_{SW} \tan\frac{\tau}{G_{SW}} \tag{5-9}$$

The displacement of the barrier layers can be solved using the same steps, and these values are substituted in Equation 5-8 to get the damping layer displacement. The damping layer displacement can then be substituted in Equation 5-5, which will give the shear angle γ_{BL} which can be substituted in Equation 5-2 to get the calculated shear modulus G_{BL}. The calculated shear moduli, along with the shear moduli of the damping sandwiches, the shear moduli of the barrier layers, and the shear moduli of the damping material neglecting the damping layer (assumes all the shearing is in damping material) are shown in Table 5-4. The calculated moduli range from 10.3 psi (FT 1125 with polyester) to 12.8 psi (FT 1125 with Kapton) are all lower than the 17.4 psi shear modulus extrapolated from the manufacturer's nomogram, but the error in extrapolation from a log-scale nomogram is high so this is not an unreasonable difference. The calculated moduli using the barrier layer thickness are only slightly lower than the moduli calculated neglecting the barrier layer, confirming that most of the shear is indeed in the damping layer.

Table 5-3. Barrier layers films used in tests.

Film	Type of film	Thickness
DuPont Tedlar®	Polyvinyl Fluoride (PVF)	0.00078”
DuPont Kapton®	Polyimide (PI)	0.00032”
Polyester (PE)	Polyester (PE)	0.00032”

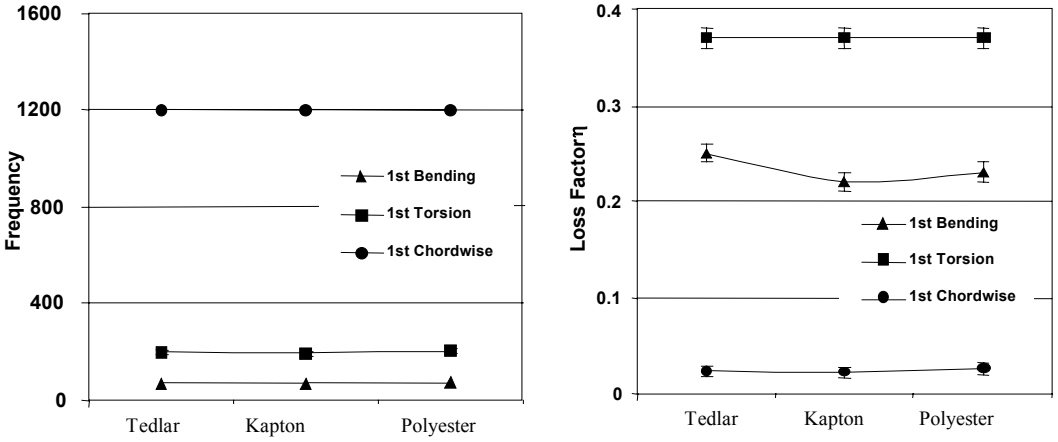

Figure 5-6. Frequencies and Loss Factor of 1st bending, 1st torsion, and 1st chordwise modes of polymeric [0/+15/-15/+15/0/barrier layer/1125 damping material/barrierlayer/0/+15/-15/+15/0] composite plates made with Avery FT 1125 damping material and Tedlar, Kapton, and polyester barrier layers.

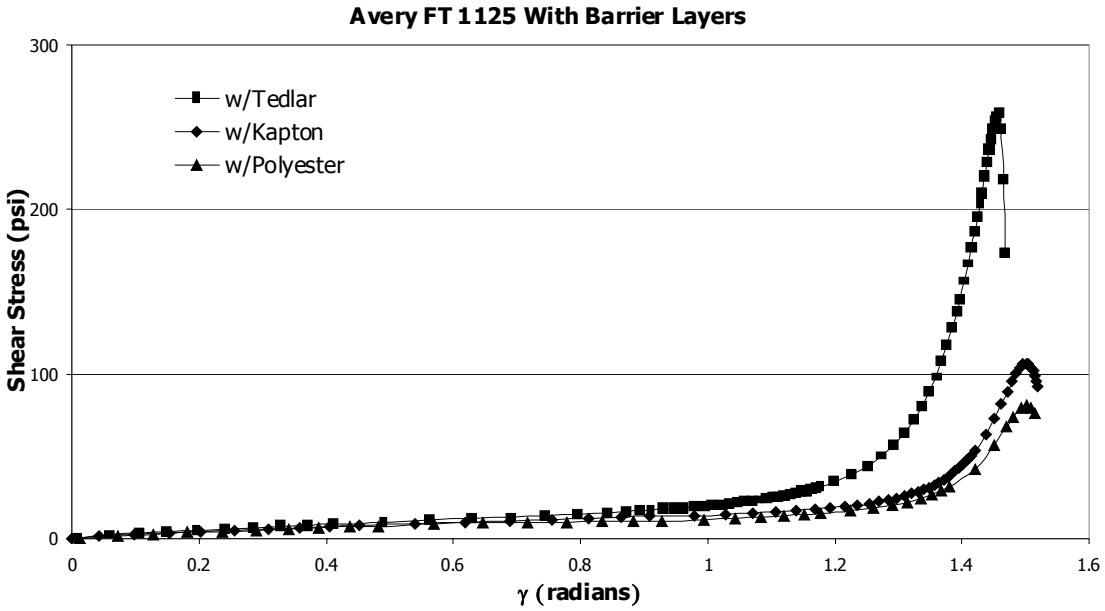

Figure 5-7. Shear Stress vs. Shear angle γ for "damping sandwiches": Avery FT 1125 damping material with various barrier layers.

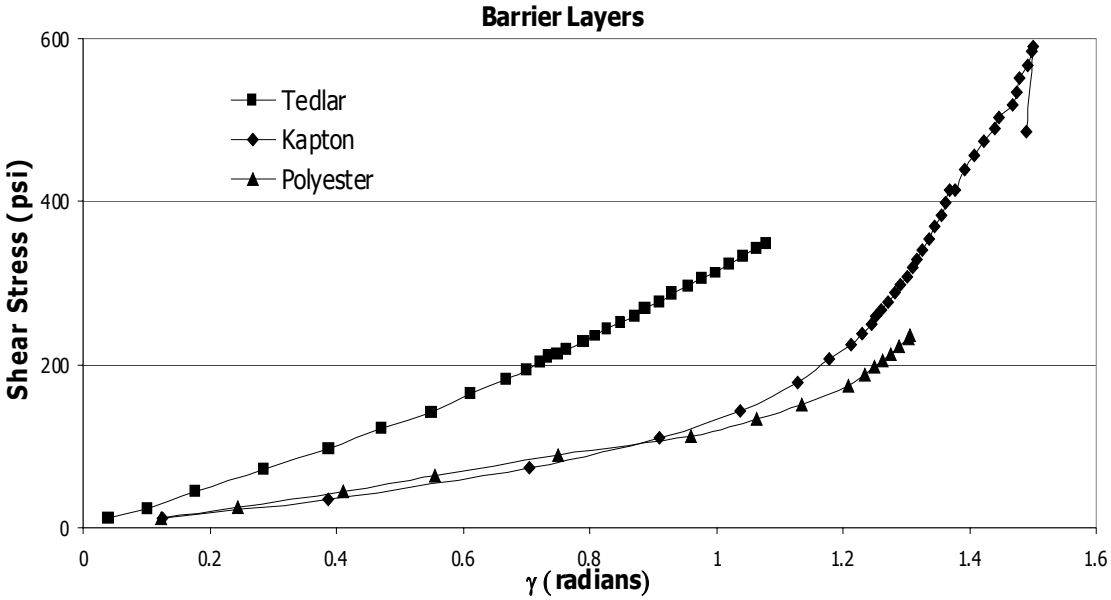

Figure 5-8. Shear Stress vs. Shear angle γ for barrier layers only.

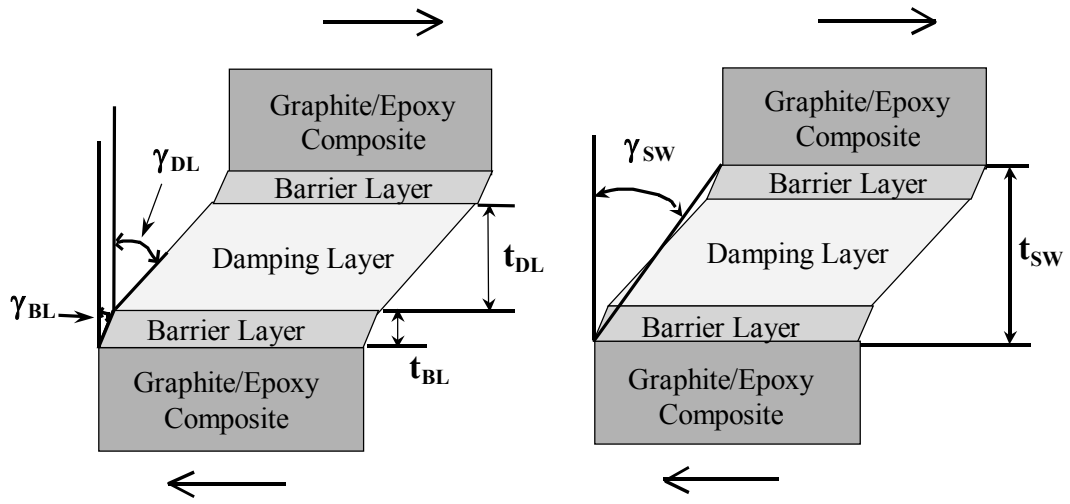

Figure 5-9. Schematic of shear test showing the shear angles (γ) and thicknesses (t) of a composite with a damping layer and barrier layers. BL – Barrier Layer, DL – Damping Layer, SW - Sandwich

Table 5-4. Calculation of shear moduli of Avery FasTape 1125 cocured with barrier layer when barrier layer moduli are considered.

Barrier Layer	Shear modulus of entire "damping sandwich", (psi)	Shear modulus of barrier layer (psi)	Shear modulus neglecting barrier layer thickness(psi)	Calculated shear modulus of Avery FT 1125 (psi)
Tedlar	16.6 ± 0.3	260.9 ± 5.4	14.3 ± 0.2	12.8
Kapton	13.3 ± 2.9	116.2 ± 9.7	12.5 ± 2.7	11.9
PE	11.5 ± 0.7	118.0 ± 8.5	10.6 ± 0.7	10.3

5.6 Shear moduli of cocured damping materials with Tedlar barrier film

In the previous section it was indicated that Tedlar appears to have superior bonding with the acrylic-based damping materials. In this section shear tests were performed on graphite/epoxy samples with various damping materials (Avery FT 1125, Avery FT 1191, Avery FT 1182, and 3M ISD-112) and a Tedlar barrier layer to compare the moduli to the manufacturer's listed moduli. Figure 5-10 shows the shear stress vs. shear angle for the "damping sandwiches" made with Tedlar barrier layer

and damping materials. The initial modulus was fairly similar for the damping materials: 16.6 psi for FT 1125, 52.1 psi for FT 1182, 22.7 psi for FT 1191, and 11.2 psi for ISD-112. The secondary modulus, however, was much higher for FT 1191 (18,920 psi) than the other materials (1927 psi for FT 1125, 2785 psi for FT 1182, and 5000 psi for ISD-112). The FT 1191 is a rubber-based damping material whereas the other three are acrylic-based. A comparison of the measured shear moduli and calculated moduli using the barrier layer modulus (using the same procedure as in the previous section) along with manufacturers' predicted values is given in Table 5-5. The calculated shear moduli are at most 12psi different than the moduli taken from the manufacturer's nomograms (the maximum was for FT 1182 where the given shear modulus is 18.9 psi and the calculated shear modulus is 30.9 psi). The nomograms for the Avery materials required extrapolation to 0.1 Hz.; the differences with manufacturers supplied data sheets are most likely due to the extrapolation or inaccuracies in advertised material nomograms.

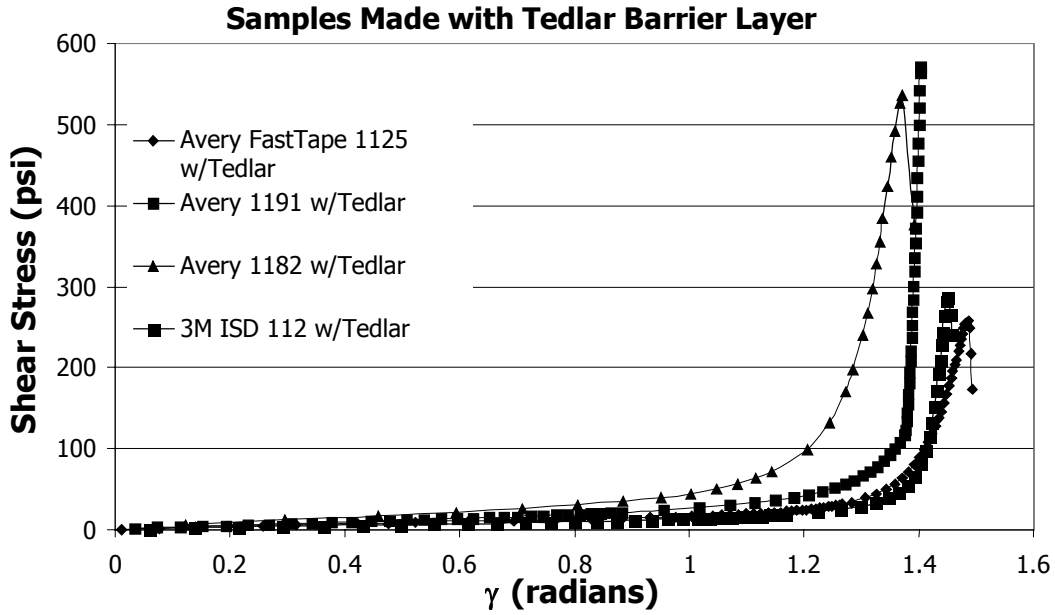

Figure 5-10. Shear stress vs. shear angle γ for "damping sandwiches": various damping material with Tedlar barrier layers.

Table 5-5. Calculation of shear moduli of damping materials cocured with Tedlar when Tedlar modulus is considered.

Damping Material	Modulus of entire "damping sandwich"(psi)	Modulus of Tedlar (psi)	Modulus neglecting barrier layer thickness(psi)	Calculated modulus of Damping Material (psi)	Manufact .given modulus (psi)
Avery FT 1125	16.6 $\pm$ 0.3	260.9 $\pm$ 5.4	14.3 $\pm$ 0.2	12.8	17.4
Avery FT 1182	52.1 $\pm$ 1.8	260.9 $\pm$ 5.4	31.3 $\pm$ 1.0	30.9	18.9
Avery FT 1191	22.7 $\pm$ 1.0	260.9 $\pm$ 5.4	20.3 $\pm$ .9	19.8	24.7
3M ISD-112	11.2 $\pm$ 3.2	260.9 $\pm$ 5.4	9.3 $\pm$ 2.4	8.5	10.9

5.7 Shear moduli of cocured damping materials having an embedded mesh (no barrier film)

Often a loose-weave mesh is inserted in the damping material to help prevent the damping material from creeping. Two types of loose-weave mesh were used in this experiment. The first was a 0.006" thick loose weave fiberglass and the other was a 0.009" thick tighter weave nylon mesh. No barrier film was used in the shear tests

(tests with a barrier film are described in the next section) and thus some infiltration of the laminate epoxy into the damping material and loose-weave mesh was expected. The samples were cocured, and thus went through an autoclave cure cycle that included 100 psi pressure and a vacuum of 12.3 psi. The pressure and vacuum worked to press the damping material into the mesh.

The shear stress vs. strain angle of the samples made with Avery FT 1125 and fiberglass mesh at $0^o/90^o$, $\pm 45^o$, and $+22.5^o/-67.5^o$, nylon mesh at $0^o/90^o$, and a control with no mesh are shown in Figure 5-11. The moduli and yield shear stresses are given in Table 5-6. The control had approximately half the modulus of the samples with mesh, but it yielded at a much higher shear stress. Under small shear stresses the mesh contained the damping materials and possibly bonded somewhat to the composite because of the epoxy infusion, increasing the shear modulus. At high shear stresses (possibly after the "bond" between the mesh and composite had failed), however, the mesh was observed cutting through the damping material and thus decreased the shear stress necessary for failure. The moduli for the samples with the loose weave mesh were close but the $0^o/90^o$ fiberglass mesh was slightly higher than the other fiberglass mesh samples. The samples with the tighter weave nylon mesh had a higher initial modulus but then yielded at a lower shear stress, although by a different mechanism than the fiberglass samples. The fiberglass samples failed by debonding completely along the damping material with no mesh pull-out, meaning the mesh remained bonded to one side of the shear sample. The nylon mesh, however, pulled out and ripped apart in almost all of the samples. Figure 5-12 and Figure 5-13

are photographs of graphite/epoxy shear samples, after testing, with FT 1125 damping material and fiberglass mesh and nylon mesh, respectively.

Vibrational damping test samples were also made, with a layup of [0/15/-15/FT 1125/mesh/FT 1125/-15/15/0]. There was very little variation in frequencies of the samples, shown in Figure 5-14, with the exception of the first torsion mode of vibration for the sample with fiberglass mess (it was 168 Hz. while the first torsion mode for the nylon mesh sample had a frequency of 204 Hz.). For the first bending and first torsion modes, the loss factor for composite samples made with FT 1125 and the loose weave mesh were slightly lower overall than samples with no mesh and those made with the tighter weave nylon mesh were significantly lower, as shown in **Figure 5-15.** Damping in the chordwise mode was relatively unaffected by the mesh.

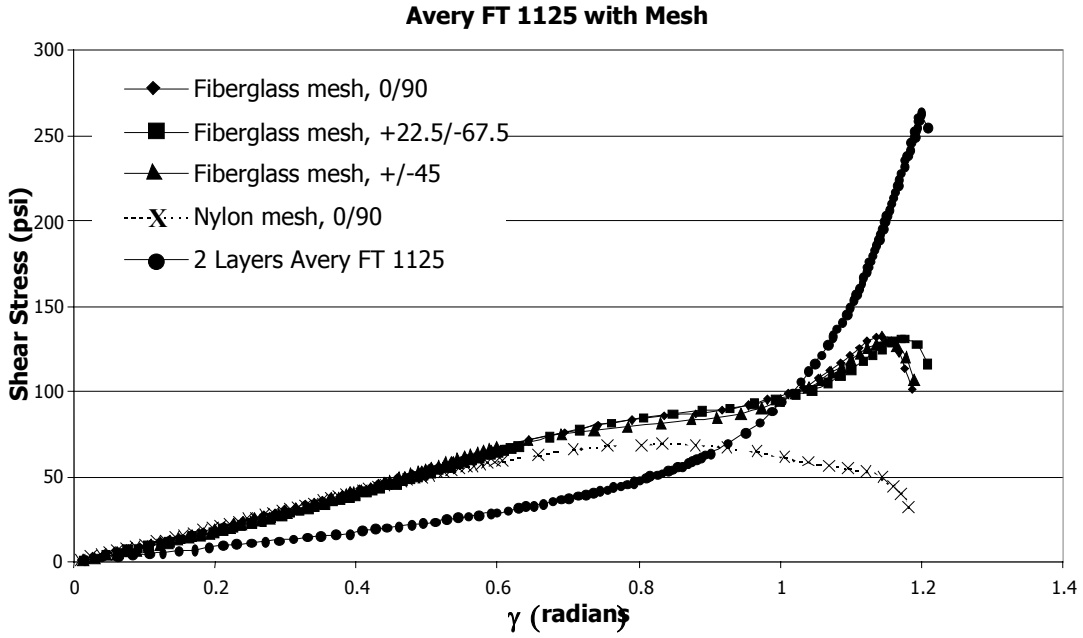

Figure 5-11. Shear stress vs. strain angle of samples made with two layers Avery FT 1125 damping material with either fiberglass or nylon mesh between the layers.

Table 5-6. Shear moduli and yield shear stress of samples shown in Figure 5-11.

Sample	Shear Modulus (psi)	Yield Shear Stress (psi)
Control, 2 Layers Avery FT 1125	42.4 ± 1.2	271.1 ± 16.5
2 Layers Avery FT 1125 with loose weave fiberglass mesh between layers at $0^o/90^o$	93.2 ± 3.3	132.1 ± 3.7
2 Layers Avery FT 1125 with loose weave fiberglass mesh between layers at ±45	89.6 ± 3.0	131.1 ± 2.7
2 Layers Avery FT 1125 with loose weave fiberglass mesh between layers at $+22.5^o/-67.5^o$	81.1 ± 4.4	133.1 ± 2.3
2 Layers Avery FT 1125 with loose weave nylon mesh between layers at $0^o/90^o$	102.1 ± 2.2	68.8 ± 2.0

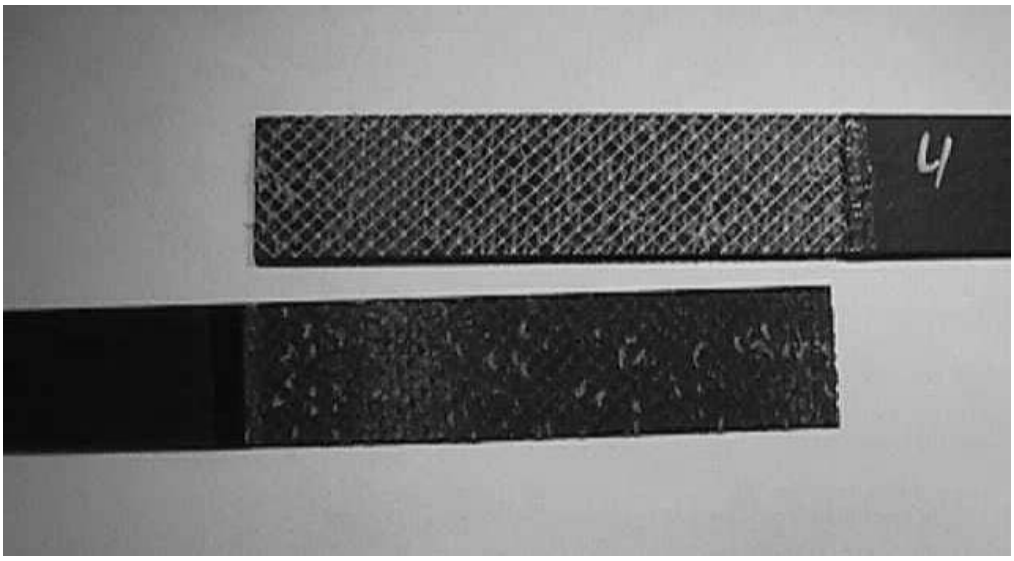

Figure 5-12. Shear sample, after testing, of graphite/epoxy with Avery FT 1125 damping material and fiberglass mesh. The mesh remained embedded in the "top" side.

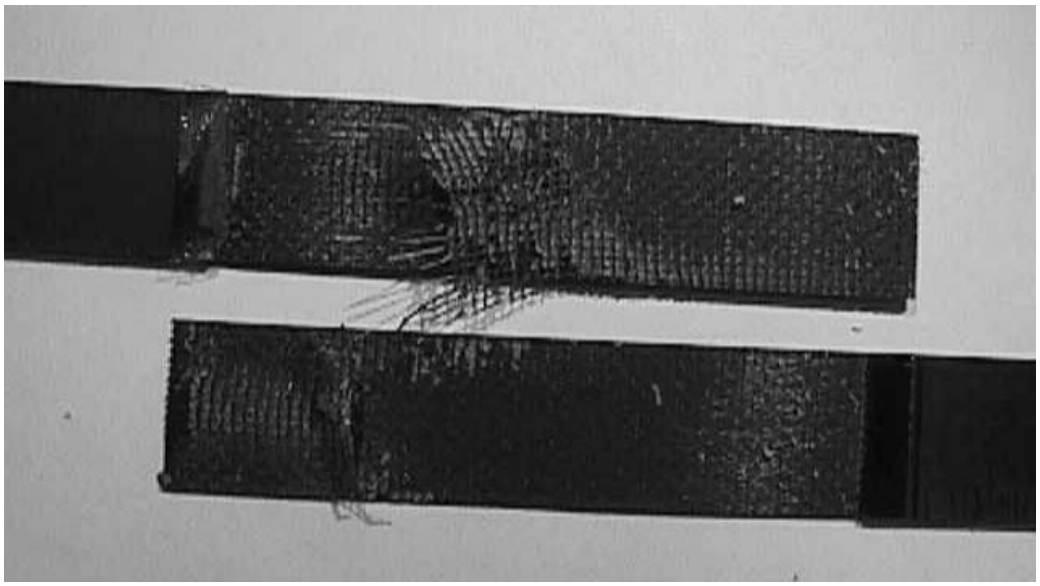

Figure 5-13. Shear sample, after testing, of graphite/epoxy with Avery FT 1125 damping material and nylon mesh. The mesh ripped apart during the shear testing.

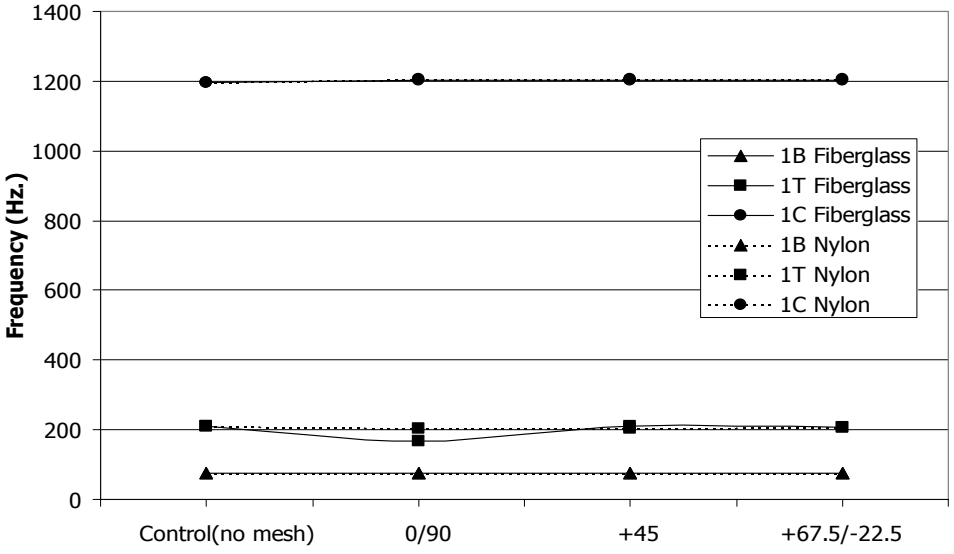

Figure 5-14. Frequency of 1st bending (▲), 1st torsion (■), and 1st chordwise (●) modes of composite samples made with no mesh (control), and both loose-weave fiberglass mesh (—) and tight-weave nylon mesh(---) at 0°/90 °, ±45 °, and +22.5°/-67.5° between two layers of Avery FT 1125.

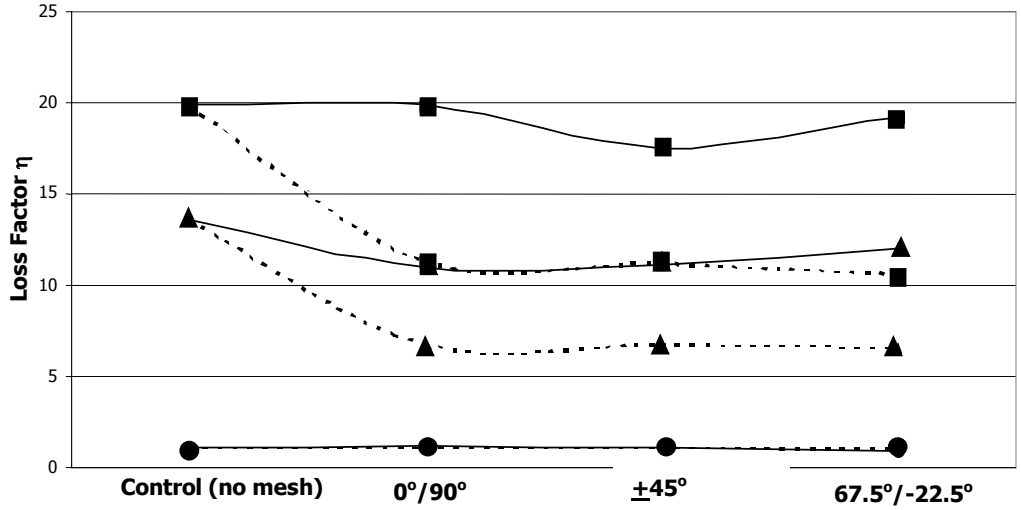

Figure 5-15. Loss Factor of 1st bending (▲), 1st torsion (■), and 1st chordwise (●) modes of composite samples made with no mesh (control), and both loose-weave fiberglass mesh (—) and tight-weave nylon mesh(---) at 0°/90 °, ±45 °, and +22.5°/-67.5° between two layers of Avery FT 1125.

5.8 Shear moduli of cocured damping materials having an embedded mesh (with barrier film)

Graphite/epoxy shear test samples were manufactured with loose weave fiberglass mesh between layers of Avery FT 1125 and a Tedlar barrier layer between the Avery FT 1125 and the composite. These were identical to those in the previous section with the addition of a Tedlar barrier layer. The shear stress vs. strain angle of the samples made with the Tedlar barrier layer and fiberglass mesh at $0^o/90^o$, $\pm 45^o$, and $+22.5^o/-67.5^o$, and a control with no mesh are shown in Figure 5-16; the initial moduli are given in Table 5-7. The samples with the mesh had only slightly higher initial moduli than the control sample without mesh (the highest was $0^o/90^o$ at 19.3 psi and the control was 16.6 psi) and a much lower yield shear stress. The $0^o/90^o$ mesh sample had a slightly higher modulus and failure load than the samples with the $\pm 45^o$ and $+22.5^o/-67.5^o$ mesh. As in the previous section, the mesh seemed to cut through the damping material and thus decrease the yield shear stress.

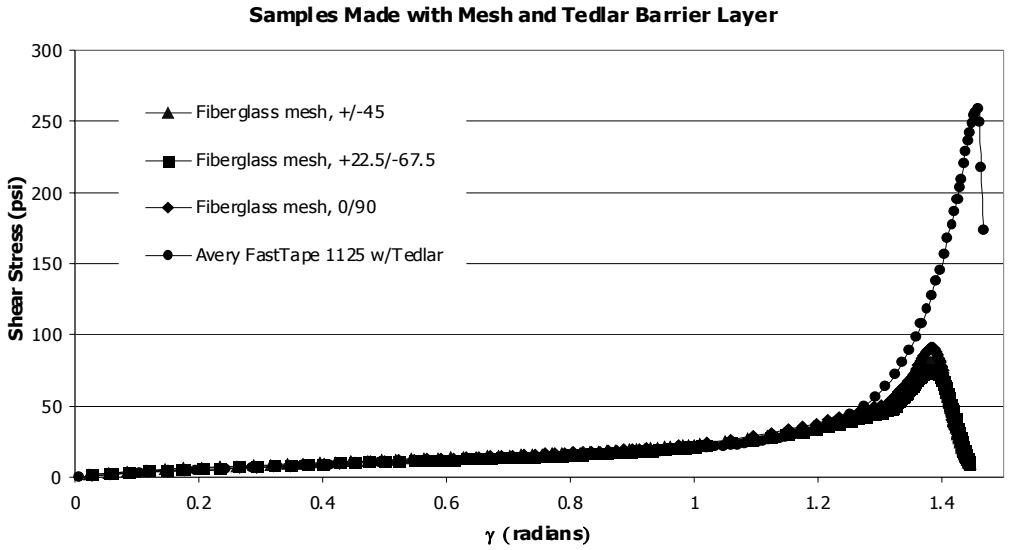

Figure 5-16 Shear stress vs. strain angle of samples made with fiberglass mesh and control with no mesh.

Table 5-7. Shear moduli and yield shear stress of samples shown inFigure 5-16.

Sample	Shear Modulus (psi)	Yield Shear Stress (psi)
Control, Avery FT 1125 with Tedlar	16.6 ± 0.3	256.3 ± 7.4
2 Layers Avery FT 1125 with loose weave fiberglass mesh between layers at $0^o/90^o$, with Tedlar	19.3 ± 0.9	87.0 ± 4.4
2 Layers Avery FT 1125 with loose weave fiberglass mesh between layers at ±45, with Tedlar	17.0 ± 0.8	78.3 ± 2.9
2 Layers Avery FT 1125 with loose weave fiberglass mesh between layers at $+22.5^o/-67.5^o$, with Tedlar	17.4 ± 2.6	76.9 ± 3.0

5.9 Conclusions

The shear test results in this investigation help characterize viscoelastic damping materials cocured within graphite/epoxy composites. It was shown that the shear moduli of the acrylic-based cocured samples ranged from 1.5 (ISD-130) to 10.4 (ISD-

112) times higher than the manufacturer's given non-cocured damping material moduli. This increase was caused by epoxy penetration into the damping material during the cure. The rubber-based Avery FT 1191 material shear modulus was within 8.5% of the shear modulus taken from the manufacturer's nomogram, and thus it appeared relatively unaffected by the epoxy. The EAR CN-06 shear modulus was tremendously less than the shear modulus taken from the manufacturer's nomogram and although the cause for that is unknown it was suspected that a hot-press operation to get it to the desired thickness might have been the cause.

Three barrier layer films, used to prevent epoxy/damping material interaction, were tested: Tedlar, Kapton, and polyester. Composite samples made with the three barrier layers had comparable damping capabilities and initial shear moduli, although the Tedlar had a much higher shear modulus at high strains and also a much higher yield shear stress. Composite samples having Tedlar barrier film and different damping materials (Avery FT 1125, 1182, 1191, and 3M ISD-112) had shear moduli that were within 20% (for Avery FT 1191) to 57% (for Avery FT 1182) of shear moduli taken from the manufacturer's supplied nomograms.

The last shear test performed involved placing "scrim cloth" or a loose-weave mesh between two layers of Avery 1125 damping material, both with and without a barrier layer. In the samples without a barrier layer, the loss factor in the 1st bending and 1st torsion modes of the loose weave glass mesh were better than the more tightly woven nylon mesh (the nylon mess sample loss factors were typically 40% less than the fiberglass mesh sample loss factors). The shear tests showed that the glass mesh

nearly doubled the modulus over the no mesh sample, but its yield shear stress load was significantly lower. Under small loads, the mesh contained the damping materials and decreased the amount of strain (i.e. increases shear stiffness). At high loads, however, the mesh cut through the damping material. The modulus for the $0^o/90^o$ fiberglass mesh was slightly higher than the other fiberglass mesh orientations. The fiberglass samples failed by debonding completely along the damping material. The nylon mesh, however, pulled out and ripped apart in all samples. Samples with the mesh and the barrier layer had much smaller initial moduli than samples without the barrier layer but were only slightly higher than the barrier layer control sample without the mesh. The yield shear stress, however, was much smaller for the samples with the mesh. As in the samples without the barrier layer, the mesh seemed to cut through the damping material in samples with the barrier layer.

This shear test method used composite laminates with a symmetric lay-up and 0^o ply layers next to the material being sheared. Future work would include investigating the importance of ply angle adjacent to the damping material. For very low modulus materials it is assumed the effects would be negligible but it's possible that higher modulus damping materials might be behave differently when cured next to, for example, a 90^o composite layer compared to a 0^o layer.

This chapter, in part, will be submitted for publication to the *Journal of Composite Materials* with the title "Shear Measurements of Cocured Viscoelastic Damping Materials". The dissertation author was the primary investigator and co-authored the article with advisor J. B. Kosmatka.

Chapter 6 Directional Damping Tests

Viscoelastic damping materials behave isotropically which means that their stiffness and damping properties are the same in all directions. There is a desire to develop damping materials that behave orthotropically so that the stiffness and damping properties vary with material orientation. Thus, a designer can directionally tailor the stiffness and damping properties within the laminate to better damp (or control) a particular mode without suppressing other more desirable modes. A low modulus material could be made orthotropic by embedding strands of a stiffer material while a "high-modulus" material (in this case acrylic) could be made to act in an orthotropic manner by cutting many fine parallel off-angle slots in the material. The slotted acrylic has significant directional stiffness that follows classic lamination theory.[70] The presence of the acrylic slots significantly changes the energy loss (damping) mechanism of the material, from a single pure shear (isotropic) mechanism to three (orthotropic) mechanisms that depend upon the mode type and acrylic orientation angle. These three mechanisms, which have been proposed by other researchers, involve unique damping coefficients for longitudinal, transverse, and longitudinal-shear deformations.[71-74]

The objective of this research was to make a directional damping layer using isotropic materials within an isotropic sandwich so that there would be no interference with the directional damping material layer. Frequency and loss factors were measured for six out-of-plane vibration modes. Acrylic (with silicone damping

material embedded in slots) was used for the "directional layer" and polycarbonate was used for the outside sandwich layers.

6.1 Sample Fabrication

The test specimens were manufactured by sandwiching a 0.060" thick Plaskolite Optix® acrylic directional layer between 0.020" thick standard polycarbonate layers, as shown in Figure 6-1. The overall cut dimensions were 11.00" by 4.00". The directional acrylic layer was made using a LaserCAMM™ Model 2410 CO_2 laser to cut out 0.050" wide slots with 0.070" spacing between the cuts. Slots were cut from 0^o to 90^o in 15^o increments. A 0.33" border was left on the three unclamped sides for handling purposes and a 3.00" length was left on the clamping end. Acrylic was chosen because it was easily cut by the LaserCAMM™ and retained dimensional stability even when the thin slots were being cut. Polycarbonate sheets were used on the outside layers; polycarbonate was chosen because the thin sheets had consistent thicknesses.

Both sides of the acrylic and the inner sides of the polycarbonate were sanded to improve bonding. One polycarbonate outer layer was glued to the acrylic using 1.0 $\pm$ 0.05 grams of standard two-part epoxy. The epoxy was applied evenly with a paintbrush and then the two pieces were placed in a vacuum bag for two hours to press the sides together and ensure good bonding during cure. The silicone damping material, consisting of 30% Dow Corning Sylgard® 182 two-part silicone elastomer and 70% Dow Corning Sylgard® 527 two-part dielectric silicone gel, was then mixed

and added to the cut-out slots. A combination was used because the 527 gel, which had greater damping, was too "sticky" when cured (and thus would pull out of the slots when the plastic layer used during cure was removed) and the addition of the 182 gel made it easier to handle. The shear modulus of the gel was 15 psi and the loss factor of the combination ranged from 0.07 to 0.15, depending on the frequency. To make certain that the silicone damping material cured flush with the acrylic a piece of easy release plastic was placed over the uncured damping material, the outer layer was placed on top, and then the entire sandwich was placed in a vacuum bag that pressed the "sandwich" together and squeezed out all the excess damping material. After curing the plastic was peeled off and the exposed acrylic very lightly sanded again to improve bonding to the outer layer. The second polycarbonate outer layer was then coated with epoxy and placed on the acrylic/damping material layer. Again, the sample was placed in a vacuum bag for two hours while the epoxy cured.

The border was then cut off of the samples using the LaserCAMM™; the final samples were 3.29" wide, 10.70" long, and 0.10" thick. Figure 6-2 shows the dimensions before and after the final cut and Figure 6-3 is a photograph of the 0^o sample.

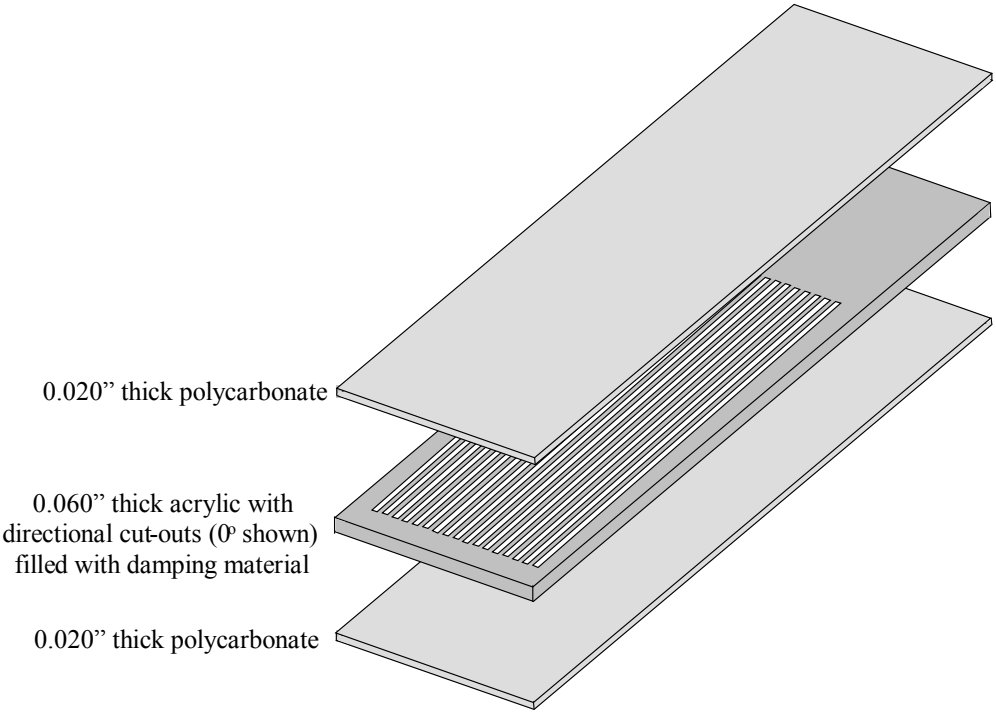

Figure 6-1. Lay-up showing acrylic directional damping layer (slots filled with Dow Corning Sylgard® 182 elastomer and Sylgard 527® dielectric gel) and polycarbonate outer layers.

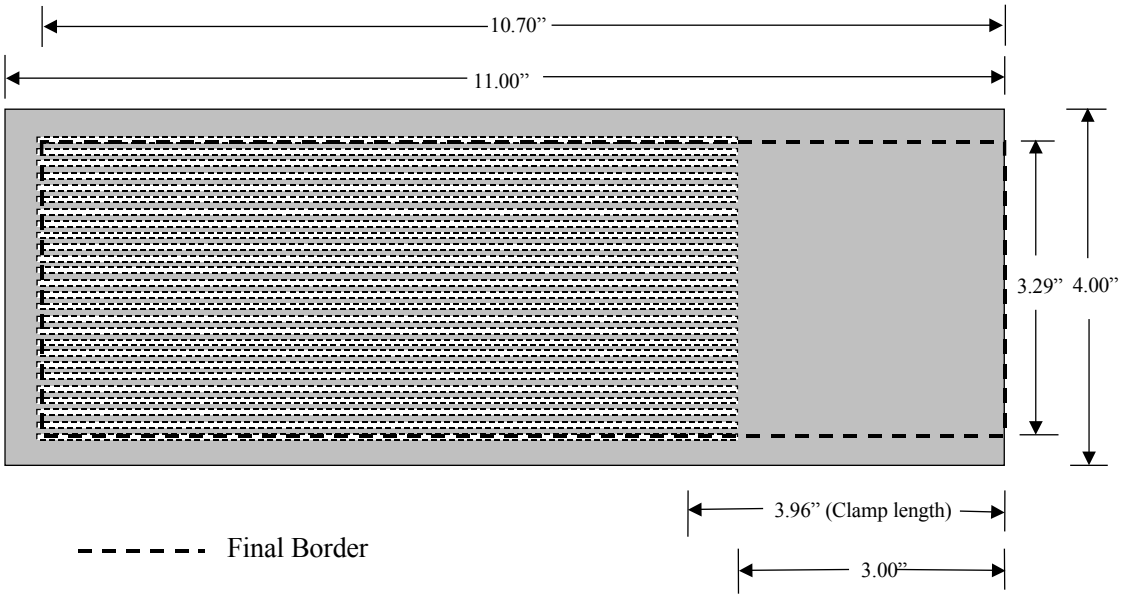

Figure 6-2. Assembled dimensions and dimensions after final cut (- - -) of sample with acrylic directional damping layer (slots filled with Dow Corning Sylgard® 182 elastomer and Sylgard 527® dielectric gel) and polycarbonate outer layers.

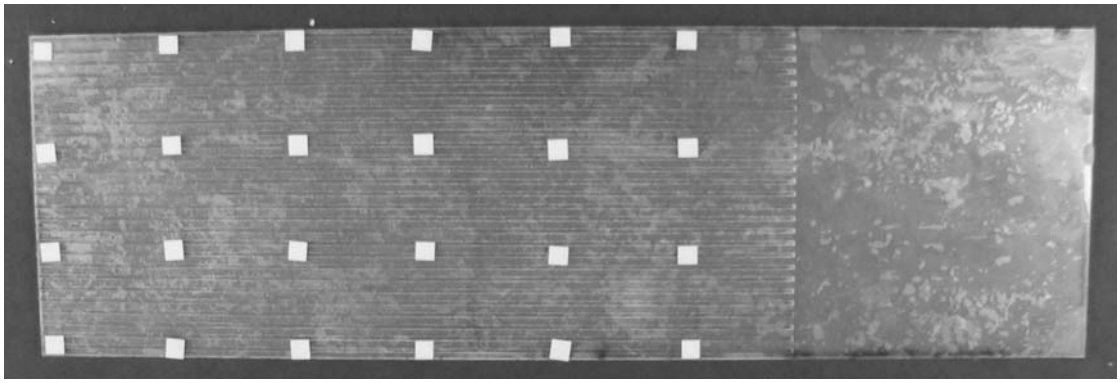

Figure 6-3. Photo of the 0^o test sample. The silver squares are the reflective tape used for the laser vibrometer testing.

6.2 Vibration Testing

Vibration tests were performed on the samples in order to obtain natural frequency and damping results for the first, second, and third bending modes, the first and second torsion mode, and the chordwise mode. Vibration tests were performed with a 3.96" clamp length (0.96" into the directional area) to minimize clamping effects. A speaker was used to provide broadband excitation from 0 to 700 Hz. and a scanning laser vibrometer (Polytec PI) was used to measure the plate velocity response. An initial area scan was performed on the 0^o sample to characterize the modes and then the samples were compared using a single point scan on the outer corner. The damping was measured using LMS's Cada X software, which used a time domain multi-degree-of-freedom curvefitter. One specimen was tested per angle and each specimen was tested twice. All tests were performed at room temperature.

6.3 Results

As predicted by classic lamination theory, the frequency decreased steadily with increased directional layer angle in all the bending modes; the changes from the sample with the 0^o directional layer to the sample with a 90^o directional layer were 10% to 12%. Table 6-1 lists the frequencies and loss factors for all the samples and modes. Figure 6-4, Figure 6-6, and Figure 6-8 show plots of the frequencies of the first bending, second bending, and third bending modes, respectively.

The loss factor values for the bending modes also decreased with increased angle; the damping for first bending, second bending, and third bending modes are shown in Figure 6-5, Figure 6-7, and Figure 6-9, respectively. The relative changes were quite large; for example in first bending the loss factor for the 90^o sample was approximately 54% of the loss factor for the 0^o sample.

Because the torsion mode is twisting rather than bending the first torsion mode showed a different trend than the bending modes. As shown in Figure 6-10, the frequency was highest for the 0^o sample (93.3 Hz.), decreased slightly for the 15^o and 30^o samples, increased for the 45^o sample (91.2 Hz.) and then decreased as the angle increased; the lowest frequency was for the 90^o sample (87.2 Hz). The loss factor, shown in Figure 6-11, was highest for the 45^o sample at 0.0160 and drops to 0.0128 for the 90^o sample.

The chordwise mode is bending across the width of the sample (rather than along it as in bending) and therefore the samples with the higher angles have higher frequencies and loss factors. The frequencies, shown in Figure 6-14, had a minimum

of 595.6 Hz. for the 15^{o} sample, although the 30^{o} sample wasn't much higher at 596.7 Hz. The maximum frequencies occurred at 60^{o} and 75^{o}: 616.9 Hz. and 616.3 Hz. The loss factor, shown in Figure 6-15, followed a similar trend.

Tests were also performed on a control sample with a 30^{o} directional layer and no silicone damping material. The control sample had essentially the same damping as the as the 30^{o} sample with silicone embedded in it. Figure 6-16 and Figure 6-17 show the frequency response functions of the two samples over two frequency ranges, 5 to 200 Hz. and 200 to 700 Hz., respectively. The sample with no added silicone had higher frequencies because of its smaller mass. The acrylic was tested to determine the damping. Its loss factor was found to be 0.070 at 20 Hz., very close to the silicone loss factor. Polycarbonate was also tested and it was determined to have a loss factor of 0.016 at 20 Hz.

Table 6-1 Frequencies and Loss Factors of the various modes for samples with directional damping layer angles ranging from 0^o to 90^o.

	1st Bending		1st Torsion		2nd Bending		3rd Bending		2nd Torsion		ChordWise	
Angle	Frequency (Hz)	Loss Factor	Frequency (Hz)	Loss Factor	Frequency (Hz)	Loss Factor	Frequency (Hz)	Loss Factor	Frequency (Hz)	Loss Factor	Frequency (Hz)	Loss Factor
0^o	22.1	0.0198	93.3	0.0158	139.7	0.0190	391.1	0.0166	585.7	0.0166	602.8	0.0124
15^o	21.3	0.0204	90.8	0.0152	134.6	0.0188	380.8	0.0164	576.3	0.0164	595.6	0.0118
30^o	21.2	0.0176	90.8	0.0156	132.8	0.0170	372.4	0.0148	566.2	0.0148	596.7	0.0120
45^o	20.9	0.0156	91.2	0.0160	130.2	0.0160	366.4	0.0138	563.0	0.0148	607.9	0.0132
60^o	20.2	0.0136	89.2	0.0152	126.7	0.0140	355.2	0.0124	551.3	0.0136	616.9	0.0144
75^o	19.8	0.0110	87.5	0.0136	125.2	0.0122	351.6	0.0102	546.3	0.0124	616.3	0.0148
90^o	19.8	0.0106	87.2	0.0128	123.6	0.0116	347.7	0.0096	541.2	0.0118	612.8	0.0144

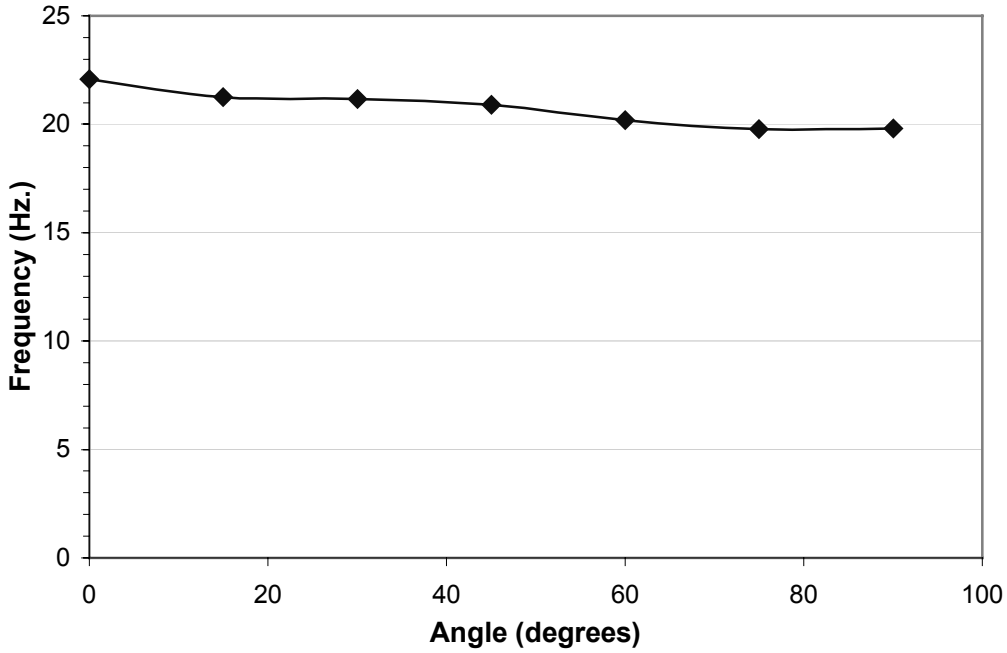

Figure 6-4. Frequency of the first bending mode of samples with an acrylic directional layer at varying angles and polycarbonate outer layers.

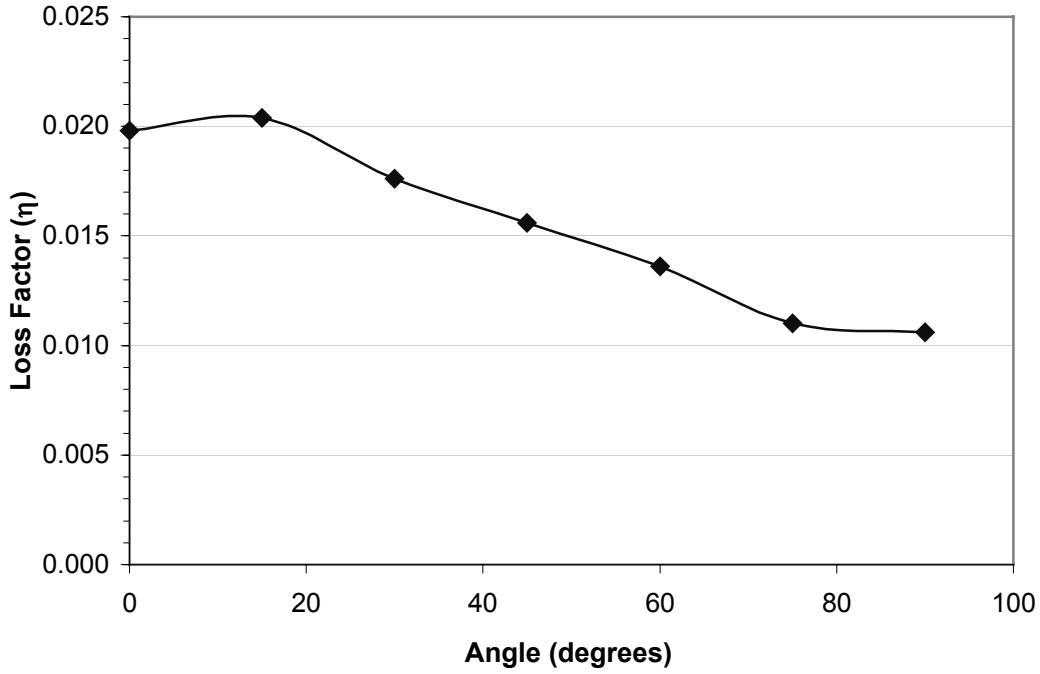

Figure 6-5. Loss factor of the first bending mode of samples with an acrylic directional layer at varying angles and polycarbonate outer layers.

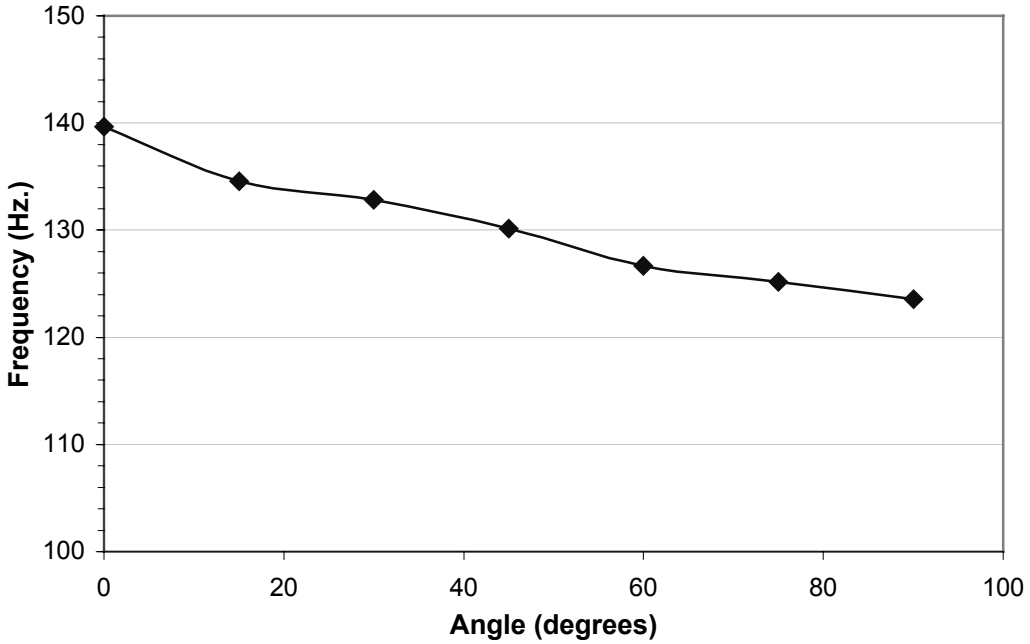

Figure 6-6 Frequency of the second bending mode of samples with an acrylic directional layer at varying angles and polycarbonate outer layers.

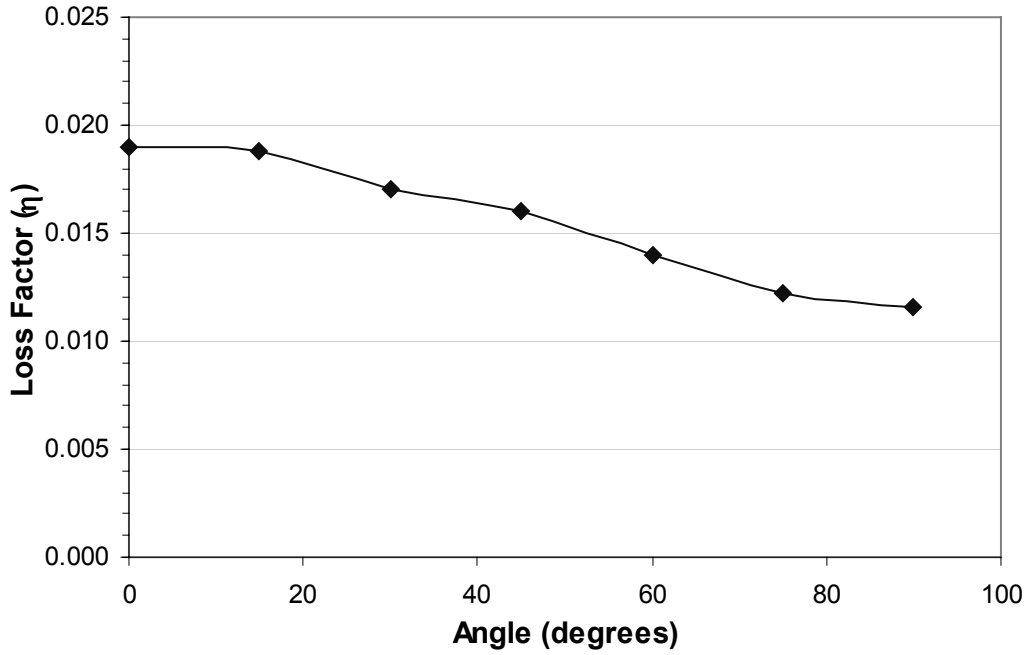

Figure 6-7. Loss factor of second bending mode of samples with an acrylic directional layer at varying angles and polycarbonate outer layers.

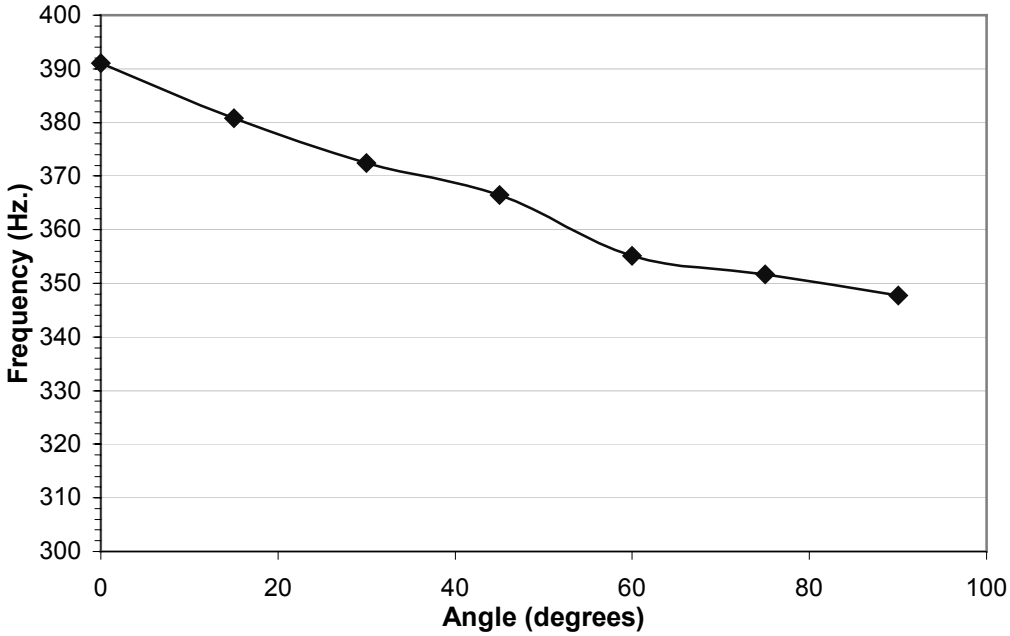

Figure 6-8. Frequency of the third bending mode of samples with an acrylic directional layer at varying angles and polycarbonate outer layers.

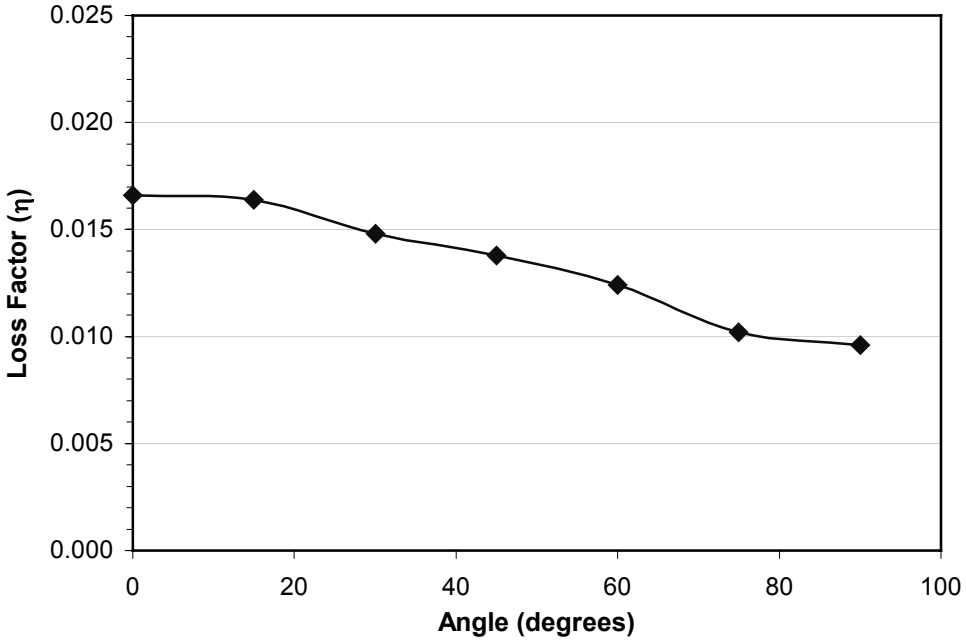

Figure 6-9. Loss factor of the third bending mode of samples with an acrylic directional layer at varying angles and polycarbonate outer layers.

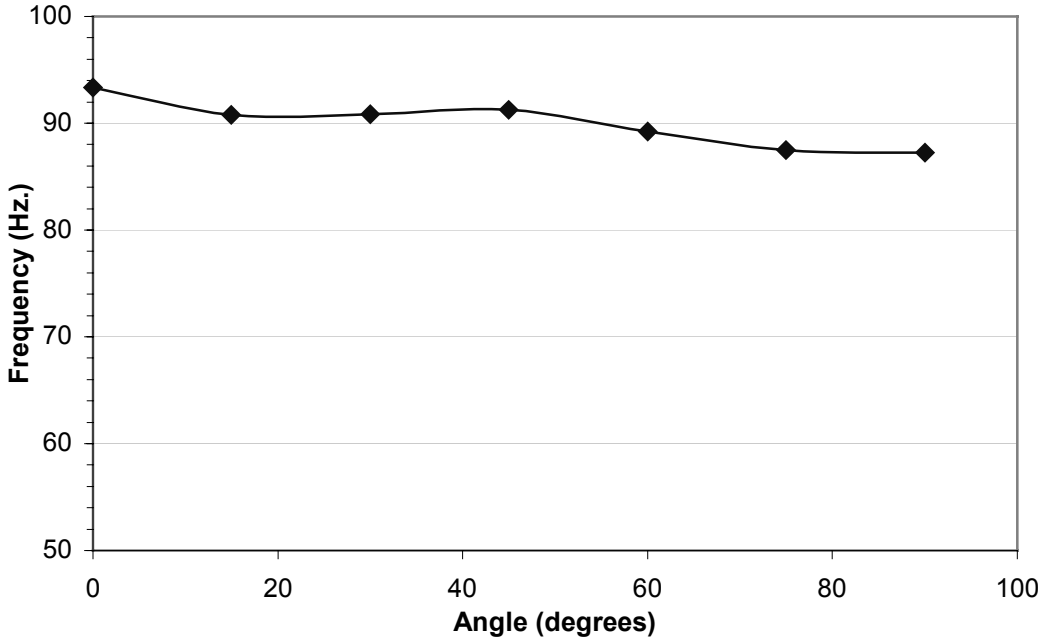

Figure 6-10. Frequency of the first torsion mode of samples with an acrylic directional layer at varying angles and polycarbonate outer layers.

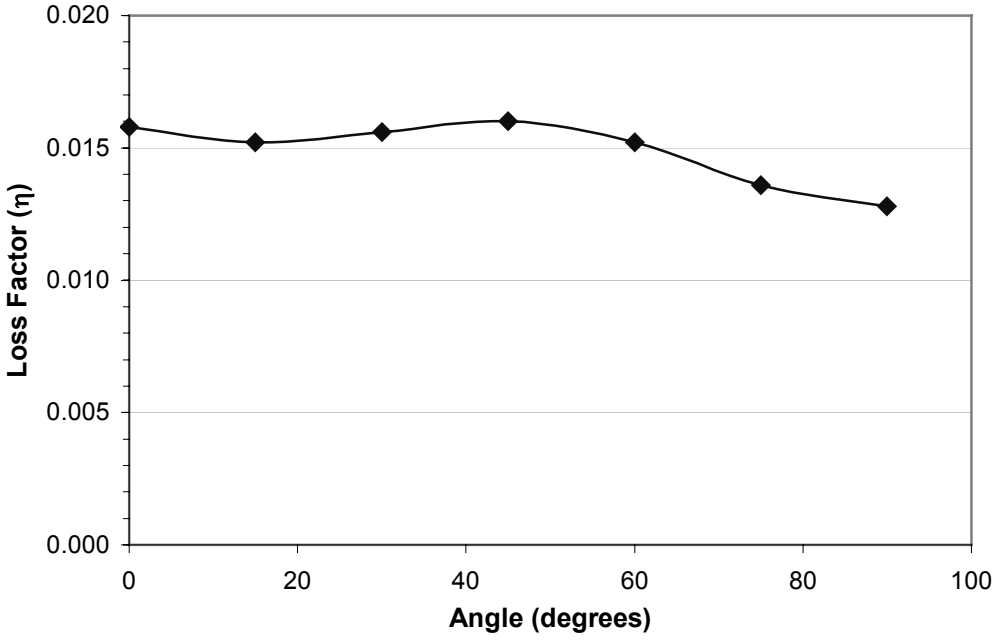

Figure 6-11. Loss factor of the first torsion mode of samples with an acrylic directional layer at varying angles and polycarbonate outer layers.

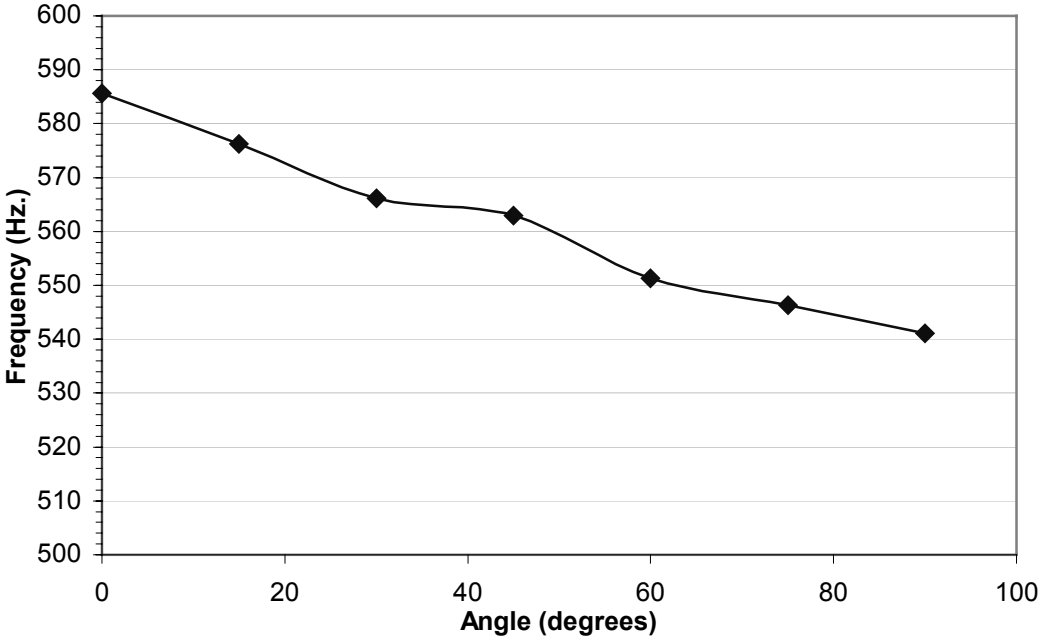

Figure 6-12 Frequency of the second torsion mode of samples with an acrylic directional layer at varying angles and polycarbonate outer layers.

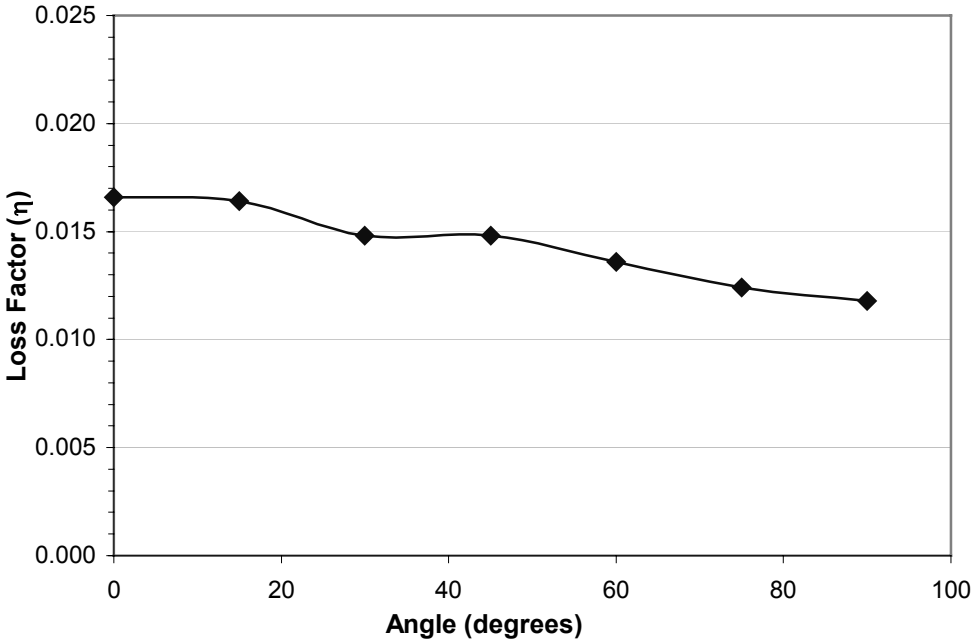

Figure 6-13. Loss factor of the second torsion mode of samples with an acrylic directional layer at varying angles and polycarbonate outer layers.

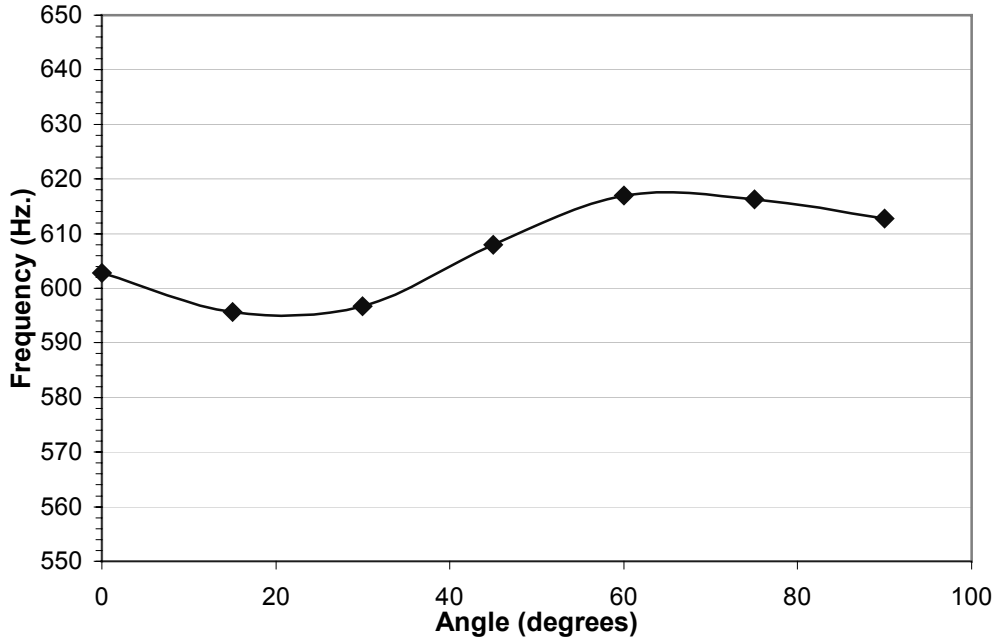

Figure 6-14. Frequency of the first chordwise mode of samples with an acrylic directional layer at varying angles and polycarbonate outer layers.

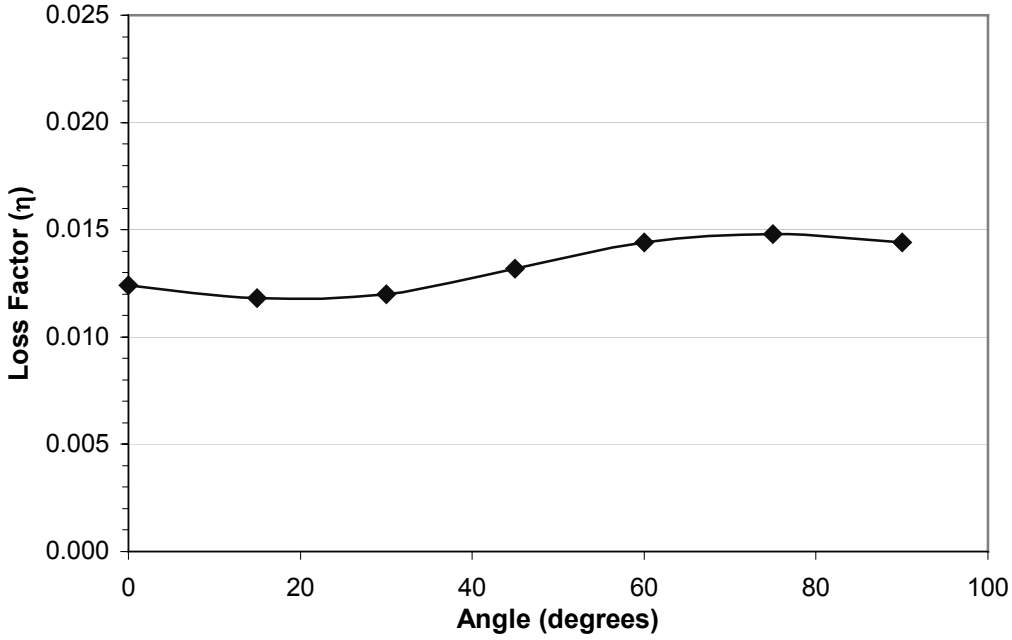

Figure 6-15. Loss factor of the first chordwise mode of samples with an acrylic directional layer at varying angles and polycarbonate outer layers.

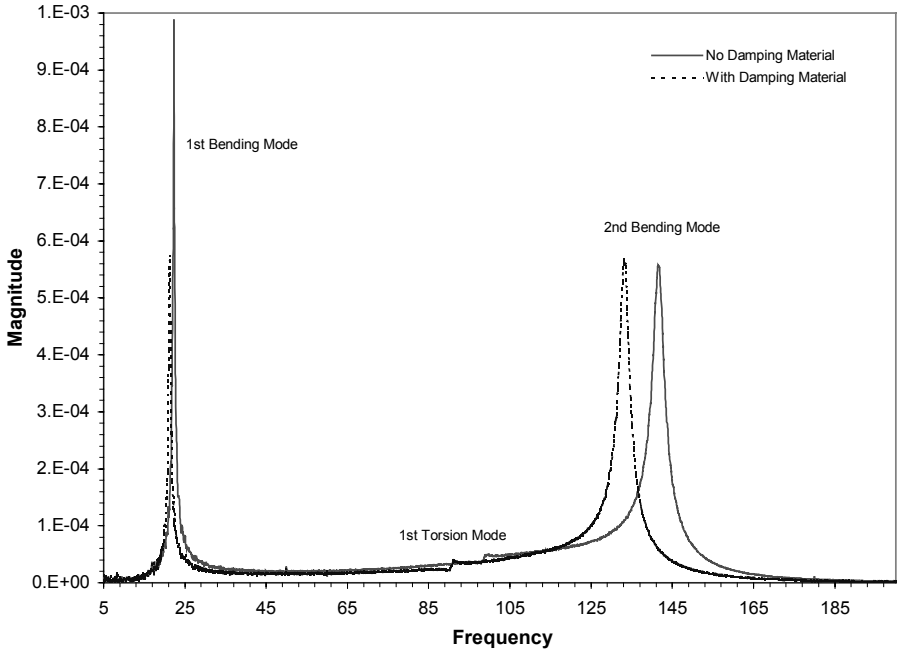

Figure 6-16. FRF from 5 to 200 Hz. of samples with a 30^{o} directional damping layer.

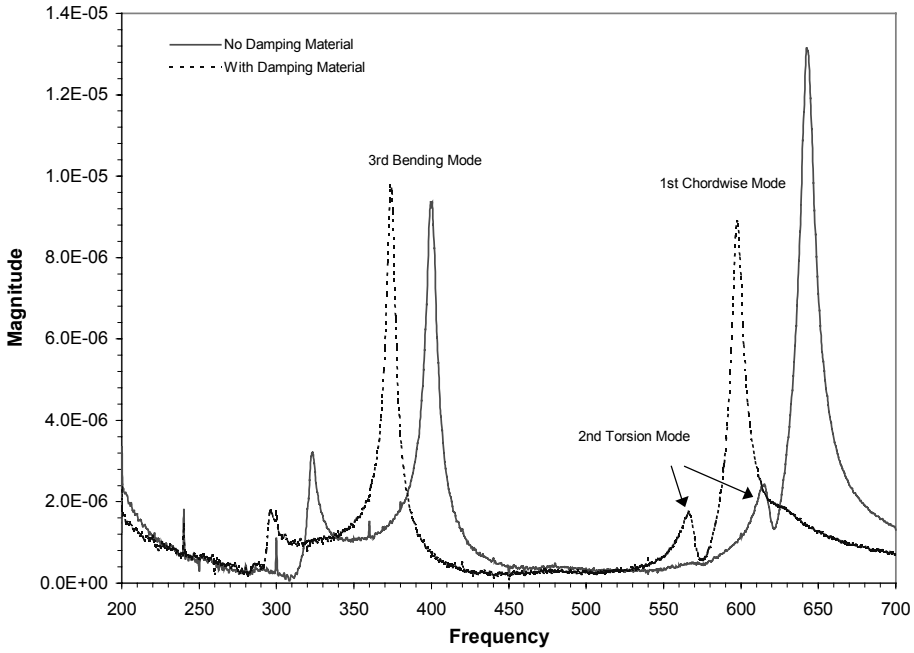

Figure 6-17. FRF from 200 to 700 Hz. of samples with a 30^{o} directional damping layer.

6.4 Discussion

The many trends described above can be simplified by noting that higher frequencies (thus higher stiffness) corresponded with higher loss factors. The frequencies and loss factors of the bending modes all decreased as the directional damping layer angle increased. The first torsion mode, which involves twisting, had a loss factor peak at 45^o, although the highest frequency was unexpectedly at 0^o. The chordwise mode, which involves bending along the length of the plate, had the highest frequencies and damping at the larger angles (60^o, 75^o, and 90^o). Because the loss factors of the three types of modes (bending, torsion, and chordwise) have different trends the modal loss factor ratios change with angle. For example, to maximize the loss factor in the chordwise mode the directional layer would be oriented to 75^o. The chordwise loss factor then increases from 0.0124 (at 0^o) to 0.0148 (a 19% increase) while the bending loss factor decreases from 0.0198 (at 0^o) to 0.0110 (a 44% decrease). Therefore the modal loss factor ratio of chordwise to bending increased a total of 115%. Likewise the modal loss factor ratio of chordwise to torsion is 39% greater when the directional layer angle is oriented at 75^o compared to 0^o. Similarly, the loss factor for torsion was greatest when the directional material layer is at 45^o. The loss factor when the directional layer was oriented to 45^o was only slightly higher than at 0^o for the torsion mode (0.0160 and 0.0158, respectively, but the bending mode decreased (0.0198 at 0^o and 0.0156 at 45^o) so the modal loss factor ratio of torsion to bending increased 29%.

Finite element models (using MSC Nastran^{TM}) of the samples were created to compare with the experimental results. Complex eigenvalue analysis was used to predict the damping. The material properties used in the models are shown in Table 6-2; the final properties were determined after looking at published material properties, vibration tests (acrylic and polycarbonate sheets), shear tests (silicone damping material), and, finally, model iterations. The model frequencies and loss factors of the first bending and first torsion modes are plotted along with experimental results in Figure 6-18 (frequency) and Figure 6-19 (loss factor). The frequency predictions matched well, especially for the first bending mode, although the loss factor predictions were off by up to 20%. The loss factor curves also had slightly different trends, such as the model torsion loss factor peaked at 30^{o} whereas the experimental loss factor peaked at 45^{o}, but matched the overall curves.

The models showed that virtually all the directional damping layer strain energy, which corresponds to damping, was in the acrylic. This was expected in bending of the sample with the 0^{o} directional damping layer because the strains in the silicone and the acrylic are equal, assuming no interface slippage, and they have similar loss factors. The strain energy is equal to the area under the stress-strain curve and the stress is much higher in the acrylic (because of the much higher modulus). Figure 6-20 shows the first bending mode strain energy distribution for all samples. All of the silicone areas are white, which indicate that the strain energy is near zero. In all samples the maximum strain energy is at the clamped end. The strain energy in the acrylic is measurable over a significantly smaller area of the sample with 90^{o}

directional damping layer than the other samples at other angles; the 90° acrylic lines transfer load across the width rather than the length. Strain energy distributions for the torsion mode are shown in Figure 6-21. The samples have similar strain energy distributions in the torsion mode, with the outer edges next to the clamp having the maximum shear energy and the middle of the sample next to the clamp and the outer corners having the least strain energy. The sample with the largest strain energy concentration, occurring at the outer edges next to the clamp, is the 30° sample which was predicted to have the highest loss factor. Figure 6-22 shows the strain energy distribution for the chordwise mode. The overall distributions are similar with the maximum occurring at the midpoint of the outside edge and the minimum occurring at the midpoint of the clamped edge. The largest strain energy concentrations were in the 60°, 75°, and 90° samples, which had the highest loss factors in the chordwise mode.

The lack of strain energy in the silicone damping material is also consistent with experimental comparison of the 30° samples, which had the same loss factor with and without silicone damping material. The silicone was added with the intent of amplifying the directional damping but it had little or no effect.

Table 6-2. Material properties used in finite element models.

Property	Acrylic	Polycarbonate	Silicone Damping Material
E (ksi)	564	345	33.8
G (ksi)	200	123.2	12.0
υ	0.41	0.40	0.41
ρ (lb/in^3)	0.043	0.043	0.036
η	0.07	0.016	0.08

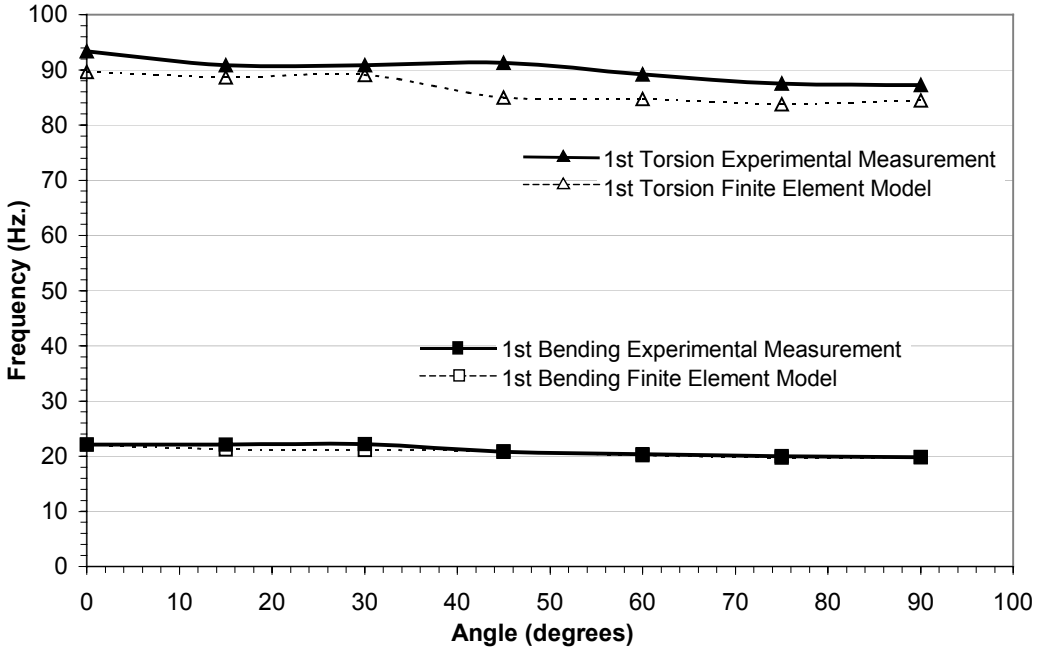

Figure 6-18. Frequency of 1st bending and 1st torsion modes of vibration of samples with 0° to 90° directional damping layers compared to finite element models.

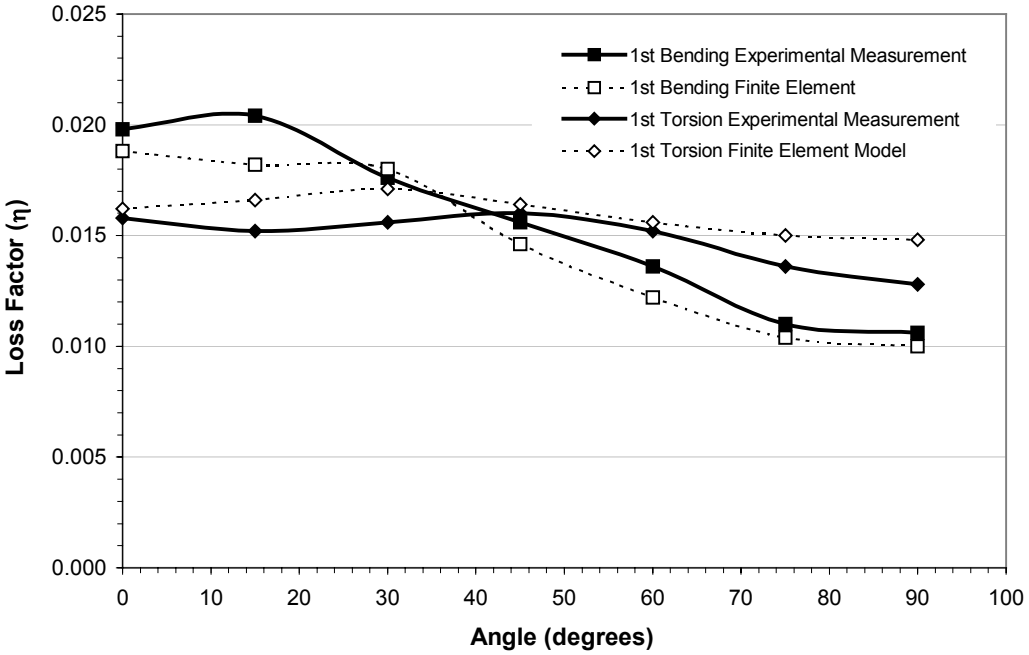

Figure 6-19. Loss factor of 1st bending and 1st torsion modes of vibration of samples with 0° to 90° directional damping layers compared to finite element models.

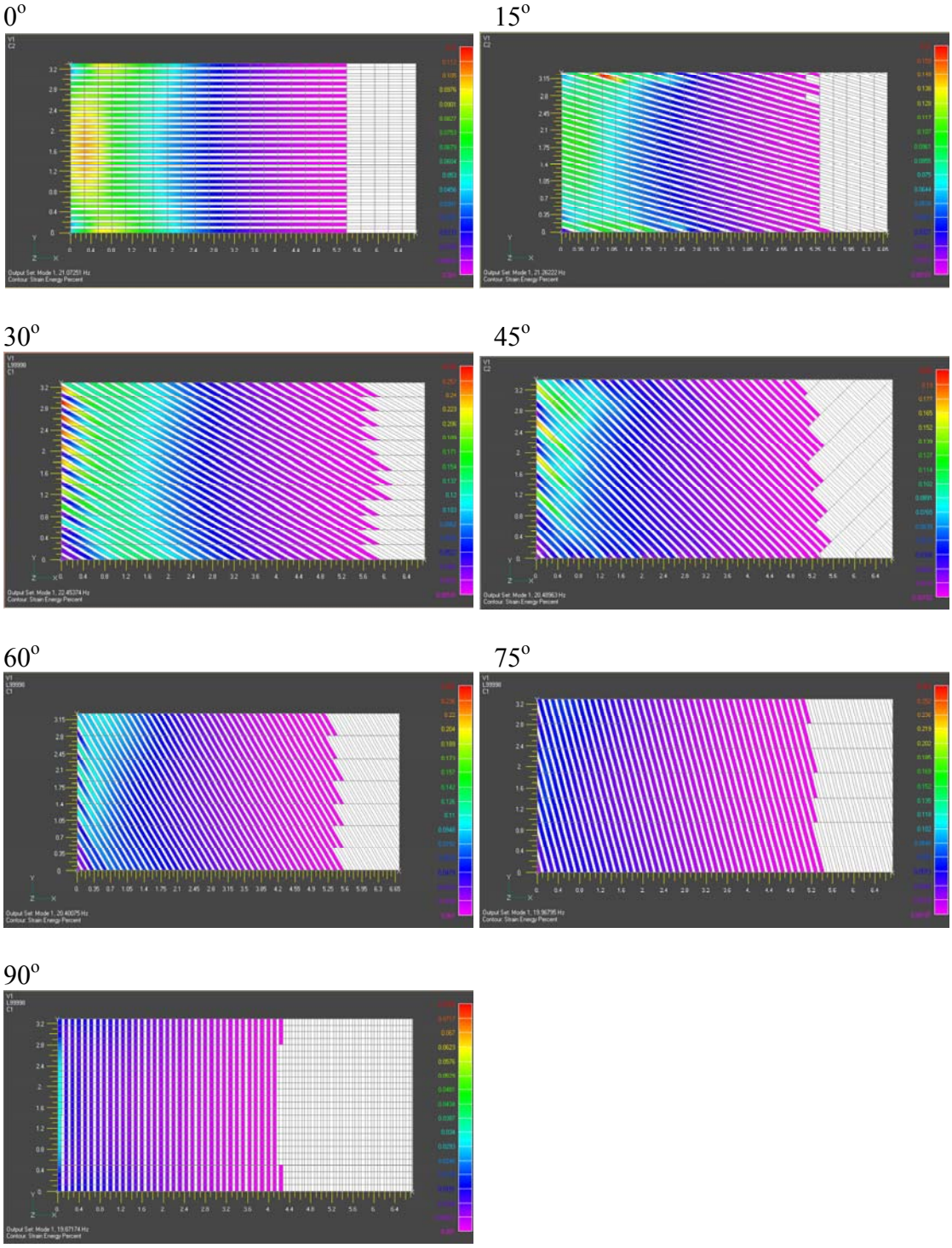

Figure 6-20. Strain energy distribution of the middle directional layer in the first bending mode of vibration. Light gray areas (including all silicone areas) have strain energy percents approaching zero.

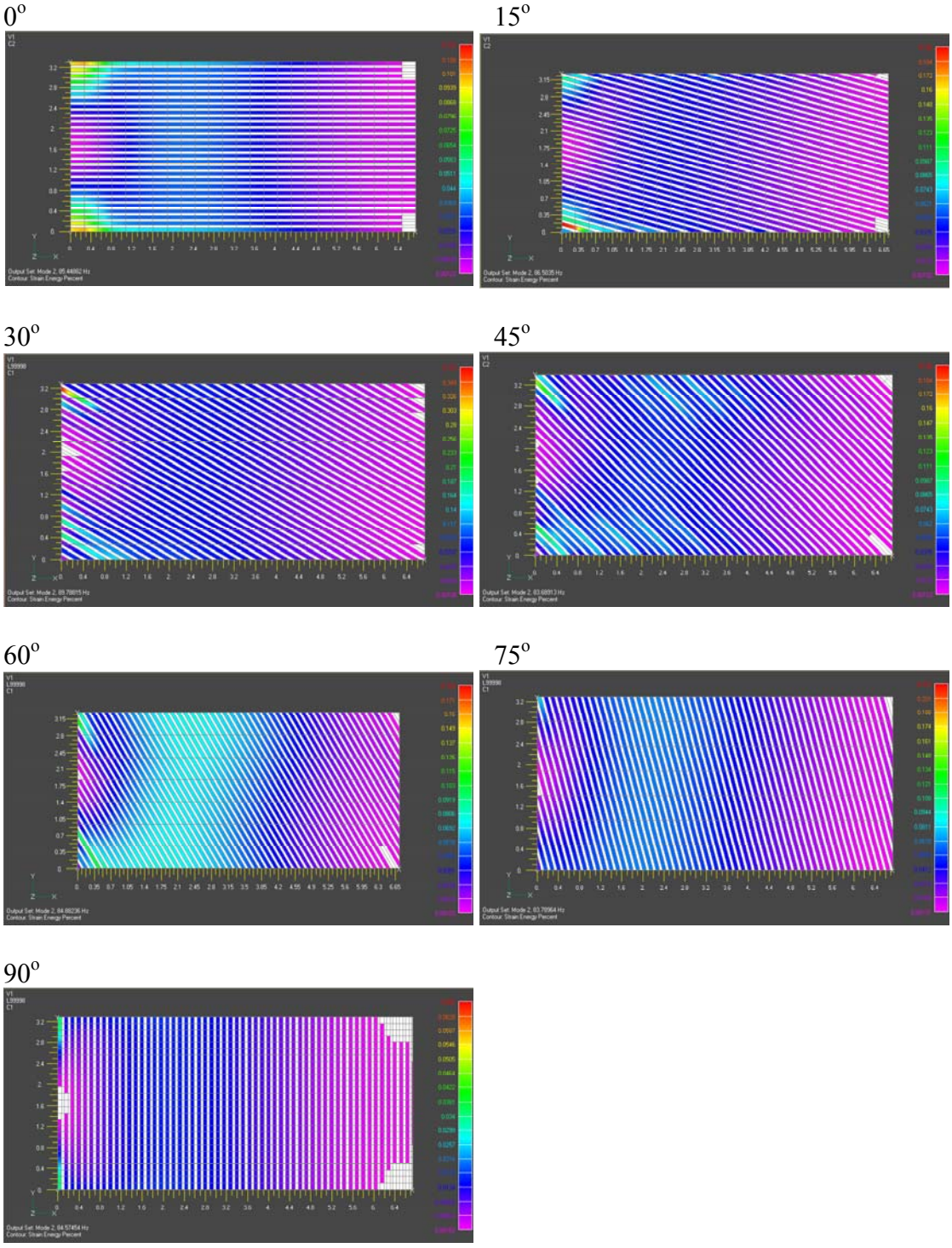

Figure 6-21. Strain energy distribution of the middle directional layer in the first torsion mode of vibration. Light gray areas (including all silicone areas) have strain energy percents approaching zero.

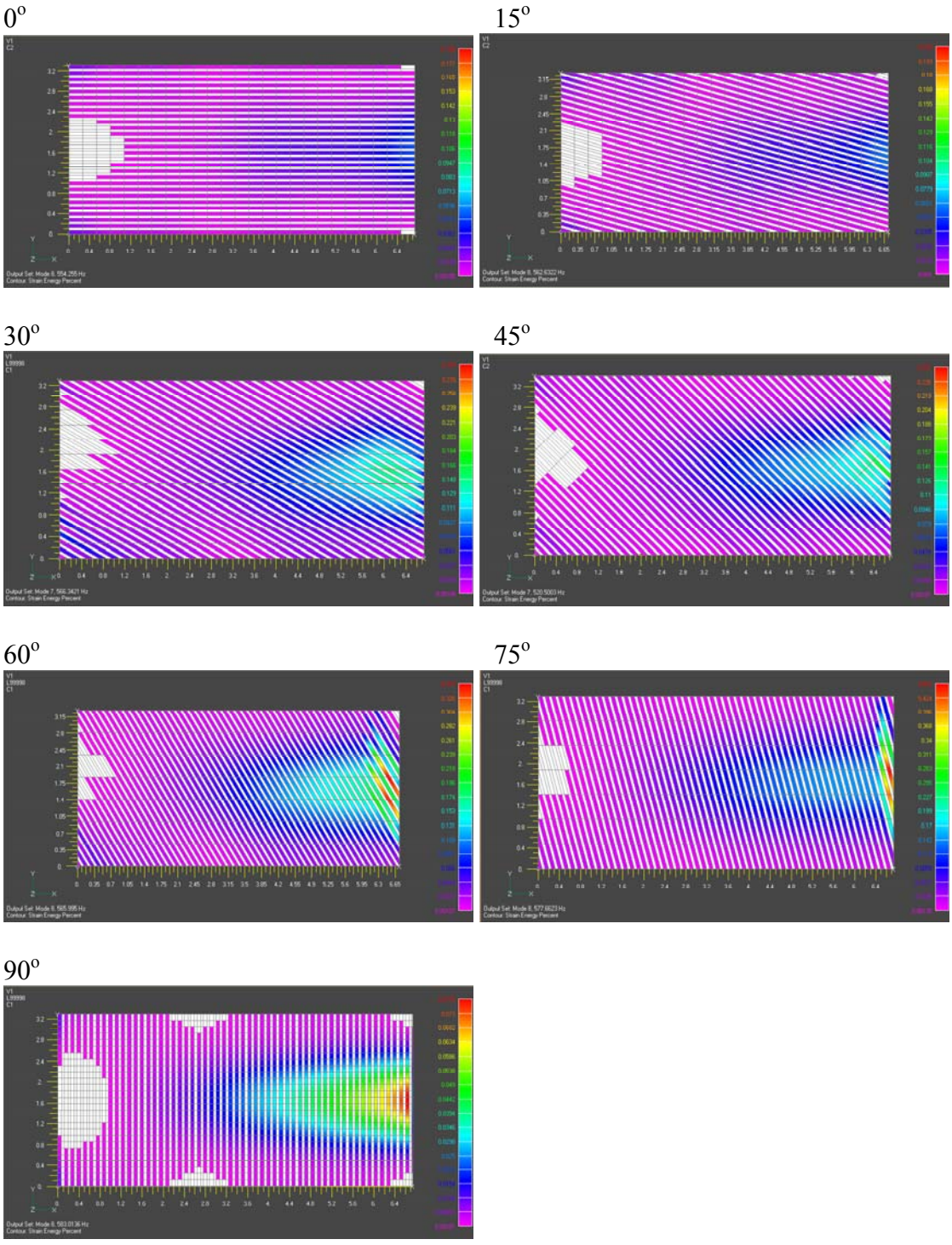

Figure 6-22. Strain energy distribution of the middle directional layer in the first chordwise mode of vibration. Light gray areas (including all silicone areas) have strain energy percents approaching zero.

6.5 Conclusions

The samples with an acrylic directional damping layer and polycarbonate outer layers showed large changes with damping layer angle variations in both frequency and loss factor. The frequency and loss factor followed the same general trends for each mode, i.e. the frequency and loss factor both decreased with increasing angle for the bending modes. The changes in frequency and loss factor were quite significant, especially for the bending modes: in first bending mode the frequency for the sample with a 90^o directional damping layer was 10% less than the sample with a 0^o directional damping layer and the loss factor for the sample with a 90^o directional damping layer was 46% less than the sample with a 0^o directional damping layer. The first torsion mode had peaks with a 45^o directional damping layer for both frequency and loss factor (although the highest frequency was actually at 0^o). The chordwise mode had the highest frequencies and loss factors at the larger angles. Finite element models showed similar results.

This research demonstrated the stiffness and damping tailorability of the directional acrylic. Other methods of creating a directional damping material could include inserting high stiffness strands in a low stiffness highly damped material or vice versa, depending on the application.

This chapter, in part, will be submitted for publication to *Composites, Part A* with the title. “Directional Damping Properties of Slotted Acrylic”. The dissertation author was the primary investigator and co-authored the article with advisor J. B. Kosmatka.

Chapter 7 Use of Particulate Toughners to Improve Composite Damping

This research involved adding small toughening particulates to graphite/epoxy composites. Currently, liquid nitrile rubber is commonly added to the epoxy matrix to toughen the composite. When the crack is progressing through the composite, the elastic energy stored in the rubber during stretching is dissipated when the rubber fails.[75,76] Adding rubber toughening particles might increase the damping because most rubber is a viscoelastic material that exhibits damping when strained and since the particles are discreet, then there could be damping from the particle/matrix interface interaction.

Other researchers have added different particles to composites, such as thermoplastic powders and whiskers[77], carbon fiber filaments[78], and tin-zinc alloy particles[79]. The thermoplastic powders and whiskers were added for toughness and the damping properties were not investigated. The damping characteristics of the composites with both the carbon fiber filaments and the tin-zinc alloy particles were examined: the carbon fiber filaments increased the damping in the transverse bending modes but only slightly in the longitudinal bending modes and the tin-zinc particles increased the damping but also increased the density by 34% and were only studied at low frequencies (<4 Hz.).

The objective of this research was to determine if damping can be increased by adding toughening particles to graphite/epoxy composite materials and if so, how the damping values (loss factors) compare to other damping methods. This was

accomplished by adding toughening particles to the interlaminar regions of the composite. The damping achieved by adding particles was then compared to the damping increase obtained when other materials are added, such as an acrylic damping material layer, a thermoplastic damping material layer, or an epoxy layer. The tensile and bending moduli were also compared for the samples.

7.1 Manufacturing and Testing

The prepreg composite material used in these tests had a Toray M40J fiber with epoxy matrix. Three types of particle tougheners manufactured by Zeon Chemical Incorporated were added: carboxy modified acrylonitrile/butadiene polymer (DuoMod DP5078), non-carboxy modified acrylonitrile/butadiene polymer (DuoMod DP5047), and acrylic polymer (DuoMod DP5097). The particles were added by placing a prepreg layer in a bag with an excess of the particle toughener. The entire bag was placed under vacuum and heated up slightly to 110^{o}F for 15 minutes. This temperature was chosen just high enough to increase the "tack" of the resin but not high enough to initiate the cure. A monolayer of particles then adhered to the prepreg. This was done for each layer then the laminate was assembled and autoclaved at 250^{o}F and 100 psi for 2.5 hours.

Other layers added for comparison purposes include: Avery Dennison FT^{TM} 1125, an acrylic viscoelastic material; 3M AF32, a nitrile phenolic adhesive; EAR CN-06, a thermoplastic alloy; and Newport NCT-304 epoxy, a rubber-toughened epoxy.

Tensile tests were performed according to ASTM Standard 3039. Three point bending tests were performed using ASTM Standard D 790-97. Shear tests were performed using a double lap shear tests method described in Chapter 5. Vibration tests were performed on the beams in order to obtain natural frequency and damping results for the first bending mode, torsion mode, and chordwise mode. The plates were 3.5" wide and were cantilevered with a length of 5" to 6". A speaker was used to provide a broad band excitation from 0 - 1000 Hz. The input into the speaker was used as the reference and a Polytec PI laser vibrometer was used to measure beam velocity response. The damping was measured with LMS's Cada X software, which uses a time domain multi-degree-of-freedom curvefitter. One specimen was tested per sample and each specimen point was analyzed twice and the two values were averaged; damping values were typically within 1% of each other. The coherence was excellent near resonance. All tests were performed at room temperature.

7.2 Results and Discussion

The tests can be divided up into three categories: 1) comparison of different particles, 2) comparison of adding a layer of particles to a layer viscoelastic damping material, and 3) comparison of adding a layer of particles to other additions, including an epoxy layer, an adhesive layer, and a thermoplastic damping material layer.

7.2.1 Comparison of Particles

The first set of samples tested had a layup of $[0_3/90/0_3]$. Duomod DP 5047, DP 5078, and DP 5097 particles were added to both sides of the prepreg (except the outer

side of the outermost layers). One sample was prepared with DuoMod DP 5078 particles on just one side of the prepreg for comparison purposes. Table 7-1 shows the mass and thicknesses for these samples. The sample mass increase resulting from adding the particles ranged from 0.008885 lbm for the DuoMod DP 5078 added to one side (a 18.6% increase) to 0.016344 lbm for the DuoMod DP 5047 added to both sides (a 34.3% increase). Adding the particles to both sides of the prepreg increased the thickness of the sample by 0.012" to 0.014" (40.0% to 46.4%) while adding DuoMod DP 5078 to one side increased it by 0.009" (30.0%). Vibration tests were performed on the samples; Figure 7-1 shows the frequency response functions (FRFs) and Figure 7-2 to Figure 7-4 zoom in on the frequency ranges of the first three modes of vibration: 1st bending, 1st torsion, and 1st chordwise, respectively. The frequencies of the samples are plotted in Figure 7-5. Adding the particles increased the frequencies of all the samples, which was a result of the increased laminate thickness from the added particles. The increased thickness increased the overall laminate bending stiffness. A better way of comparing the samples is to look at the bending modulus. For a beam in three point bending, the stiffness k is

$$k = \frac{48 E_B I}{L^3} \tag{7-1}$$

where E_B is the bending modulus, L is the support span, and I is the area moment of inertia. One can then solve for the bending modulus:

$$E_B = \frac{L^3 k}{4 b d^3} \tag{7-2}$$

where b is the width of the sample and d is the thickness of the sample. The bending modulus for the vibrations samples is shown in Figure 7-6. Adding the particles decreased the bending modulus in all cases: from 30.4 Msi (control) to 28.0 Msi for DP 5047 double side, to 25.8 Msi for DP 5078, and to25.9 for DP 5097. The bending modulus decreased for the samples with particles because 1) the addition of particles increased the thickness and lowered the fiber volume fraction and 2) the shear modulus of the particle layer is much smaller than the shear modulus in regions with fibers (shear tests like those described in Chapter 5 showed that the shear modulus of the layer with DuoMod DP 5078 particles to only be 4 ksi). Figure 7-7 plots the increase in loss factor obtained by adding the various particles. All three types of particles increased the loss factor for the three modes of vibration. DuoMod DP 5078 particles were particularly effective, increasing the loss factor by at least 143% over the control for all modes: from 0.0055 (control) to 0.0135 (DuoMod DP 5078) in first bending, from 0.0061 to 0.0122 in first torsion, and from 0.0092 to 0.0251 in first chordwise. Adding DuoMod DP 5078 particles to only one side rather than both sides had little effect on the loss factor of the first bending mode, decreased the loss factor from 0.0147 (both sides) to 0.0122 (one side) in the first torsion mode, and decreased the loss factor significantly from 0.0251 (both sides) to 0.0171 (one side) in the first chordwise mode.

Table 7-1. Thickness and mass of graphite/epoxy samples without (control) and with particles. The layup was [0_3/90/0_3].

Sample	Thickness (in.)	Mass (lbs)
Control	0.030	0.04770
DuoMod DP 5097 Double Particle Layer	0.044	0.06058
DuoMod DP 5047 Double Particle Layer	0.042	0.06404
DuoMod DP 5078 Double Particle Layer	0.042	0.06131
DuoMod DP 5078 Single Particle Layer	0.039	0.05678

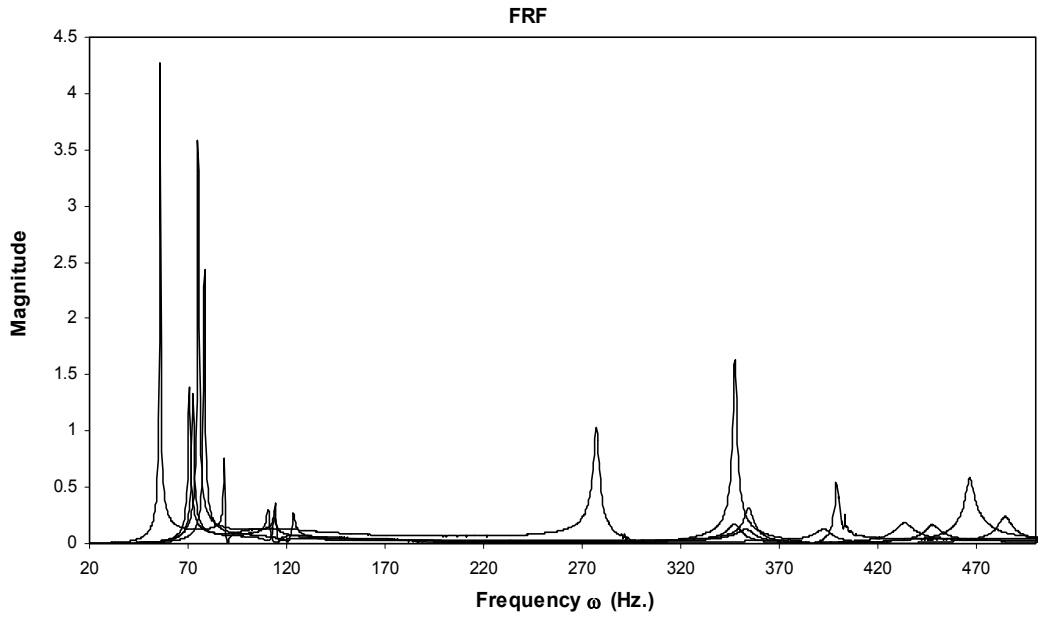

Figure 7-1. Frequency response functions (FRFs) of graphite/epoxy composite samples with and without (control) embedded particle tougheners. The layup was [0_3/90/0_3]. Labeled close-ups of individual modes of vibration are shown in Figure 7-2 to Figure 7-4.

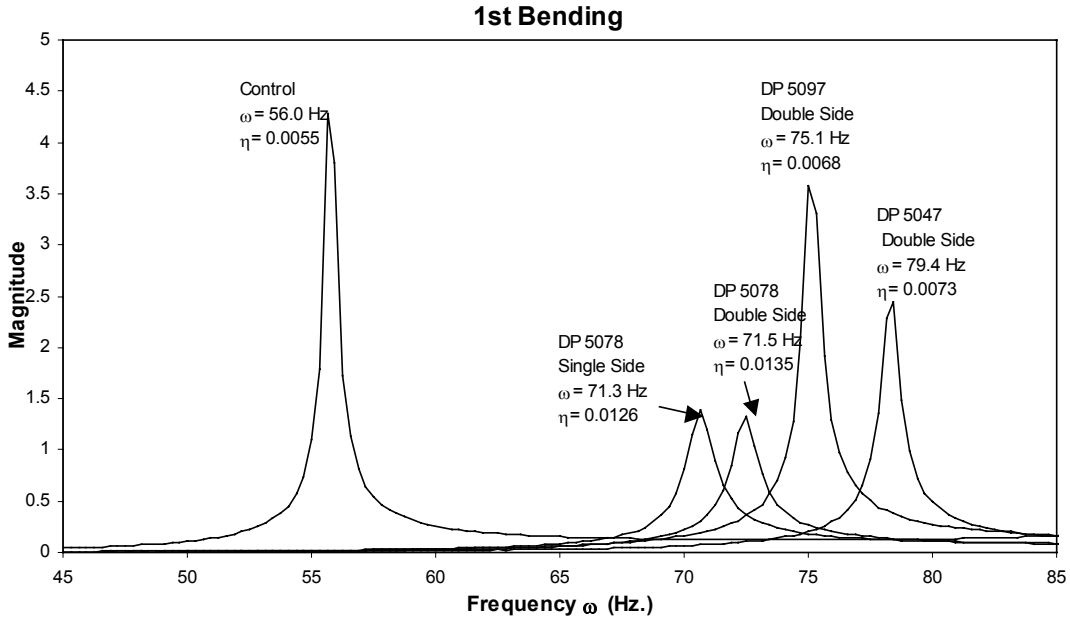

Figure 7-2. FRF of the 1st bending mode of vibration of graphite/epoxy composite samples with and without (control) embedded particle tougheners.

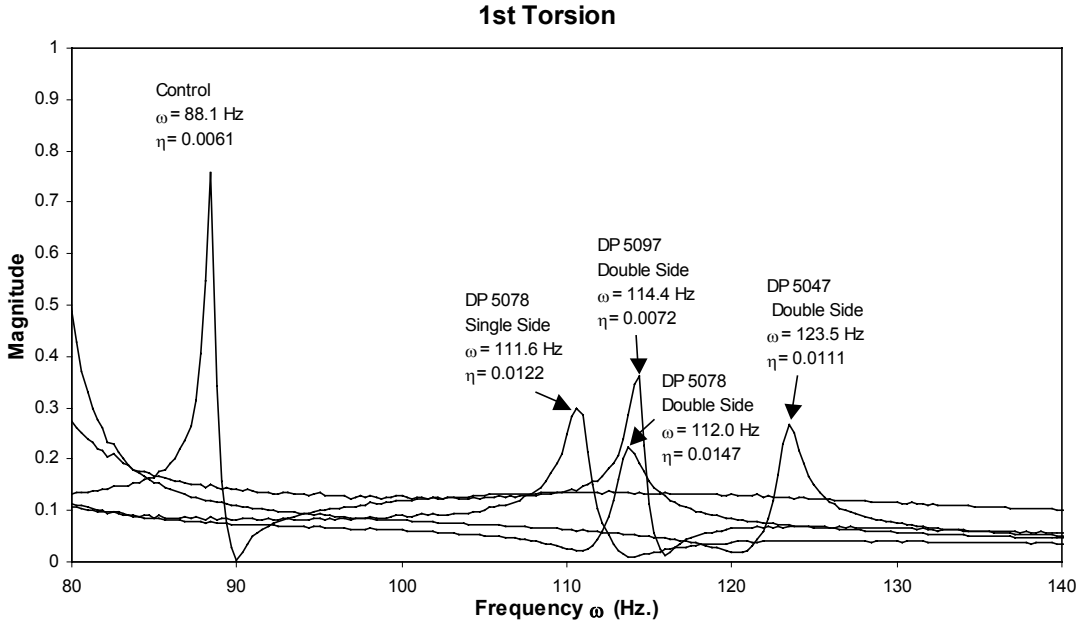

Figure 7-3. FRF of the 1st torsion mode of vibration of graphite/epoxy composite samples with and without (control) embedded particle tougheners.

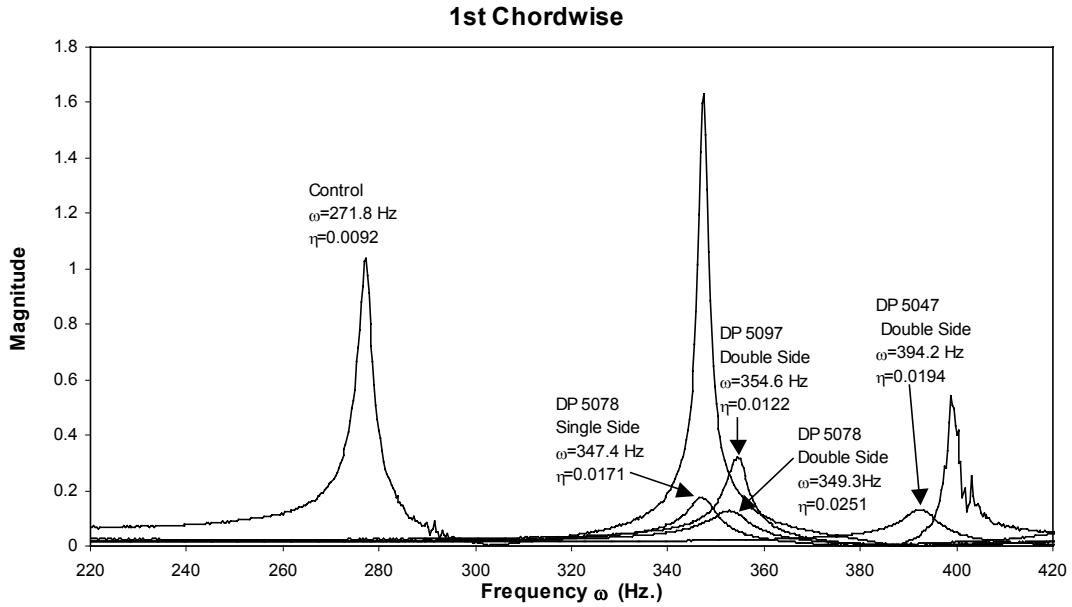

Figure 7-4 FRF of the 1st chordwise mode of vibration of graphite/epoxy composite samples with and without (control) embedded particle tougheners.

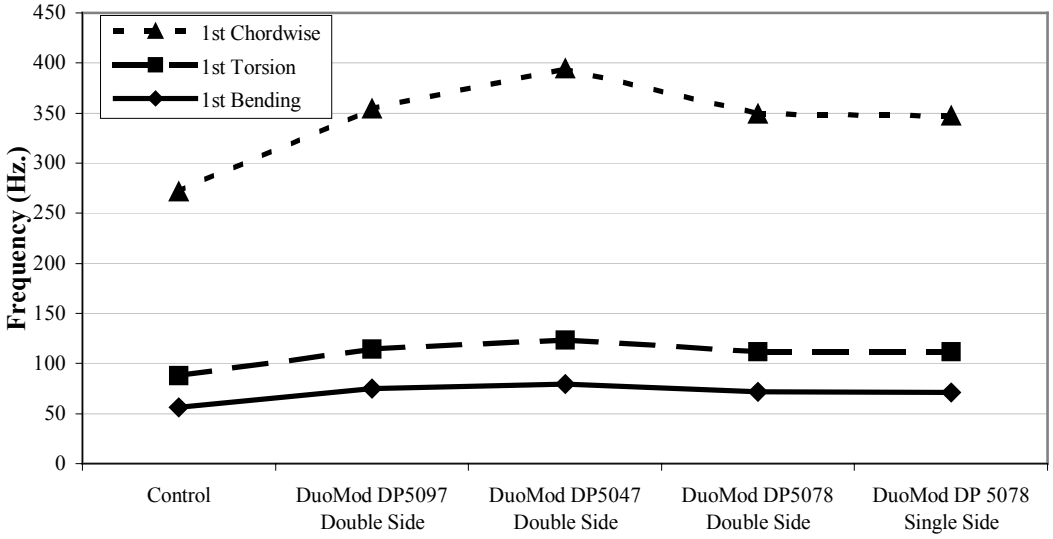

Figure 7-5. Frequencies of various modes of vibration of graphite/epoxy composite samples with and without (control) embedded particle tougheners.

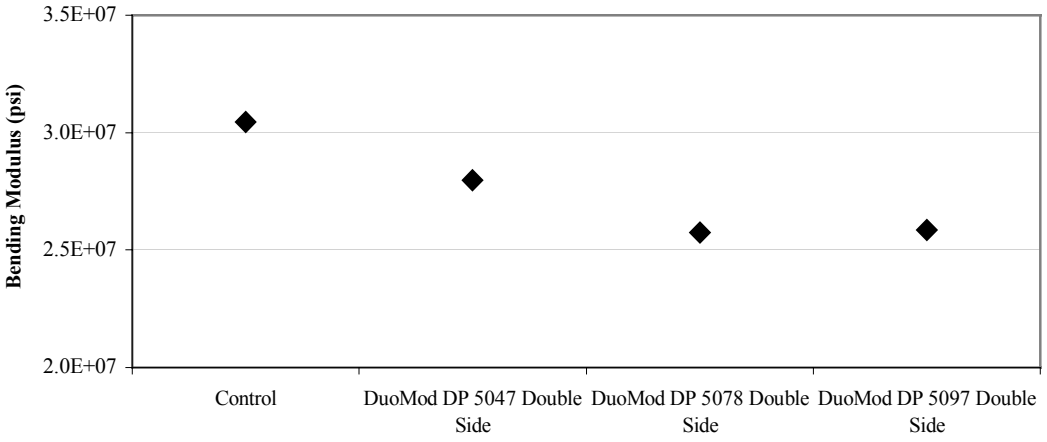

Figure 7-6. Bending moduli of graphite/epoxy samples without (control) and with particles.

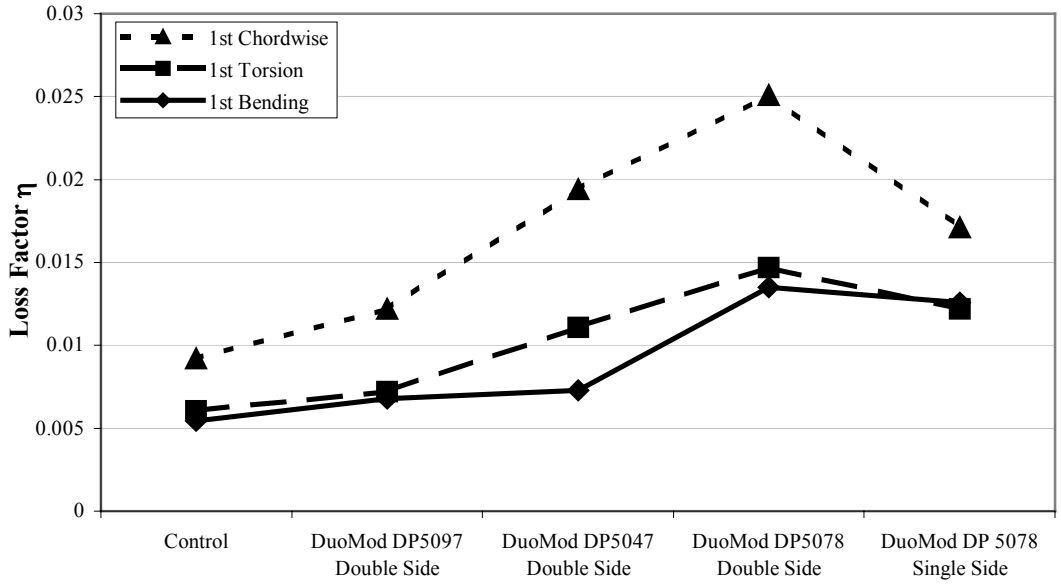

Figure 7-7. Loss factors of various modes of vibration of graphite/epoxy composite samples with and without (control) embedded particle toughenners.

7.2.2 Particle and Viscoelastic Damping Material Comparison

The next tests compared the damping and properties of samples with particles to those with an embedded cocured layer of Avery Dennison FT™ 1125 viscoelastic material (VEM). Three configurations were made with the VEM. First, the VEM was simply cocured into the composite. The second sample had particles placed between the VEM layer and the graphite/epoxy to see if the particles acted as a "barrier layer" and would prevent epoxy penetration into the VEM. Epoxy penetration into the VEM layer has been shown to decrease the damping capability of the VEM, as discussed in Chapter 4. The last sample was manufactured with a Kapton™ barrier layer between the VEM and graphite/epoxy. The sample with the particles was made with only three double-sided layers of DuoMod DP 5078 particles so the thickness of the sample would be similar to that of the samples with the VEM. The control sample was made with an extra layer of graphite/epoxy so it, too, would be similar in thickness to the samples with VEM and the sample with particles. The layups and thicknesses for these samples are listed in Table 7-2. The thicknesses varied from 0.048" (with VEM and VEM with a particle layer) to 0.050" (with VEM and barrier layer). Vibration tests were performed on these samples; Figure 7-8 shows the FRFs and Figure 7-9 to Figure 7-11 zoom in on the first three modes of vibration: 1st bending, 1st torsion, and 1st chordwise. Figure 7-12 plots the frequencies of the modes of vibration. The frequency of the control sample was higher than the other samples in the 1st bending mode but in the 1st torsion and 1st chordwise modes the sample with particles was slightly higher. This was a result of the increased thickness of the sample with

particles. The frequencies of the samples with VEM were significantly lower than the frequencies of the control sample; this decrease can be accredited to the lower shear, bending, and tensile modulus of the samples with VEM. Shear tests reported in Chapter 5 showed the shear modulus of the layer of cocured FT™ 1125 was 57.6 psi; the same testing showed the layer with DuoMod DP5078 particles was 4001 psi. Table 7-3 describes the tensile samples with particles and FT™ 1125 VEM and the tensile moduli are shown in Figure 7-13. The sample with a double layer of DuoMod DP 5078 particles had a tensile modulus that was 10.3 Msi (28%) less than the control, which had a tensile modulus of 37.2 Msi. The sample with a single layer of DuoMod DP 5078 had a tensile modulus that was 4.4 Msi (12%) less than the control, and samples with VEM have tensile moduli that were 7.8 Msi to 11.0 Msi (21% to 30%) less than the control. Three point bending tests were performed on the samples used in the vibration tests. The bending moduli are shown in Figure 7-14. The bending modulus for the samples with particles was 2.5 Msi (8%) less than the control, which had a bending modulus of 32.9 Msi, while the samples with FT™ 1125 VEM had bending moduli that were 22.6 Msi to 25.6 Msi (69% to 78%) less than the control.

The loss factors of the first three modes of vibration (1^{st} bending, 1^{st} torsion, and 1^{st} chordwise) are plotted in Figure 7-15. The control sample had loss factors of 0.0054 for the 1^{st} bending mode, 0.0040 for 1^{st} torsion mode, and 0.0078 for 1^{st} chordwise mode. The sample with the DuoMod DP 5078 particles showed an increase in loss factor over the control of 0.0024 (44%) for the 1^{st} bending mode, 0.0024 (60%) for the 1^{st} torsion mode and 0.0014 (18%) for the 1^{st} chordwise mode. The samples

with the layer of FT™ 1125 VEM (by itself and with the barrier layer and particle layer) had much higher loss factors than control sample. In the 1st bending mode the loss factor increase ranged from 0.2200 (for VEM only) to 0.2738 (for VEM with barrier layer), in the 1st torsion mode the increase ranged from 0.1850 (VEM only) to 0.1990 (VEM with barrier layer), and in the 1st chordwise mode the increase ranged from 0.0880 (VEM only) to 0.0924 (VEM with barrier layer).

Table 7-2. Layups of graphite/epoxy samples with embedded Avery Dennison FT™ 1125 viscoelastic material (VEM) and DuMod DP 5078 Particles.

Sample	Layup	Thickness
Control	[0/+15/-15/+15/0_3/+15/-15/+15/0]	0.0485”
w/ PL	[0/+15/-15/+15/**PL**/0/**PL**/0/**PL**/+15/-15/+15/0]	0.0495”
w/ VEM	[0/+15/-15/+15/0/**VEM**/0/+15/-15/+15/0]	0.048”
w/ VEM and PL	[0/+15/-15/+15/0/**PL/VEM/PL**/0/+15/-15/+15/0]	0.048”
w/ VEM and BL	[0/+15/-15/+15/0/**BL/VEM/BL**/0/+15/-15/+15/0]	0.050”

*PL – Particle Layer, BL – Barrier Layer

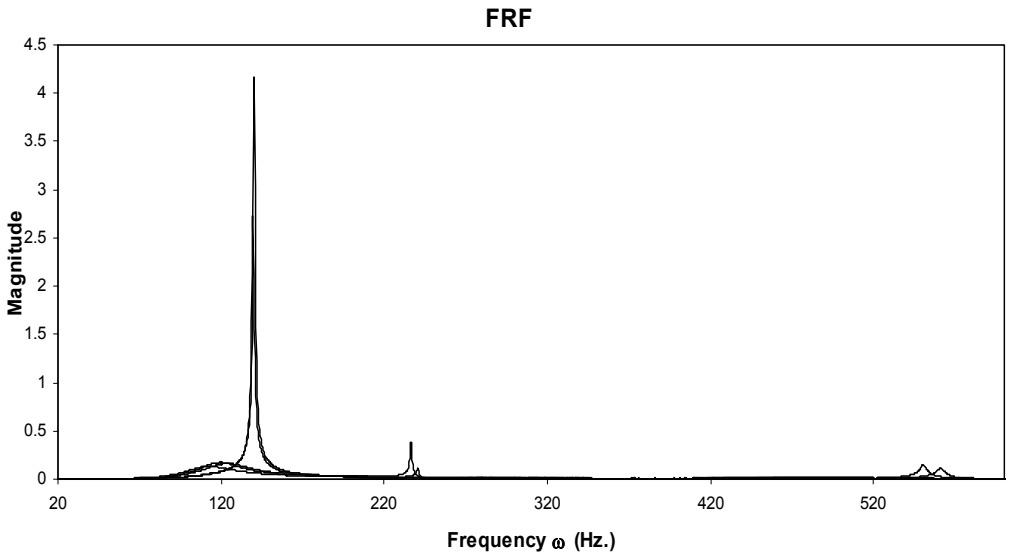

Figure 7-8. FRFs of graphite/epoxy samples with embedded Avery Dennison FT™ 1125 viscoelastic material (VEM) and DuMod DP 5078 Particles. Labeled close-ups of individual modes of vibration are shown in Figure 7-9 to Figure 7-11.

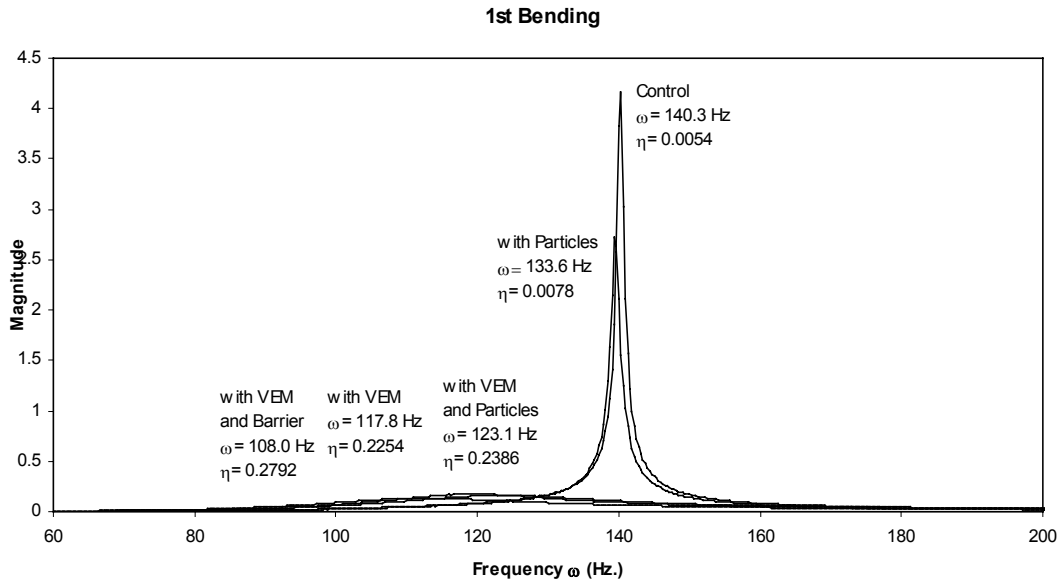

Figure 7-9. FRFs of the 1st bending mode of vibration of graphite/epoxy samples with embedded Avery Dennison FT™ 1125 viscoelastic material (VEM) and DuMod DP 5078 Particles.

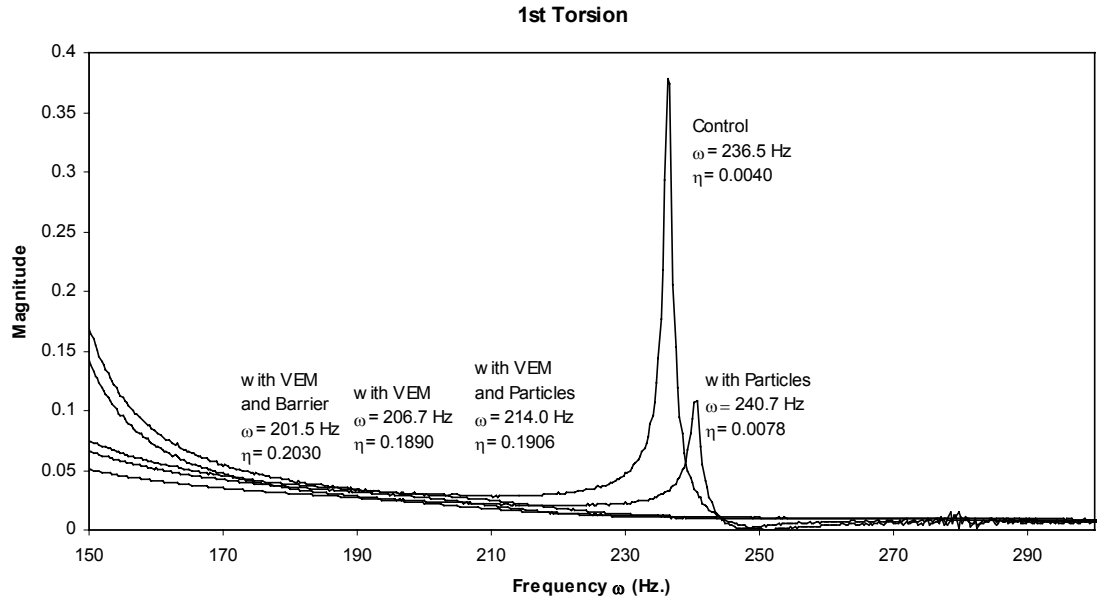

Figure 7-10. FRF of the 1st torsion mode of vibration of graphite/epoxy samples with embedded Avery Dennison FT™ 1125 viscoelastic material (VEM) and DuMod DP 5078 Particles.

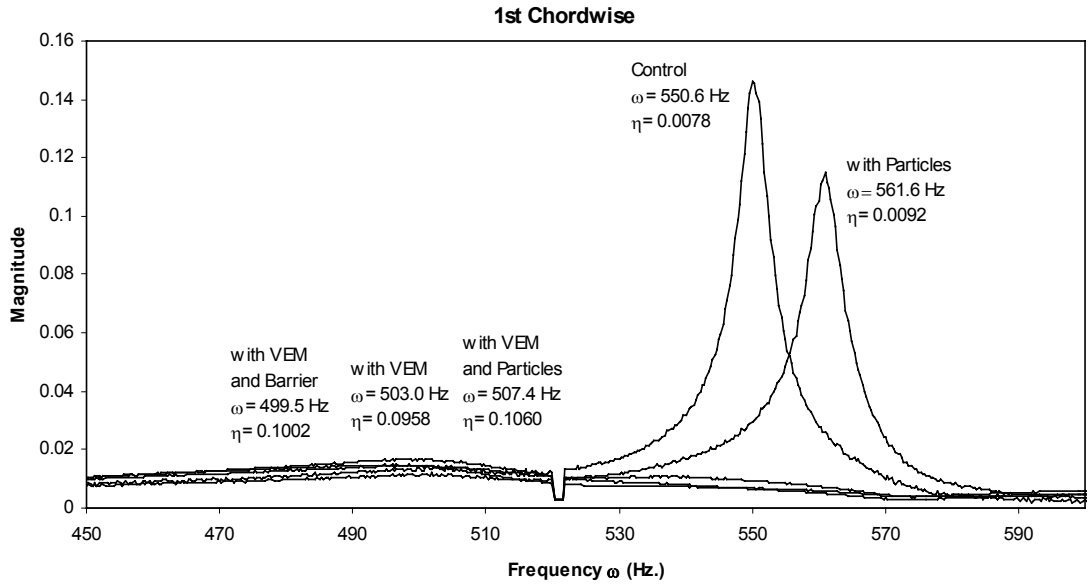

Figure 7-11. FRF of the 1st chordwise mode of vibration of graphite/epoxy samples with embedded Avery Dennison FT™ 1125 viscoelastic material (VEM) and DuMod DP 5078 Particles.

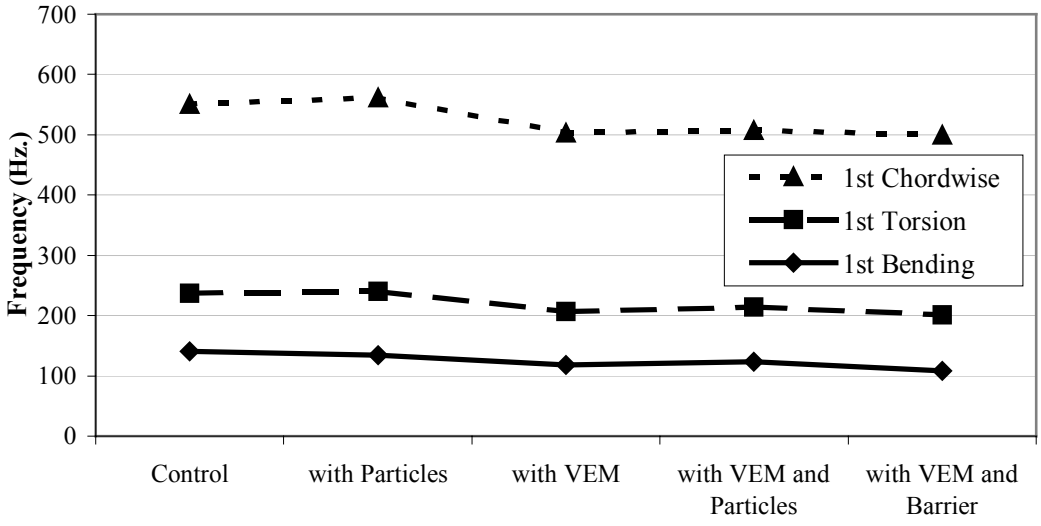

Figure 7-12. Frequencies of the 1st bending, 1st torsion, and 1st chordwise modes of vibration of graphite/epoxy samples with embedded Avery Dennison FT™ 1125 viscoelastic material (VEM) and DuMod DP 5078 Particles.

Table 7-3. Description of graphite/epoxy tensile test samples shown in Figure 7-13. VEM is FT™ 1125 and Particles are DuoMod DP 5078.

Sample	Layup	Thickness
Control	0_8	.036
with VEM	0_3/VEM/0_2/VEM/0_3	.045
with VEM and PL	0_3/**PL/VEM/PL**/0_2/**PL/VEM/PL**/0_3	.049
with VEM and BL	0_3/**BL/VEM/BL**/0_2/**BL/VEM/BL**/0_3	.050
with Double PL	0_8 with double PL between every layer	.0495
with Single PL	0_8 with SPL between every layer	.044

*PL – Particle Layer, BL – Barrier Layer

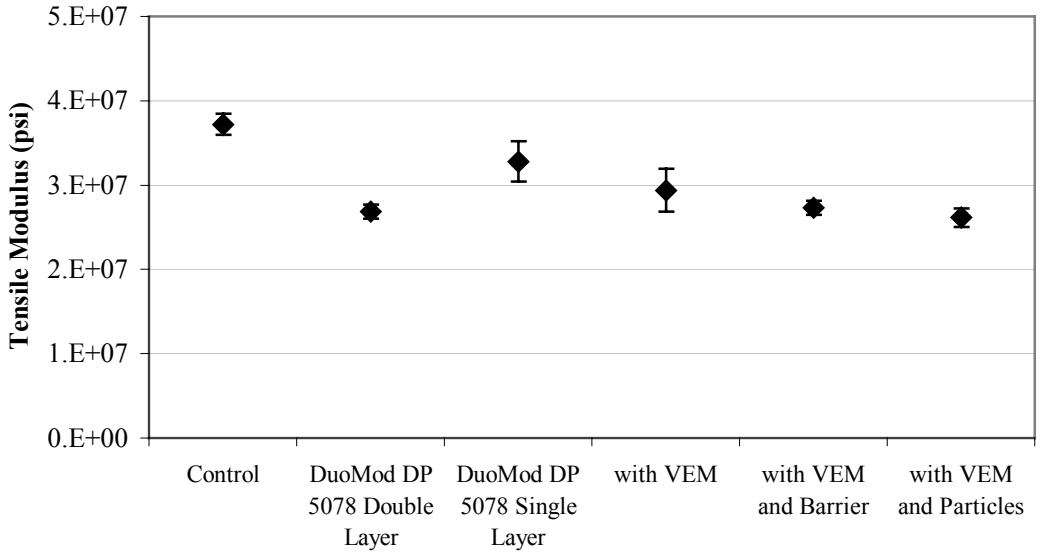

Figure 7-13 Tensile moduli (0^o) of various samples described in Table 7-3. VEM is FT™ 1125 and Particles are DuoMod DP 5078.

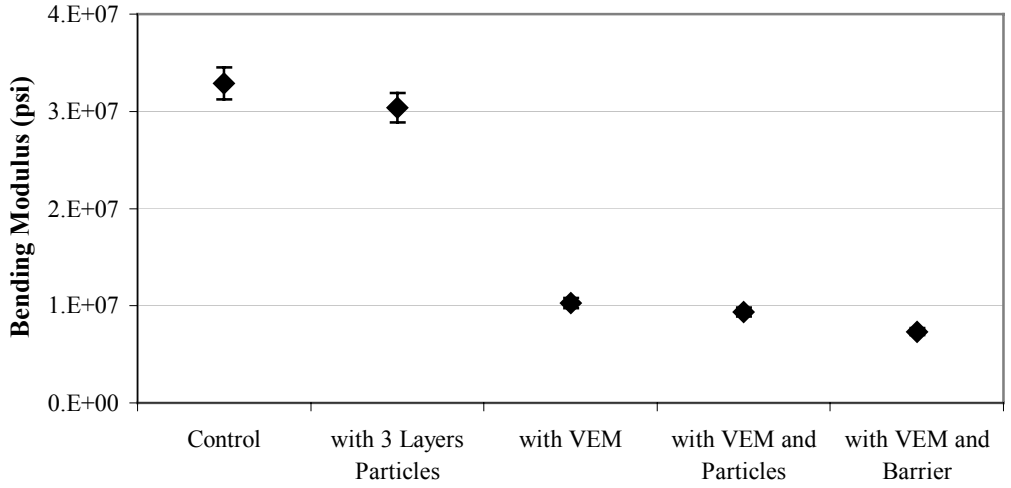

Figure 7-14. Bending moduli of graphite/epoxy samples with embedded Avery Dennison FT™ 1125 viscoelastic material (VEM) and DuMod DP 5078 Particles.

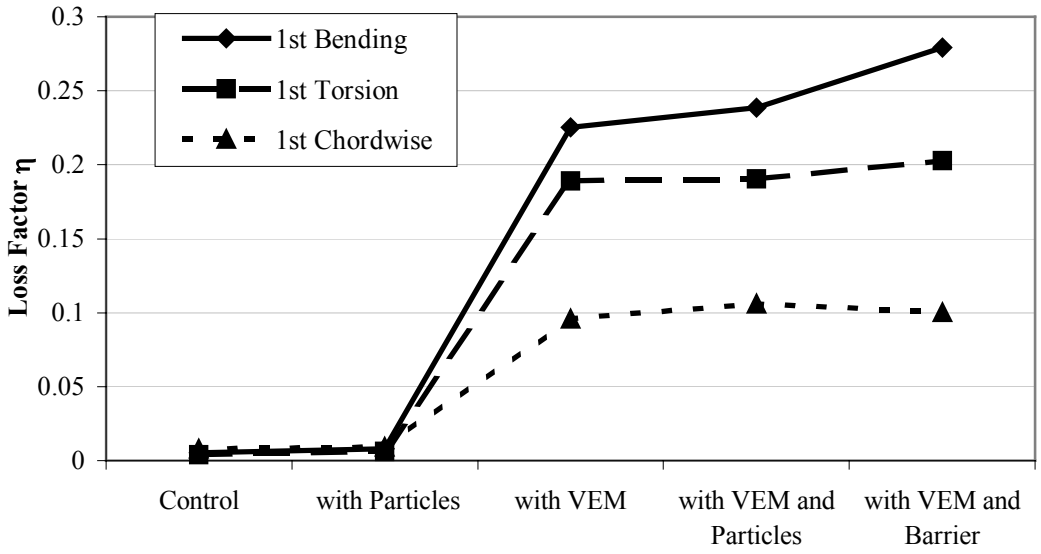

Figure 7-15. Loss factors of the 1st bending, 1st torsion, and 1st chordwise modes of vibration of graphite/epoxy samples with embedded Avery Dennison FT™ 1125 viscoelastic material (VEM) and DuMod DP 5078 Particles.

7.2.3 Comparison of particles to other additions

These tests compared a graphite/epoxy sample with 3 layers of DuoMod DP 5078 particles to five other graphite/epoxy samples: 1) with a layer of Newport NCT-304 rubber toughened epoxy, 2) with a layer of 3M AF32 adhesive, 3) with a layer of EAR CN-06 thermoplastic damping material, 4) with one layer of CN-06 flakes, and 5) with three layers of CN-06 flakes. Table 7-4 shows the layups and thicknesses of these samples. Vibration tests were performed on these samples; Figure 7-16 shows the FRFs and Figure 7-17 to Figure 7-19 zoom in on the first three modes of vibration: 1st bending, 1st torsion, and 1st chordwise. The frequencies of the samples are plotted in Figure 7-20; the sample with the CN-06 layer has the highest frequency in all three modes of vibration. It is the thickest sample (0.055") which explains the higher frequency. The bending moduli are shown in Figure 7-21. The control sample, the epoxy layer sample and the CN-06 single flake layer sample all had similar moduli (32.9 Msi, 33.4 Msi and 34.1 Msi, respectively) while the three particle layer sample and three CN-06 flake layer sample were slightly lower (30.4 Msi and 30.8 Msi, respectively). The bending moduli of the AF32 layer and CN-06 layer samples were significantly lower (21.7 Msi and 18.9 Msi, respectively) than the other samples.

The loss factors are shown in Figure 7-22. The AF32 layer sample had significantly higher loss factors than the other samples in all three modes of vibration; it was 0.0364 compared to 0.0054 for the control sample in the 1st bending mode, 0.0328 compared to 0.0034 in the 1st torsion mode, and 0.0266 compared to 0.0070 for

the 1st chordwise mode. Although significantly less than the AF32 layer sample, the loss factor of the CN-06 layer sample was still much greater than the other samples: 0.0316, 0.0248, and 0.0156 for the 1st bending, 1st torsion, and 1st chordwise modes of vibration, respectively. The epoxy layer sample had a 23% higher loss factor than the particle sample (and 78% higher than the control) for the first bending mode but was lower than the particle sample in the first torsion and chordwise modes (31% and 15%, respectively) and was approximately the same as the control in first torsion and chordwise modes. A single layer of CN-06 flakes did not significantly improve the loss factor over the control sample. Three layers of CN-06 flakes, however, increased the loss factor slightly in the first bending mode (19%) and chordwise mode (26%) but had no effect on the torsion mode.

Table 7-4. Layups of graphite/epoxy samples with various added layers.

Sample	Layup	Thickness
Control	[0/+15/-15/+15/0_3/+15/-15/+15/0]	0.0485”
w/ PL	[0/+15/-15/+15/**PL**/0/**PL**/0/**PL**/+15/-15/+15/0]	0.0495”
w/ Epoxy	[0/+15/-15/+15/0/**Epoxy**/0/+15/-15/+15/0]	0.051”
w/ AF32	[0/+15/-15/+15/0/**AF32**/0/+15/-15/+15/0]	0.052”
w/ CN-06	[0/+15/-15/+15/0/**CN-06**/0/+15/-15/+15/0]	0.055”
w/ 1FL	0/+15/-15/+15/0/**FL**/0/+15/-15/+15/0]	0.046”
w/ 3FL	[0/+15/-15/+15/**FL**/0/**FL**/0/**FL**/+15/-15/+15/0]	0.049”

*PL – DuoMod DP 5078 Particle Layer, FL – CN-06 Flake Layer

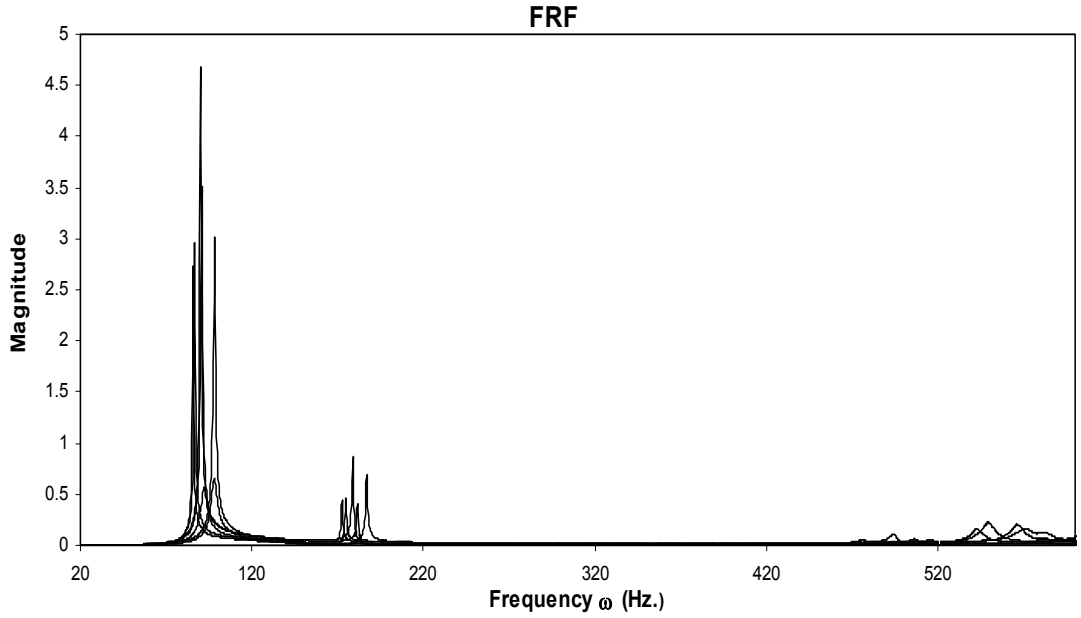

Figure 7-16. FRFs of graphite/epoxy samples with embedded layers of epoxy, CN-06 damping material, CN-06 damping material flakes, AF32 damping material, or DuoMod DP 5078 particles. Labeled close-ups of individual modes of vibration are shown in Figure 7-17 to Figure 7-19.

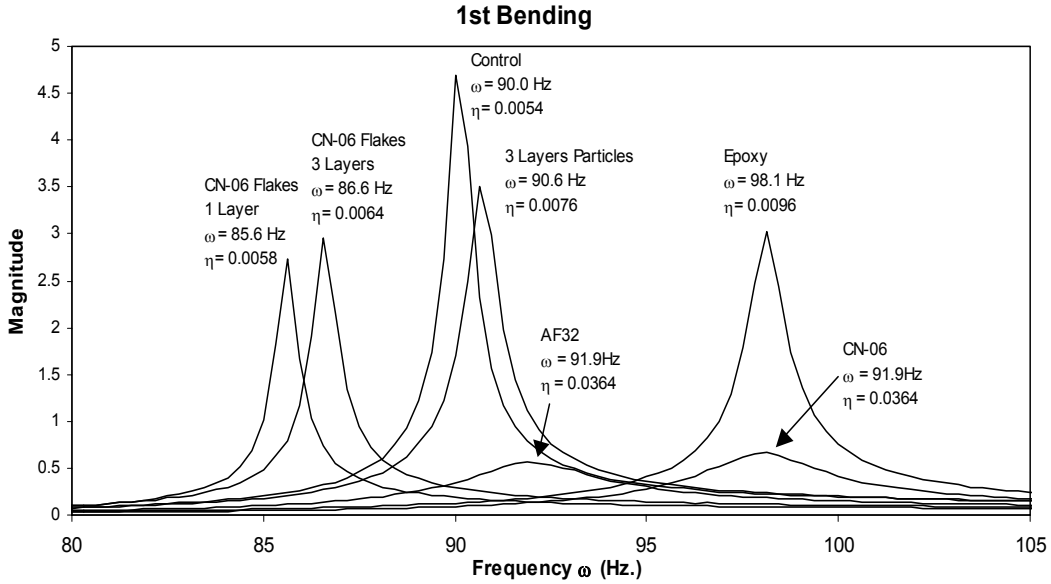

Figure 7-17. FRFs of 1st bending mode of vibration of graphite/epoxy samples with embedded layers of epoxy, CN-06 damping material, CN-06 damping material flakes, AF32 damping material, or DuoMod DP 5078 particles.

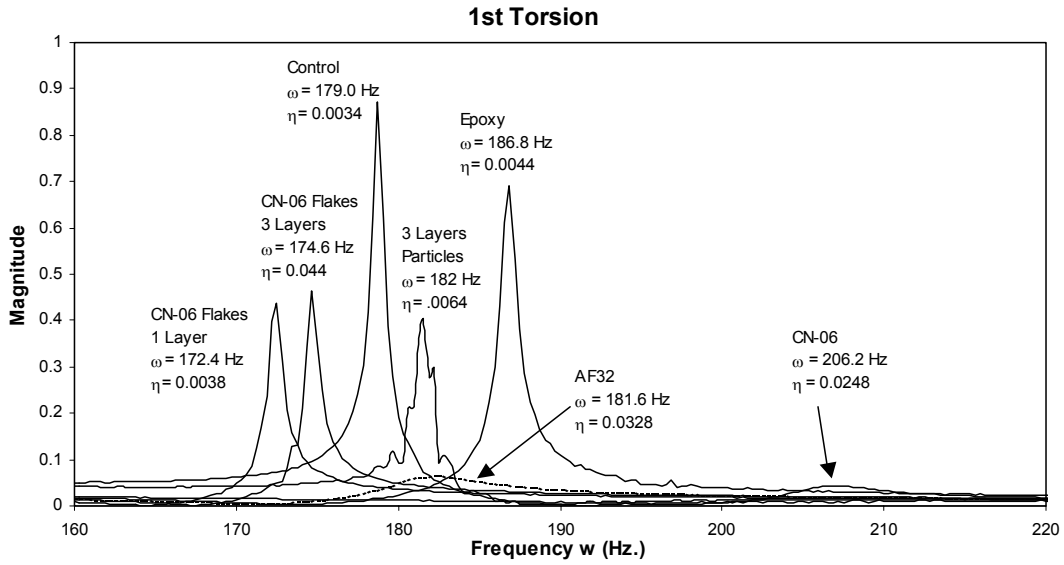

Figure 7-18 FRFs of 1st torsion mode of vibration of graphite/epoxy samples with embedded layers of epoxy, CN-06 damping material, CN-06 damping material flakes, AF32 damping material, or DuoMod DP 5078 particles.

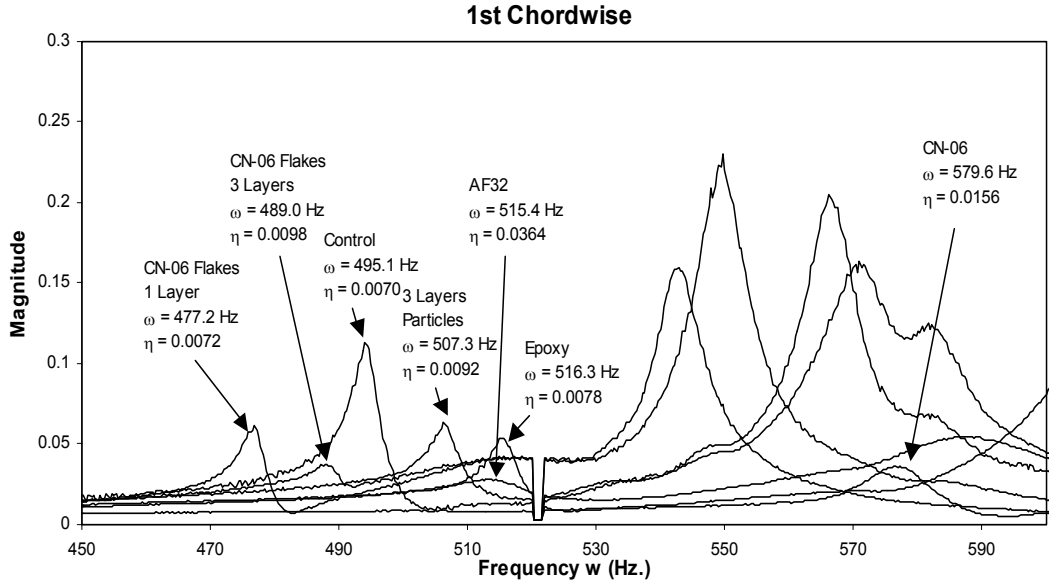

Figure 7-19 FRFs of the 1st chordwise mode of vibration of graphite/epoxy samples with embedded layers of epoxy, CN-06 damping material, CN-06 damping material flakes, AF32 damping material, or DuoMod DP 5078 particles.

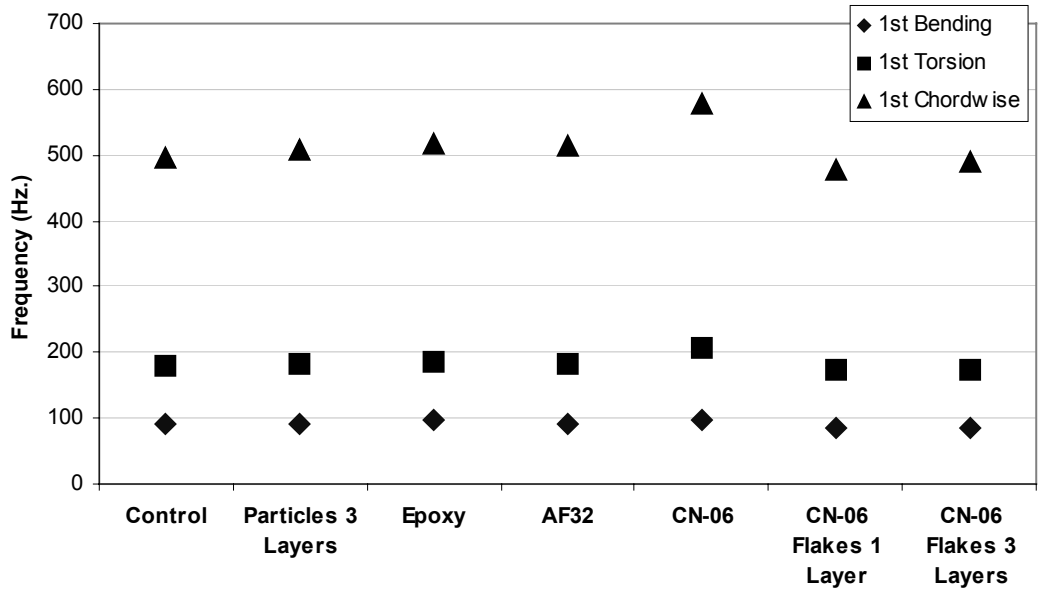

Figure 7-20. Frequencies of the first three modes of vibration (1st bending, 1st torsion, and 1st chordwise) of graphite/epoxy samples with embedded layers of epoxy, CN-06 damping material, CN-06 damping material flakes, AF32 damping material, or DuoMod DP 5078 particles.

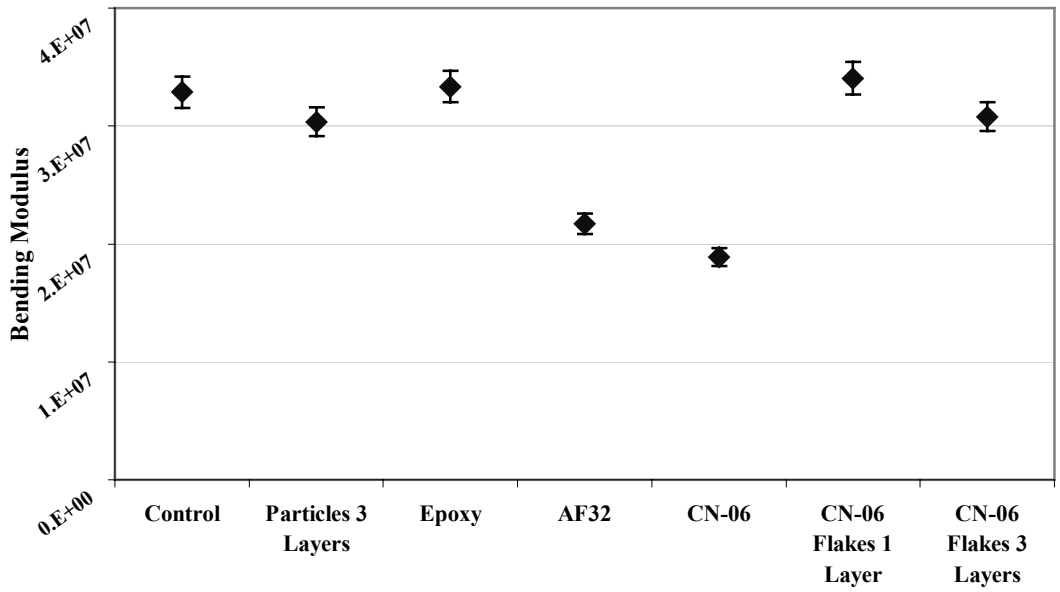

Figure 7-21. Bending moduli of graphite/epoxy samples with embedded layers of epoxy, CN-06 damping material, CN-06 damping material flakes, AF32 damping material, or DuoMod DP 5078 particles.

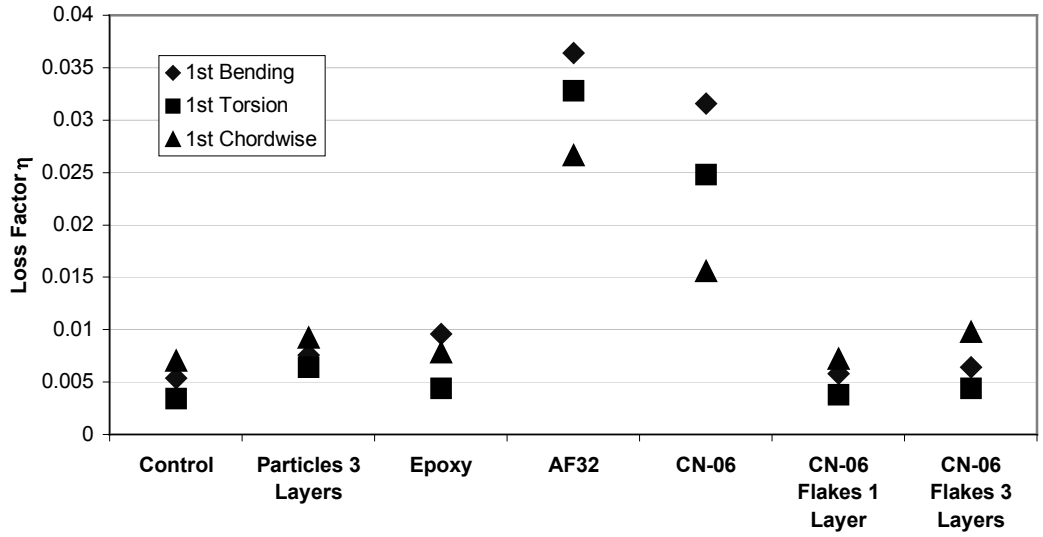

Figure 7-22. Loss factors of the first three modes of vibration (1st bending, 1st torsion, and 1st chordwise) of graphite/epoxy samples with embedded layers of epoxy, CN-06 damping material, CN-06 damping material flakes, AF32 damping material, or DuoMod DP 5078 particles.

7.3 Conclusions

The addition of three types of toughening particles to graphite/epoxy composite samples increased the loss factor for the bending, torsion, and chordwise modes of vibration. Samples with DuoMod DP 5078 particles were particularly effective with more than a 140% loss factor increase over the control sample for all three tested modes of vibration (1st bending, 1st torsion, and 1st chordwise). The bending modulus for the sample with DP 5078 particles was 8% less than the control (30.4 Msi compared to 32.9 Msi). For comparison purposes samples were made with a layer of Avery Dennison FT™ 1125 VEM damping material, a layer of rubber toughened epoxy, a layer of 3M AF32 adhesive, a layer of EAR CN-06 thermoplastic damping

material, and one or three layers of CN-06 flakes. The layer of 1125 VEM greatly increased the loss factor (10 to 30 times the loss factor than the sample with DuoMod DP 5078 particles) but the bending modulus was 69% to 78% less than the control. Also, the shear modulus of the layer of cocured VEM was much less than the shear modulus of the layer of DuoMod DP5078 particles: 57.6 psi and 4001 psi, respectively. Therefore while the damping is much greater for the samples with a VEM layer than those with particles, the much higher bending modulus and shear modulus of the samples with particles make them advantageous in stiffness critical parts. Samples with AF32 and CN-06 layers had substantially higher loss factors than both the control sample and particle sample in all three modes of vibration (i.e. in 1st bending mode the loss factors for the control sample, particle layer sample, AF32 layer sample, and CN-06 layer sample were 0.0054, 0.0076, 0.0364, and 0.0316, respectively) but had a 35% to 43% lower bending modulus. The sample with a layer of rubber toughened epoxy had a 23% higher loss factor than the sample with particle layers in the 1st bending mode of vibration but had a smaller loss factor in 1st torsion and 1st chordwise modes (31% and 15%, respectively). The bending modulus of the sample with layer of rubber toughened epoxy had a higher bending modulus than the sample with particle layers (33.4Msi compared to 30.4Msi).

This chapter, in part, will be submitted for publication to the *Journal of Composite Materials* with the title "Addition of Particulate Toughners to Increase Damping of Composite Laminates". The dissertation author was the primary investigator and co-authored the article with advisor J. B. Kosmatka.

Chapter 8 Electroviscoelastic Materials as Active Dampers

The ability to tailor damping response is highly desirable. Structures such as space satellites experience tremendous temperature shifts and also may need damping over a wide frequency range. There are no single damping materials that have the desirable damping characteristics throughout the entire temperature and frequency range. Thus, multiple layers of different damping material are needed to provide damping, which leads to an over-weight and inefficient design solution. Moreover adding damping in a passive constrained layer not only knocks down the resonant peaks, but also increases the response in the anti-resonant region, thus the response actually increases when excited in these regions. What is needed are viscoelastic damping materials that can be added to (or embedded within) structural components, where the damping levels and stiffness properties of the damping materials can be changed (or controlled) for different operating conditions (i.e. lower the damping levels when operating near an anti-resonance condition, and increase the damping levels when operating near a resonant condition). In Figure 8-1, typical ranges for stiffness and damping for different types of structural materials are presented, where a proposed single electroviscoelastic material (EVEM) can span a broad stiffness and frequency range.

Currently, electro-rheological materials have been developed that exhibit both changes in stiffness and damping as a function of voltage, but these materials are not self-supporting and thus can not be easily added to (or embedded within) structural

components. These fluid-like materials contain a suspension of fine particles (up to 50 microns) in non-conducting fluids that can stiffen into a semi-solid (very soft gel), within milliseconds, when subjected to a voltage and increases in viscosity by factors up to 10^5 have been observed. They are best used to build physical dampers that can be added discretely to mechanical systems having kinematic motion. Commercial acceptance has been slow because they are not self-supporting, can only operate in a small temperature range, have long-term storage instability problems, and have poor quality control. The few successful examples include automotive seat suspension components.

The development of an EVEM for damping applications was initially proposed by Shiga et. al.[41,42,44] They developed several electroviscoelastic gels and went as far as to suggest the gel could be used for "actively reducing sounds and vibrations", although no more mention was made of it and no damping studies were performed.

In this research, the goal is to develop an EVEM that can be used to actively control vibrations by using a single EVEM layer. EVEMs are similar to electrorheological fluids except the semiconducting particles are suspended in a self-supporting gel rather than a fluid. By applying a voltage across the material, properties such as modulus and loss factor can be varied and controlled, depending on the structural needs. The EVEM used in this research was a silicone gel with poly(p-phenylene) (PPP) particles doped with $FeCl_3$. When a voltage is applied across the EVEM, the modulus increases because the particles become attracted to each other. It is then harder to move the particles apart when a force is applied. The degree of

increase depends on the particles used, the amount of particles in the gel, and the type of silicone gel used.

The expected effect of applying voltage across the EVEM on the material loss factor is unclear. For a typical damping material, the loss factor curve peaks at a specific frequency, whereas the shear modulus increases until it levels off at the glassy modulus, as shown in Figure 8-2. At low frequencies, the loss factor increases with increased frequency (and higher shear modulus). At frequencies higher than the maximum loss factor frequency, however, the loss factor decreases with increased frequency (and higher shear modulus). It was unknown what part of the loss factor curve the EVEM will be in and it can be speculated that at a different frequency range the change in loss factor with applied voltage would be very different**.**

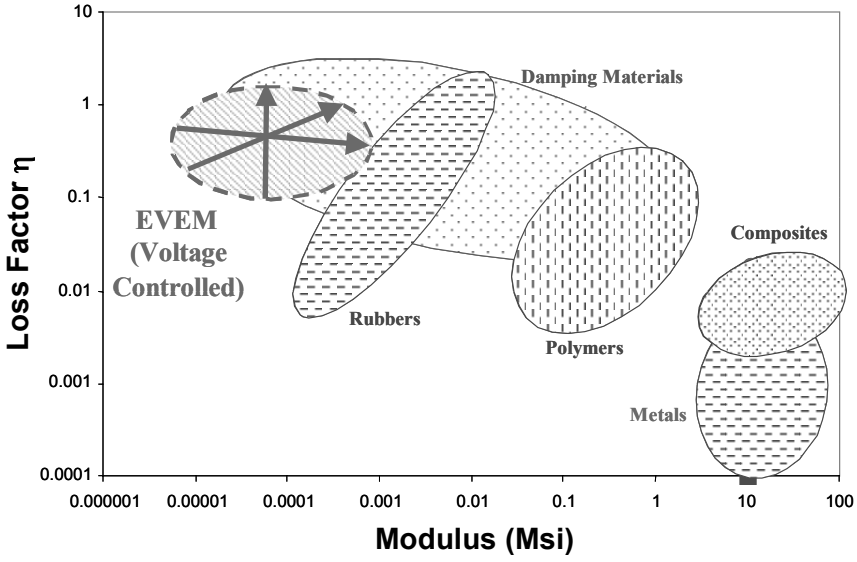

Figure 8-1. Stiffness and damping ranges for typical structural materials.

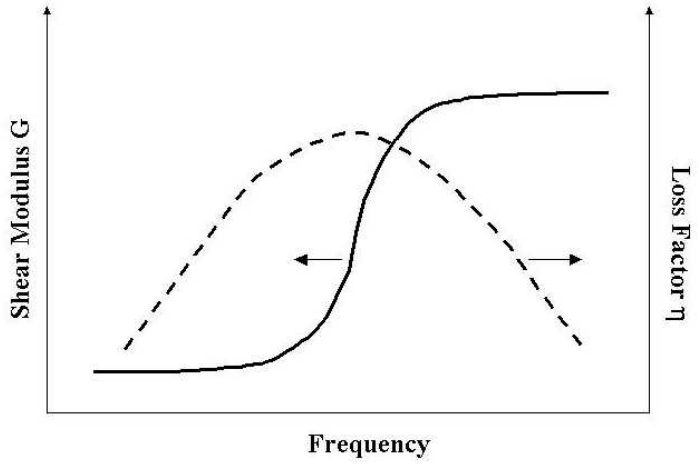

Figure 8-2. Shear modulus and loss factor variation with frequency for a typical damping material.

8.1 Polymer Development

The EVEMs are composed of a non-conducting gel or polymer with fine chargeable powders suspended in it. In the current study, two different silicone gels were combined to get a workable initial zero-voltage stiffness. Dow Corning Sylgard® 527 silicone dielectric gel (referred to as DEG) was used as the base material because it's soft enough to allow particle interaction and it has a high loss factor. Alone, however, it was difficult to handle because it could easily be "squeezed out" under small compression loads. Dow Corning Sylgard® 182 silicone elastomer (referred to as elastomer) was added to the Sylgard® 527 silicone dielectric gel to increase the stiffness. The densities of the elastomer and DEG were similar: 0.038 lb/in^3 and 0.035 lb/in^3, respectively.

The PPP particles were synthesized by coupling benzene using aluminum chloride and cupric chloride.[80] The particles were then doped with $FeCl_3$ by

suspending the PPP particles in ethanol and anhydrous $FeCl_3$ at 140^oF for 24 hrs. The particles were then dried at 302^oF. The powder tended to clump together so a grinder was used to make the particles finer and more uniformly sized. The powder was then dried again.

The powder was mixed with the silicone gel (in ratios varying from 10% to 25% by mass) and then placed under vacuum until there were no visible bubbles; this was typically 1-3 hours. The samples were made by curing the gel between 0.03" thick x 0.5" x 1.5" copper plates. The sample configuration is shown in Figure 8-3. Non-conducting Teflon spacers were placed between the copper plates to separate them and give the EVEM a uniform thickness of 0.025". Tape was placed around the bottom of the sample to keep the gel from leaking out during curing. The gel was placed in the sample a little at a time and frequently placed under vacuum to reduce voids. Once the gel had reached the top of the copper the samples were placed under vacuum for approximately 4 hours. A dc voltage of 1 kV was applied across the samples (except for a control sample with no voltage) for 1 hour to allow the particles to align. The 1 kV voltage was chosen because above that voltage some of the uncured samples shorted. The sample was then placed on a hot plate at 300^oF and 1 kV was again applied so the sample cured under the applied voltage. Once the EVEM was cured the tape and spacers were removed.

The gel was transparent, so one can use a microscope to see how well the particles are aligned. Figure 8-4 and Figure 8-5 are photograph from an optical microscope showing a sample cured with no voltage and under a 1 kV voltage,

respectively. Figure 8-5 illustrates the strong alignment of the particles as a result of curing under applied voltage. This sample was approximately 15% particles and 85% gel (80% DEG/20% Elastomer).

A series of samples were made to investigate: 1) the change in gel properties with mixture ratio, 2) the effect of varying the ratios of gel and particles, 3) the change in properties when particles were added and 4) the difference in samples cured with and without voltage. Table 8-1 shows the composition of the samples. Samples A1 to A5 were considered control samples because they were made to test the gel ratios (no particles); they were cured under a 1 kV voltage. Samples B1 to B5 were samples with particles that were cured under a voltage of 1 kV with particle ratios that varied from approximately 10% to 25% by mass and gel ratios that varied from approximately 50% DEG/50% elastomer to 90% DEG/10% elastomer. Sample C1 had particles but was cured without applied voltage. Figure 8-6 is a tertiary plot that more clearly describes the mass percentages of the three components: particles, DEG, and elastomer. A line is drawn at the particle mass limit of 0.25 because above that ratio the sample would short when voltage was applied.

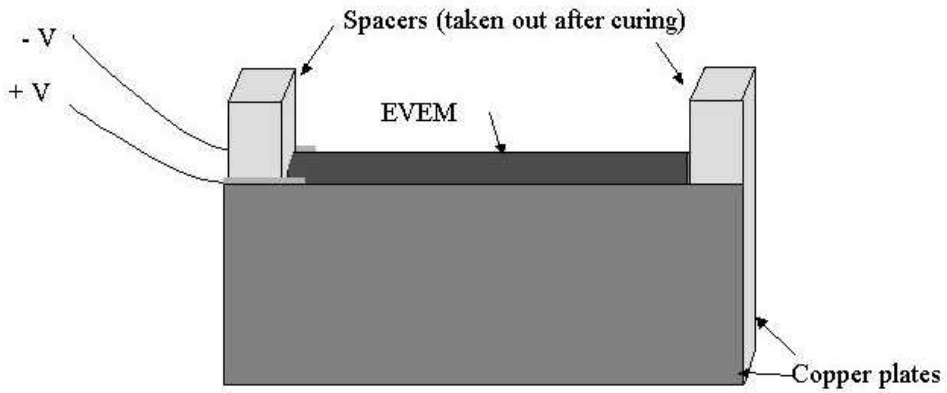

Figure 8-3. Sample configuration

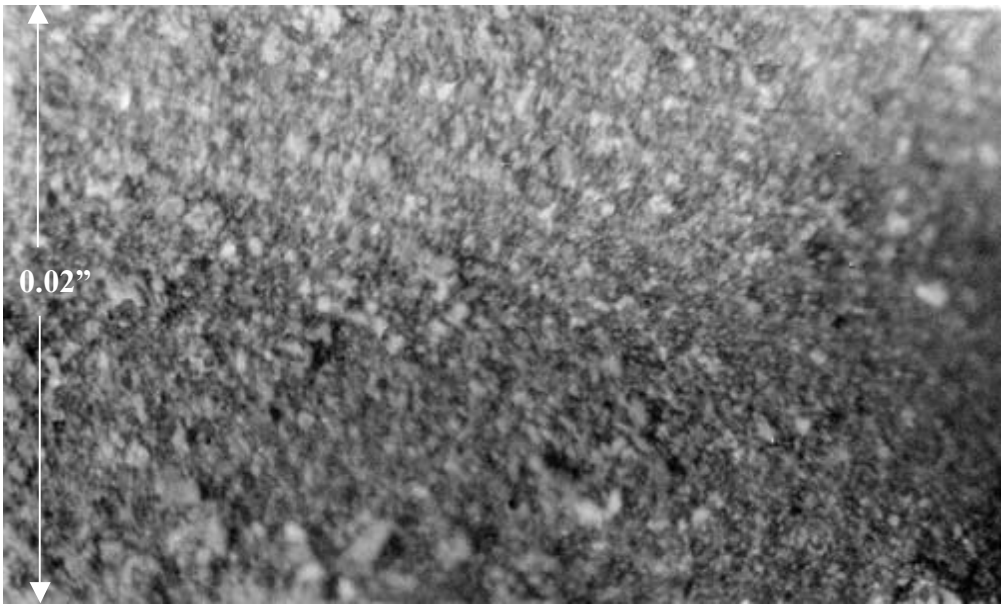

Figure 8-4. Optical photo of the cross-section of sample cured with no applied voltage. The PPP particles doped with FeCl show no allignment. The sample consisted of 15% particles and 85% gel (80% DEG/20% elastomer).

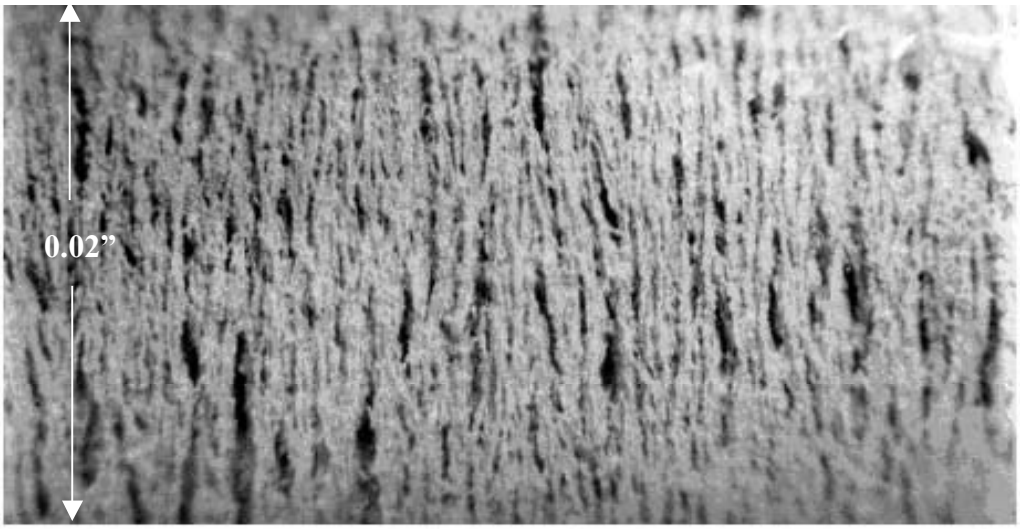

Figure 8-5. Optical photo of the cross-section of sample cured under 1 kV applied voltage. The PPP particles doped with $FeCl_3$ aligned across the sample. The sample consisted of 15% particles and 85% gel (80% DEG/20% elastomer).

Table 8-1. Sample descriptions. DEG refers to Dow Corning Sylgard® 527 silicone dielectric gel and elastomer refers to Dow Corning Sylgard® 182 silicone elastomer.

Sample	1 kV DC voltage applied during cure?	Particle mass %	Gel mass %	Gel composition	
				DEG mass %	Elastomer mass %
A1	Yes	0.00	100.00	0.00	100.00
A2	Yes	0.00	100.00	50.03	49.97
A3	Yes	0.00	100.00	79.99	20.01
A4	Yes	0.00	100.00	90.12	9.88
A5	Yes	0.00	100.00	100.00	0.00
B1	Yes	10.01	89.99	80.03	19.97
B2	Yes	20.09	79.91	80.03	19.97
B3	Yes	25.01	74.99	80.03	19.97
B4	Yes	19.90	80.10	50.14	49.86
B5	Yes	19.63	80.37	89.88	10.12
C1	No	19.98	80.02	80.02	19.98

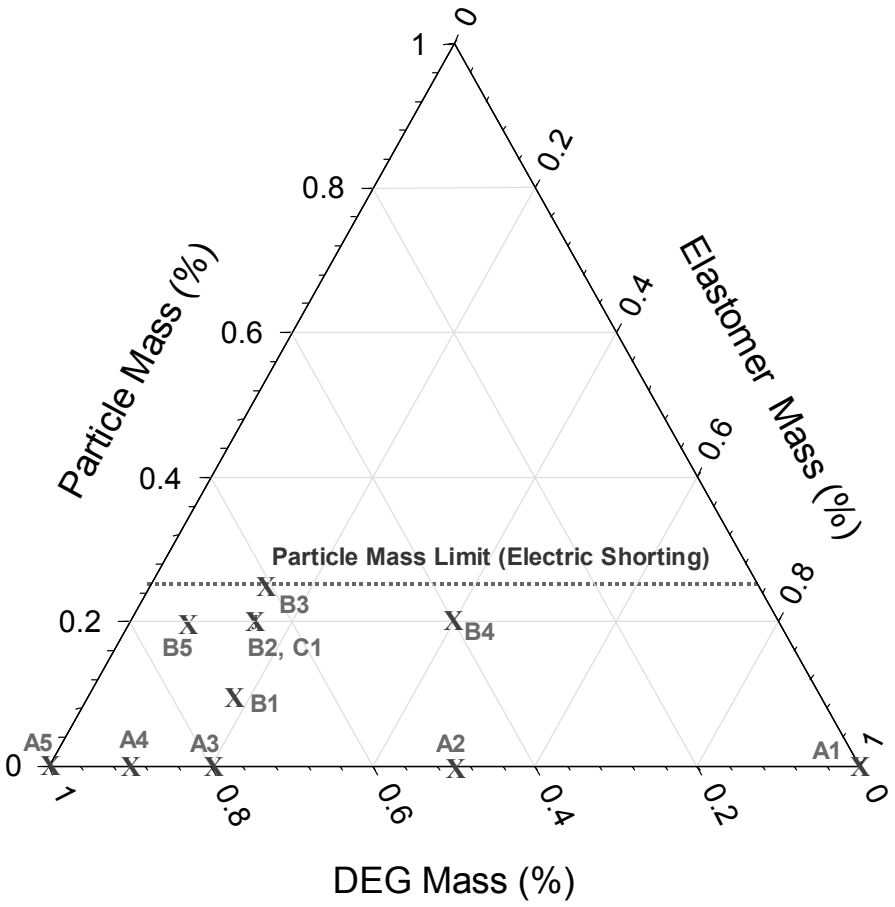

Figure 8-6. Diagram showing the mass percentages of the samples described in Table 8-1.

8.2 Experimental Testing

A new experimental test system[81] was developed that allows for the direct measurement of the complex stiffness and damping properties as a function of applied voltage and temperature. The test hardware consisted of a double-lap shear type refrigerated test fixture utilizing a laser vibrometer to measure the dynamic response from an applied harmonic excitation, as shown in Figure 8-7. One side of each specimen was bonded to either side of a moving mass and the other side of each specimen was bonded to a stationary block. The moving mass was attached to a nylon

stinger through a Kistler force transducer to a 50-lb shaker to accurately measure the input harmonic forces. Harmonic chirp excitations in the range from 20 to 300 Hz. were applied. A refrigeration system was added to control the temperature of the stationary and moving masses as well as to perform high and low temperature testing. All of the components were insulated so that a DC voltage of up to 2 kV could be applied across the specimens. A Polytec laser vibrometer was used to measure the velocity response of the mass and check the motion of the stationary blocks.

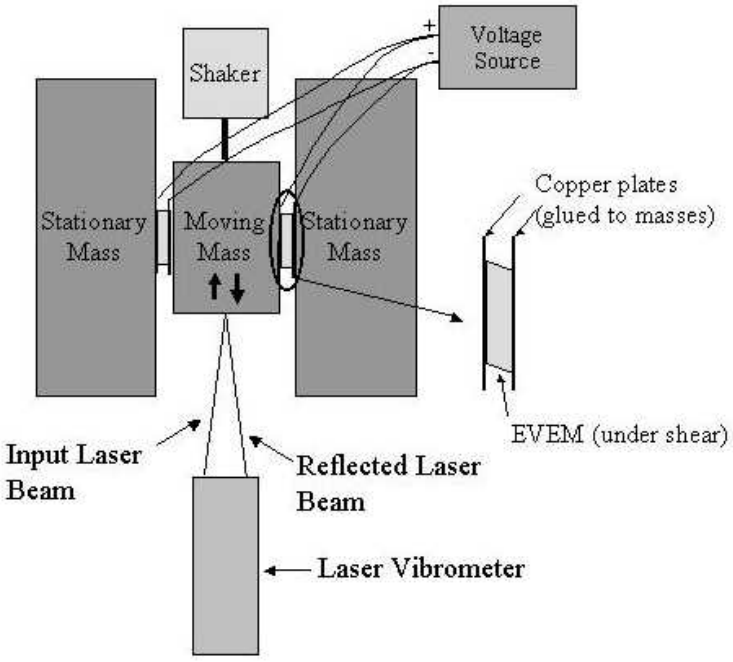

Figure 8-7. Testing configuration.

8.3 Results and Discussion

Three sets of samples were manufactured: 1) control samples without particles (samples A1-A5), 2) samples with particles cured with a DC voltage of 1 kV (40 kV/inch) (samples B1-B5) and 3) a sample with particles cured without voltage (sample C1).

8.3.1 Control samples

Five control samples (samples without particles) were made with various DEG and elastomer mass ratios. The tested frequency range was 20 Hz. to 120 Hz.; the intended maximum frequency was 300-500 Hz. but the scatter was too great at the higher frequencies. The maximum applied voltage was 2 kV and the current was zero. The testing was performed at room temperature ($70^{o}F \pm 1^{o}F$). Sample A1 was tested at $-5^{o}F$, $25^{o}F$, $70^{o}F$ and $140^{o}F$. Figure 8-8 and Figure 8-9 show how temperature variations affect the shear modulus and loss factor, respectively, of sample A1. The shear modulus and the loss factor both decreased significantly as the temperature increased. The shear modulus saw its largest drop when the temperature increased only $30^{o}F$ from $-5^{o}F$ to $25^{o}F$, where it went from 188.0 psi to 146.4 psi at 100 Hz. The shear modulus then decreased to 109.4 psi after an increase in temperature to $140^{o}F$, a temperature rise of $115^{o}F$. The loss factor was 0.26 at $-5^{o}F$ and 100 Hz. and decreased to 0.10 at $140^{o}F$ and 100Hz., an overall decrease of 62%.

Next, specimens A1-A5 were tested, at room temperature, over the frequency range 0-120 Hz. with 0V and 2kV applied voltage. See Figure 8-10 and Figure 8-11 for the measured shear modulus and loss factor results, respectively. The 0 V and 2

kV shear modulus and loss factor data were basically indistinguishable in all samples. Sample A1 (100% elastomer) had a shear modulus that was significantly higher than the other samples; for example at 70 Hz. the shear modulus for sample A1 (at both 0 V and 2 kV) was 129.5 psi while the next highest was 31.7 psi for sample A2 (50.03% DEG/49.97% elastomer). Samples A3 (79.99% DEG/20.01% elastomer), A4 (90.12% DEG/9.88% elastomer), and A5 (100% DEG) all had very low shear moduli at 70 Hz: 10.4 psi, 3.5 psi, and 2.8 psi, respectively. Clearly, as the percentage of DEG increased in the specimen the shear modulus dropped significantly. The difficulty in working with sample A5 (it was much too soft and easily squeezed or leaked out of the sample) led to its elimination as a suitable gel for EVEMs and is why the stiffer elastomer was added.

The maximum loss factor, 0.27 at 0 V and 50 Hz., was seen in sample A5 (100% DEG). The loss factor then decreased with increasing elastomer ratio through sample A2 (49.97% elastomer/50.03% DEG), which had a loss factor of 0.04. The loss factor of sample A1 (100% elastomer) was 0.16, significantly higher than the loss factor of both sample A2 and A3 (0.04 and 0.10, respectively). This is contrary to the predictions of the Rule of Mixtures that is discussed in the following paragraphs.

It was thought that the sample shear modulus G' of the samples A2-A4, which are a mixture of DEG and elastomer, would follow the rule of mixtures:

$$G' = V_{DEG} G'_{DEG} + (1 - V_{DEG}) G'_{elastomer} \tag{8-1}$$

where V_{DEG} is the volume fraction of DEG, G'_{DEG} is the modulus of the DEG, and $G'_{elastomer}$ is the shear modulus of the elastomer. To get the volume ratios the mass

ratios were simply divided by the densities, although since the densities of the two polymers were similar there was little difference. A plot of the shear moduli at 70°F, 70 Hz., and 0 V, shown in Figure 8-12, indicates that the samples do not follow the rule of mixtures. The shear moduli of samples A2-A4 are all significantly below what would be predicted with the rule of mixtures. If, however, the volume fractions from Equation 8-1 are squared:

$$G' = (V_{DEG})^2 G'_{DEG} + (1 - V_{DEG})^2 G'_{elastomer} \tag{8-2}$$

the fit is actually much closer. Sample A3 has the largest difference in predicted and experimental data; the experimental data is 10.4 psi and the Equation 8-2 predicted value (referred to as the "modified rule of mixtures") is 6.4 psi. The modified rule of mixtures predicted values for samples A2 and A4 are within 4% of the experimental values.

The loss factor at 70°F, 70 Hz., and 0 V, shown in Figure 8-13, didn't come close to following the rule of mixtures:

$$\eta = (V_{DEG})\eta_{DEG} + (1 - V_{DEG})\eta_{elastomer} \tag{8-3}$$

For sample A2 (50.03% DEG/49.97% elastomer), the rule of mixtures would predict a loss factor of 0.227, while the measured loss factor was 0.039. Similar to the shear modulus, a "modified rule of mixtures" where the volume fractions are raised to a power of 3.5:

$$\eta = (V_{DEG})^{3.5}\eta_{DEG} + (1 - V_{DEG})^{3.5}\eta_{elastomer} \tag{8-4}$$

provides a much better fit. The modified rule of mixtures prediction for samples A2 and A3 are within 8% of the experimental values; for sample A4 the modified rule of mixtures prediction is 16% lower than the experimental value.

The low shear moduli leads to a suspicion that in the combination samples the elastomer was not able to completely cure because of polymer interaction with the DEG. The fact that the loss factors of the combination samples (samples A2, A3, and A4) are all lower than the loss factors of the single-polymer samples (samples A1 and A5) also indicates the polymers didn't simple "mix".

8.3.2 Samples with particles

Five samples were made with particles. The first three samples (B1-B3) were made with a gel that had a target mass ratio (more exact percentages shown in Table 8-1) of 80% DEG/20% elastomer. The purpose was to test increasing the target particle mass ratio: in sample B1 it was 10%, in B2 it was 20%, and in B3 it was 25%. Samples B4 and B5 had 20% particle mass target ratios but different gel compositions: B4 had a target gel ratio of 50% DEG/50% elastomer and B5 had a target gel ratio of 90% DEG/10% elastomer. The samples with particles were tested from 20 Hz. to 300 Hz. The maximum voltage had to be limited to 1.5 kV for the samples with particles because at 2 kV most of them shorted.

Sample B1 had the smallest particle amount (10.01% particles, 89.99% gel) and a gel composition of 80.03% DEG/19.97% elastomer. The shear modulus, shown in Figure 8-14, increased to 1.5 psi with a 1.5 kV applied voltage; however, with such

small shear moduli that was a significant percent increase (i.e. at 100 Hz. the increase was 24%). The loss factor, shown in Figure 8-15, appears to decrease slightly at some frequencies with applied voltage but the scatter is large making it difficult to quantify.

Sample B2 had double the particles as sample B1 (20.09% particles, 79.91% gel) and the same gel composition (80.03% DEG/19.97% elastomer). The shear modulus and loss factor are shown in Figure 8-16 and Figure 8-17, respectively. The increase in shear modulus with 1.5 kV applied voltage was dramatic; at 100 Hz. the shear modulus was 30.0 psi at 0 V and 79.8 psi at 1.5 kV, an increase of 166%. The loss factor saw a significant decrease with applied voltage. At 100 Hz. the loss factor was 0.48 and at 1.5 kV it decreased to 0.31, a 35% decrease.

The particles were again increased in sample B3, this time to 25.01%. The gel was the same as in B1 and B2 (80.03%DEG and 19.97% elastomer). The sample was deemed untestable because of problems both with manufacturing and testing. The uncured gel and particle mix was very thick and even under a 28" Hg vacuum for 24 hours the air bubbles could not be removed. When voltage was applied to the sample for cure only a relatively small voltage (<40 V) was applied before the sample began shorting.

Sample B4 was made with 19.90% particles but a much stiffer gel than samples B1-B3: the gel was composed of 50.14% DEG and 49.86% elastomer. The shear modulus, shown in Figure 8-18, did measurably increased with an applied 1.5 kV voltage; the increases was 7.2% at 100 Hz. The loss factor, shown in Figure 8-19,

looks to have decreased very slightly above approximately 80 Hz. with an applied voltage of 1.5 kV.

Sample B5 had 19.63% particles and a very soft gel (89.88% DEG and 10.12% elastomer). Having a softer matrix apparently allowed the particles to interact easily because the property changes with a 1.5 kV applied voltage was very large; Figure 8-20 and Figure 8-21 show the dramatic increase of the shear modulus and loss factor, respectively. At 100 Hz. the shear modulus jumped from 16.6 psi at 0 V to 82.3 psi at 1.5 kV. The loss factor also had a dramatic response; at 100 Hz. and 0 V the loss factor was 0.71 and at 1.5 kV the loss factor dropped to 0.30.

The shear modulus of samples made with target mass ratio of 80% DEG/20% elastomer – samples A3, B1 and B2 – are shown together in Figure 8-22 (shear modulus vs. frequency) and Figure 8-23 (shear modulus vs. particle mass% at 100 Hz.). Sample B1, with 10% particles, had a lower shear modulus than the gel alone (sample A3), although both were quite low; at 100 Hz. the shear modulus for sample B1 was 3.9 psi at 0V and 4.8 psi at 1.5 kV and the shear modulus for sample A3 was 10.50 psi at both 0V and 2 kV. The shear modulus for Sample B2 (20% particles) jumped to 30.4 psi at OV and 79.8 psi at 1.5 kV. The fact that sample B1 (10% particles) had relatively small changes with applied voltage indicates there was very little particle interaction. If the particles didn't bond well with the polymers but also didn't interact or bond with each other the shear modulus would decrease with the addition of a small number of particles. With sample B2 the large number of particles increased the shear modulus, either by bonding with each other or interacting (i.e.

such as not allowing the particles to move past one another when sheared). Other samples also showed an increase in modulus when 20% particles (by mass) were added. Both sample A2 and sample B4 had gel ratios of 50% DEG/50% elastomer, with sample B4 having the additional 20% particles; Figure 8-24 shows the shear modulus comparison of the two samples. At 100 Hz. sample A2 had a shear modulus of 31.7 psi at both 0V and 2 kV and sample B4 had a shear modulus of 106.1 psi at 0 V and 113.8 psi at 1.5 kV. Similar results were seen in samples A4 and B5 which had 90% DEG/ 10% elastomer gel compositions as shown in Figure 8-25. At 100 Hz. sample A4 had a shear modulus of 3.6 psi at both 0V and 2 kV and sample B5 had a shear modulus of 16.6 psi at 0V and 106.1 psi at 1.5 kV.

The loss factors of samples A3, B1 and B2 are shown together in Figure 8-26 (loss factor vs. frequency) and Figure 8-27 (loss factor vs. particle mass% at 100 Hz.). The addition of particles drastically increased the loss factor but once there were enough particles to increase the modulus (indicating an interaction) then the loss factor decreased somewhat: the loss factor for sample A3 (no particles) had the lowest loss factor (0.15 at 0V and 2 kV), sample B1 (10% particles), had the highest loss factor (0.70 at 0V and 0.64 at 1.5 kV), and sample B2 (20% particles) had a loss factor of 0.48 at 0V and 0.31 at 1.5 kV. As shown in Figure 8-28 adding particles also increased the loss factor for samples with 50% DEG/50% elastomer: at 100 Hz. the loss factor for sample A2 (no particles) was 0.05 at OV and 2 kV and sample B4 (20% particles) had a loss factor of 0.25 at 0V and 0.24 at 1.5 kV. Samples with 90% DEG/10% elastomer, shown in Figure 8-29**,** had an increase in loss factor with added

particles at 0V but at increased voltage (1.5 or 2 kV) the loss factor was similar with or without particles: at 100 Hz. sample A4 (no particles) had a loss factor of 0.28 at 0V and 2 kV and sample B5 (20% particles) had a loss factor of 0.71 at 0V and 0.29 at 1.5 kV.

8.3.3 Sample with particles cured without voltage

Sample C1 was made with a composition of 19.98% particles and 80.02% gel (80.02% DEG/19.98% elastomer) and was cured without voltage. The applied voltage before and during curing was expected to "line up" the particles in the liquid uncured gel so when the gel cured the particles were close together and could interact with an applied voltage. Sample C1 was made to explore whether the particles needed to be "lined up" for the material properties to change with applied voltage. Surprisingly, both the shear modulus and loss factor changed significantly with applied voltage in sample C1; the shear modulus is shown in Figure 8-30 and the loss factor is shown in

Figure 8-31. At 100 Hz. the modulus increased from 23.5 psi at 0 V to 47.3 psi at 1.5 kV (a 101% increase) and the loss factor at 100 Hz. decreased from 0.47 at 0 V to 0.36 at 1.5 kV (a 23% decrease).

Sample C1 had the same target composition as sample B2 and the only manufacturing difference was that sample C1 was cured without voltage and sample B2 was cured with a voltage of 1 kV. Comparisons of shear modulus and loss factor are shown in Figure 8-32 and Figure 8-33, respectively. For both properties the changes with applied voltage were significantly greater in sample B2 than in sample C1; at 100 Hz. the shear modulus increased 166% with applied voltage in sample B2

whereas it increased 101% in sample C1 and the loss factor decreased 35% in sample B2 whereas it decreased 23% in sample C1. It appears that while lining up the particles does increase the sample reaction to applied voltage, the sample properties will still change when there are a large amount of particles (as in sample C1) because the particles are still close enough to interact.

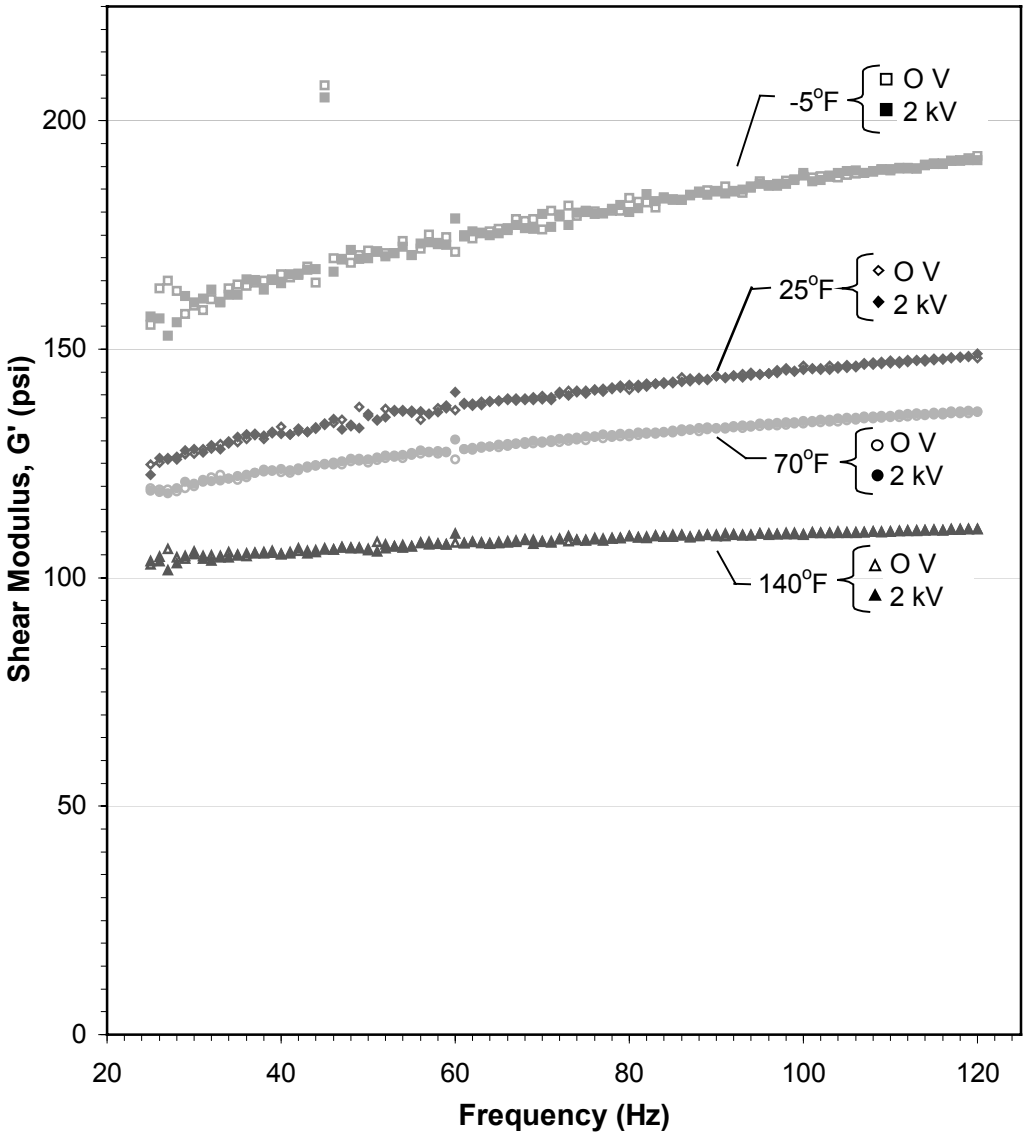

Figure 8-8. Shear moduli of sample A1 (100% elastomer, no particles) as a function of frequency, voltage, and temperature.

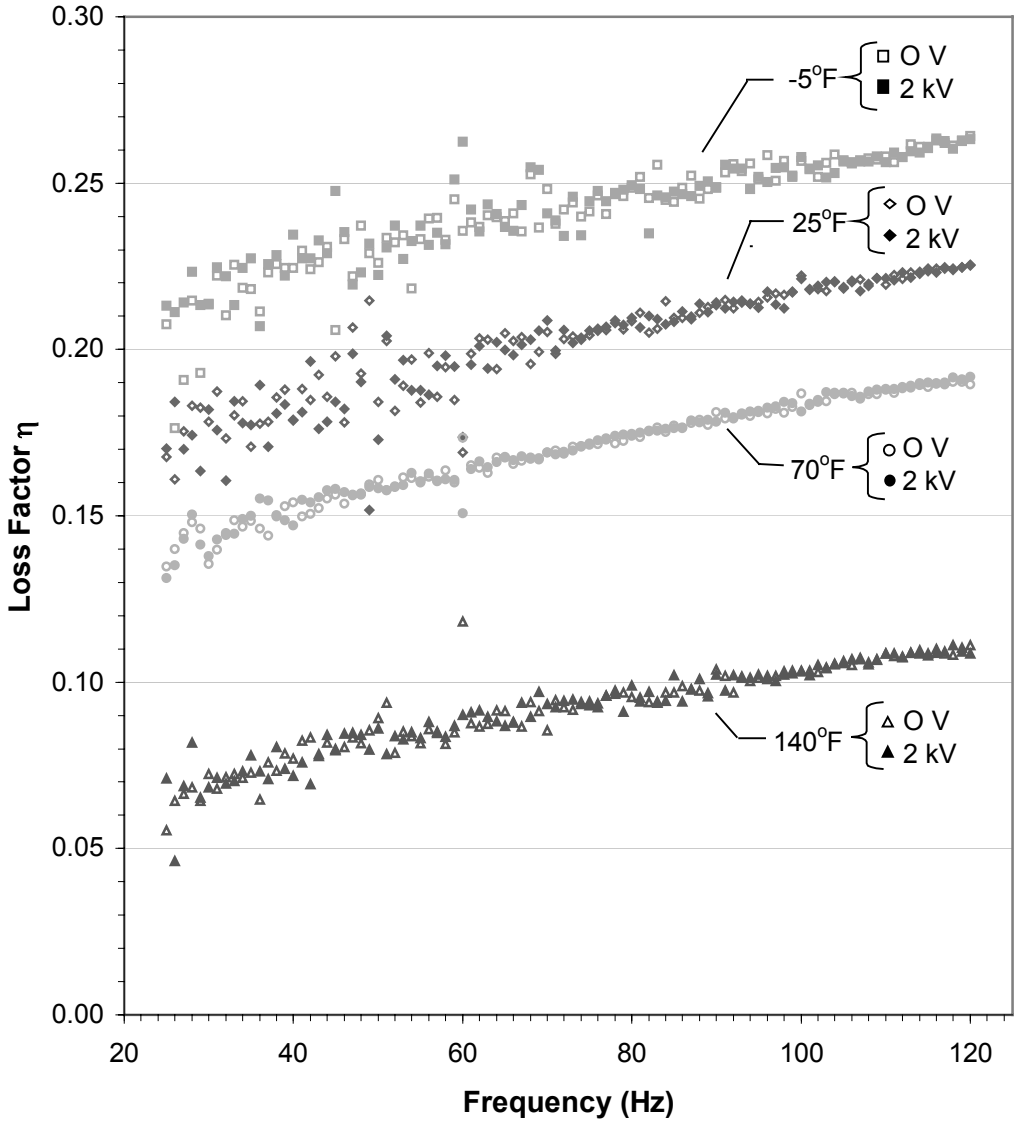

Figure 8-9. Loss factors of sample A1 (100% elastomer, no particles) as a function of frequency, voltage, and temperature.

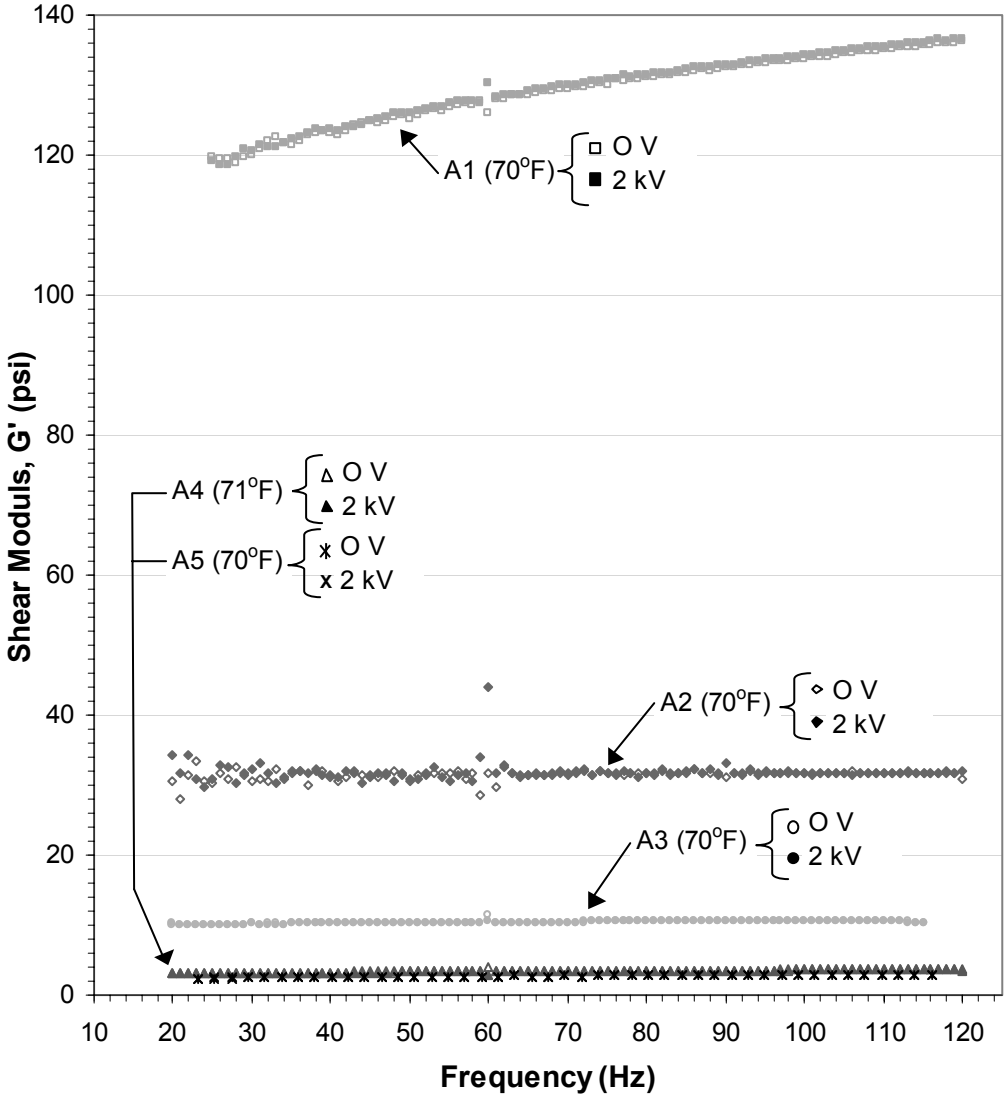

Figure 8-10. Shear moduli of samples A1 to A5 as a function of frequency (20 to 120 Hz.) and voltage (0 V and 2 kV). Target compositions: A1 (100% elastomer), A2 (50% DEG/50% elastomer), A3 (80% DEG/20% elastomer), A4 (90% DEG/10% elastomer), A5 (100% DEG).

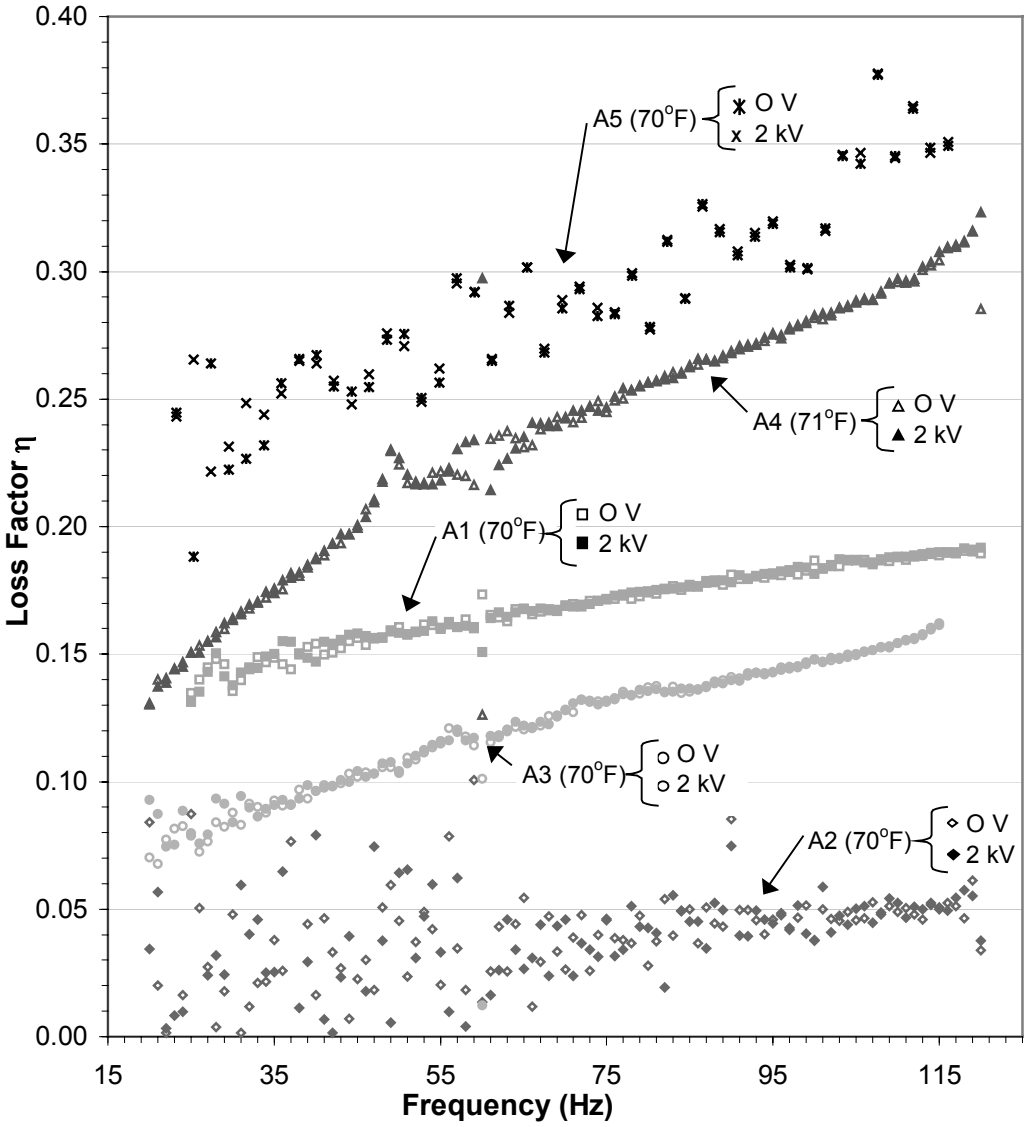

Figure 8-11. Loss factors of samples A1 to A5 as a function of frequency (20 to 120 Hz.) and voltage (0 V and 2 kV). Target compositions: A1 (100% elastomer), A2 (50% DEG/50% elastomer), A3 (80% DEG/20% elastomer), A4 (90% DEG/10% elastomer), A5 (100% DEG).

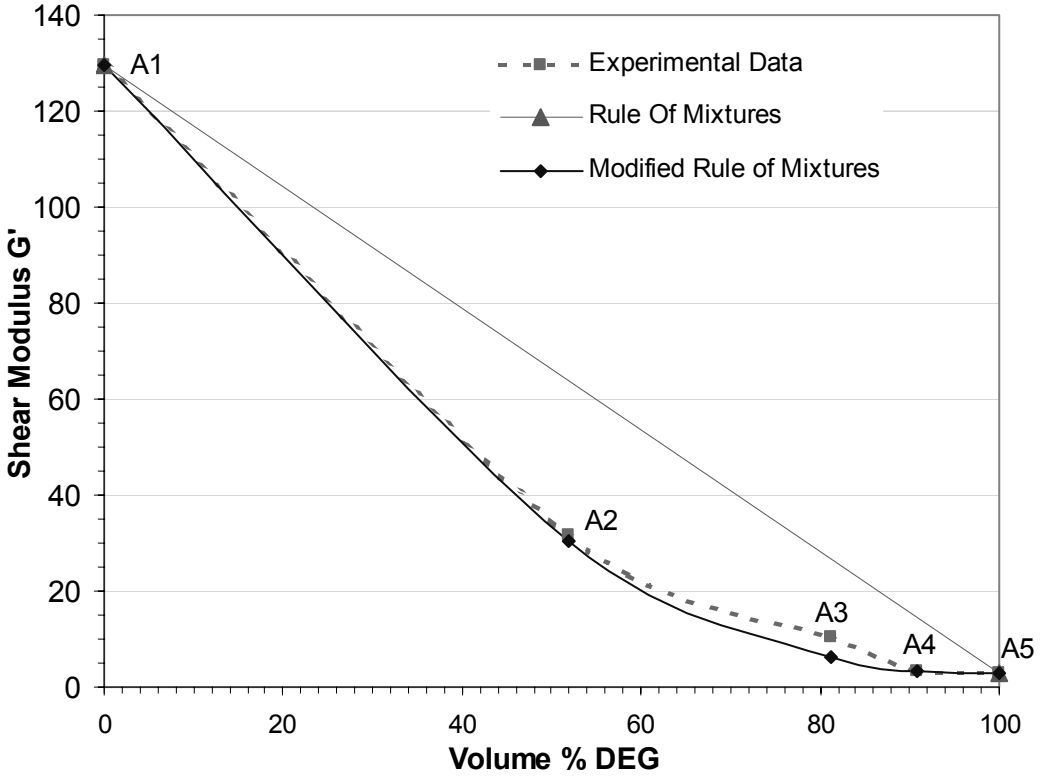

Figure 8-12. Shear moduli of samples A1-A5 at 70°F, 70 Hz., and 0 V vs. the volume fraction DEG. Also plotted are the predicted shear moduli from the rule of mixtures and the "modified rule of mixtures" (Equations 8-1 and 8-2, respectively).

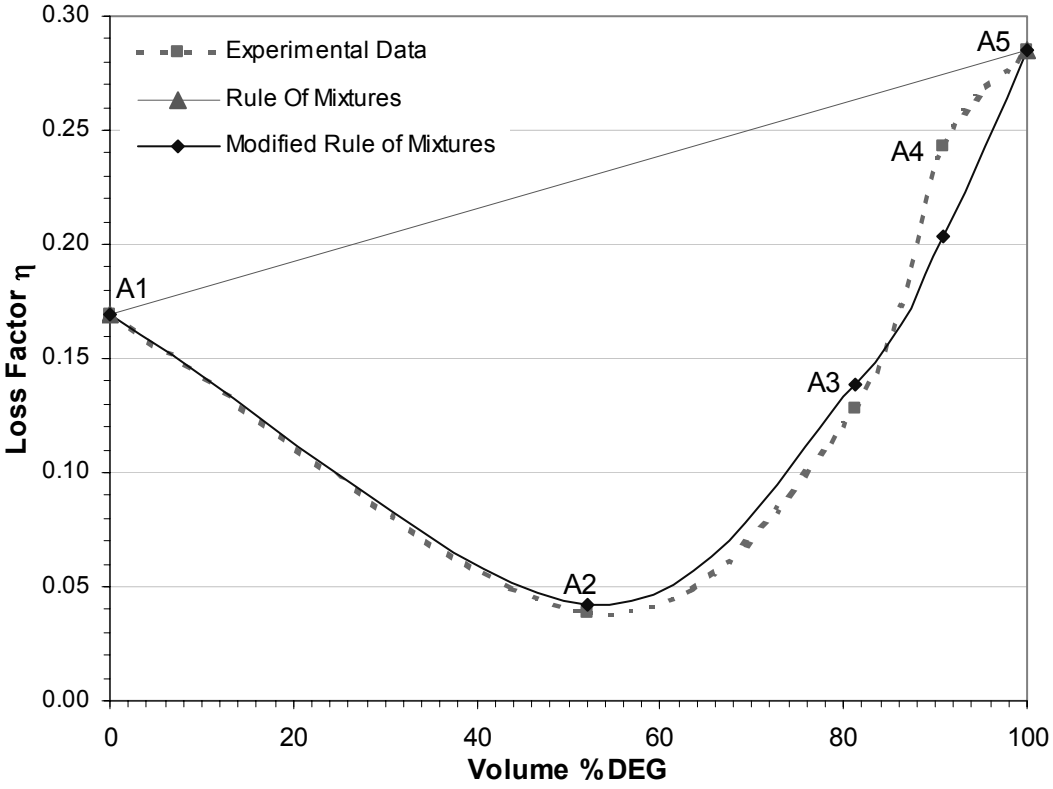

Figure 8-13. Loss factors of samples A1-A5 at 70°F, 70 Hz., and 0 V vs. the volume fraction DEG. Also plotted are the predicted loss factors from the rule of mixtures and the "modified rule of mixtures" (Equations 8-3 and 8-4, respectively).

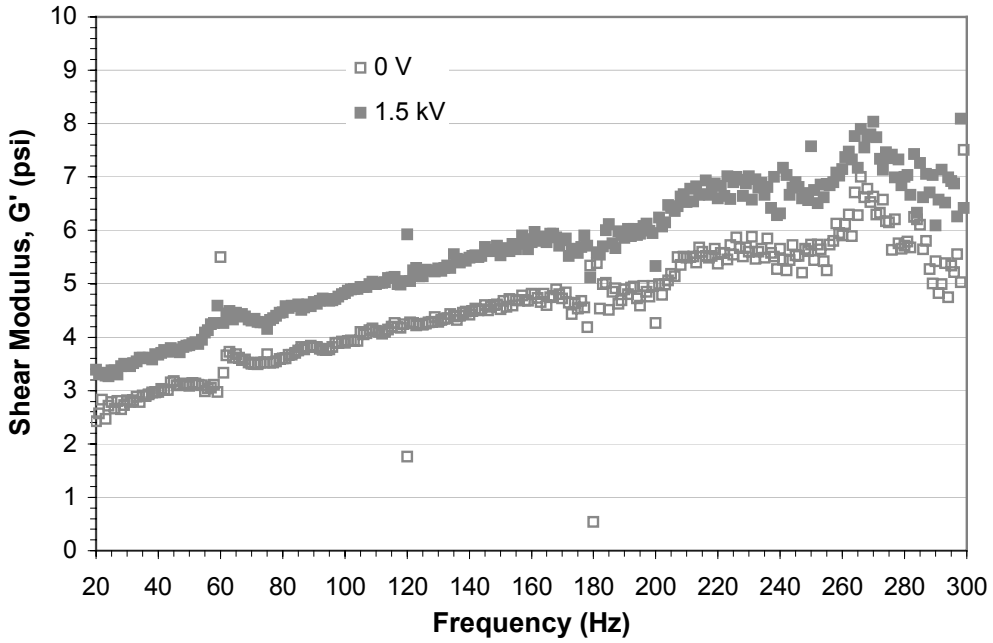

Figure 8-14. Shear modulus of sample B1 (10% particle, 72% DEG, 18% elastomer) at 71°F.

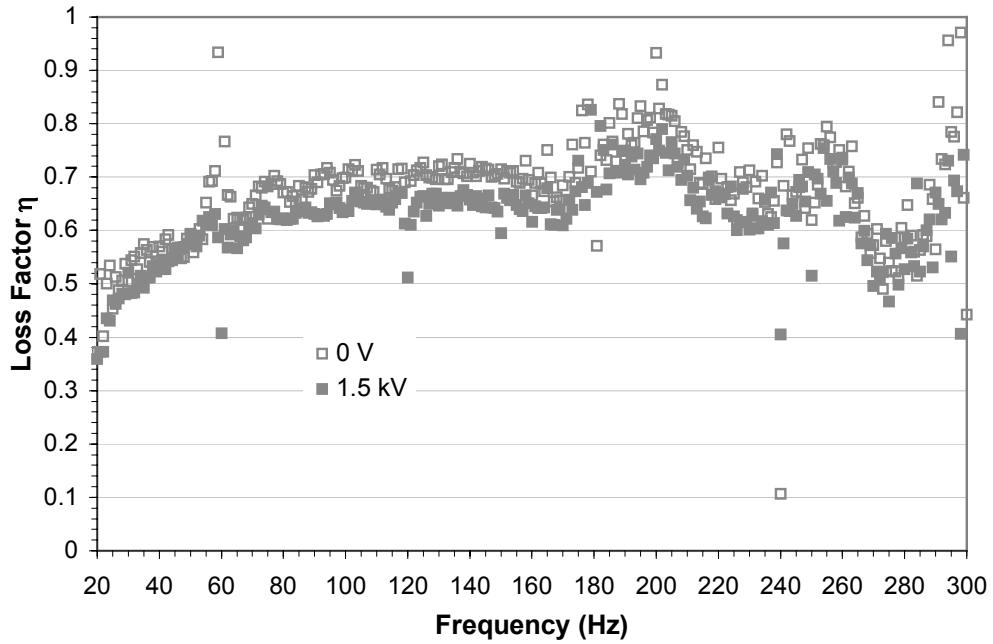

Figure 8-15. Loss factor of sample B1 (10% particle, 72% DEG, 18% elastomer) at 71°F.

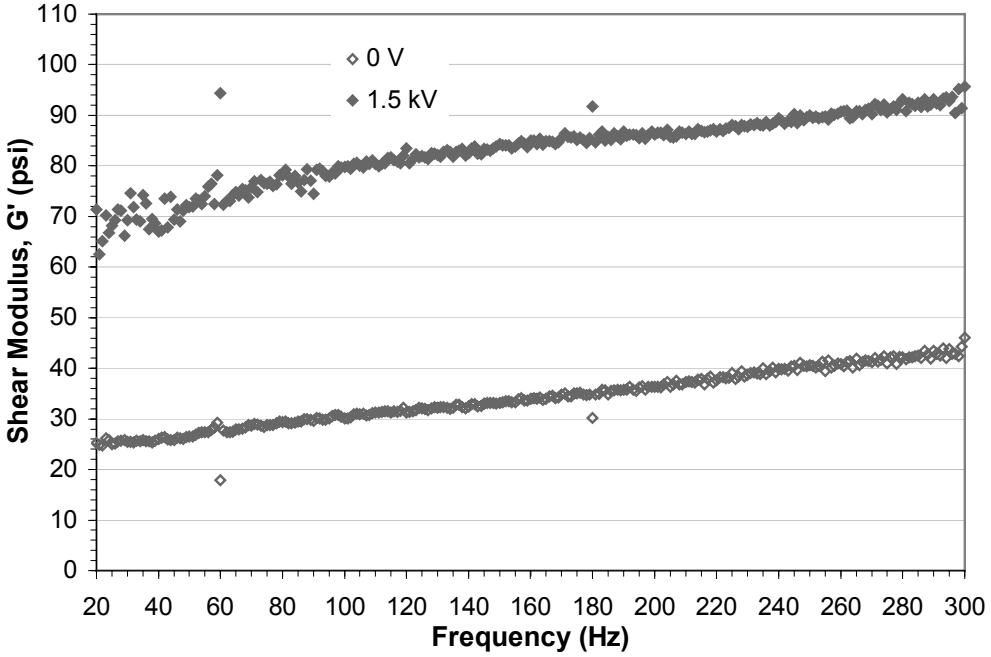

Figure 8-16. Shear modulus of sample B2 (20% particle, 64% DEG, 16% elastomer) at 71°F.

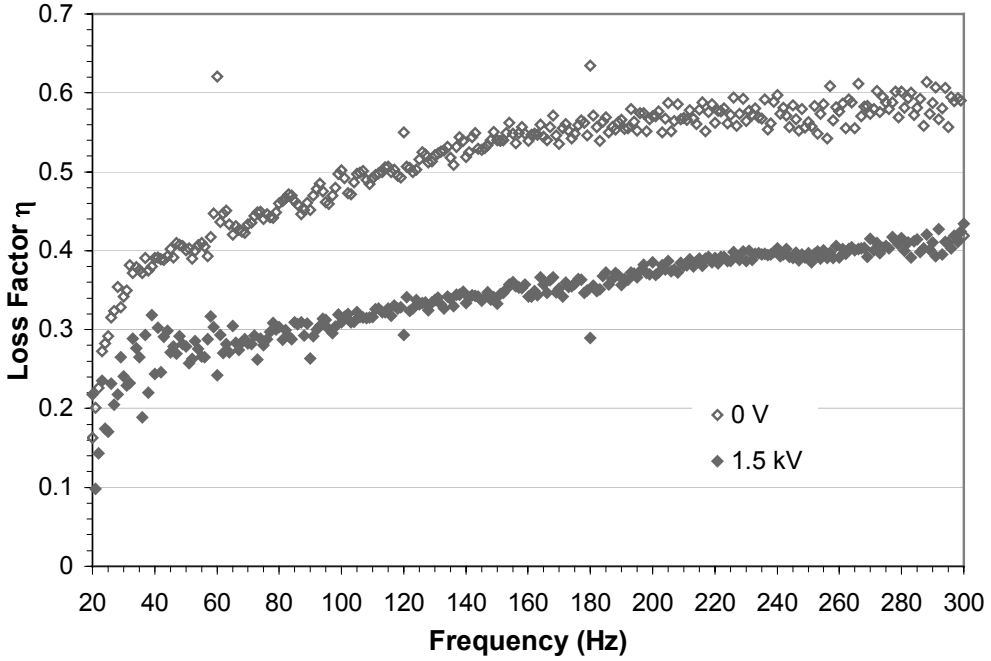

Figure 8-17. Loss factor of sample B2 (20% particle, 64% DEG, 16% elastomer) at 71°F.

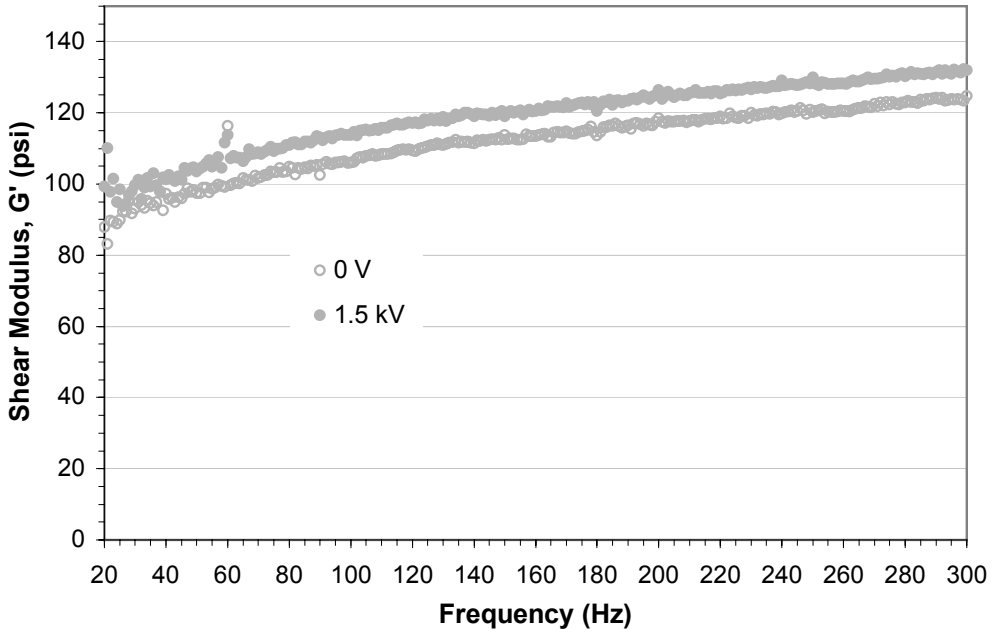

Figure 8-18. Shear modulus of sample B4 (20% particle, 40% DEG, 40% elastomer) at 71°F.

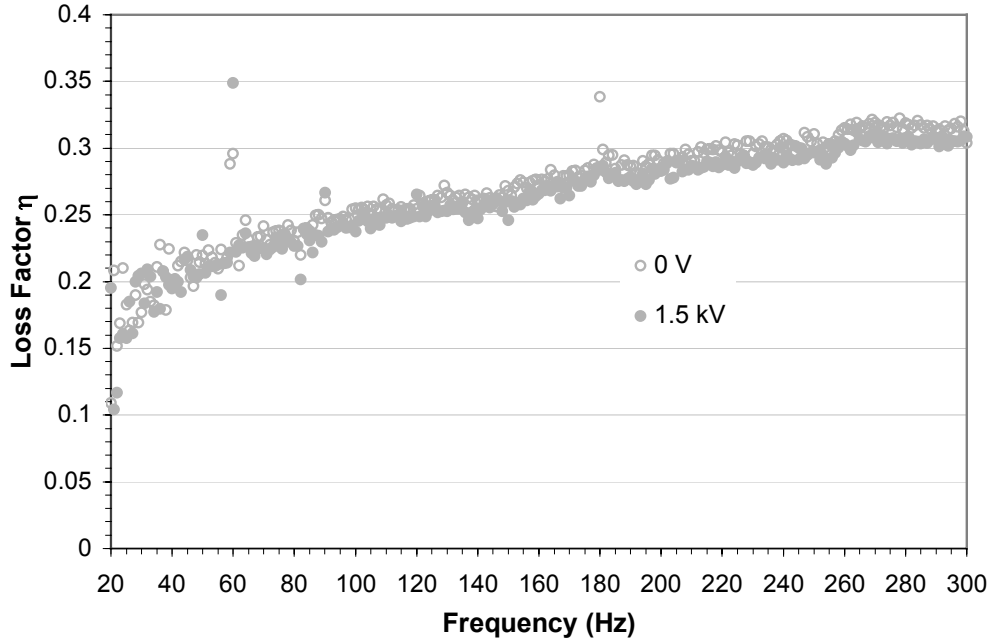

Figure 8-19. Loss factor of sample B4 (20% particle, 40% DEG, 40% elastomer) at 71°F.

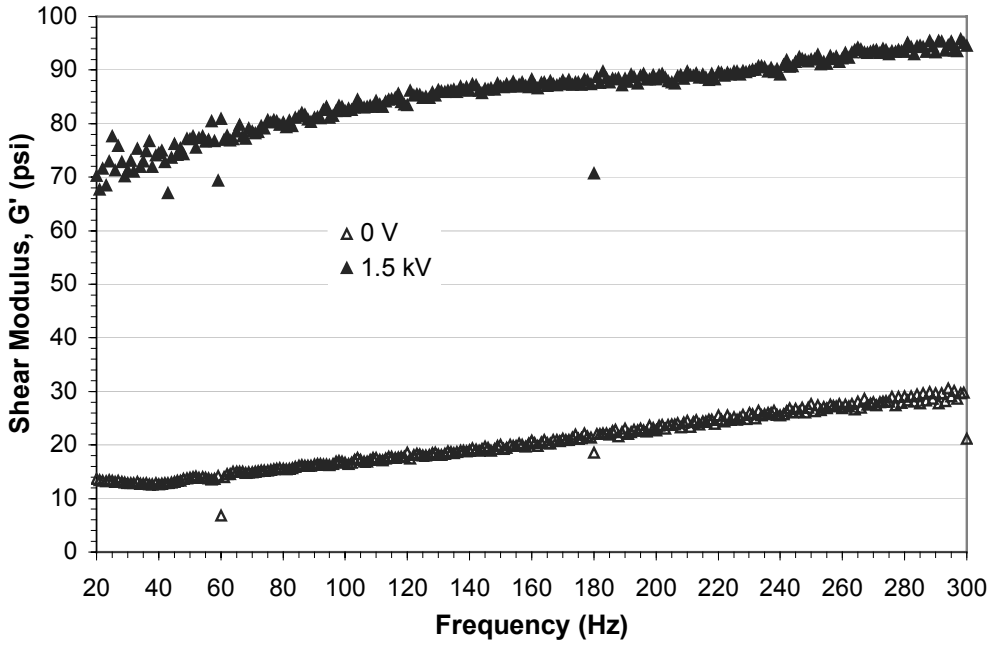

Figure 8-20. Shear modulus of sample B5 (20% particle, 72% DEG, 8% elastomer) at 71°F.

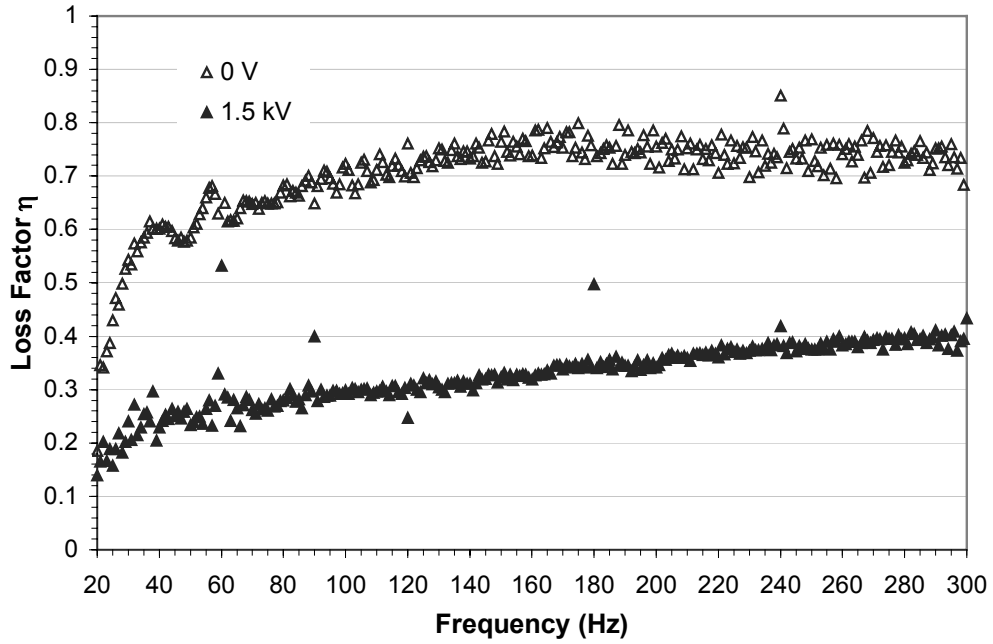

Figure 8-21. Loss factor of sample B5 (20% particle, 72% DEG, 8% elastomer) at 71°F.

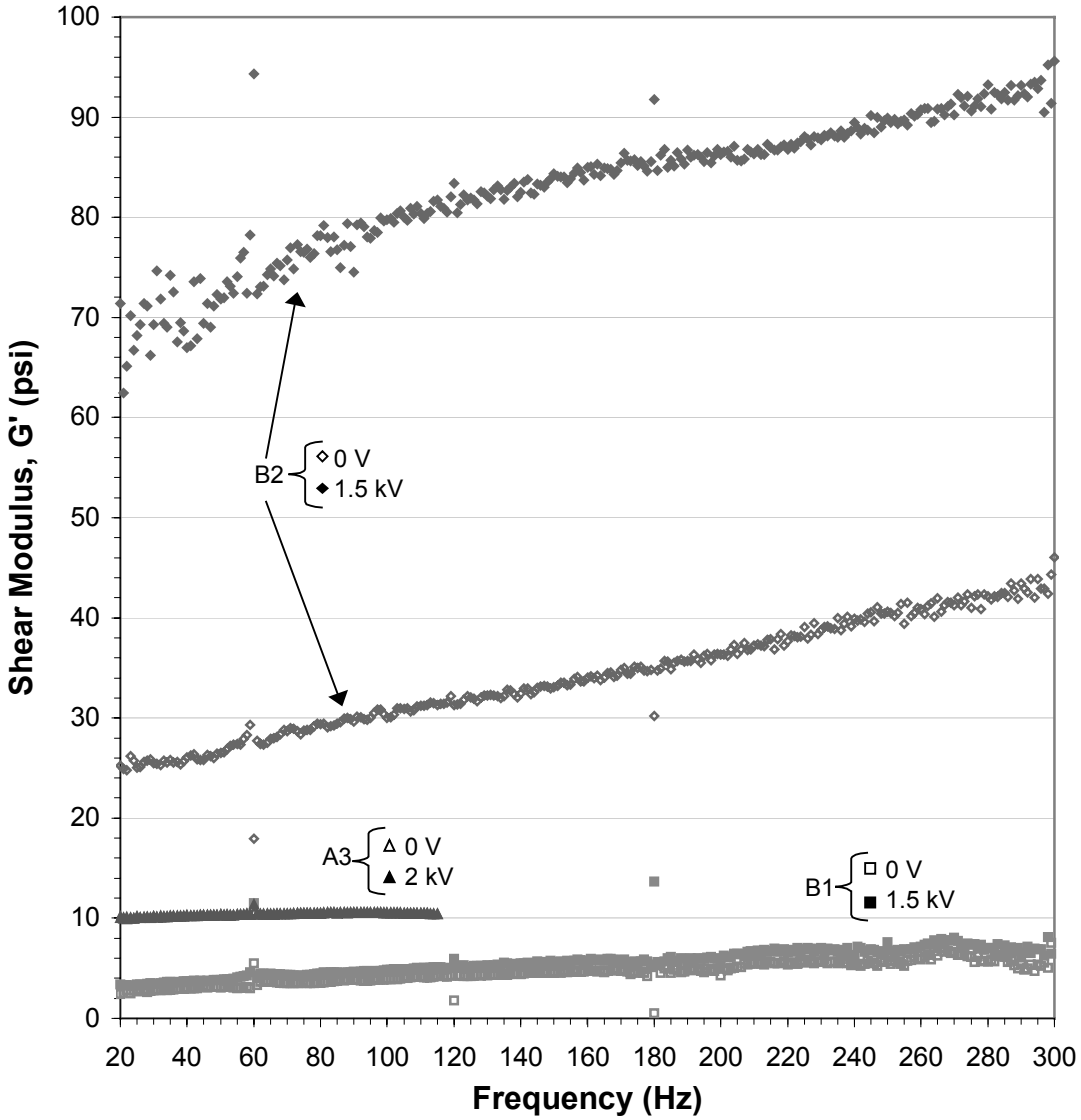

Figure 8-22. Shear moduli of samples with a target gel composition (by mass) of 80% DEG/20% elastomer. Sample A3 has zero particles, B1 has 10% particles (total composition 10% particle, 72% DEG, 18% elastomer), and B2 has 20% particles (total composition 20% particle, 64% DEG, 16% elastomer) at 71 $\pm$ 1°F.

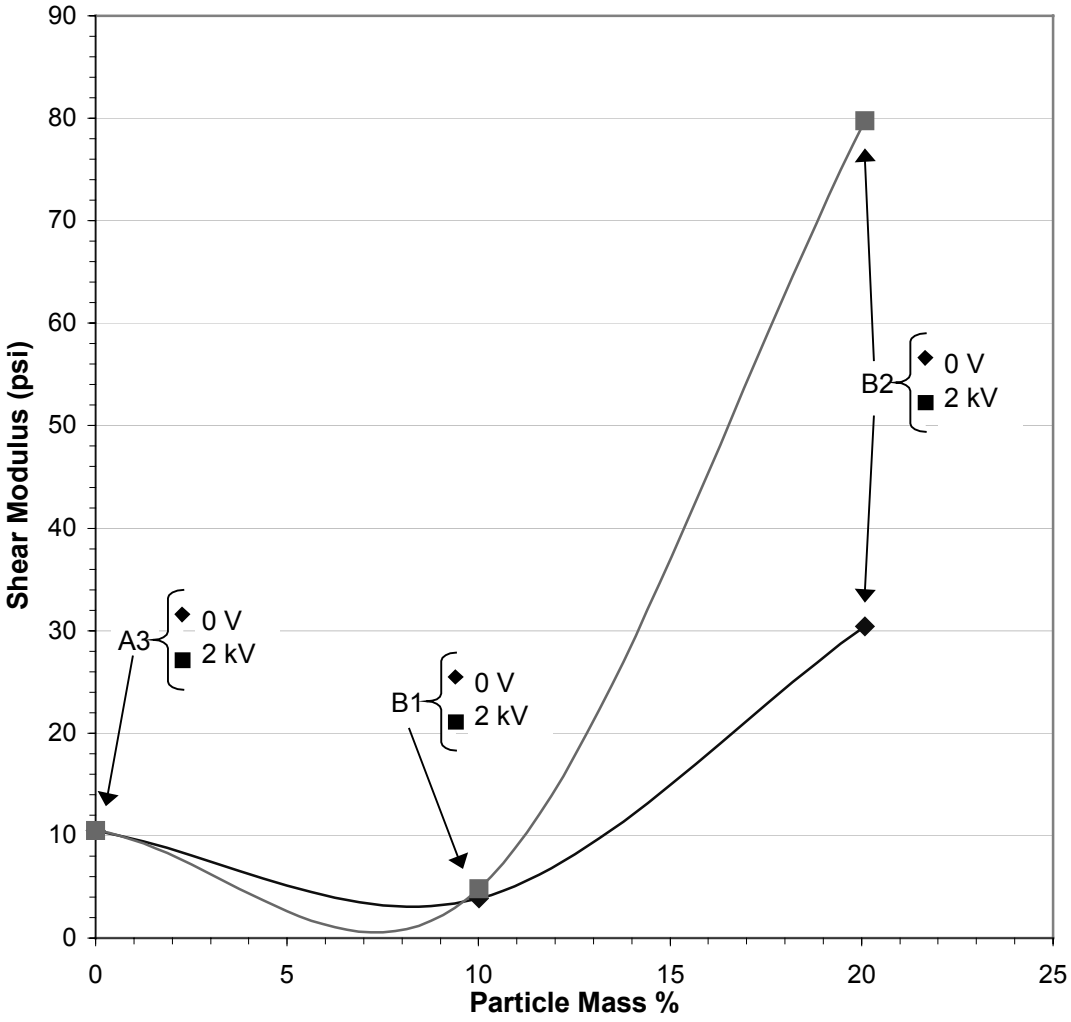

Figure 8-23. Shear moduli vs. particle mass of samples with a target gel composition (by mass) of 80% DEG/20% elastomer. Sample A3 had zero particles, B1 had 10% particles (total composition 10% particle, 72% DEG, 18% elastomer), and B2 had 20% particles (total composition 20% particle, 64% DEG, 16% elastomer) at 71 $\pm$ 1°F and 100 Hz.

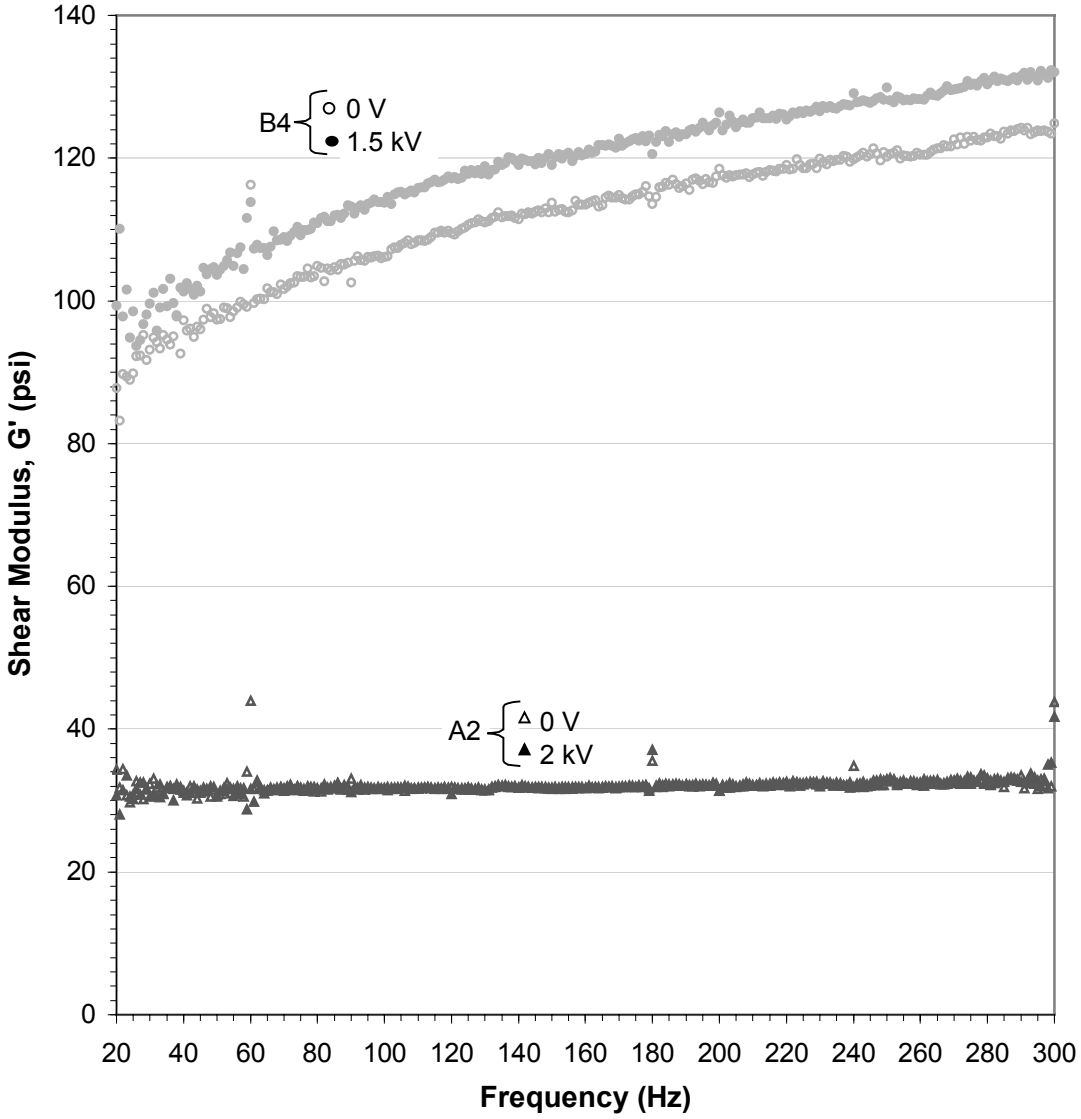

Figure 8-24. Shear moduli of samples with a target gel composition (by mass) of 50% DEG/50% elastomer. Sample A2 had zero particles and B4 had 20% particles (total composition 20% particle, 40% DEG, 40% elastomer) at 71 $\pm$ 1°F.

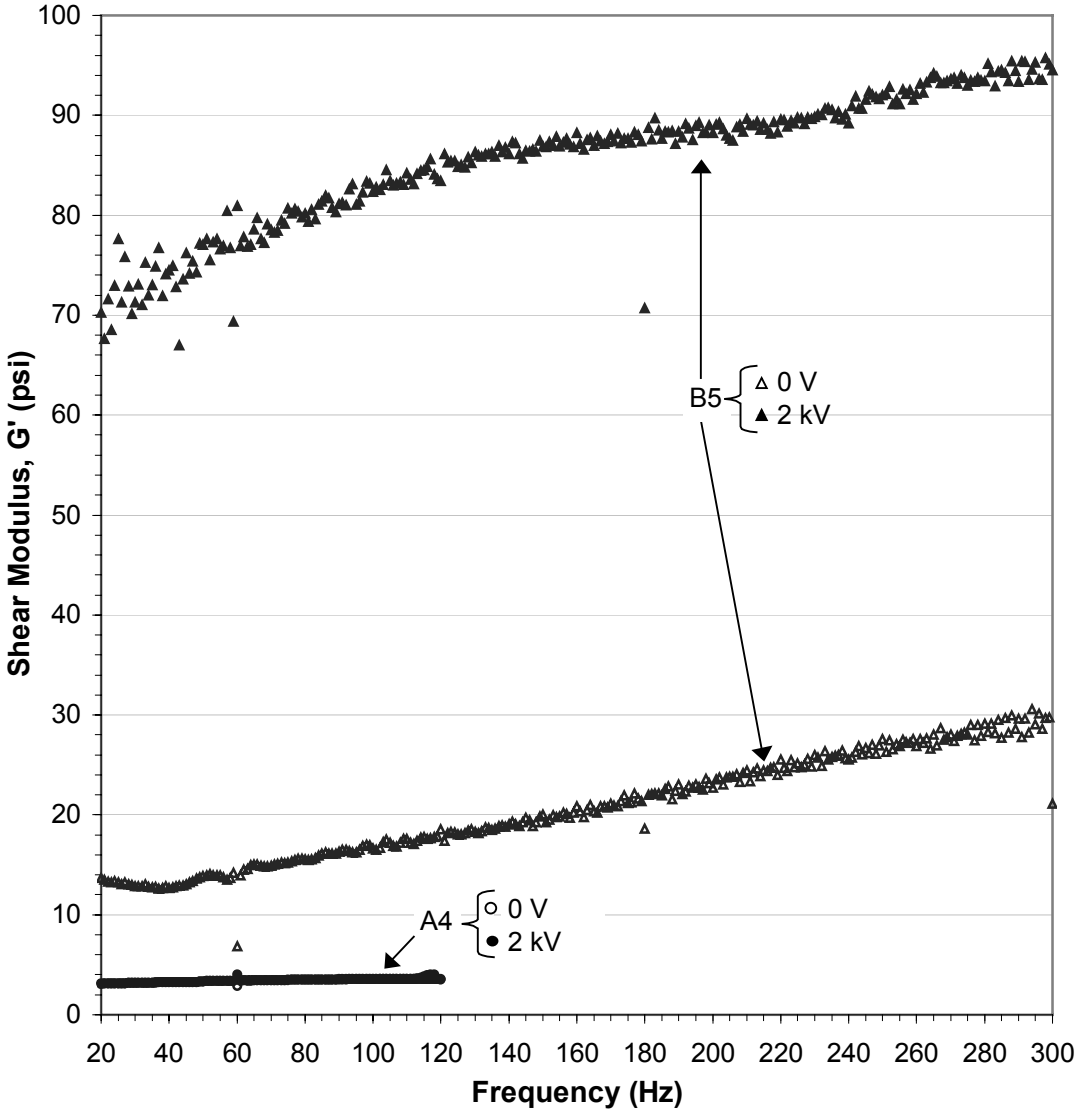

Figure 8-25. Shear moduli of samples with a target gel composition (by mass) of 90% DEG/10% elastomer. Sample A4 had zero particles and B5 had 20% particles (total composition 20% particle, 72% DEG, 8% elastomer) at 71 $\pm$ 1°F.

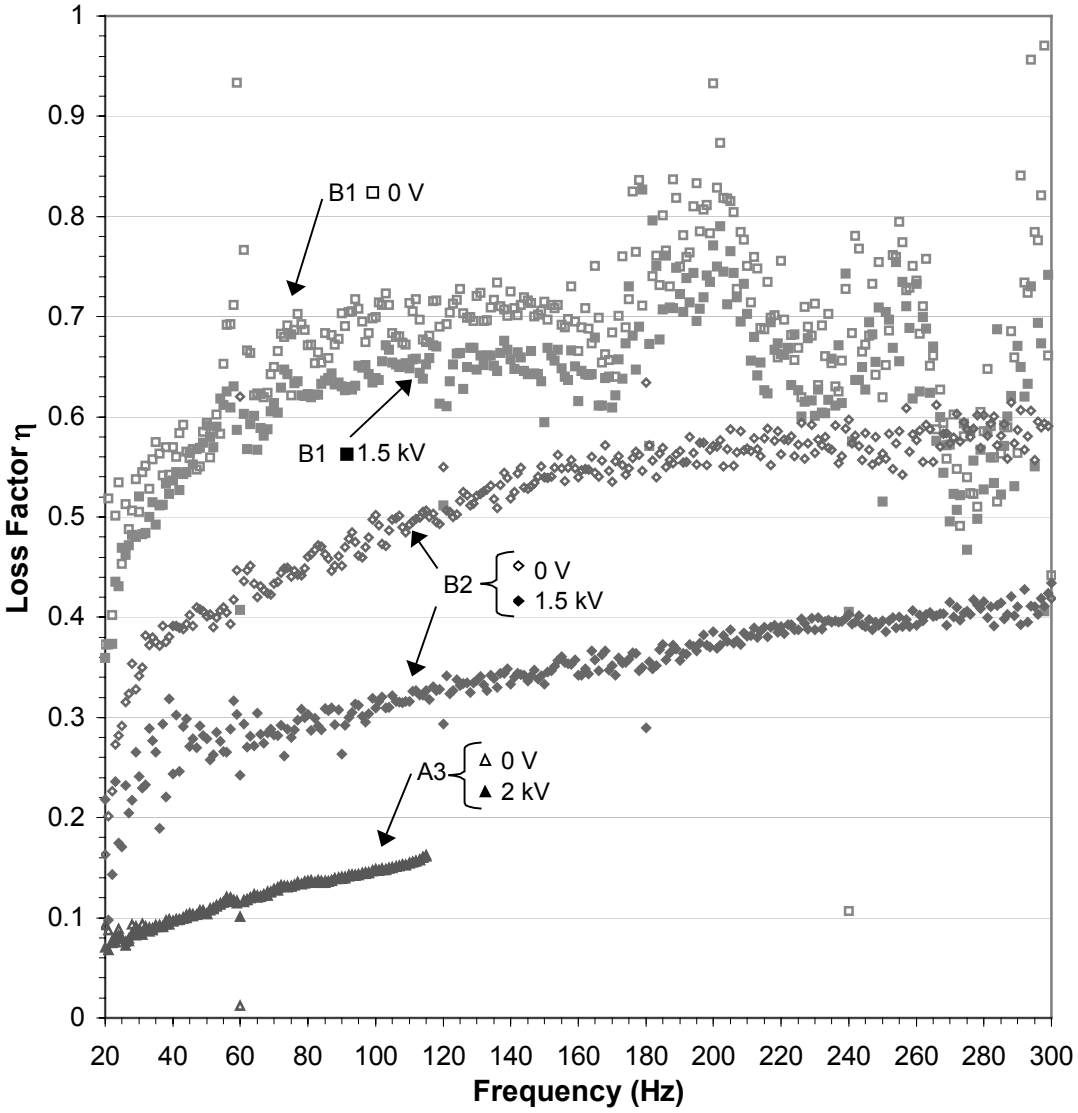

Figure 8-26. Loss factor of samples with a target gel composition (by mass) of 80% DEG/20% elastomer. Sample A3 had zero particles, B1 had 10% particles (total composition 10% particle, 72% DEG, 18% elastomer), , and B2 had 20% particles (total composition 20% particle, 64% DEG, 16% elastomer) at 71 $\pm$ 1°F.

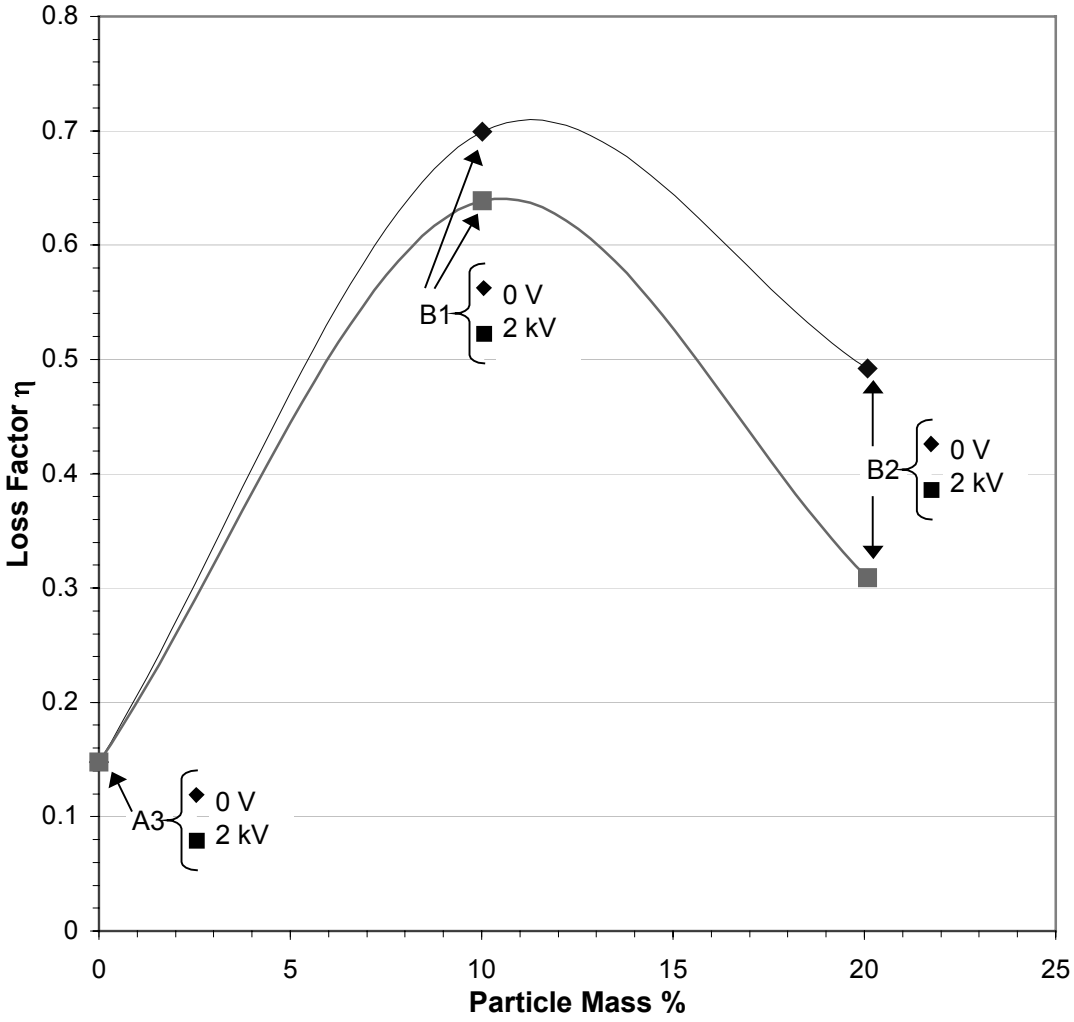

Figure 8-27. Loss factor vs. particle mass of samples with a target gel composition (by mass) of 80% DEG/20% elastomer. Sample A3 had zero particles, B1 had 10% particles (total composition 10% particle, 72% DEG, 18% elastomer), and B2 had 20% particles (total composition 20% particle, 64% DEG, 16% elastomer) at 71 $\pm$ 1°F and 100 Hz.

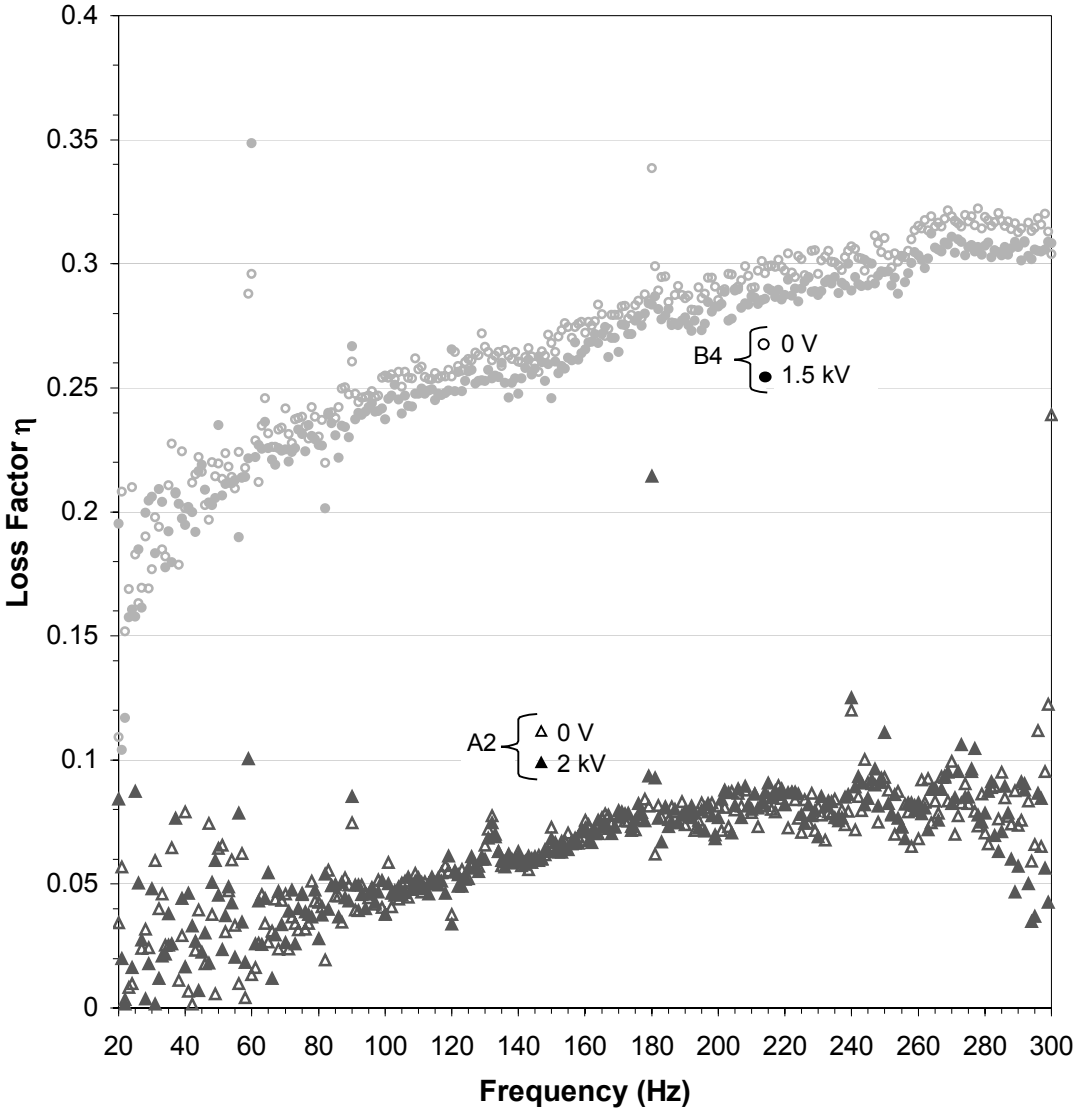

Figure 8-28. Loss factor of samples with a target gel composition (by mass) of 50% DEG/50% elastomer. Sample A2 had zero particles and B4 had 20% particles (total composition 20% particle, 40% DEG, 40% elastomer) at 71 $\pm$ 1°F.

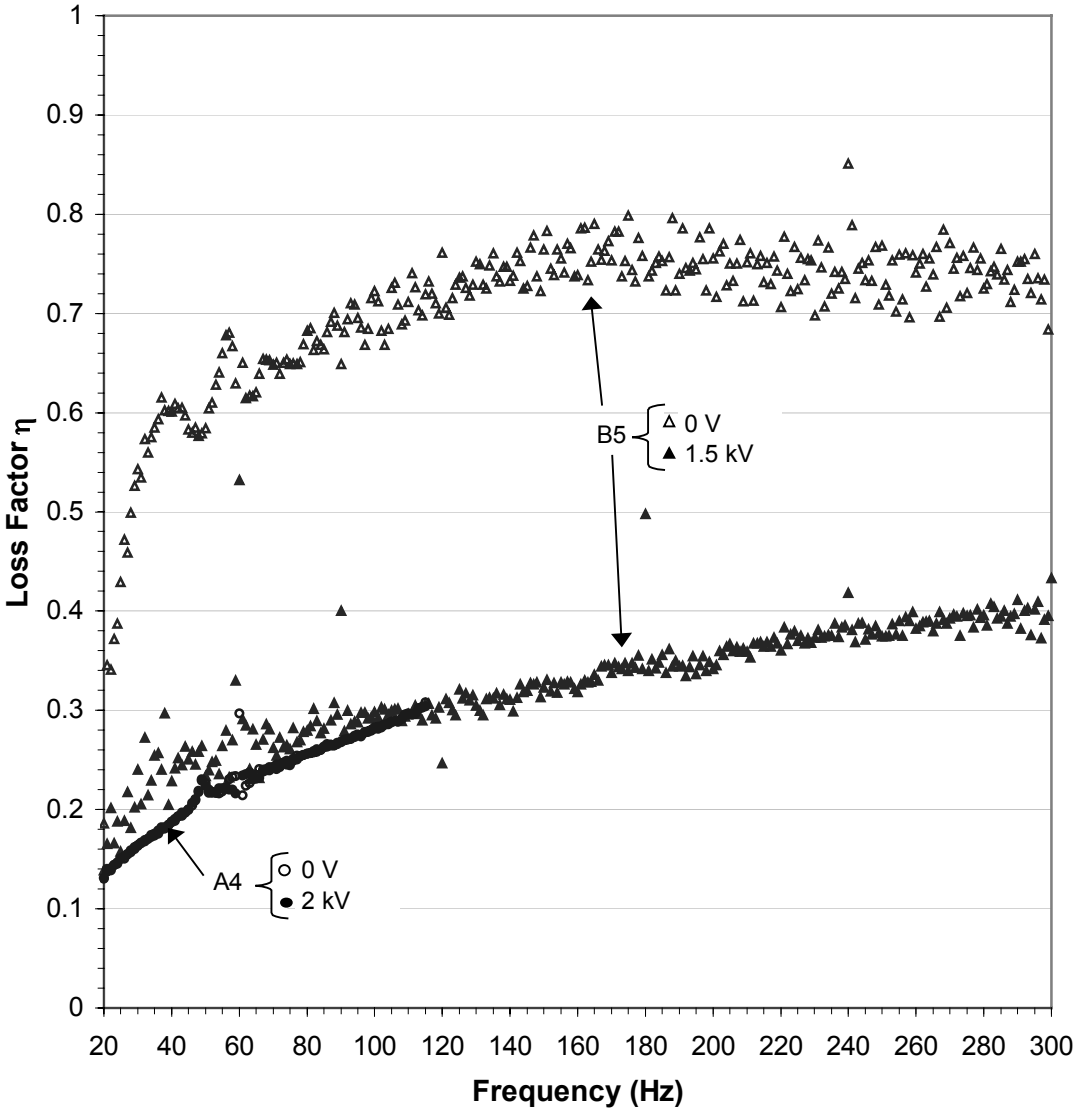

Figure 8-29. Loss factor of samples with a target gel composition (by mass) of 90% DEG/10% elastomer. Sample A4 had zero particles and B5 had 20% particles (total composition 20% particle, 72% DEG, 8% elastomer) at 71 $\pm$ 1°F.

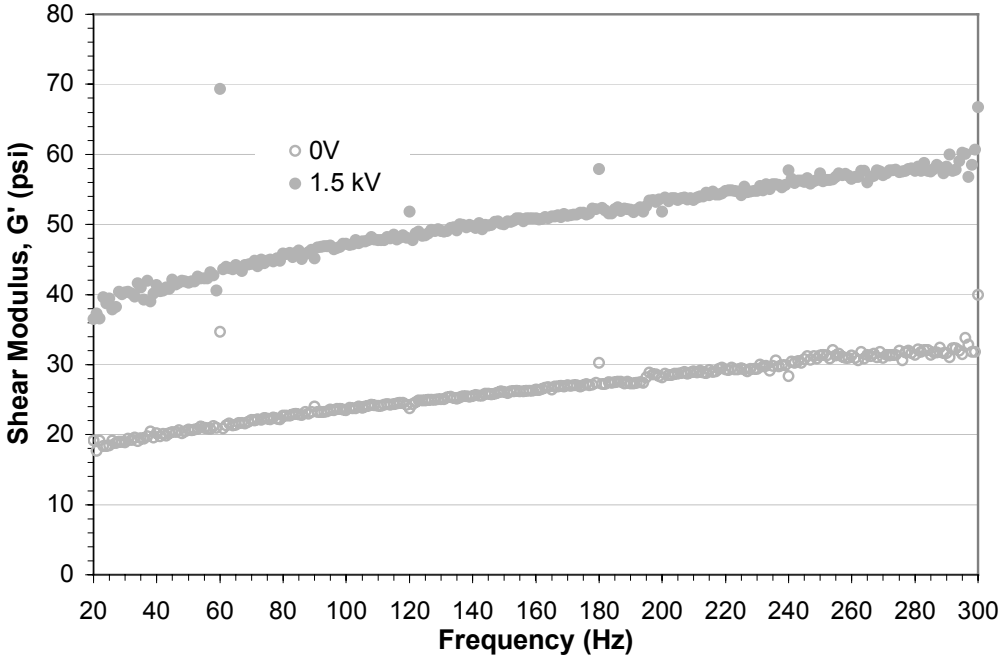

Figure 8-30. Shear modulus of sample C1 (20% particle, 64% DEG, 16% elastomer, cured without voltage) at 71°F.

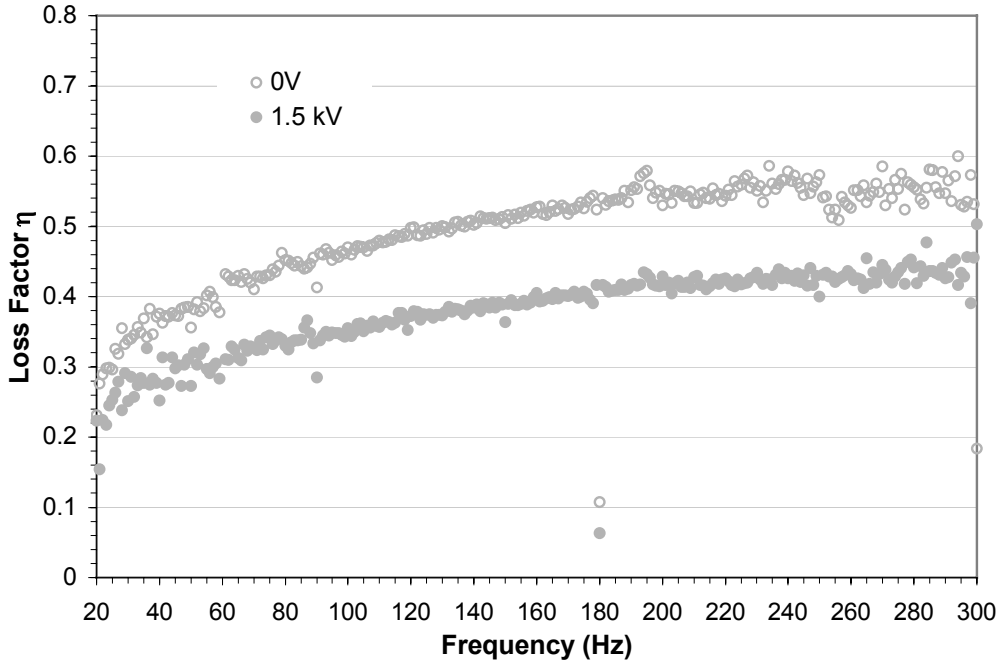

Figure 8-31. Loss factor of sample C1 (20% particle, 64% DEG, 16% elastomer, cured without voltage) at 71°F.

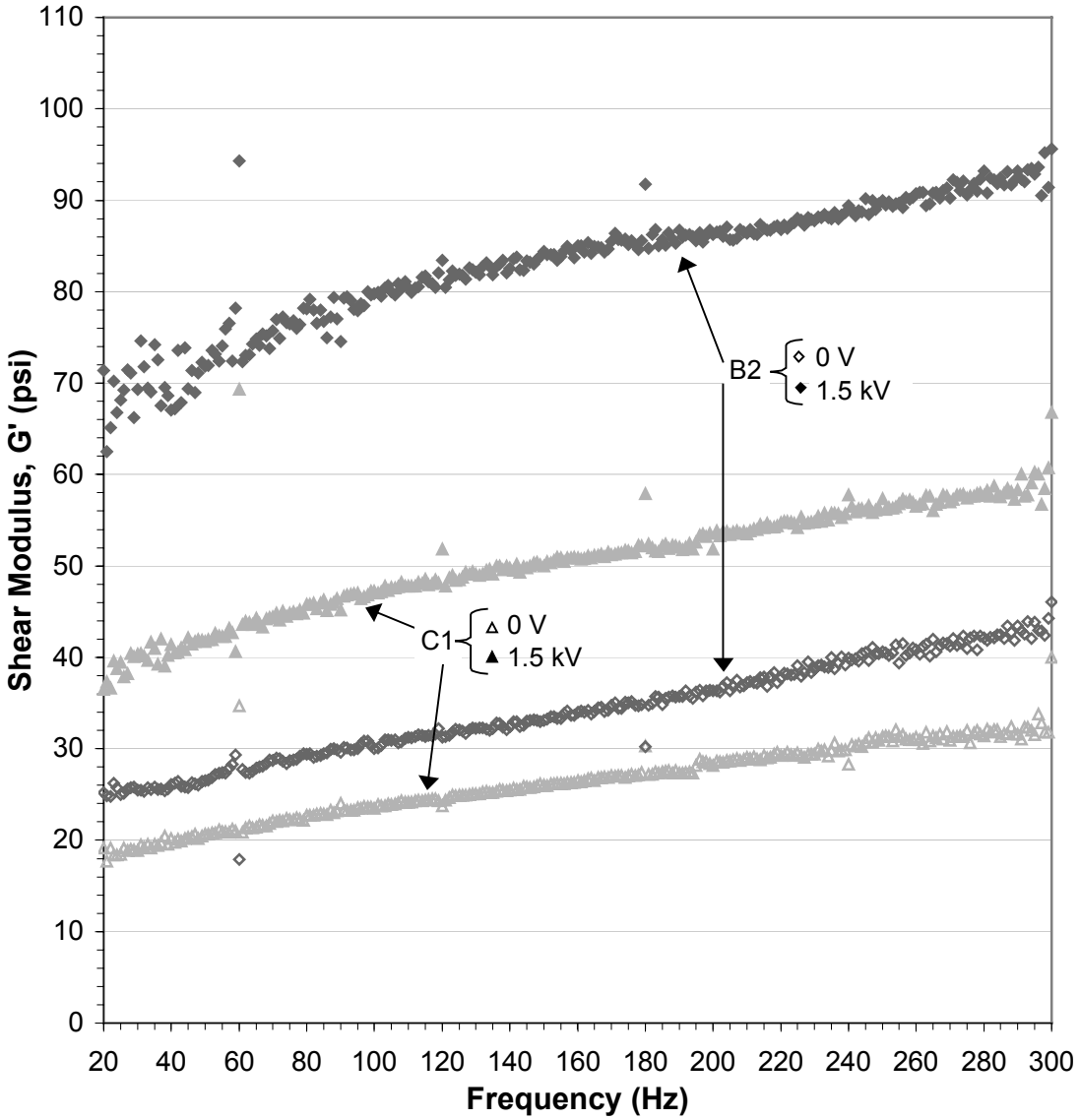

Figure 8-32. Shear modulus of sample C1 (20% particle, 64% DEG, 16% elastomer, cured without voltage) and sample B2 (20% particle, 64% DEG, 16% elastomer, cured with a voltage of 1 kV) at 71°F.

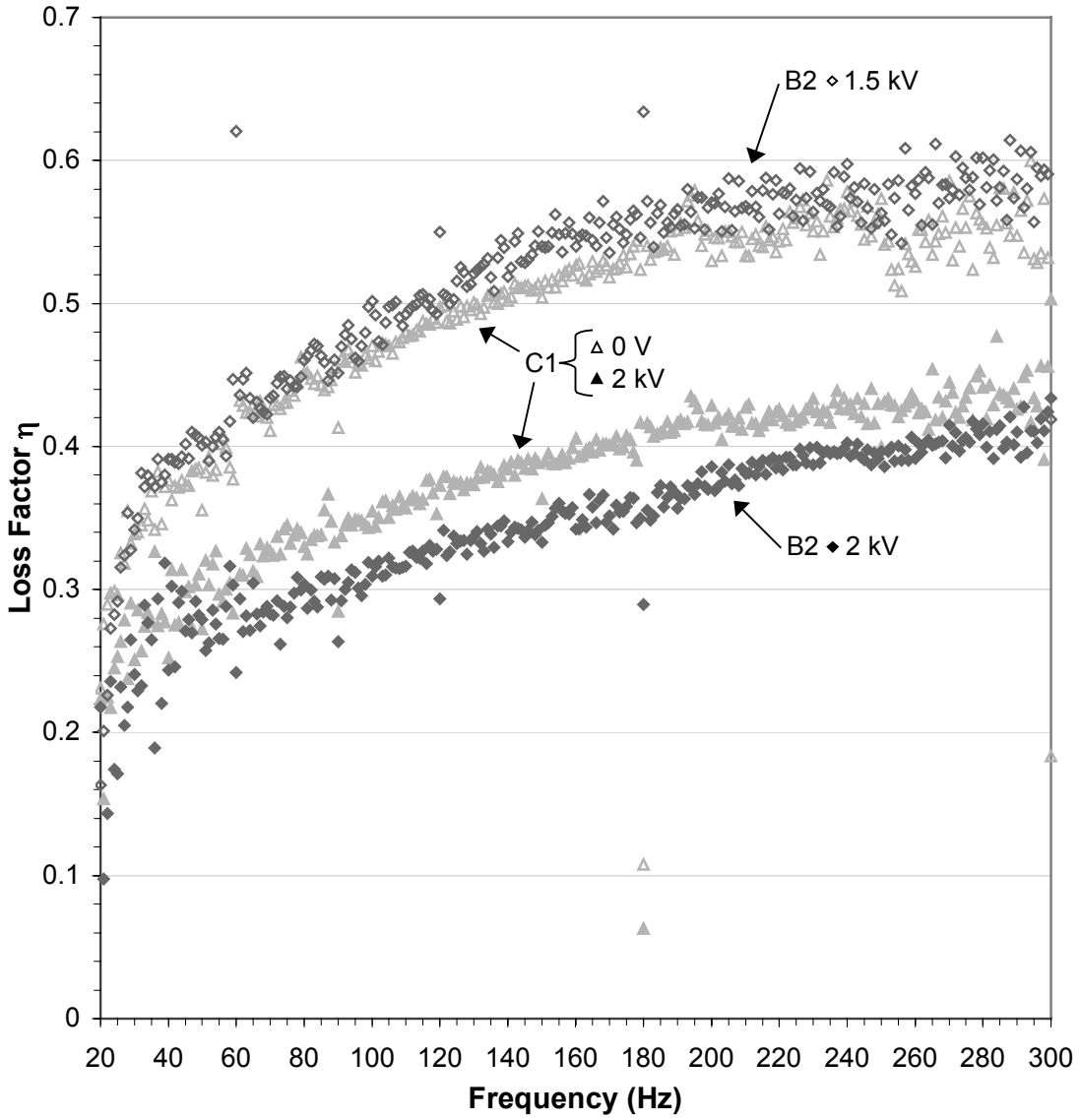

Figure 8-33. Loss factor of sample C1 (20% particle, 64% DEG, 16% elastomer, cured without voltage) and sample B2 (20% particle, 64% DEG, 16% elastomer, cured with a voltage of 1 kV) at 71°F.

8.4 Modeling

An attempt was made to model the behavior of the EVEMS. The goal was to develop an equation that could predict the shear modulus and loss factor as functions of composition, frequency, and voltage. Looking at all the data, however, it is clear that one formula would not cover all of these variables. The main obstacle was that change in frequency and voltage affected each sample very differently. A simple linear fit of the shear modulus vs. frequency of the control samples showed slopes ranging from 0.004 (sample A5) to 0.17 (sample A1). The slopes were a little more similar in the samples with particles - the range was 0.01 to 0.10 – but still not close enough for modeling Voltage also affected samples in various ways. Thus a model of the most successful sample, sample B5, was made and included voltage and frequency. Next a simple model of all the samples as a function of composition alone was created.

8.4.1 Model of shear modulus and loss factor vs. frequency of Sample B5

These materials are considered viscoelastic, meaning they have both viscous and elastic properties. There are several types of viscoelastic models but the simplest model that routinely fits material data is called the Four-Parameter Fractional Model. The equation derivations can be found in Chapter 2. The shear modulus and loss factor are found, respectively, to be:

$$G' = \frac{B + (BA + C)\omega^{\alpha} \cos(\frac{\alpha\pi}{2}) + C\omega^{2\alpha} A}{1 + 2A\omega^{\alpha} \cos(\frac{\alpha\pi}{2}) + A^2\omega^{2\alpha}} \tag{8-5}$$

$$\eta = \frac{(C - BA)\omega^{\alpha} \sin(\frac{\alpha\pi}{2})}{B + (BA + C)\omega^{\alpha} \cos(\frac{\alpha\pi}{2}) + C\omega^{2\alpha} A} \tag{8-6}$$

A, B, C, and α can be approximated (explanations are shown in Chapter 2):

$$A = \sqrt{\frac{G_e}{G_g}} \frac{1}{(2\pi f_{\eta \max})^{\alpha}} \tag{8-7}$$

$$B = G_e \tag{8-8}$$

$$C = AG_g \tag{8-9}$$

$$\alpha = \frac{2}{\pi} \tan^{-1}(\eta_{\max}) \tag{8-10}$$

where G_e is the equilibrium modulus (modulus as ω approaches zero), G_g is the glassy modulus (modulus as ω approaches infinity), η_{max} is the maximum loss factor, and $f_{\eta max}$ is the frequency of the maximum loss factor. To model all the data, the 0V samples were fit and then multiplied by a factor (discussed later) that would shift the curves for the higher voltages. The shear modulus is plotted in Figure 8-34 and the loss factor in Figure 8-35. Because only a relatively small frequency range was tested, the equilibrium modulus G_e is the only unknown that won't be largely estimated; it appears to be approximately 12 psi. The glassy modulus G_g is not determined because the tested frequencies are too low, although with the small slope it is estimated to be between 100 psi and 300 psi; 100 psi is the initial guess. The loss

factor seems to be leveling off around 300 Hz. so the maximum is estimated to be 0.42 at 350 Hz.

The shear modulus for sample B5 at 20 Hz. for each voltage (0V, 0.5 kV, 1.0 kV, or 1.5 kV) was plotted, as shown in Figure 8-36, to determine the offsets. The data was quite linear so adding the factor 0.422 multiplied times the voltage to Equation 8-5 allowed the applied voltage data to be included. The loss factor data is unstable at the lower frequencies thus the offsets were taken at 150 Hz. to find the equation. The offsets are shown in Figure 8-37 and the two-order polynomial curvefit is:

$$Z = 1.49 * 10^{-7} * V^2 + 5.59 * 10^{-5} V \qquad (8\text{-}11)$$

Adding the results of Equation 8-11 to the loss factor equation allows the samples with applied voltage to be included.

Using these approximations the 4 Parameter Model curves are shown in Figure 8-38 (shear modulus) and Figure 8-39 (loss factor). The fits are obviously not ideal. There are significant shortcomings in the approximations. One, the formulas for the factors A, B, C, and α were made assuming that the glassy modulus is much greater than the equilibrium modulus, which is not the case with this material. Also, the tested frequency range is very small making the factors difficult to determine. However, a range of values for G_g, η_{max}, and $f_{\eta max}$ were tried with no more success than the initial estimates.

Another method of looking at the data for sample B5 is to use simple curve fits of all the data. A plot of the shear modulus of sample B5 at various voltages and 71^{o}F

is shown in Figure 8-40. Each plot was curve fit with both a linear fit and a two-order polynomial. The fits were only marginally better for the two-order polynomials so they were assumed to be linear. The slopes, listed in the equations in Figure 8-40, were averaged to get a slope of 0.074, giving the equation:

$$G' = 0.074\omega + Z \tag{8-12}$$

where ω is the frequency and Z is the offset. The offsets, plotted in Figure 8-36, were quite linear so the linear fit (displayed on the plot) was simply substituted for the offset Z in Equation 8-12:

$$G' = 0.074\omega + 0.0422V + 9.609 \tag{8-13}$$

where V is the voltage. Figure 8-41 demonstrates how closely Equation 8-13 fits the experimental values. The difference in the predicted values using Equation 10 and the average experimental values is no larger than 5% except below 40 Hz. where there is a large amount of scatter.

A similar procedure was performed to fit the loss factor. Figure 8-42 shows the loss factors of sample B5 at various voltages and 71°F. Two-order polynomials were used to curvefit the data. The x^2 and x terms (shown in the equations in Figure 8-42) were averaged resulting in the following equation:

$$\eta = -2.66 * 10^{-6} * \omega^2 + 0.00157 * \omega + Z \tag{8-14}$$

where η is the loss factor. Since the data is unstable at the lower frequencies the offsets were taken at 150 Hz. to find the equation then a correction factor was subtracted. The offsets are shown in Figure 8-37 and the two-order polynomial curvefit is:

$$Z = 1.49 * 10^{-7} * V^2 + 5.59 * 10^{-5} V + 0.143 \quad (8\text{-}15)$$

Substituting Equation (8-15) into Equation (8-14) produces the final equation for the loss factor:

$$\eta = -2.66 * 10^{-6} * \omega^2 + 0.00157 * \omega + 1.49 * 10^{-7} * V^2 + 5.59 * 10^{-5} V + 0.143 \quad (8\text{-}16)$$

Figure 8-43 shows how the curvefit equations match the experimental loss factor data. The curvefits are within a few percent for the 0.5 kV, 1 kV, and 1.5 kV data above 50 Hz. The fit is not as good for the 0 V sample, especially above 200 Hz. where the experimental loss factor decreases slightly; however, the curvefit is still no more than 10% above the average value.

8.4.2 Curvefits of shear modulus and loss factor vs. composition

A plot was made of the gel composition vs. the shear modulus of the control samples at 70 Hz. (a mid-range frequency), 70°F, and 0 V. The shear modulus was curve-fit using a two-order polynomial:

$$G' = 0.0133(M_{DEG})^2 - 2.5837(M_{DEG}) + 129.32 \quad (8\text{-}17)$$

where G' is the shear modulus and M_{DEG} is the mass ratio of the DEG. The R^2 value was 0.999. The curve-fit of samples A1-A5 is shown in Figure 8-44 and the values are shown in Table 8-2.

The samples with the added particles were then considered, and it can be seen that the samples with approximately 20% particles by mass that were cured with voltage (samples B2, B4, and B5) have a little over three times the modulus of the gels

alone, regardless of the gel composition. Surprisingly, the sample with 10% particle (sample B1) has a slightly lower modulus than either the measured shear modulus or the predicted shear modulus curve. A simple way to incorporate the particle addition into to Equation 6 is to multiply it by a factor that includes the particle percentage:

$$G' = (0.0133(M_{DEG})^2 - 2.5837(M_{DEG}) + 129.32)(1.06199\text{^}M_{Part}) \quad (8\text{-}18)$$

where M_{DEG} is the mass ratio of the DEG in the gel portion of the sample and M_{Part} is the mass ratio of the particles. As shown in Table 8-3, the predicted shear moduli are within 10% of the experimental values for samples B2, B3, and B4 (all with approximately 20% particles) although the predicted shear modulus for sample B1, 14.1 psi, was slightly more than four times the measured value, 3.5 psi.

The same process can be used to predict the loss factor of the samples. At 70 Hz. and 70°F the control samples were curve-fit using a two-order polynomial:

$$\eta = 7.817\text{E-}05(M_{DEG})^2 - 6.537\text{E-}03(M_{DEG}) + 0.1689 \quad (8\text{-}19)$$

where η is the loss factor and M_{DEG} is the mass ratio of the DEG. The R^2 value is 0.966. Figure 8-45 shows the loss factors at 70 Hz. and 70°F. Table 8-4 shows how the predicted loss factors compare with the experimental values; the largest difference is 13%.

The samples with added particles were then included. The loss factors for the samples with particles were higher than the gel alone in all cases. Both the gel composition and the particle ratio seem to affect the loss factor. As with the shear modulus, however, the sample with approximately 10% particles by mass (sample B1) does not follow the trend of the other samples; it has a much higher loss factor than

would be expected. To best fit all four samples, Equation 8-19 is multiplied by a factor that includes both the particle percentage and gel composition:

$$\eta = (7.817\text{E-}05(M_{DEG})^2 - 6.537\text{E-}03(M_{DEG}) + 0.1689) * 111^{\frac{M_{Part}}{M_{DEG}}} \quad (8\text{-}20)$$

where M_{DEG} is the mass ratio of the DEG in the gel portion of the sample. As shown in Table 8-5, the predicted loss factors are within 10% of the experimental values for samples B2, B3, and B4 (all with approximately 20% particles) although the predicted loss factor for sample B1, 0.261, was significantly smaller than the experimentally measured loss factor, 0.650.

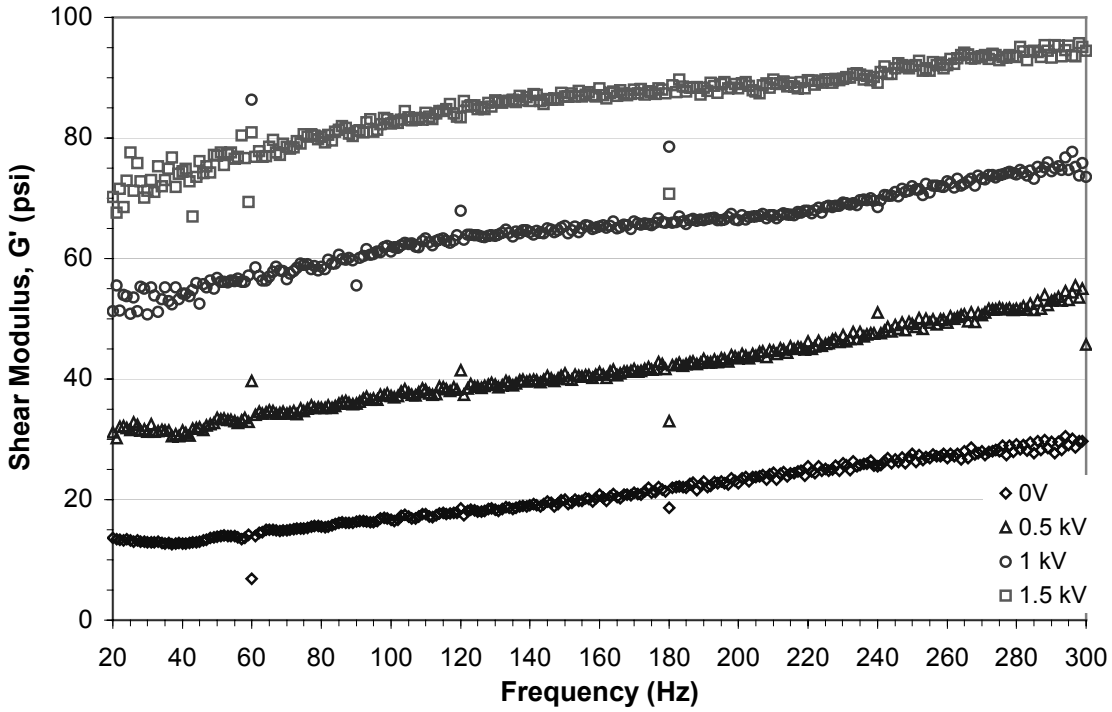

Figure 8-34. Shear modulus of sample B5 at 0 V, 0.5 kV, 1.0 kV, and 1.5 kV.

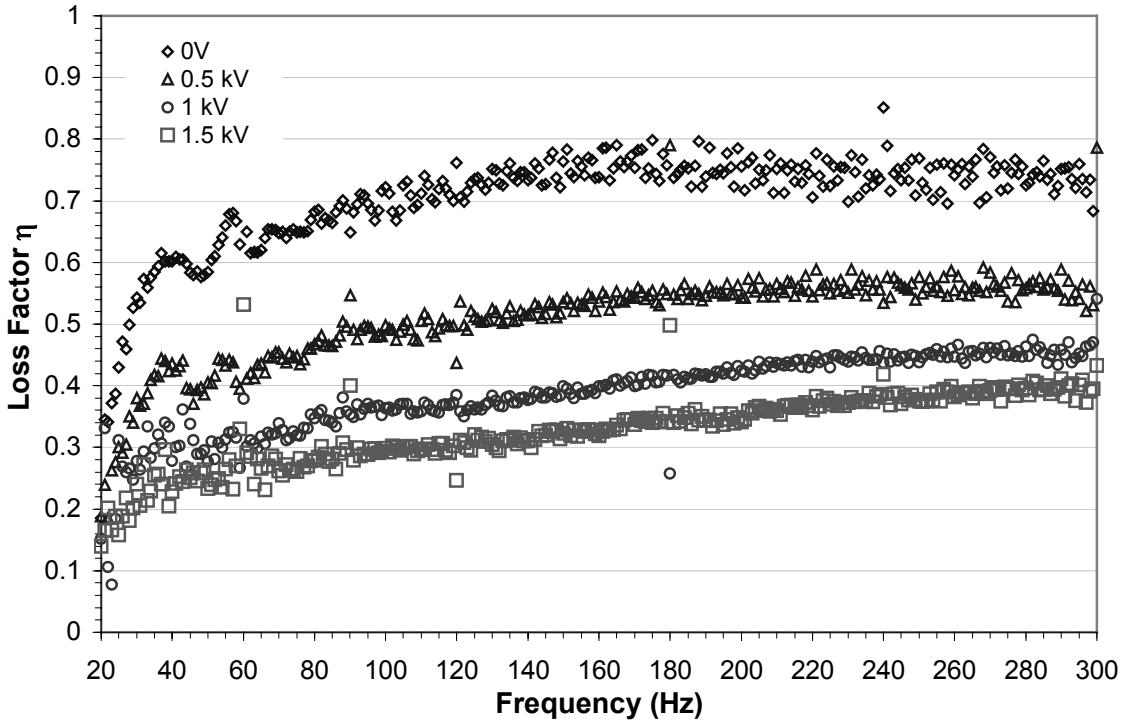

Figure 8-35 Loss factor of sample B5 at 0 V, 0.5 kV, 1.0 kV, and 1.5 kV.

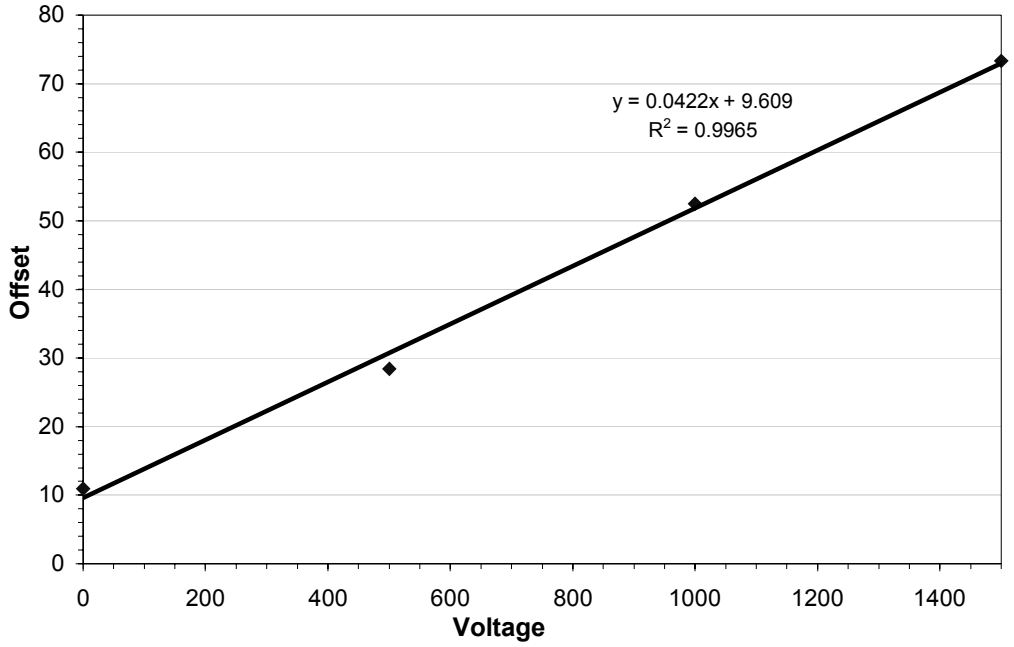

Figure 8-36. Plot of the offsets of the shear moduli of sample B5 at 150 Hz. in Figure 8-34.

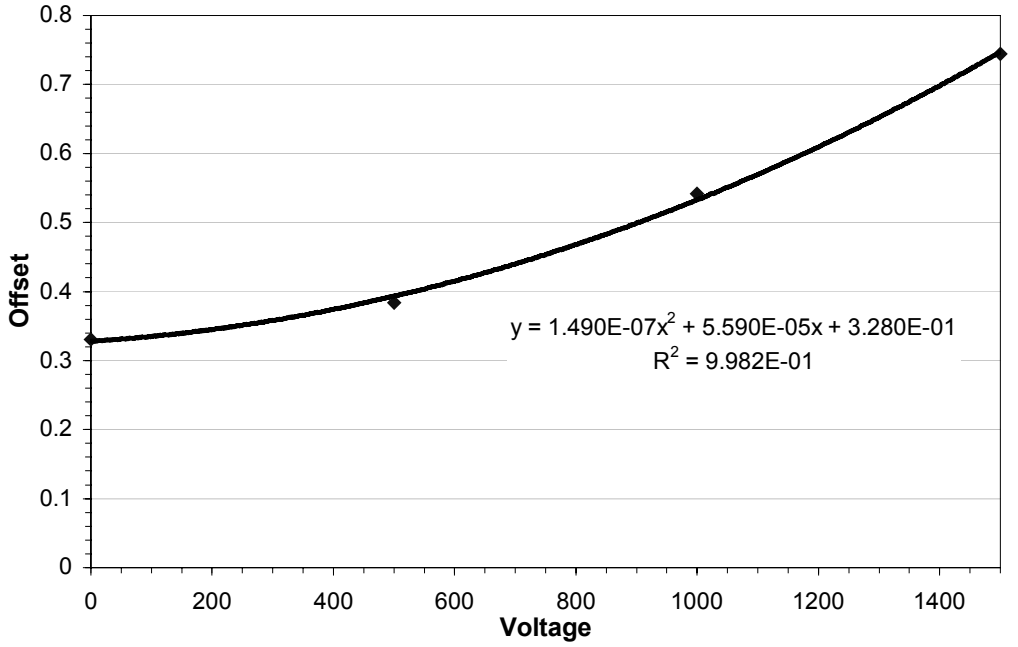

Figure 8-37. Plot of the offsets of the loss factor of sample B5 at 150 Hz. of the curvefits in Figure 8-35.

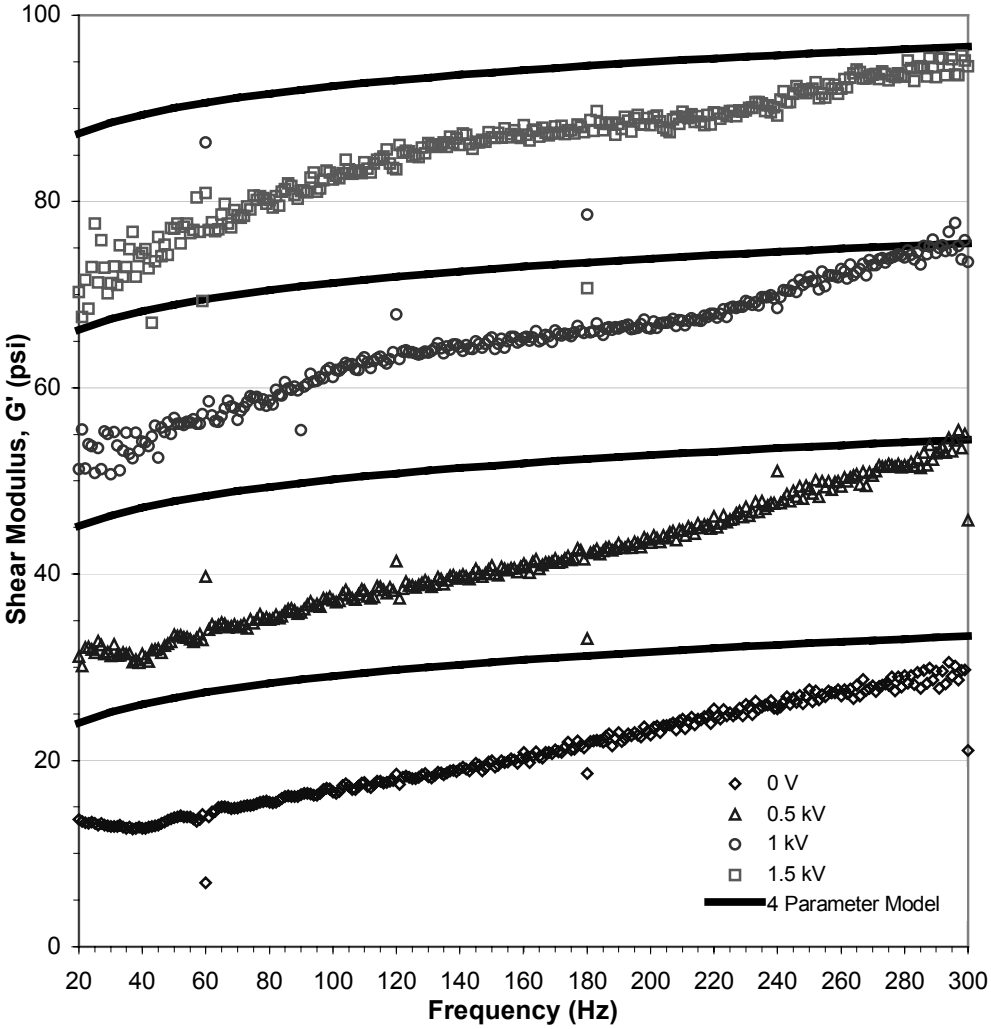

Figure 8-38. Plot showing how the 4 Parameter model fits the experimental shear modulus data for sample B5.

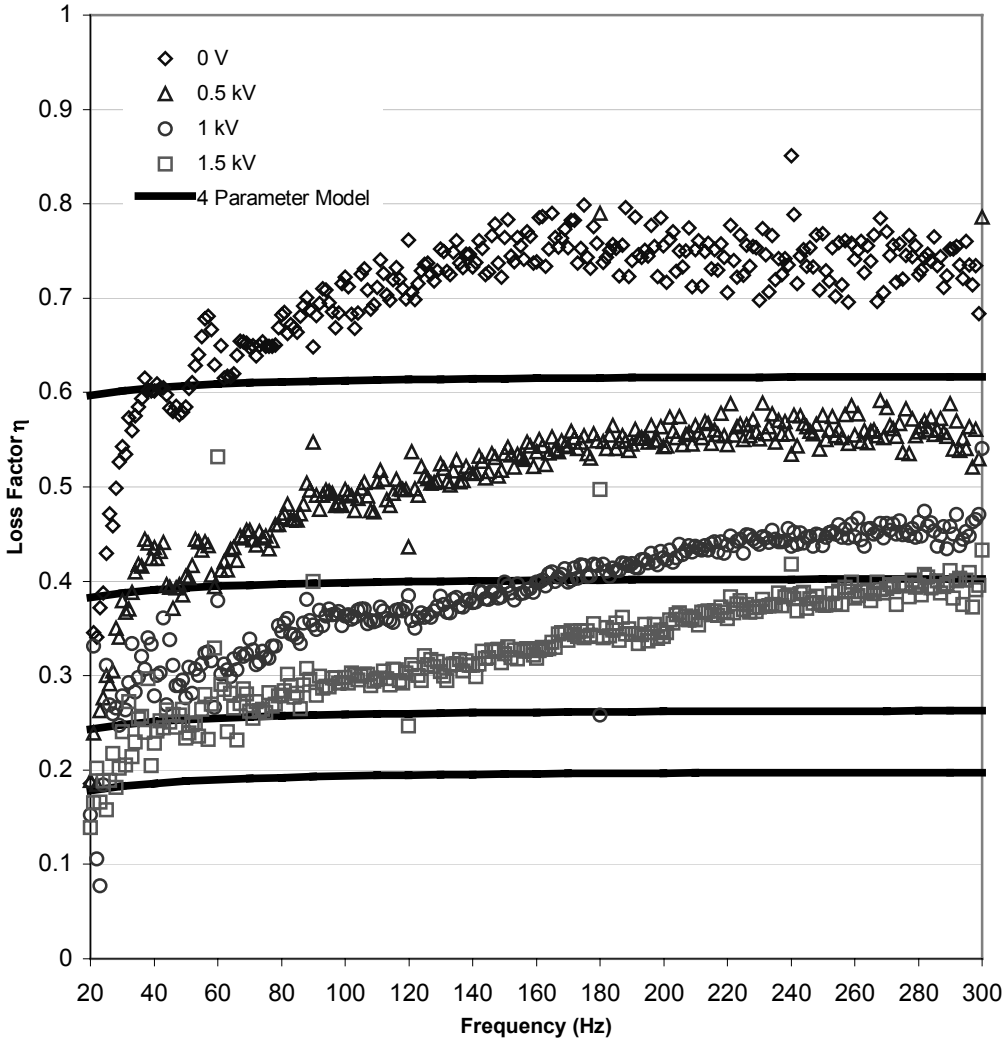

Figure 8-39. Plot showing how the 4 Parameter model fits the experimental loss factor data for sample B5.

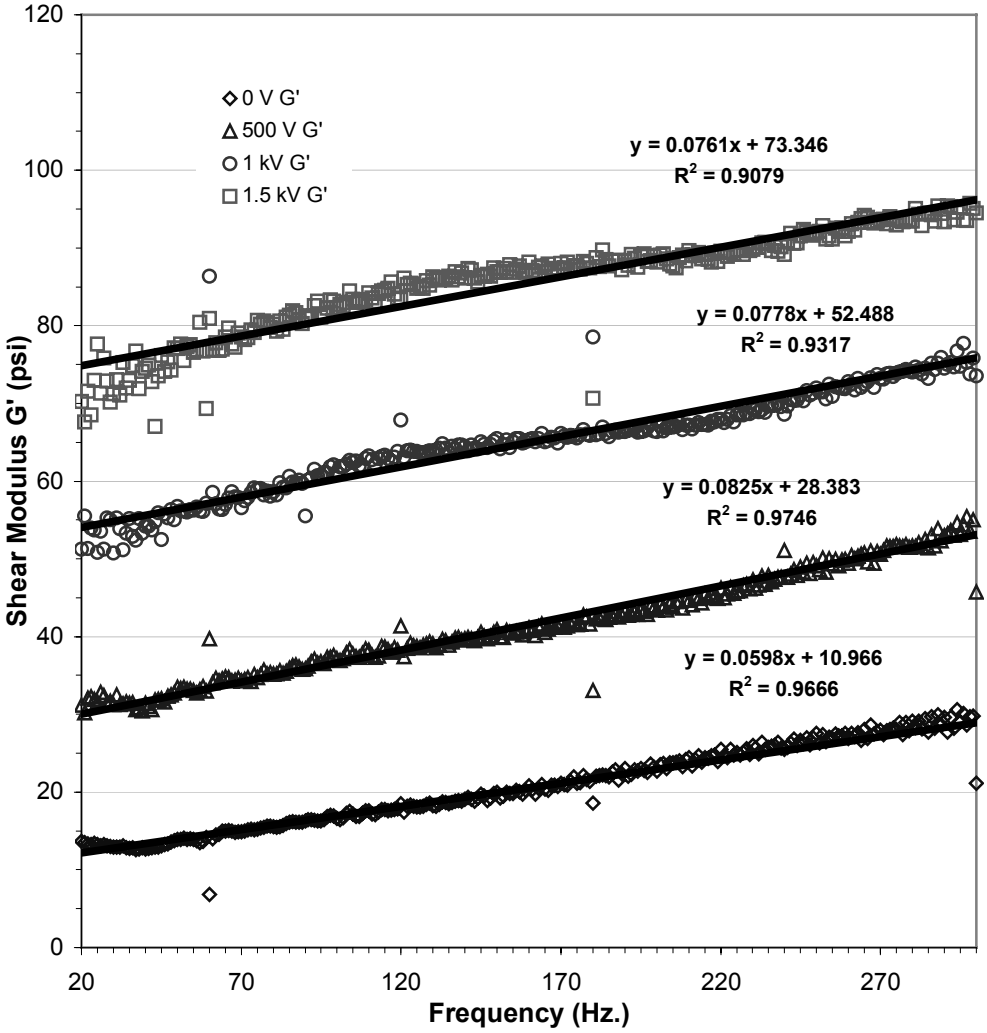

Figure 8-40. Shear moduli of sample B5 at 71°F and 0 V, 0.5 kV, 1 kV, and 1.5 kV with individual curvefits for each voltage.

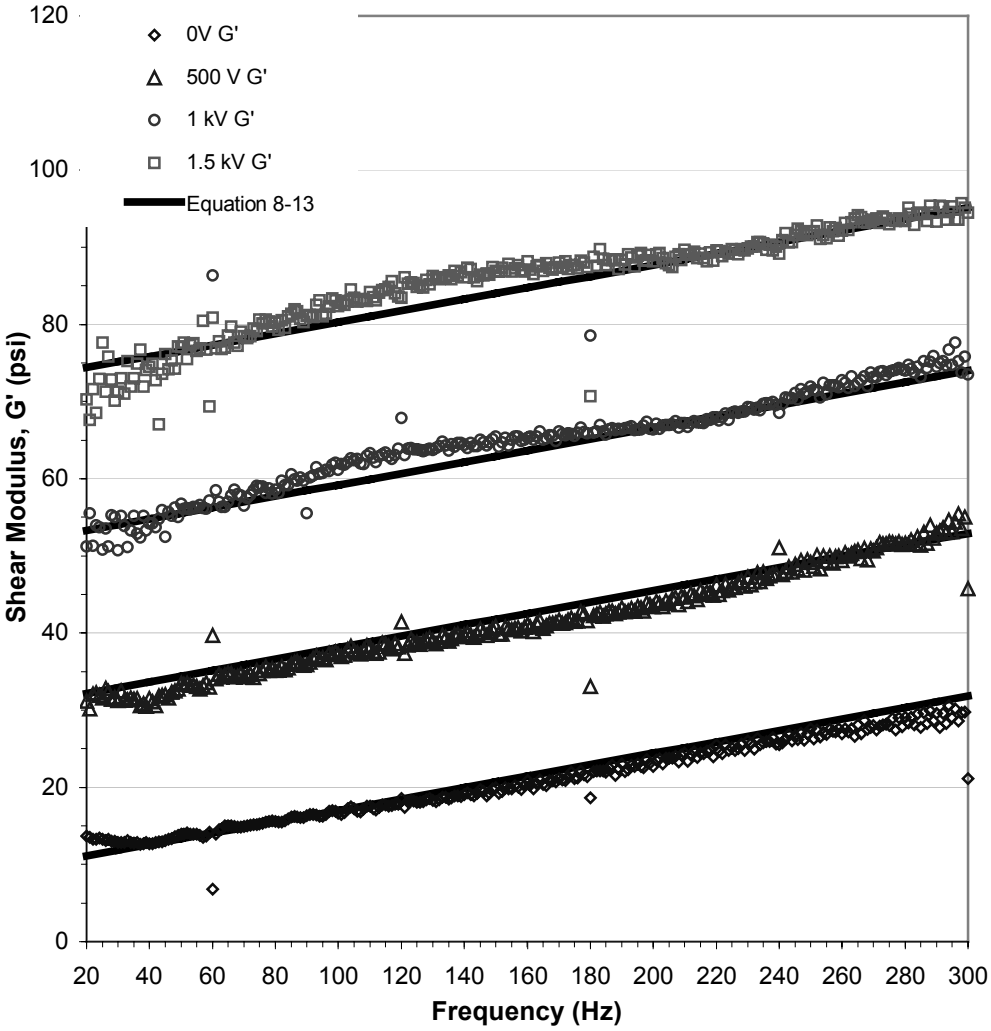

Figure 8-41. Plot of the single curvefit (Equation 8-13) of the shear moduli of sample B5 from 0 V to 1.5 kV.

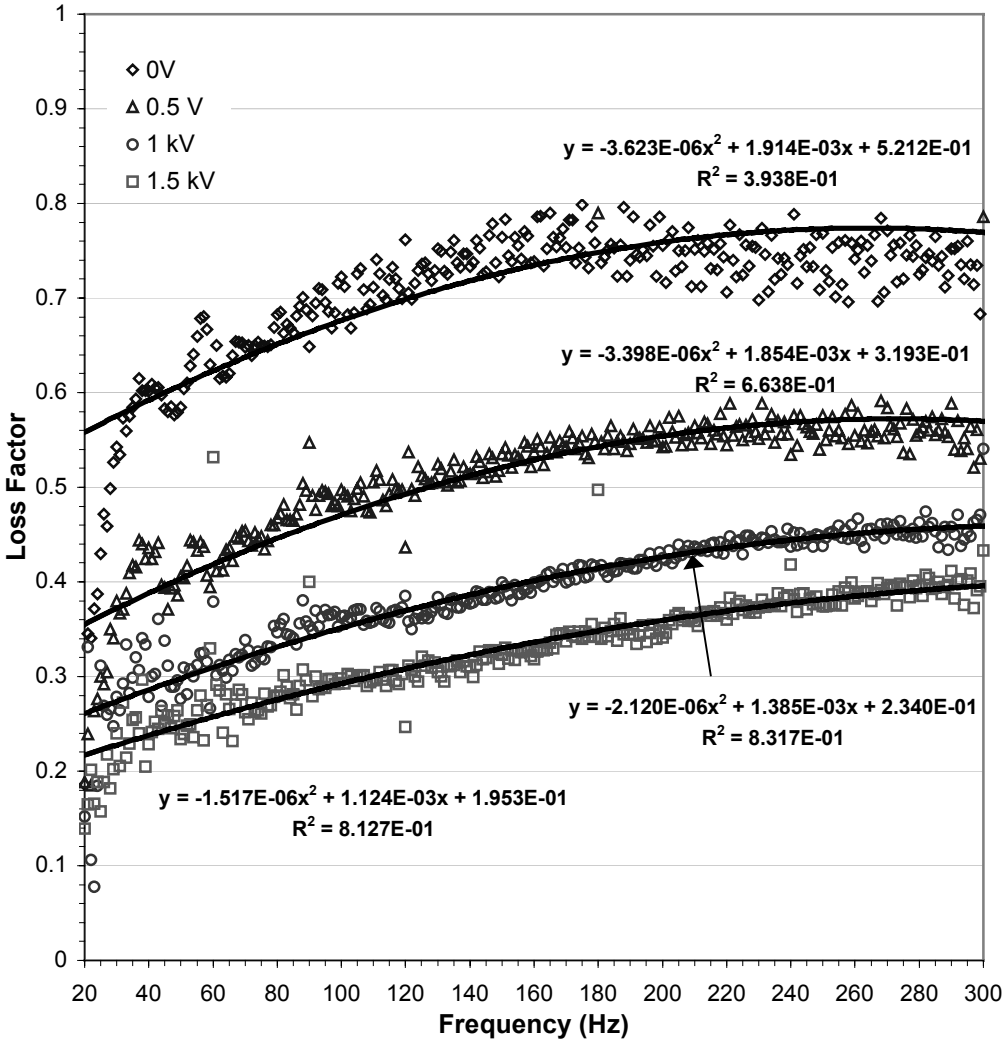

Figure 8-42. Loss factors of sample B5 at 71°F and 0 V, 0.5 kV, 1 kV, and 1.5 kV with individual curvefits for each voltage.

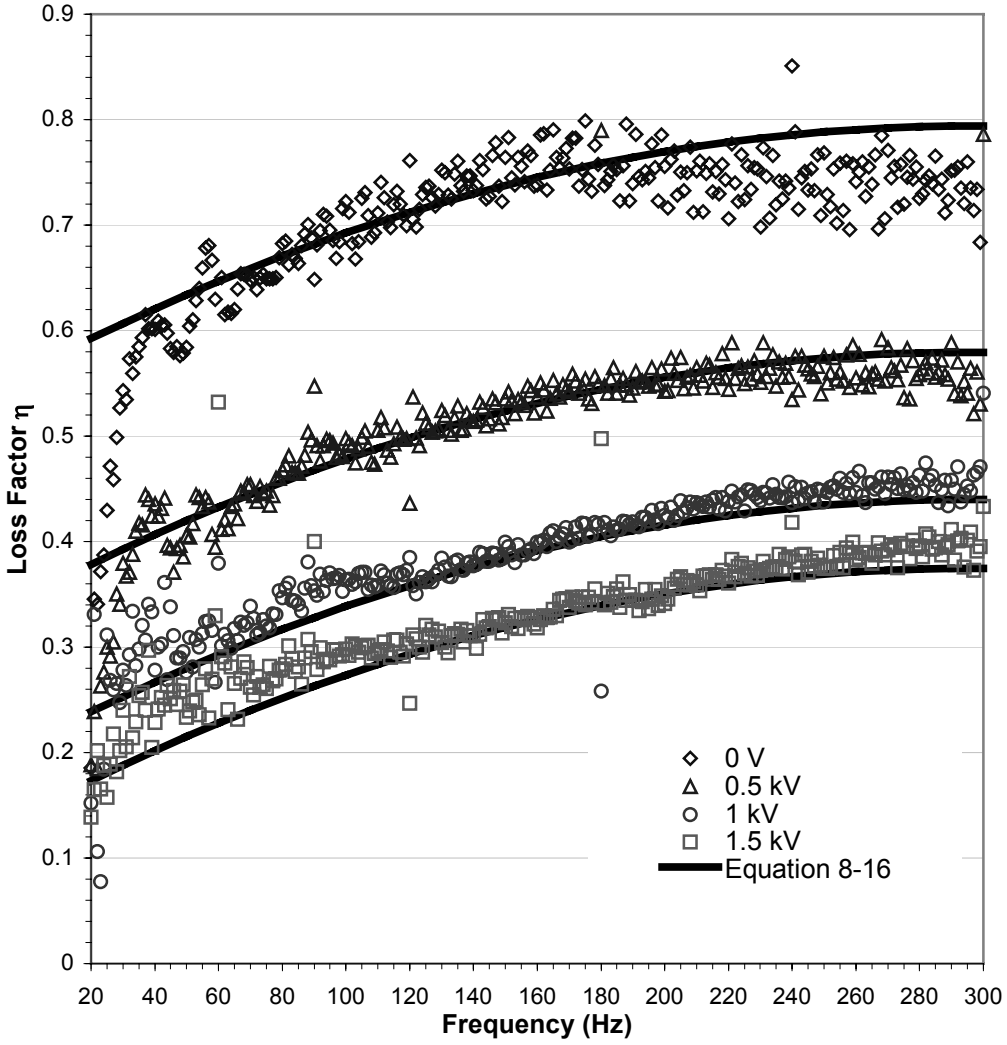

Figure 8-43. Plot of the single curvefit (Equation 8-16) of the loss factor of sample B5 at various voltages.

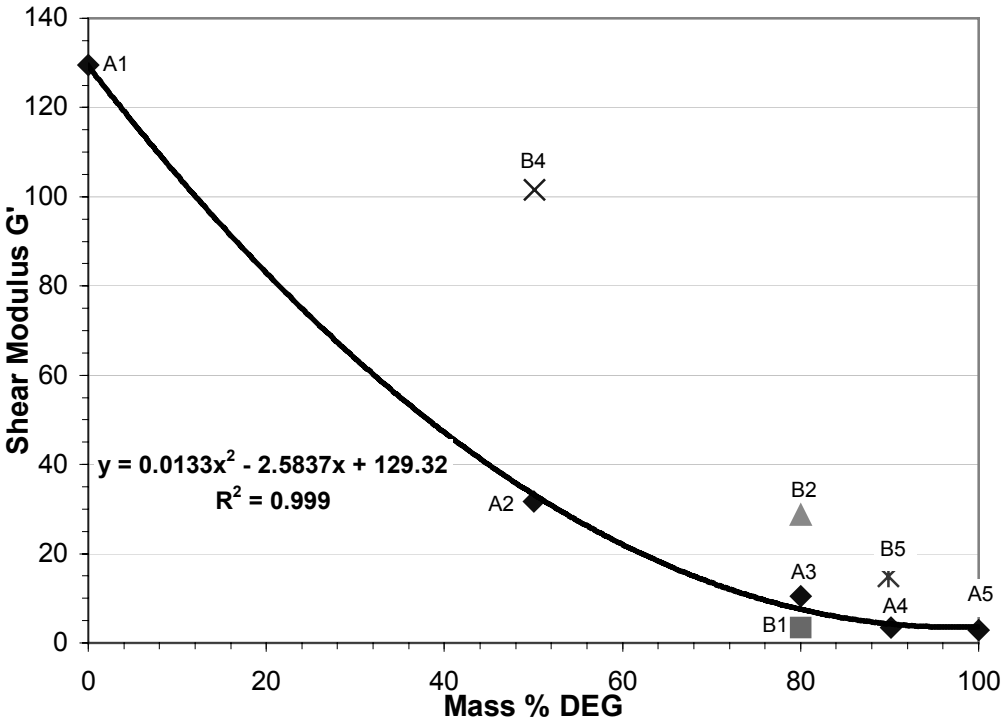

Figure 8-44. Shear moduli of samples at 70 Hz., 70°F, and 0V. The curvefit is of samples A1-A5.

Table 8-2. Predicted shear moduli (using Equation 8-17) as compared to experimentally measured shear moduli.

Sample	% DEG (as part of gel)	% Particles	Predicted G'	Experimental G'	% Difference
A1	0	0	129.3	129.6	-0.2
A2	50.03	0	33.3	31.7	5.0
A3	79.99	0	7.7	10.4	-26.0
A4	90.12	0	4.5	3.5	28.6
A5	100	0	4.0	2.8	42.9

Table 8-3. . Predicted shear moduli (using Equation 8-18) as compared to experimentally measured shear moduli.

Sample	% DEG (as part of gel)	% Particles	Predicted G'	Experimental G'	% Difference
B1	80.03	10.01	14.1	3.5	302.9
B2	80.03	20.09	25.9	28.7	-9.8
B4	50.14	19.9	109.9	101.6	8.2
B5	89.88	19.63	14.8	14.9	-0.7

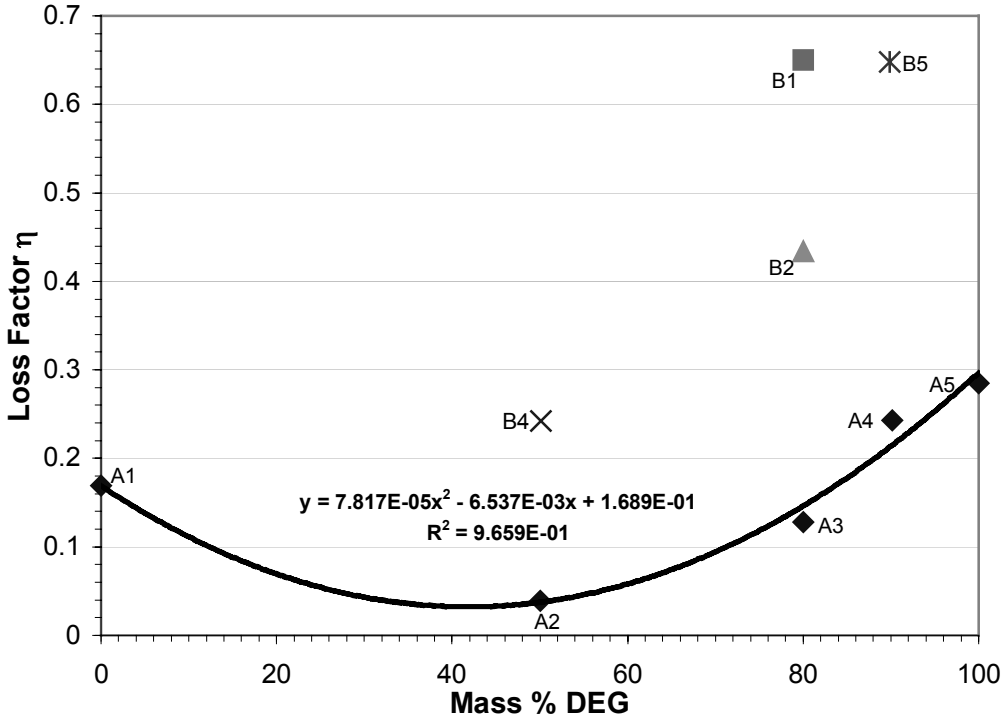

Figure 8-45 Loss factors of samples at 70 Hz.,70^{o}F, and 0V. The curvefit is of samples A1-A5.

Table 8-4. Predicted loss factors (using Equation 8-19) as compared to experimentally measured loss factors.

Sample	% DEG (as part of gel)	% Particles	Predicted η	Experimental η	% Difference
A1	0	0	0.169	0.169	0
A2	50.03	0	0.037	0.039	-5.1
A3	79.99	0	0.145	0.128	13.3
A4	90.12	0	0.213	0.243	-12.3
A5	100	0	0.295	0.285	3.5

Table 8-5. Predicted loss factors (using Equation 8-20) as compared to experimentally measured loss factors.

Sample	% DEG (as part of gel)	% Particles	Predicted η	Experimental η	% Difference
B1	80.03	10.01	0.261	0.650	-59.8
B2	80.03	20.09	0.473	0.434	9.0
B4	50.14	19.9	0.240	0.242	-0.8
B5	89.88	19.63	0.591	0.648	-8.8

8.5 Conclusions

An EVEM was developed that produced large changes in shear modulus and loss factor with applied voltage. The material exhibits many of the same properties as an electrorheological (ER) fluid, except the current material is self-supporting and thus can be used in applications where viscoelastic materials are used. The EVEM is composed of three components: 1) poly (p-phenylene) (PPP) particles doped with $FeCl_3$, 2) Dow Corning Sylgard® 527 silicone dielectric gel, and 3) Dow Corning Sylgard® 182 silicone elastomer. The dielectric gel had a high loss factor but was too soft by itself thus the elastomer was added to increase the stiffness of the gel. Experimental harmonic tests using a double-lap shear test and 0.025" thick specimens between 20 and 300 Hz. reveal shear modulus increases of up to a factor of almost five and a 58% decrease in loss factor with an applied DC voltage of 1.5 kV. The reason for the change in properties is the attraction between the particles, which became charged when a voltage was applied. It was also confirmed that curing the samples under a 1 kV voltage increased the change in material properties when a voltage was applied across the cured sample although the sample cured without

voltage also saw significant changes in shear modulus and loss factor with applied voltage. Samples with softer gels (with less elastomer) tended to show more change in material properties with applied voltage; the softer sample allowed more particle interaction. The sample that showed the greatest change in shear modulus and loss factor with applied voltage was sample B5, which had the maximum particle ratio (approximately 20% by mass) and least elastomer (approximately 10% by mass of the gel) and therefore was the softest sample.

This chapter, in part, will be submitted for publication to *Mechanics of Advanced Materials and Structures* with the title "The Development of Electroviscoelastic Materials As Active Vibrational Dampers". The dissertation author was the primary investigator and co-authored the article with advisor J. B. Kosmatka.

Chapter 9 Conclusions

With this research new methods for damping vibrations in composite materials were developed and currently utilized methods were greatly enhanced. First, the loss factors of composite samples made with embedded cocured viscoelastic damping materials were increased significantly by the addition of a barrier layer; the barrier layer prevented epoxy from infiltrating the damping materials and tremendously reducing the damping capacity. It was shown that most common damping materials are not greatly affected by the temperature and pressure of typical composite cure cycles.

A shear test method was developed to test the shear modulus and strength of materials cocured in a composite sample. Shear tests were performed on viscoelastic damping materials to measure the effects of cocuring vs. secondarily bonding. Shear tests were also performed on various barrier layers and damping material with embedded fiberglass and nylon mesh scrim cloth.

A directional damping material was manufactured by adding silicone into slots cut out of an acrylic sheet at various angles and then bonded between sheets of polycarbonate, chosen because it is isotropic and will have no angle interaction. The loss factor and frequency both varied substantially with angle change of the acrylic/silicone directional damping layer.

Several types of toughening particles (carboxy modified acrylonitrile/butadiene polymer, non-carboxy modified acrylonitrile/butadiene

polymer, and acrylate polymer) were added to graphite/epoxy composites interlaminar regions. They were found to greatly increase the damping without decreasing the shear and bending modulus to the extent that typical viscoelastic damping material do.

An electroviscoelastic material (EVEM) was developed that produced dramatic changes in shear modulus and loss factor when a voltage was applied across the material. The EVEM was composed of poly (p-phenylene) particles doped with $FeCl_3$ mixed in a silicone gel, which was a mixture of a silicone dielectric gel and a silicone elastomer. Curing the silicone under an applied voltage lined up the particles and increased the changes measured when voltage was applied during testing.

References

1 Fujimoto, Jun, and Tetsuya Tamura. 1993. “Mechanical Properties for CFRP/Damping-Material Laminates”, *Journal of Reinforced Plastics and Composites*, **12**:738-51.

2 Adam Quilter. 2005. "Composites in Aerospace Applications" IHS Inc. White Paper.

3 Harris, Charles E. and Mark J. Shuart. 2001. “An Assessment of the State-of-the-Art in the Design and Manufacturing of Large Composite Structures for Aerospace Vehicles”, NASA Technical Reports, NASA/TM-2001-210844

4 www.airbus.com

5 Appuhn, Geoffrey. 2002. “Integrally damped 1st stage composite fan blades”, M.S. Thesis, University of California San Diego

6 Kosmatka, John. 2000. “Building Better Turbine Blades”, *NASA at UC: A Publication on NASA Research on the University of California,* Autumn edition.

7 http://www.geae.com/aboutgeae/presscenter/ge90/ge90_20051012.html (General Electric)

8 Kosmatka, J. B., A. J. Lapid, and O. Mehmed. 1996. “Passive Vibration Control of Advanced Composite Turbo-Fan Blades Using Integral Damping Materials”, *Proceeding so the AIAA/ASME/ASCE/AHS/ASC 32nd Structures, Structural Dynamics, and Materials Conference*, AIAA-96-1598-CP:2459-69.

9 Swartz, Dave, and Larry Ilcewicz. 2002. "Fatigue and Damage Tolerance Perspectives for Composite Aircraft Structures", *FAA/DOD/NASA Aging Aircraft Conference*

10 Norris, Guy; Geoffrey Thomas; Mark Wagner, and Christine Forbes Smith. 2005. *Boeing 787 Dreamliner - Flying Redefined*, Aerospace Technical Publications International Pty Ltd.

11 Finegan, Ioana C., and Ronald F. Gibson. 1999. “Recent Research on Enhancement on Damping in Polymer Composites”, *Composite Structures*. **44**:89-98.

12 Pulgrano, L. J. and L. H. Miner. 1983. "Effects of Fiber and Resin on the Vibration Damping of Composites Reinforced wit Fiberglass, Graphite, and Aramid", *28th National SAMPE Symposium*, 56-64.

13 Adams, R. D. and D. G. C. Bacon. 1973. "Effect of Fibre Orientation and Laminate Geometry on the Dynamic Properties of CFRP", *J. Composite Materials*, 7(5):402-428.

14 Lin, D. X., R. G. Ni and R. C. Adams. 1984. "Prediction and Measurement of the Vibrational Damping Parameters of Carbon and Glass Fiber Reinforced Plastic Plates", *J. Composite Materials*, 18(2):132-152.

15 Ni, R. G. and R. D. Adams. 1984. "The Damping and Dynamic Moduli of Symmetric Laminated Composite Beams – Theoretical and Experimental Results", *J. Composite Materials*, 18(2):104-121.

16 Hwang, S. J. and R. F. Gibson. 1991. "The Influence of Vibration Coupling Effects on Damping of Laminated Composites", *Proceeding so the AIAA/ASME/ASCE/AHS/ASC 32nd Structures, Structural Dynamics, and Materials Conference*, AIAA-91-1129-CP:2397-2404.

17 Bronowicki, Allen J., and Henry P. Diaz. 1989. "Analysis, Optimization, Fabrication and Test of Composite Shells with Embedded Viscoelastic Layers", *Proceedings of Damping '89 Conference*, **AFWAL-TR-89-3116**:GCA1-21.

18 Maly, Joseph R., and Conor D. Johnson. 1996. "Cocured Viscoelastic Composites," *SPIE Proceedings on Smart Structures and Materials*, San Diego CA, 365-376.

19 Schmidt, K., F. Curtis, and E. Muziani. 1989. "Relsat Damped Equipment Panels – Fabrication", *Proceedings of Damping '89 Conference*, **AFWAL-TR-89-3116**:JBD1-18.

20 Belknap, F.L, and J.B. Kosmatka. 1991. "Vibration Suppression of Thin-Walled Composite Tubes Using Embedded Viscoelastic Layers," *Proceedings of the Damping '91 Conference*, HAC1-16.

21 Belknap, Frank. 1991. "Vibration Reduction of Composite Structures Using Constrained Layer Damping Techniques", *AIAA/ASME/ASCE/AHS/ASC 32nd Structures, Structural Dynamics, and Materials Conference*, AIAA-91-1128-CP:2391-6.

22 Barrett, David J. 1991. “Damped Composite Structures”, *Composite Structures*, **18**:283-294.

23 Rotz, C.A., and D.J. Barrett. 1991. “Cocured Damped Layers in Composite Structure,” *Sampe Quarterly*, 43-47.

24 Saravanos, D. A., and J. M. Pereira. 1992. “Effects of Interply Damping Layers on the Dynamic Characteristics of Composite Plates”, *AIAA Journal*. **30**:2906-13.

25 Gerst, D., M.D. Rao, and S.He. 1992. “Damping of Cocured Composite Structures Incorporating Viscoelastic Materials,” *Proceedings of the Damping of Multiphase Inorganic Materials Symposium*, Chicago, 85-93.

26 Rao, M.D., and S.He. 1993. “Dynamic Analysis and Design of Laminated Composite Beam with Multiple Damping Layers,” *AIAA Journal*, 31:736-745.

27 Harvey, James A., James L. Koury, Thomas D. Kim, and Michael L. Drake. 1993. “Integrally Damped Composites – a Study on Fabrication, Dynamics, and Statics Effects,” *SPIE Proceedings on Smart Structures and Materials*, Albuquerque NM, 634-40.

28 Sattinger, S. S., and Z. N. Sanjana. 1993. “Damping Thin-Walled Composite Structures with Embedded Constraining Layers”. *Proceedings of Damping ’93 Conference*, GCD1-14.

29 Saravanos, D. A., and J. M. Pereira, 1995. “Dynamic Characteristics of Specialty Composite Structures with Embedded Damping Layers”, *Transactions of the ASME*, **117**:62-9.

30 Kosmatka, J. B., and O. Mehmed. 1998. “Vibrational Reduction in Integral Damped Composite Fan Blades: Experimental Results”, *SPIE Proceedings on Smart Structures and Materials*, San Diego CA, 115-127.

31 Napolitano, K.L., W. Grippo, J.B. Kosmatka, and C.D. Johnson. 1998. “A Comparison of Two Cocured Damped Composite Torsion Shafts,” C*omposite Structures*, 43:115-125.

32 Kunz-Douglass, S., P. W. R. Beaumont, and M. F. Ashby. 1980. “A Model for the Toughness of Epoxy-Rubber Particulate Composites”, *Journal of Materials Science*, 15:1109-1123.

33 Jang, B.Z., J. Y. Liau, L. R. Hwang, and W. K. Shih. 1990. "Particulate and Whisker Modifications of Matrix Resin for Improved Toughness of Fibrous Composites". *Journal of Reinforced Plastics and Composites*, **9**:314-21.

34 Hudnut, Steven W., and D. D. L. Chung. 1996. "Highly Damped Carbon-Fiber Polymer-Matrix Composites", *Proceedings of the 1996 SPIE Symposium on Smart Materials and Structures*, 2720:358-64.

35 Hudnut, Steven W., and D. D. L. Chung. 1996. "Enhancing Loss Modulus of Carbon Fibre Polymer Matrix Composites by Addition of Particles in Interlaminar Region", *Plastics, Rubber and Composites Processing and Applications*. **25**:77-81.

36 http://www.elsie.brandeis.edu/er/index.html

37 Winslow, W. M. 1947. U. S. Patent 2417850.

38 http://www.mrfluid.com/

39 Davis, L. C. 1999. "Model of Magnetorheological Elastomers", *Journal of Applied Physics*, **85**:3348-3351.

40 Shiga, T., Y. Hirose, A. Okada, and T. Kurauchi. 1991. "Electroviscoelastic Effect of Polymer Gel Containing Fine Particles", *Kobunshi Ronbunshu*, **48**:47-51.

41 Shiga, Tohru, Takashi Ohta, Yoshiharu Hirose, Akane Okada, and Toshio Kurauchi. 1993. "Electroviscoelastic Effect Of Polymeric Composites Consisting Of Polyelectrolyte Particles And Polymer Gel", *Journal of Materials Science*, **28**:1293-1299.

42 Shiga, Tohru, Akane Okada, and Toshio Kurauchi. 1993 "Electroviscoelastic Effect of Polymer Blends Consisting of Silicone Elastomer and Semiconducting Polymer Particles", *Macromolecules*, **26**:6958-63.

43 Shiga, T., A. Okada, and T. Kurauchi. 1995. "Electroviscoelastic effect of doped poly (3-hexylthiophene)", *Journal of Materials Science Letters*, **14**:514-15.

44 Shiga, T. 1998. "Deformation and viscoelastic behavior of Polymer Gels in Electric Fields", *Proceedings of the Japan Academy*, **74(B)**:6-11.

45 Shiga, Tohru, Akane Okada, and Toshio Kurauchi. 1995. "Magnetroviscoelastic Behavior of Composite Gels", *Journal of Applied Polymer Science*, **58**:787-92.

46 Aklonis, John J., William J. MacKnight, and Mitchel Shen. *Introduction to Polymer Viscoelasticity*, Wiley-Interscience, New York, 1972.

47 Zinoviev, Peter A. and Yury N. Ermakov. *Energy Dissipation in Composite Materials*, Technomic Publishing Company, Lancaster, 1994.

48 Lakes, Roderic S. *Viscoelastic Solids*, CRC Press, Boca Raton, 1999.

49 Drozdov, Aleksey. *Viscoelastic Structures*, Academic Press, San Diego, 1998.

50 Haddad, Y. M. *Viscoelasticity of Engineering Materials*, Chapman and Hall, 1995.

51 Escobedo-Torres, J. 1997. "Solution Methods for the Dynamic Response of Structures with Viscoelastic Materials," Ph.D. Dissertation, Lehigh University, Bethleham, PA.

52 Bagley, R. L., 1983. "A Theoretical Basis for the Application of Fractional Calculus to Viscoelasticity", *Journal of Rheology*, **27**:201-210.

53 Bagley, Ronald L. and Peter J. Torvik, 1983. "Fractional Calculus – A Different Approach to the Analysis of Viscoelastically Damped Structures", *AIAA Journal*. **21**:741-8.

54 Bagley, Ronald L. and Peter J. Torvik, 1985. "Fractional Calculus in the Transient Analysis of Viscoelastically Damped Structures", *AIAA Journal*. **23**:918-925.

55 Bagley, Ronald L. and Peter J. Torvik, 1986. "On the Fractional Calculus Model of Viscoelastic Behavior", *Journal of Rheology*, **30**:133-55.

56 Bagley, Ronald L. 1989. "Power Law and Fractional Calculus Model of Viscoelasticity", *AIAA Journal*. **27**:1412-7.

57 Bagley, R. L. and P. J. Torvik, 1987. "Fractional Derivatives in the Description of Damping Materials and Phenomena", *11th Biennial Conference on Mechanical Vibration and Noise*, **5**:125-34.

58 McTavish, D. J. and P. C. Hughes. 1993. "Modeling of Linear Viscoelastic Space Structures", *Journal of Vibration and Acoustics*, **115**:103-110.

59 Lesieutre, G. A. and E. Bianchini. 1995. "Time Domain Modeling of Linear Viscoelasticity Using Anelastic Displacement Fields", *Transactions of the ASME*, **117**:424-430.

60 Jones, David I. G. 1978. “A Reduced-Temperature Nomogram for Characterization of Damping Material Behavior”, *The Shock and Vibration Bulletin*, **48**:13-22.

61 Rogers, Lynn. 1981. “Damping: On Modeling Viscoelastic Behavior”, *The Shock and Vibration Bulletin*, **51**:55-69.

62 Eichenlaub, James A. and Lynn Rogers. 1985. “Temperature Shift Effects on Complex Modulus”, *The Shock and Vibration Bulletin*, **55**:85-88.

63 ASTM Standard E 756-5, Standard Method for Measuring Vibration-Damping Properties of Materials.

64 Suarez, S. A., R. F. Gibson, and L. R. Deobald. 1984. “Random and Impulse Techniques for Measurement and Damping in Composite Materials”, *Experimental Techniques*, **8**:19-24.

65 Suarez, S. A. and R. F. Gibson. 1987. “Improved Impulse-Frequency Response Techniques for Measurement of Dynamic Mechanical Properties of Composite Materials”, Journal of Testing and Evaluation, 114-121.

66 Brodt, M., L. S. Cook, and R. S. Lakes. 1995. “Apparatus for Measuring Viscoelastic Properties over Ten Decades: Refinements”, Review of Scientific Instruments, **66**:5292-7.

67 Nashif, Ahid D. and Tom M. Lewis. 1991. “Data Base of the Dynamic Properties of Materials”, Sound and Vibration, Materials Reference Issue, 14-24.

68 Rao, Singiresu S. Mechanical Vibrations. Addison-Wesley Publishing Company, Reading, Massachusetts, 1995.

69 Biggerstaff, J.M, and J.B. Kosmatka, 1999. “Damping Performance of Cocured Graphite/Epoxy Composite Laminates with Embedded Damping Materials”, *Journal of Composite Materials*, **33**:1457-69.

70 Jones, R. M.; *Mechanics of Composite Materials*, Hemisphere Publishing Corporation, New York, 1975.

71 Adams, R. D. and D. G. C. Bacon. 1973. “Effect of Fibre Orientation and Laminate Geometry on the Dynamic Properties of CFRP”, *J. Composite Materials*, 7(5):402-428.

72 Lin, D. X., R. G. Ni and R. C. Adams. 1984. "Prediction and Measurement of the Vibrational Damping Parameters of Carbon and Glass Fiber Reinforced Plastic Plates", *J. Composite Materials*, 18(2):132-152.

73 Ni, R. G. and R. D. Adams. 1984. "The Damping and Dynamic Moduli of Symmetric Laminated Composite Beams – Theoretical and Experimental Results", *J. Composite Materials*, 18(2):104-121.

74 Hwang, S. J. and R. F. Gibson. 1991. "The Influence of Vibration Coupling Effects on Damping of Laminated Composites", *Proceeding so the AIAA/ASME/ASCE/AHS/ASC 32nd Structures, Structural Dynamics, and Materials Conference*, AIAA-91-1129-CP:2397-2404.

75 Kunz-Douglass, S., P. W. R. Beaumont, and M. F. Ashby. 1980. "A Model for the Toughness of Epoxy-Rubber Particulate Composites", *Journal of Materials Science*, **15**:1109-1123.

76 Nakao, Kazumune and Yoshihiro Yamashita. 1986. "Effect of Modification of Epoxy Matrix with Liquid Nitrile Rubber on Bond Strength between Carbon Fiber and Epoxy Matrix in Composites". *Composites '86: Recent Advances in Japan and the United States, Tokyo*, 743-50.

77 Jang, B.Z., J. Y. Liau, L. R. Hwang, and W. K. Shih. 1990. "Particulate and Whisker Modifications of Matrix Resin for Improved Toughness of Fibrous Composites". *Journal of Reinforced Plastics and Composites*, **9**:314-21.

78 Hudnut, Steven W., and D. D. L. Chung. 1996. "Highly Damped Carbon-Fiber Polymer-Matrix Composites", *Proceedings of the 1996 SPIE Symposium on Smart Materials and Structures*, **2720**:358-64.

79 Hudnut, Steven W., and D. D. L. Chung. 1996. "Enhancing Loss Modulus of Carbon Fibre Polymer Matrix Composites by Addition of Particles in Interlaminar Region", *Plastics, Rubber and Composites Processing and Applications*. **25**:77-81.

80 Kovacic, P. and A. Kyriakis. 1963. "Polymerization of Benzene to *p*-Polyphenyl by Aluminum Chloride-Cupric Chloride", Journal of the American Chemical Society, **85**:454.

81 Mak, Stanley, C., and J. B. Kosmatka, 2002, "A New Method for Characterizing the Dynamic Properties of Electroviscoelastic Materials," *Proceedings of the 9th Annual International Symposium on SPIE Smart Structures and Materials*, **4695**:277-285.